Applied Voxel-based Morphometry in Health and Neurological disease

Catriona Diana Good

Thesis submitted for the degree of Doctor of Philosophy, 2003
Institute of Neurology, University College London, London UK

ProQuest LLC
789 East Eisenhower Parkway
P.O. Box 1346
Ann Arbor, MI 48106-1346

ABSTRACT

The importance of brain structure is indisputable. It forms the framework on which functional parameters can be mapped and referenced. The classical region of interest based morphometric methods that have hitherto formed the mainstay of structural neuroimaging have a number of drawbacks not least because they are spatially constrained and operator dependent. In light of substantial advances in magnetic resonance imaging techniques and concomitant computational post processing innovations, new insights into brain structure are now possible. A new generation of whole brain imaging techniques can now inform about brain structure in a more holistic way with enhanced precision. Computational neuroanatomy is a new method employing the versatile framework of statistic parametric mapping and volumetric high-resolution magnetic resonance images of the brain. It consists of a triad of interactive techniques: voxel-based morphometry (VBM) which provides voxel-wise inferences about regional grey and white matter, deformation-based morphometry (DBM) which characterises global brain shape differences and tensor-based morphometry (TBM) which characterises local shape differences with high precision.

This thesis examines the application and usefulness of voxel-based morphometry with particular reference to its practicality, reproducibility, validity and sensitivity to characterise brain structure. VBM is first applied to a large normative database to characterise physiological variations in normal brain structure in order to create a canonical framework against which pathology can be measured. VBM is then rigorously compared with classical morphometrics in patients with two distinct forms of dementia and in patients with mesial temporal sclerosis in order to establish validity and sensitivity. VBM is then applied to a variety of disease groups where classical morphometrics have failed to reveal consistent brain structural phenotypes in order to reveal morphological changes in functionally implicated regions. Finally VBM is used as a tool to allow genotype-phenotype mapping. The strengths and weaknesses of this new technique are discussed with reference to its applicability and usefulness for neurologists and neuroradiologists

COPYRIGHT

ACKNOWLEDGEMENTS

This work is the result of a stimulating and richly rewarding four years at the Wellcome Department of Imaging Neuroscience. First and foremost I would like to thank my supervisors, Richard Frackowiak and Karl Friston. Quite simply it has been a joy to work for Richard. He has provided constant intellectual stimulation, provocation and sound advice imbued with human kindness and a wicked sense of humour. Karl has provided tremendous support and wisdom, patiently and generously answering my stream of questions relating to the finer points of SPM and VBM. I am also hugely indebted to John Ashburner; Karl and John are the masterminds behind VBM, and without them this thesis would not be possible. At each and every stage of this work, John has provided image processing support and guidance. I lay any wisdom of this thesis at feet of these three.

Many others have made significant specific contributions to the individual studies reported here including, Ingrid Johnsrude and Rick Henson (chapters 3 and 4), Rachael Scahill and Nick Fox (chapter 5), Mathias Koepp (chapter 6), Manjit Matharu and Peter Goadsby (chapter 7), Hugo Critchley, Hema Ananth and Ioana Popescu (chapter 8), Hugo Critchley and Chris Mathias (chapter 9), David Skuse, Kate Elgar, Simon Thomas, Lars Oreland, Rebecca Akkers and Cathy Price (chapter 10), Andrew Duggins and Mike Thieben (chapter 11), Nicola Giffin, Manjit Matharu and Peter Goadsby (chapter 12).

I am particularly grateful to all my friends and colleagues at the FIL. I received tremendous technical and personal support from James Rowe, Ingrid Johnsrude, Bal Athwal, Anne Lise Giraud, Andreas Kleinschmidt, Dave McGonigle, Julie Grezes and Nick Ward - our supervisees meetings with Richard were a highlight of each week. Special thanks to Ralf Deichmann for his kindness and support and for producing high-resolution structural images of the finest quality. Amanda Brennen, Paul Bland, Helen Gallagher, Karen Hawkins, Eleanor Maguire, Bryan Strange, Oliver Josephs, Stefan Kiebel, Chloe Hutton, Bob Turner and Ray Dolan have all provided invaluable advice and support. Terry Morris has helped me at every step with administrative issues and equipment and I thank him for securing me a desk with a fine view of Queen Square (enhanced most misty mornings by a postman doing t'ai chi). I thank all the patients and volunteers who participated in my studies and the Wellcome Trust for their generous support. Finally I thank my family.

TABLE OF CONTENTS

LIST OF FIGURES

LIST OF TABLES

CHAPTER 1

INTRODUCTION

The importance of brain structure

One of the fundamental goals of neuroscience is to understand the complex functions of the human brain in health and its adaptations to disease. To this end, increasing importance has been placed on brain structure not only to establish links between structure and function, but also to allow brain function to be mapped precisely into a neuroanatomical framework. Brain structure can be expressed at a macroscopic scale (e.g., global or regional grey matter, regional asymmetries), at a mesoscopic scale (e.g., cortical thickness) or at a microscopic scale (e.g., cytoarchitectonics). Large multicentre databases are now integrating several components of structural information such as cytoarchitectonics, myeloarchitectonics, neurochemical receptor distribution and diffusion properties of white matter tracts with functional imaging data from PET, fMRI, EEG and MEG, and genetic profiles in order to create a more holistic map of the human brain. It is now increasingly important to have a standardised accurate anatomical framework to enable multiple sources of information to be pooled and compared between laboratories.

There has been recent renewed interest in brain macroscopic and mesoscopic structural imaging in light of substantial advances in computational power and analytical expertise that permit objective analyses of high resolution three-dimensional MRI scans. The great challenge for structural imaging is to accommodate the full spatial and temporal complexity of macroscopic brain anatomy during normal development and its adaptations to physiological senescence. It is only after the dynamic physiological asymmetries and heterogeneities of normal cerebral anatomy are realised, that perturbations of disease can be properly appreciated. This requires sophisticated registration and analysis of MRI scans. The relationship between brain structure and function is complex; abnormalities in structure are not necessarily

associated with functional deficits, and the spatial extent of a structural lesion does not necessarily determine the degree of functional deficit. Despite this, the importance of anatomy is indisputable and it remains the infrastructure upon which brain function is mapped.

Macroscopic cerebral anatomy

Crude descriptions of cerebral anatomy originate from ancient Egyptian times, but at that time the cerebrum was passed off as a functionless organ. It was not until the early nineteenth century that the important functions of the cerebral cortex were recognised. By the late nineteenth- and early twentieth-century pioneering work by anatomists allowed the first detailed labelling of brain surface structures and formed the foundations of modern neuroanatomy. With the introduction of modern scanning techniques, detailed labelling of deeper brain structures began - and today comprehensive and detailed brain atlases map the brain in its entirety with great precision in three dimensions.

Brain size and gross morphology

The human brain lies within the cranial cavity attached to the spinal cord at the cervico-medullary junction. The brain and spinal cord are surrounded by fibrous membranes, the meninges, which comprise three layers: a dense outer dura mater, an intermediate arachnoid membrane and a thin inner pia mater. Cerebrospinal fluid circulates in the subarachnoid space around the brain and spinal cord in free continuity with the ventricles. The basic divisions of the brain are into two cerebral hemispheres, the brainstem and cerebellum. The right and left cerebral hemispheres are separated by the falx cerebri that lies within the interhemispheric fissure. A broad commissure of white matter fibres, the corpus callosum, connects the hemispheres. Each hemisphere comprises an outer mantle of grey matter (the cerebral cortex) and underlying white matter that extends down to the ventricular system. Embedded deep within the white matter are additional grey matter structures, the grey matter nuclei (e.g. accumbens, basalis, caudate, lentiform, thalamic, hypothalamic, subthalamic, parafascicular, red and septal). The grey matter contains the cell bodies of neurons whereas the white matter consists of bundles of myelinated axons emerging from cell bodies. The cortical surfaces are markedly convoluted into a complex system of gyri and sulci.

The hemispheres are generally divided into six lobes: frontal, temporal, parietal, occipital, insula and limbic. The frontal lobe is the only lobe that can be clearly separated from the other lobes on the lateral surface. It is bounded posteriorly by the central sulcus and inferiorly by the Sylvian fissure, and is divided into four frontal gyri: precentral, superior, middle and inferior. Some of the boundaries of the temporal, parietal and occipital lobes are less distinct and are conventionally defined on arbitrary criteria that have no anatomical, histological or functional basis. The parietal lobe is clearly separated from the frontal lobe by the central sulcus, but its boundary with the temporal lobe is based on an arbitrary convention: a horizontal line extending posteriorly from the point that the Sylvian fissure becomes vertical. The division between the occipital, temporal and parietal lobes is usually based on a theoretical straight line running from the parieto-occipital fissure (visible on the medial surface of the brain) to the temporo-occipital incisure. The parietal lobe is divided into the postcentral and the superior and inferior parietal gyri. The temporal lobe is divided into superior, middle and inferior temporal gyri. The occipital lobe anatomy is so complex and variable that most classic anatomy textbooks avoid detailed descriptions. In general it is divided into superior, middle and inferior occipital gyri. The insula is situated in the bottom of the lateral fossa and can only be seen once the lateral operculum has been removed. It is shaped as a small inverted triangle and is separated from the lateral operculum by the circular insular sulcus. The insula is divided into anterior and posterior portions by the central insular sulcus. The limbic lobe is a complex structure consisting of large convolutions of the medial hemisphere and is separated from surrounding structures by the limbic fissure. The limbic lobe may be divided into limbic and intralimbic gyri. The limbic gyrus comprises the subcallosal gyrus, cingulate gyrus, isthmus and parahippocampal gyrus. The intra-limbic gyrus comprises the pre-hippocampal rudiment, the indusium griseum and the hippocampus.

Sulcal and gyral anatomy

It is beyond the scope of this text to provide a comprehensive account of each and every sulcus and gyrus, particularly considering the wide variations in sulcal anatomy not just between different brains, but also between hemispheres of the same brain. This section will document the most consistent and major surface anatomical landmarks that are used as reference points by most brain imagers. Variability of structures and inconsistencies of nomenclature will also be highlighted. Anatomical

descriptions and nomenclature are in general based on Henri M. Duvernoy's comprehensive and excellent brain atlas (Duvernoy 1999).

The **Sylvian fissure**, also termed the lateral fissure forms a deep depression on the lateral fossa whose banks constitute the lateral operculum. It is divided into basal and lateral parts, and the lateral part is further subdivided into anterior, middle and posterior segments. Its start marks the division between the frontal and temporal lobes and it bifurcates posteriorly into a small downward curving segment and a larger vertical portion called the terminal ascending segment.

The **central sulcus**, also termed fissure of Rolando, separates the frontal and parietal lobes, and more importantly delineates the boundary between the primary motor and sensory cortices. It is usually clearly identifiable on MRI and serves as an important reference point for the identification of other sulci. (That said, occasionally even the most experienced anatomists have problems identifying the central sulcus). On superior axial slices the central sulcus displays a typical notch and does not connect with sulci orientated in a different direction (such as the superior frontal and intraparietal sulci). At the level of the vertex the precentral, central and postcentral sulci form a typical triad of parallel lines. On para- sagittal sections the central sulcus forms a notch just anterior to the end of the callosomarginal sulcus. On lateral sagittal slices, the central sulcus is the third sulcus after the ascending branch of the Sylvian fissure.

Frontal lobe sulci: The superior and inferior frontal and precentral sulci divide the frontal lobe into precentral, superior, middle and inferior frontal gyri. The horizontally orientated superior and inferior frontal sulci branch into ascending and descending rami at their caudal ends. These rami form the inferior and superior precentral sulci, which may remain separate or merge to form a single precentral sulcus lying anterior and parallel to the central sulcus. The superior frontal sulcus frequently intersects the precentral sulcus (usually the inferior segment) and is easily identifiable on axial MR slices, helping to differentiate the precentral sulcus from the central sulcus. The lateral surface of the superior frontal gyrus (F1) is often divided by an additional longitudinal sulcus that may be discontinuous. The middle frontal gyrus (F2) is often divided into superior and inferior parts by a middle frontal sulcus that sometimes merges with the frontomarginal sulcus. The inferior frontal gyrus (F3) may merge with the orbital lobe inferiorly or be separated from it by a lateral orbital sulcus. The ascending and horizontal rami of the Sylvian fissure divide the inferior frontal

gyrus into three parts: the *pars orbitalis* inferiorly, the pars triangularis centrally and the *pars opercularis* posteriorly. An additional *sulcus diagonalis* may arise from the inferior frontal sulcus to divide the pars triangularis and a vertical groove, the *sulcus diagonalis* may be seen on the pars opercularis. Confusion may arise over terms such as dorsolateral prefrontal cortex (generally considered to be the superior and middle frontal gyri excluding the posterior portions) and ventrolateral prefrontal cortex (generally considered to be the middle and anterior parts of the inferior frontal gyrus). The frontal pole is a transitional area between the lateral, medial and orbital surfaces of the frontal lobe. Most of the medial surface of the frontal lobe comprises the superior frontal gyrus (F1), which is bounded posteriorly by the small paracentral sulcus. Caudal to this is the paracentral lobule, which bridges the frontal and parietal lobes. The medial surface of the frontal lobe is separated from the limbic lobe by the cingulate sulcus. In the subcallosal region one or two supraorbital sulci separate the medial surface of the frontal lobe from the gyrus rectus, which forms part of the inferior surface of the frontal lobe (also termed the orbital lobe)

Parietal lobe sulci: The parcellation of the parietal lobe is very variable. On the lateral surface only one sulcus is clearly visible, the intraparietal sulcus, which divides the parietal lobe into the postcentral and superior and inferior parietal gyri. The intraparietal sulcus usually comprises three segments: an anterior segment that ascends, an intermediate segment that lies horizontally and a posterior segment that descends. The anterior segment, also termed the inferior postcentral sulcus, runs parallel to the central sulcus. There may also be a separate superior postcentral sulcus. The posterior segment descends until it reaches the theoretical boundary between the parietal and occipital lobes then becomes the intra-occipital sulcus. The postcentral gyrus is often narrower than the precentral gyrus. The subcentral gyrus (ventrally) and the paracentral lobule (dorsally) form a superficial link between the pre- and postcentral gyri. The superior parietal gyrus (P1) is clearly identifiable, limited anteriorly by the postcentral sulcus and inferiorly by the intraparietal sulcus. At the level of the parieto-occipital fissure P1 is linked to the superior occipital gyrus by a transitional area called the parieto-occipitalis and there may be bridging lobules connecting the superior and inferior parietal gyri. The inferior parietal gyrus (P2) is highly variable and complex. It is divided by a descending ramus of the intraparietal sulcus into two parts: the supramarginal gyrus and the angular gyrus. The supramarginal gyrus is an arched lobule surrounding the end of the Sylvian fissure.

The angular gyrus is a narrow lobule surrounding the ascending posterior segment of the superior temporal sulcus. To complicated matters the left superior temporal sulcus often has a double parallel termination, and in this scenario there is no consensus on the anterior and posterior limits of the angular gyrus, with some authors ascribing part of the angular gyrus to the parietal lobe and others ascribing it to the occipital lobe. The confusion is further confounded by the cytoarchitectonics of this region (Brodmann's area 39), which cannot be clearly separated from the occipital and temporal regions. The medial surface of the parietal lobe comprises the precuneus, which is part of the superior parietal gyrus (P1). The marginal segment of the cingulate sulcus separates the anterior border of the precuneus from the paracentral lobule. Posteriorly the parieto-occipital fissure separates the precuneus from the occipital lobe. The subparietal sulcus partially separates the precuneus from the cingulate gyrus.

Temporal lobe sulci: The superior and inferior temporal sulci divide the temporal lobe into superior, middle and inferior temporal gyri. The superior temporal sulcus runs parallel to the Sylvian fissure and is easy to identify. It is usually divided into an anterior and posterior segment. The anterior segment is sometimes termed the anterior temporal sulcus as it reaches the temporal pole. The posterior segment is variable. It may be a single sulcus or, as is most often the case, it branches into an ascending posterior segment (sulcus angularis) and a horizontal segment. The inferior temporal sulcus is not only highly variable, but it is difficult to define along its course, particularly posteriorly, where it may be termed the anterior occipital sulcus. As a result the delineation between the posterior limits of the middle and inferior temporal gyri and the adjacent inferior occipital gyrus is unclear. The medial temporal lobe comprises the amygdala, the complex folded allocortex of the hippocampal formation (subicular cortices, hippocampus and dentate gyrus) and the surface allocortical and peri-allocortical layers of the parahippocampal gyrus (T5) that cover them. Confusion in nomenclature arises because many of the "medial temporal" structures are formally part of the limbic lobe (see below for details). The inferior surface of the temporal lobe consists of three gyri: the inferior temporal gyrus (T3), the fusiform gyrus (T4) and the parahippocampal gyrus (T5) separated by the lateral occipitotemporal and collateral (medial occipitotemporal) sulci respectively. The fusiform gyrus does not extend to the temporal pole and is bounded rostrally by the anterior transverse collateral sulcus and caudally by the posterior transverse collateral sulcus.

Occipital lobe sulci: laterally, the occipital lobe is separated from the other

lobes by a theoretical line running from the parieto-occipital fissure to the temporo-occipital incisure. Although parcellation of the occipital lobe is by no means consistent, Duvernoy (Duvernoy 1999) describes superior and inferior occipital sulci on the lateral surface forming superior (O1), middle (O2) and inferior (O3) occipital gyri. The superior occipital sulcus (or intra-occipital sulcus) is usually the continuation of the intraparietal sulcus. The inferior occipital sulcus is variable and usually difficult to identify. A transverse occipital sulcus is also described. On the medial surface the occipital lobe is clearly separated from the parietal lobe by the parieto-occipital fissure. On the inferior surface, there are no clear boundaries between the occipital and temporal lobes. The fourth occipital gyrus (O4) and its paired temporal homologue (T4) together form the fusiform (lateral occipitotemporal) gyrus. The lingual gyrus (O5) and the parahippocampal gyrus (T5) together form the medial occipitotemporal gyrus. The cuneus (O6) is the only well defined occipital gyrus bordered by the parieto-occipital fissure and the calcarine sulcus. Occasionally a bridging lobule links the cuneus to the lingual gyrus. On the occipital pole, the calcarine sulcus branches off into the retro-calcarine sulcus, which demarcates a small lobule, called the gyrus descendens of Ecker, which marks the caudal boundary of the striate cortex. The striate cortex is situated in the gyrus of Ecker, superior and inferior banks of the calcarine sulcus proper and extending rostrally along the inferior bank of the anterior calcarine sulcus without reaching its end.

Limbic lobe sulci: The limbic fissure demarcates the limbic lobe, but problems arise because this fissure is complex and difficult to define. It is formed by a succession of different and discontinuous sulci (subcallosal, cingulate, subparietal, anterior calcarine, collateral and rhinal), which constitute the limbic fissure only for part of their course. The limbic gyrus is made up of several parts: the subcallosal gyrus, cingulate gyrus, isthmus and parahippocampal gyrus. The subcallosal gyrus is bordered by the anterior para-olfactory (subcallosal) sulcus and the posterior para-olfactory sulcus, which separates it from the paraterminal gyrus. There are inconsistencies with terminology here. The subcallosal gyrus is sometimes termed the area adolfactoria, in which case the paraterminal gyrus is called subcallosal gyrus. The cingulate gyrus courses around the corpus callosum from which it is separated by the pericallosal sulcus. A narrow bridge of cortex, the isthmus, connects the cingulate gyrus to the parahippocampal gyrus beneath the splenium of the corpus callosum. The parahippocampal gyrus, confusingly termed T5, and the lingual gyrus (O5) together

form the medial occipitotemporal gyrus. The parahippocampal gyrus is usually divided into two parts. A larger anterior segment called the piriform lobe, which consists of the anterior part of the uncus and the entorhinal cortex. The narrower posterior segment has a flat superior surface, the subiculum, which is separated from the hippocampus by the hippocampal sulcus. The uncus is divided into anterior and posterior portions. The anterior portion is part of the piriform lobe. Two protrusions are conspicuous in this region: the semilunar gyrus (part of the amygdala) and the ambient gyrus. The ambient gyrus is often misidentified as uncus because it bulges medially in a similar fashion, but the ambient gyrus actually arises from medial entorhinal cortex and is always a few millimetres anterior to uncus and in the same plane as the posterior portion of the amygdala. The posterior portion of the uncus belongs to the intralimbic gyrus and comprises the uncinate gyrus, the band of Giacomini and the uncal apex. The entorhinal cortex (Brodmann's area 28) is the largest cortical field of the parahippocampal gyrus and forms the lower part of the piriform lobe. This structure is difficult to differentiate from surrounding anatomy; the sulcus semilunaris separates it from the amygdala, but posteriorly it merges with the lingual part of the occipital lobe near the anterior tip of the calcarine fissure and medially it merges with the subicular part of the hippocampal formation. Its borders are thus usually defined by arbitrary criteria (see chapter 4). The perirhinal cortex also causes confusion and is often ignored in anatomy texts. It forms the lateral border of the parahippocampal gyrus and corresponds to Brodmann's area 35 which constitutes the medial bank of the collateral sulcus intervening between the entorhinal cortex and the inferior temporal cortex (Brodmann's area 36). Its exact configuration depends on the positioning and depths of the rhinal and collateral sulci.

Macroscopic anatomical variability

Sulcal variability

Features such as neocortical expansion and complex gyrification help to differentiate the human brain from the brains of lesser primates. As unique as the human brain is relative to other species, there are considerable interindividual variations in neuroanatomy including global size and shape differences as well as regionally specific differences in gyral and sulcal geometry. The spatial variations in

sulcal and gyral geometry relate in part to the timing of sulcal formation during brain development. The more consistent sulci are generally those that develop early such as the primary and secondary sulci, while those developing later (after the 28th week of gestation) show greater complexity and variation. The early sulci include the interhemispheric fissure (8th week), Sylvian fissure (14th week), parieto-occipital sulcus, central sulcus and calcarine fissure (16th week). The precentral, postcentral, intraparietal, middle temporal and superior frontal sulci develop between the 24th and 28th weeks and finally in the third trimester, the tertiary sulci and gyri (such as the inferior temporal, inferior parietal, angular and supramarginal gyri) develop. This complex variability between individuals and across different regions presents a huge challenge for anyone attempting to create an anatomical reference frame. A fixed brain atlas cannot truly represent the individual brain and direct averaging of digital brain maps is only valid if homologous regions are accurately mapped. For this reason, sophisticated computational morphometric models are integral to modern brain mapping.

Cerebral asymmetries

An important and specific form of cerebral variability is asymmetry. Morphological left-right asymmetry appears to be the rule rather than the exception in biological systems (Geschwind and Galaburda 1985a; Geschwind and Galaburda 1985b; Geschwind and Galaburda 1985c; Kimura 1973). Even single-celled organisms are commonly asymmetric, and greater organisational complexity may be reflected in greater functional specialisation and thus in more elaborate asymmetry of function and structure. Certainly human beings are structurally asymmetric; from the size of their feet, sex organs and hands to the placement of visceral organs and facial features (Kimura, 1973; Levy, 1978; Purves *et al.*, 1994) and they exhibit lateralised behaviour as early as 10 weeks gestation (Hepper *et al.*, 1998).

Structural asymmetries in the human brain have been sought and studied for over a century (Geschwind and Galaburda 1985a) (Geschwind and Galaburda 1985b) (Geschwind and Galaburda 1985c) and observations of macroscopic structural asymmetries in areas known to be functionally asymmetric have proliferated in the last two decades. The main and most consistent observations include the right frontal and left occipital petalia; marked indentations of the inner table of the skull resulting from the greater protrusion of the adjacent cerebral lobes (Chiu and Damasio 1980; Gundara

and Zivanovic 1968; LeMay 1986). This term is now used in reference to the lobar asymmetries themselves. One of the earliest reported brain asymmetries is also one of the most consistent: the trajectory of the Sylvian fissure is angled upwards (dorsally) more steeply in the right hemisphere (Cunningham 1892; Geschwind and Galaburda 1985a; Loftus *et al.* 1993; Ratcliff *et al.* 1980; Thompson *et al.* 1998; Thompson *et al.* 2001a; Westbury *et al.* 1999). This trajectory asymmetry is very probably related to another well-known posterior Sylvian asymmetry - one probably more easily detectable by voxel-based morphometry (VBM) - the leftward volume asymmetry of the planum temporale (Geschwind and Levitsky 1968; Steinmetz *et al.* 1989; Wada *et al.* 1975; Watkins *et al.* 2001) and of cytoarchitectonic area Tpt, characteristically found in this region (Galaburda *et al.* 1978).

Other macrostructural asymmetries can be found on the superior temporal plane: the first gyrus of Heschl, containing primary auditory cortex, appears to be larger on the left side (Penhune *et al.* 1996; Rademacher *et al.* 1993). This difference has been ascribed to a larger volume of white matter rather than grey matter (Penhune *et al.* 1996). Finally recent studies corroborate and extend older reports of a larger Broca's area (areas 44 and 45 of Brodmann) in the left hemisphere (Foundas *et al.* 1998b; Annett 1970; Annett 1976; Falzi *et al.* 1982; Foundas *et al.* 1995; Foundas *et al.* 1996; Geschwind and Galaburda 1985a). Chapter 4 examines human brain asymmetries on a voxel-wise scale and documents the effects of sex and handedness.

Relationship between macroanatomy and microanatomy

The microanatomy of the brain has to a large extent already been mapped in detail. In 1909 in the famous book *Vergleichende Lokalisationslehre der Grosshirnrinde in ihren Prinzipien dargestellt auf Grund des Zellenbaues*, Korbinian Brodmann provided detailed mapping of architectonic fields (Brodmann 1909). The basis of Brodmann's cortical localisation is its subdivision into 'areas' with similar cellular and laminar structure. He compared localisation in the human cortex with that in a number of other mammals, including primates, rodents and marsupials. In man, he distinguished 47 areas, each carrying an individual number, and some being further subdivided. To this day Brodmann's work forms the basis for localisation of function in the cerebral cortex, with most neuroanatomical texts referring to Brodmann's areas

(Brodmann 1909). In early times, specific cognitive functions were assumed to be directly predicated by specific cytoarchitectural fields. But since the advent of functional imaging, it is now clear that there is not an exact correspondence between cytoarchitectonic anatomy and function, for example in areas 17,18 and 19 of the human occipital cortex, the myelo- and cytoarchitecture do not correspond with the putative boundaries of functional visual areas (Clarke and Miklossy 1990). It is thus more appropriate to parcellate the microstructure of the human cerebral cortex using multiple criteria based on quantitative measurements of microstructural variables, such as neuron densities, neurotransmitter receptor densities and enzyme densities (Roland and Zilles 1998). Although architectonic fields often show a characteristic relationship to macroscopic landmarks such as gyri and sulci, there are several areas such as Brodmann's areas 9 and 46 in prefrontal cortex where cytoarchitectonic fields and macroscopic landmarks do not correlate (Rajkowska and Goldman-Rakic 1995b; Rajkowska and Goldman-Rakic 1995a). The "primary" cytoarchitectonic neocortical fields, Brodmann's areas 17, 41, 3b, and 4 bear a characteristic relationship to a set of bounding anatomic landmarks, in particular gyri, fissures, and sulci that can be readily defined by MRI. In general there are two types of variability. In the first case, variability is not predictable from visible landmarks as exemplified by the extracalcarine distributions of area 17 or the extent of area 4 on the paracentral lobule. In the second case, variability is predictable from visible landmarks as exemplified in the marked interindividual or interhemispheric variation in overall size or shape of a field. Because of the prominence of this second class of variability, direct reference to landmarks that frame these fields may be more reliable for functional mapping than reference to a fixed or standard template.

Brain atlases

Brain atlases have existed for many decades and their purpose is to provide an anatomical reference frame. Many of the early atlases were collections of micrographs or schematic drawings of brain sections derived from one or a few post mortem specimens depicting information such as microscopic architecture (Brodmann 1909) or neurochemical distribution (Mansour *et al.* 1995). In the early 1970s, Jean Talairach (Talairach and Tournoux 1988) combined a system of teleradiography with

ventriculography to describe brain anatomy in a statistical way within a proportional grid localisation system. His system is based on the premise that despite marked variability in brain sizes, the relationship of structures in the telencephalon to the anterior and posterior commissures is stable. Structures close to the AC or PC exhibit smaller variations in stereotactic space than those at the periphery of the brain. This methodology was originally designed as a navigational tool for functional neurosurgery, but it rapidly became an international standard for localising functional imaging data and one of the most used brain atlases that has subsequently been digitised. The atlas maps the brain of a sixty year old woman within a stereotactic coordinate system and includes the cartography of Brodmann (Brodmann 1909). One of the problems with this atlas is that it does not accurately reflect the in vivo anatomy of most of the subjects used in activation studies (usually young males). A further confound is the variable separation between atlas plates and the sometimes imprecise mapping of Brodmann areas: "The brain presented here was not subjected to histological studies and the transfer of the cartography of Brodmann usually pictured in two dimensional projections sometimes possesses uncertainties". To address these limitations the Montreal Neurological Institute (MNI) (Evans *et al.* 1993) produced a more representative brain template based on a large series of normal MRI brain scans. Initially they manually defined various landmarks on 241 normal brain MRIs, scaled each image to match the landmarks on the Talairach atlas using affine transformations (translations, rotations, zooms) and finally created a mean image. They then used an automated linear algorithm to match 305 normal MRI scans (all right handed, 239 M, 66 F, age 23.4 +/- 4.1) to the mean scaled 241-brain image. From this they generated a mean template: the MNI 305. They have subsequently generated the ICBM 152 template which is based on 152 normal MRI scans that have been affinely matched to the MNI 305 (age range 18-44, mean 24 (+/- 4.9), 56% male. This digitalised template is now the standard for the International Consortium for Brain Mapping (ICBM)(Mazziotta *et al.* 2001) and the widely used Statistic Parametric Mapping (SPM) package (Friston *et al.* 1995). However, with the introduction of the MNI templates, some confusion has arisen over reporting localisations in the Talairach coordinate system. The linear transformations have not matched the MNI templates precisely to the Talairach brain and as a result the MNI brain is slightly larger than the Talairach brain. Furthermore, mismatches are most pronounced (up to 10mm) at the periphery of the brain and least pronounced centrally. For this reason there are now

approaches for translating MNI coordinates to Talairach space.

In light of the complex interindividual variability in cortical structure, a fixed brain atlas cannot allow a precise representation of each and every brain. This is because sulci and gyri will not be precisely matched. With improvements in registration techniques, deformable MRI atlases can now be created to more accurately match individual MRI image sets. Two options exist: the incoming MRI can be warped to the atlas, or the atlas can be warped to the incoming MRI. In the former, the subject's anatomy is transformed into the anatomical framework of the atlas, removing subject specific shape differences. For example regionally specific effects can be compared having removed confounding factors such as global size and shape differences. In the latter, the information from the atlas is transferred onto the subject's anatomy, whilst preserving subject specific characteristics. For example, cytoarchitectonic architecture can be mapped onto a specific subject's brain.

These deformable brain atlases thus allow more accurate matching of brain scans, but they do not encode information on interindividual variations in cortical architecture. Complex mathematical strategies are needed to quantify the magnitude and directional biases of neuroanatomical variability. Such atlases now exist, and are referred to as digital probabilistic atlases. They encode precise statistical information on local structural variations. For example, gyral and sulcal variations can be quantified to determine whether they lie outside the normal range, which may be a sign of disease (Thompson *et al.* 1996a; Thompson *et al.* 1996c; Thompson *et al.* 2000). Pioneering work by Thompson and colleagues has allowed the generation of population-based probabilistic brain atlases in a number of important diseases including Alzheimer's disease and schizophrenia (Thompson *et al.* 1998; Thompson *et al.* 2001a; Thompson *et al.* 2001b).

Evolution of morphometry techniques

Although the quest for understanding the structure and function of the human brain started centuries ago, most of the earlier descriptions were qualitative. Quantitative assessments of anatomy and function are preferable, but are more challenging to obtain. The highly complex organisation of human cerebral cortex, including the dynamic changes with time and marked interindividual variability in

regional anatomy need to be catered for. In addition, brain function is likely to be more closely related to a combination of structural features such as cytoarchitecture, neurotransmitter receptor and enzyme densities and myeloarchitecture than simply macroscopic structure. Thus crude anatomical descriptions on a macroscopic level are generally of limited value, and more sophisticated objective morphometric methods are required. Quantitative differences in macroscopic brain structure have been assessed by a variety of techniques over the last 3 decades. As early as 1905 indirect measurements of brain volume were made post mortem by instilling water into the cranial cavity and measuring the brain/ intracranial cavity volume ratio (Reichardt 1905). Direct post mortem analyses of brain structure, whilst sensitive to microscopic and macroscopic structural differences are subject to a number of practical shortcomings. Firstly post mortem material is not readily available. Secondly these studies are time consuming, since much of the tissue preparation is performed manually. Further confounding effects such as the interval between death and fixation of brain tissue, the timing of measurements (Last and Tompsett 1953; Messert *et al.* 1972) and the inclusion or exclusion of brain stem structures and meninges (which can be difficult to control), can vary across studies, making comparisons difficult. The introduction of modern in vivo imaging techniques including cranial ultrasound, computed tomography (CT) and more recently magnetic resonance imaging (MRI) have provided the opportunity for direct, non-invasive, *in vivo* measurements of intracranial structure. MRI is now the established imaging technique of choice for accurate assessment of brain structure. Three-dimensional (volumetric) high-resolution structural MRI scans are the current standard requirement for modern brain morphometry. Another important requirement for modern brain morphometry is the use of spatial normalisation to bring brain images from different individuals and/or different modalities into a common anatomical reference space. The simplest methods apply rigid body registration (linear registration) of brain images. Linear registrations allow extrinsic differences between images to be matched. For example, rotations, translations, zooms and shears can be adequately catered for. The original Talairach linear registration transforms brain volumes to fit the so-called Talairach box (Talairach and Tournoux 1988). The drawback of linear registrations is that they cannot accommodate intrinsic shape differences and they are therefore used primarily for registering images from the same subject. For example, registration of serial images from a single subject can provide information about changes in global cerebral

volume over time (Freeborough *et al.* 1996). The simple linear transformations have generally been superseded by less constrained non-linear transformations that allow more accurate matching of brain structure. These non-linear registrations can be used within subject over time to provide information about local shape differences with time (e.g. Freeborough and Fox, 1998).

To make meaningful regional comparisons between brains from groups of subjects, confounding factors such as extrinsic differences (e.g. head position and orientation) and intrinsic differences (e.g. brain size and shape) need to be catered for. To achieve this, more complex models are required to register multiple images into a common anatomical framework enabling region by region comparisons in cross sectional or longitudinal studies followed by robust statistical analyses.

A wide variety of warping algorithms have been specifically developed for registering multiple volumetric brain MRIs, and there is a rapidly expanding literature on various non-linear registration methods. In general, they can be broadly classified as intensity-based or label-based. Intensity-based approaches employ mathematical and/or statistical criteria to match some voxel-similarity measure in MR images, where both are considered as continuous unlabelled processes. The matching criterion is usually based upon minimising the sum of squared differences or maximising the correlation between images. Examples include elastic methods (Shen and Davatzikos 2003; Davatzikos 1997a), fluid methods (Fox *et al.* 1996a; Freeborough and Fox 1998) spline-based methods (Bookstein 1997; Johnson and Christensen 2002; Lamm *et al.* 2001) and Bayesian (probabilistic) frameworks, e.g. statistic parametric mapping (SPM)(Friston *et al.* 1995). Label-based approaches identify homologous features (labels) in the source and reference images and then find the transformations that provide a best match. Label-based approaches are classified according to the anatomical features that drive them. The homologous features include points (Bookstein 1997; Davis *et al.* 1997; Neelin *et al.* 1993) (e.g. anterior and posterior commissure), curves (Subsol *et al.* 1997; Ge *et al.* 1994) (e.g. sulci) or surfaces (Thompson *et al.* 1996b; Thonpson *et al.* 1998) (e.g. three dimensional cortical surface maps). Point landmarks usually need to be identified manually and there are relatively few readily identifiable points within the brain. Curves and surfaces are preferable because they are more readily identifiable and in many instances can be extracted automatically (or at least semi-automatically). Cortical sulci and grey/white matter surfaces can then be accurately matched using elastic or fluid warping algorithms (e.g.

Davatzikos and Resnick 1998; Davatzikos *et al.* 2001b; Thompson *et al.* 1996a; Thompson *et al.* 1996c).

In theory, non-linear warps that precisely match the complex gyral patterns of one brain to another need to embody a potentially enormous number of parameters, in other words, they need to be very high dimensional. In practice, much of the spatial variability between individual brains can be captured with just a small number of parameters (Ashburner and Friston 1999). If the aim is to match global brain size and shape, whilst preserving regional differences, then warps consisting of a linear combination of smooth basis functions are adequate. The rationale for adopting a low-dimensional approach is that it allows rapid and easy modelling of global brain features without matching individual gyri and sulci precisely. If the aim is to accurately characterise sulcal and gyral differences then high dimensional approaches are more suitable.

Once brains have been mapped into the same anatomical framework, structural differences can be characterised. Morphometry methods can be broadly classified into region of interest (ROI)-based or whole brain techniques. In simple terms, ROI methods require expert anatomists to label homologous structures based upon prior hypotheses and inferences are restricted to a particular structure. Whole brain approaches interrogate each and every portion of the brain and do not require prior hypotheses. To date, a variety of ROI-based volumetric methods have evolved from simple two-dimensional (2D) or three-dimensional (3D) measurements of specified brain structures on relatively thick slice 2D CT or MRI scans, to more sophisticated volumetric measurements of chosen regions on high resolution 3D MRI scans that have been co registered and segmented into tissue compartments (Caviness *et al.* 1996; Chan *et al.* 2001; Cook 1994; DeLeo *et al.* 1985; Filipek *et al.* 1994; Jack, Jr. *et al.* 1988; Jack, Jr. *et al.* 1989; Jack, Jr. 1991; Jackson *et al.* 1990; Jernigan *et al.* 1990; Lee *et al.* 1998; Murphy *et al.* 1996; Schulz *et al.* 2002; Schwartz *et al.* 1985). 3D-fractal analysis of the grey/white interface (Free *et al.* 1996) has offered additional information about the surface complexity of the cerebral cortex. These techniques have all been interactive and operator dependent to a greater or lesser extent and subject to bias. The bias is introduced by the small number of regions and metrics used in classical morphometrics that are insensitive to changes elsewhere in the brain. In addition, ROI measurement errors are likely to be greater for smaller structures with complex architectures, particularly if anatomical borders are defined by arbitrary

criteria, for example the entorhinal cortex. Furthermore, a number of morphometric features (e.g. thinning of the cortical ribbon) may be difficult to quantify by inspection and thus could be missed by ROI-based techniques. Despite these limitations, ROI-based methods have been regarded as the best available "gold standard" and are still widely used in research studies and clinical practice. A number of unbiased whole brain techniques are emerging due to the development of sophisticated image processing tools. These whole brain approaches, of which there are many hybrids offer a number of advantages not least because they are semi or fully automated, and thus reproducible and applicable to large groups for cross sectional and longitudinal studies.

There is a wide range of whole brain approaches and in simple terms they can be generally categorised according to the types of spatial normalisation used. For example, information about global brain volume difference can be provided with analysis of serial linear registrations (Fox et al., 1996). Information about regional grey (or white) matter volume or concentration differences can be provided by voxel-wise assessment of spatially normalised (linear and non-linear) segmented images. Low dimensional spatial warps that remove global brain confounds whilst allowing regional differences to be assessed statistically at a voxel-wise level underpin the philosophy of voxel-based morphometry (VBM)(Ashburner and Friston 2000). A similar approach using higher dimensional warps and interactive sulcal matching is embodied in the Regional Analysis of Volumes Examined in Normalized Space (RAVENS) approach (Goldszal *et al.* 1998; Davatzikos *et al.* 2001a). Information about global brain shape differences can be provided by analysis of low-dimensional spatial warps e.g. deformation-based morphometry (DBM)(Ashburner and Friston 2000; Good *et al.* 2001a). At the other end of the spectrum, warps that allow precise matching of sulci and gyri need to be very unconstrained or high dimensional. This approach is necessarily time and computer intensive. The differences between brains will then be embodied in the warps themselves, which can be assessed statistically. This philosophy underpins methods such as tensor-based morphometry (TBM)(Ashburner and Friston 2000; Ashburner and Friston 2001; Good *et al.* 2001a) and precise cortical mapping techniques allowing the generation of probabilistic brain cortical atlases (Thompson *et al.* 1996c; Thompson *et al.* 1998).

Computational neuroanatomy: VBM, DBM, TBM

Computational neuroanatomy is the application of mathematical and statistical techniques to the characterisation of structural information in high-resolution MRI scans. It is emerging as an exciting new automated methodology to characterise shape and neuroanatomical configuration of structural MRI brain scans on a macroscopic and mesoscopic scale. The term was originally coined to describe the application of statistic parametric mapping (SPM) to structure rather than function, and for the purpose of this thesis I will adopt this definition, acknowlegeing that other analytical packages could potentially be used instead of SPM. Voxel-wise analysis of functional imaging data with SPM is well established in the neuroimaging community. This technique is also ideally suited to the interrogation of structural data: instead of determining whether voxels are significantly activated or not, SPM can also determine whether voxels of grey matter (or white matter or CSF) are significantly increased or decreased. An additional advantage is that the same general analytical framework encompasses both structural and functional data, facilitating comparisons between them. Computational neuroanatomy comprises a triad of techniques: Voxel-based morphometry (VBM) interrogates high-resolution structural MRI brain scans that have been warped into a common anatomical framework providing voxel-wise information about grey (or white) matter volume and density. Deformation-based morphometry (DBM) interrogates the low-dimensional warps created during spatial normalisation to inform about global differences in brain shape. Tensor-based morphometry (TBM) interrogates high-dimensional warps in order to characterise local shape differences. The basic methodologies of these techniques have already been described in some detail (Ashburner *et al.* 1998; Ashburner and Friston 2000; Ashburner and Friston 2001) and VBM and to a lesser extent DBM have been employed in preliminary neuroimaging studies (May *et al.* 1999a; Mummery *et al.* 2000; Woermann *et al.* 1999b; Wright *et al.* 1995a), however their practical implementation and clinical usefulness remain to be established. In this thesis I examine the implementation and clinical usefulness of VBM for neurologists and neuroradiologists.

Clinical neuroimaging: current status

The main purposes of imaging in clinical neurology are firstly to identify (or

exclude) global or regional structural abnormalities in a given subject relative to normal subjects. Secondly to monitor an abnormality in a given patient over time to assess the evolution of a disease or its response to therapy and thirdly to characterise the brain structural phenotypes of various diseases across groups of patients at single time points and over time. Neuroradiological appraisal of images should be quick and practical and ideally objective. Currently, clinical neuroradiological appraisal is subjective and qualitative, relying upon the experience and expertise of an individual neuroradiologist. Given that the spectrum of normal anatomy is wide and complex, it is not uncommon for subtle pathology to be misdiagnosed as normal, or indeed for normal structural variability to be misinterpreted as pathology. Furthermore, inter-rater and intra-rater variability needs to be acknowledged. There are different problems when a radiologist assesses serial scans in order to determine disease evolution or treatment effects. The scans are often technically different, particularly with respect to slice position and angulation, contrast and magnification making assessment of subtle lesional differences unreliable. Clearly, characterising disease brain structural phenotypes across groups of different subjects needs to cater for interindividual differences. For these reasons, objective morphometric methods are used increasingly in the research domain, and it is surprising that they are not used more as an ancillary clinical tool by neuroradiologists. The main reason is probably because many morphometric methods are complex (in computational terms), time intensive and operator dependent. If a relatively simple and quick automated method could be shown to produce clinically plausible, reliable results it might well be adopted by clinicians. There are a number of areas where automated registration and voxel-wise assessment of images could be clinically useful. For example, diagnosing a specific disease in an individual could be aided by supplementing the standard post processing that occurs following image acquisition with automated registration to a population and disease specific template. Voxel-wise statistical analysis using VBM could then demonstrate whether the scan deviated significantly from a normal age and sex matched population.

Assessing structural change over time

Neuroimaging at a single time point provides a static representation of brain structure, but this is generally inadequate for assessing dynamic processes such as

ageing and degenerative disease. There are two main options to model structural changes over time. The first option, as in most imaging studies, is a cross sectional study design, i.e. studying a group of subjects of different ages at one time point. Cross sectional studies are practical to implement and can accommodate wide age spectrums and large study groups, but have inherent drawbacks. Firstly, dynamic effects are not actually measured, but are inferred from measured differences between age cohorts. Secondly, systematic differences between age cohorts such as differences in body size (and corresponding brain size) can potentially reflect spuriously as age-related effects, unless accounted for. For example, body size has increased over the past century; so younger cohorts will have spuriously larger brains for age than elderly cohorts. Thirdly, subtle changes over time may be masked by the large inter-individual variability in normal cortical anatomy. In order to properly model dynamic change, a longitudinal study is required where a group of individuals is followed over time. For practical reasons such studies are generally limited to very short time windows and small study groups. Evaluating serial images of the same patient over time allows the detection of subtle pathology and automated registration of serial MRI has already proved to be a useful tool in dementia research and clinical practice (Fox *et al.* 1999; Fox *et al.* 2000)

Neuroimaging in disease

In disease, structural imaging can characterise the macroscopic neuroanatomical sequelae of underlying pathological processes in some detail. Neuroimaging is now a useful tool in the diagnostic work up of neurological disease and has an established role as a surrogate marker for disease progression in clinical trials for chronic progressive diseases such as multiple sclerosis and Alzheimer's disease. In vivo assessment of microanatomy is not yet possible, but by employing a multimodal imaging approach, functional parameters such as regional cerebral perfusion and diffusion properties, neurochemical receptor distributions, regional glucose metabolism, local tissue biochemistry and the response of brain regions to specific tasks can be refined with accurate structural localisation to inform about the underlying pathophysiology.

Of particular interest is the extent to which the human brain is plastic and whether determinants of plasticity (on a structural or functional level) may provide

hope for future therapies. For example, it may be possible to better characterise structural and functional predictors of recovery in cerebral infarcts to allow early and effective therapeutic measures. Even now, early subtle structural perturbations in the brains of individuals genetically at risk for dementia can be identified with neuroimaging before the onset of symptoms. In theory, with major advancements in the human genome project and molecular mapping of diseases coupled with refined neuroimaging, at risk populations can be identified and offered new disease modifying treatments before substantial pathology occurs.

In this thesis, I have used VBM to characterise the pathological perturbations in brain structure in a number of relatively common neurological (and psychiatric) diseases. Firstly, I have chosen diseases that have previously been examined with neuroimaging and histopathology in order to establish the face and construct validity of VBM. Secondly, I have tried to choose diseases that affect the brain in different locations, to further test the usefulness of VBM. These include diffuse cortical processes (Alzheimer's disease), regional cortical processes (Frontotemporal lobar degeneration of the semantic type), deep grey matter processes (mesial temporal sclerosis, Huntington's disease, Turner syndrome), putative brainstem processes (migraine, familial ataxic migraine) and cerebellar processes (familial ataxic migraine). I have also included diseases where the literature on structural imaging is highly variable and contradictory (schizophrenia) or diseases where structural change has hitherto been occult (primary autonomic failure).

A particular new area of interest is the extent to which genetic make up (genotype) predicates external manifestations of structure or function (phenotype). Many diseases are very heterogeneous by nature (owing to a number of genetic, environmental and idiopathic causes). As a result, the clinical and structural brain phenotypes are highly variable and unpredictable. If more homogenous groups of patients can be selected, the chance of characterising a consistent brain phenotype can be improved. With major advances in molecular mapping and genotyping it is now possible to select patient groups (pedigrees) with a specific genotype. These groups are then ideal candidates for brain phenotype characterisation. By using a sensitive unbiased whole brain technique such as VBM with the versatility provided by the statistical framework of the general linear model, it is now possible to map structural brain phenotypes to their genotypes and to employ a gene deletion mapping strategy to identify specific genetic loci that influence the structure of specific brain regions. This

is particularly important since it provides insight into the normal development and pathological alteration of specific brain regions (e.g. the amygdala, see Chapter 10). Furthermore, by characterising brain structural phenotypes in genotype positive pre-symptomatic patients VBM can be used as a surrogate marker for disease progression in clinical trials of disease modifying agents (e.g. dementia, Huntington's disease)

Summary

The importance of brain structure is indisputable. It forms the basis on which functional parameters can be mapped and referenced. What is less sure is the optimal method for characterising brain structure in health and disease. Certainly the classical region of interest approaches that have hitherto formed the mainstay of neuroimaging are flawed and do not inform about brain structure in a holistic, reproducible way. Modern whole brain morphometric techniques allow brain structure to be mapped into a standardised anatomical framework giving information about entire brain structure on a voxel-wise basis. These methods are in a constant process of evolution, and while automated methods may never quite match the most expert neuroanatomist for the appraisal of a single complex structure, they do offer an unbiased reproducible appraisal of brain structure which has distinct advantages over region of interest methods performed by a wide spectrum of variously skilled and less skilled operators leading to a vast but inconsistent literature. The purpose of this thesis is to evaluate the usefulness of voxel-based morphometry in health and disease, and to highlight the advantages and potential pitfalls of the methodology in its current state of evolution.

CHAPTER 2

METHODS

Introduction

The experiments reported in this thesis are predicated on two main methodologies. Firstly, magnetic resonance imaging of the brain and secondly computational processing and statistical analysis of high resolution volumetric brain magnetic resonance images. This chapter will address each of these methodologies, focusing especially on refinements enabling optimised appraisal of human brain structure. The concept of computational neuroanatomy will be introduced and the methodology of voxel-based morphometry will be detailed.

Structural Magnetic resonance imaging (MRI)

Basic principals of MRI

The basic principles of nuclear magnetic resonance were discovered by Bloch and Purcell in 1945 (NMR)(Bloch *et al.* 2003; Purcell *et al.* 1945) earning them the Nobel prize in 1952, but it took more than three decades before magnetic resonance (MR) images of the of the human brain were possible (Holland *et al.* 1980a; Holland *et al.* 1980b). Since that time there have been substantial advances in MR brain imaging, particularly in the last decade, not only to characterise brain structure with great precision in three dimensions, but also to provide information about an array of brain functional parameters such as blood flow (MR angiography (MRA) and venography (MRV)), cerebral perfusion (MR perfusion), biochemical properties of brain tissue (MR spectroscopy) and brain activation (functional MRI). In parallel with MR sequence refinements there have been major advances in computer power and speed accompanied by rapid expansion of a large body of skilled manpower. It is this combination of MR scientific development coupled with computational expertise that

has been the driving force behind the recent acceleration of brain imaging advancement. Another key factor in brain imaging development has been the multidisciplinary approach where ideas from physicists, computer scientists, psychologists, psychiatrists, neurologists and neuroradiologists are pooled to allow greater insights into the human brain.

Source of the MR signal

MRI depends on the gyromagnetic properties of certain nuclei. Nuclei with an odd number of protons and/or neutrons possess magnetic moment and behave like small magnets inducing local magnetic fields along their spin axis. In living organisms the most abundant source of protons is hydrogen within water molecules, and structural neuroimaging with MRI is based on the nuclear magnetism of these hydrogen protons. Other naturally occurring magnetic nuclei of biological interest include ^{31}phosphorus, ^{23}sodium and ^{13}carbon. In the presence of an external magnetic field, the precessing protons will align themselves to the magnetic field, like a compass aligning to the earth's magnetic field. The MRI scanner used in these experiments produces a 2 Tesla magnetic field which is 40 000 times stronger than the earth's magnetic field. Usually the alignment of hydrogen protons is not perfect and the axis of alignment will itself spin or precess around the direction of the external magnetic field, akin to a spinning top precessing around the earth's gravitational field. The precessional frequency (Larmor frequency), ω_0, is proportional to the strength of the magnetic field, B_0, and a gyromagnetic constant specific to each type of nucleus, γ:

$$\omega_0 = \gamma B_0$$

For a 2- Tesla magnetic field strength the Larmor frequency (ω_0) of hydrogen protons is approximately 85 MHz.

Net magnetisation

The spinning hydrogen protons may exist in two states depending on the orientation of magnetic moment with respect to the applied field; a low- (ground) energy state (spin axis parallel to the magnetic field) or a high-energy state (spin axis anti-parallel). The quantum of energy required for protons to move between these two energy states depends on the field strength. For a 2 Tesla field strength, the thermal energy at room temperature is enough to flip the spins of hydrogen protons. At

equilibrium, a greater proportion exist in the lower energy state according to the Boltzmann relation:

Parallel/anti-parallel=exp ($\gamma hB_0/KT$)

where h is Planck's constant, K is Boltzmann's constant and T the absolute temperature. The sum of all spins will give a net magnetisation that comprises a component along the applied magnetic field (longitudinal magnetisation) and a component transverse to the applied field (transverse magnetisation). By convention, the net magnetisation is based on a co-ordinate system with the applied magnetic field along the *z*-axis and the transverse magnetisation along the *xy* plane. The net magnetisation in the resting phase is termed the equilibrium net magnetisation where more spins are in the low energy state than the high-energy state. By applying an oscillating radio-frequency pulse (B1) perpendicular to the longitudinal magnetisation, spins can be excited from the low to the high-energy state and in doing so alter the net magnetisation. The most efficient energy transfer occurs when the applied frequency matches the Larmor frequency, ω_0. The net magnetisation will precess around B_1 with a different Larmor frequency, ω_1. Varying the strength and duration of the radiofrequency pulse that is usually applied in millisecond bursts modulates the angular deviation of the net magnetisation in the *xy* plane. It is this transverse component that produces a detectable NMR signal.

T1 and T2 relaxation

After excitation, the net magnetisation gradually returns to precess around the original magnetic field, B_0. As the protons return to equilibrium, with a greater proportion in the lower energy state, energy is released to neighbouring molecules (spin-lattice relaxation) or neighbouring spinning nuclei (spin-spin relaxation).

Spin-lattice or T1 relaxation is governed by the 'T1' time constant. The longitudinal magnetisation, M_L, recovers towards the equilibrium state, M_0, over time t, as:

$$\mathbf{M_L = M_0(1-e^{-[t/T1]})}$$

The transfer of energy to surrounding molecules determines the T1 constant and depends on the nature of the environment. Small mobile free water molecules resonate too rapidly for efficient energy transfer, while large protein molecules resonate too

slowly. Mid-sized fat molecules however resonate at frequencies close to the Larmor frequency and absorb the energy most efficiently. If a series of radiofrequency pulses is applied after a short time interval, relaxation will be incomplete for protons in water, but nearer completion for protons in fat. The repetition time, TR, can be adjusted to highlight differences in T1-dependent relaxation properties of various tissues. T1 differences between tissues can be highlighted with inversion recovery sequences. Here the net magnetisation is inverted by a 180° radiofrequency pulse followed by a second pulse after a short delay (known as inversion time, TI). The combination of TI and TR can be modulated to maximise the sensitivity of proton T1 relaxation to the differential molecular composition of various brain tissues, such as grey and white matter and cerebrospinal fluid. Thus T1-weighted imaging optimises the contrast between brain tissues (in particular grey and white matter) allowing the accurate appraisal of brain structure. Tissues with a short T1 such as fat and to a lesser extent white matter give a high signal and appear bright on MR images whereas tissues with a long T1 such as CSF and to a lesser extent grey matter appear dark.

The transfer of energy to neighbouring nuclei (spin-spin relaxation) results in an exponential decay of the transverse net magnetisation, M_T, determined by the T2 time constant, where:

$$M_T = M_0.e^{-[t/T2]}$$

As energy is passed from one spin to another, the phase of precession of neighbouring nuclei becomes desynchronised. If the local magnetic field is not homogeneous (given the complex nature of human tissue), then the Larmor frequencies of protons in a region will vary and they will lose coherence rapidly, which reduces the net transverse magnetisation, M_T. The effective T2 time constant, denoted T2*, is shorter than T2 proper for any given tissue type. Spin-echo (SE) pulse sequences utilise a 90° pulse followed after time τ by a 180° pulse and a further time τ. The echo time (TE) = 2τ. These sequences produce images with contrast predominantly dependent on differences in T2. On T2-weighted SE sequences tissues with long T2 such as water appear bright. These sequences are also sensitive to many acute and sub acute pathological processes but provide relatively poor contrast between grey and white matter.

Whole brain imaging

For structural brain imaging, it is necessary to measure and localize the MR signal from every part of the brain. This is achieved by a combination of three processes.

Firstly, **slice selection**. Regions of the brain are excited slice by slice and the position and width of these slices can be modulated. If a gradient is introduced along B_0, then each slice of the brain will have a distinct Larmor frequency. If the excitatory radiofrequency (RF) pulse has a narrow spectrum of frequencies, only a correspondingly narrow slice of brain will be excited. For the structural imaging studies here, slices were contiguous and 1mm or 1.5mm in thickness.

Secondly, **frequency encoding**. A weak magnetic gradient is applied transversely across Bo, thus perpendicular to the slice select gradient, so that spins are frequency encoded according to their spatial position in the x direction. By sampling the magnetic resonance signal at different frequencies, signal from different sides of the brain may be distinguished.

Thirdly, **phase encoding**. The MR signal contains phase information as well as frequency information. When the transverse gradient is applied, it may be varied in one direction and fixed in the other. A transient change in the transverse gradient along one axis will introduce phase differences in the spin along that axis. Individual phase encoding steps must be performed for each frequency encoded column

These three processes produce a grid of varying phase and frequency of radiofrequency signal following excitation. Fast Fourier Transform of this spectrum is used to reconstruct the signal for each part of the grid. A small volume of tissue with its unique phase and Larmor frequency after slice-specific excitation is known as a voxel. The signal intensity for all voxels is written in a standard radiographic format (ANALYZE) for subsequent viewing and analysis.

High resolution imaging

There are three main requirements for good structural brain imaging. First there should be high spatial resolution (1mm isotropic voxel size is preferred) to allow discrimination of small anatomic structures. Second, there should be high contrast between grey and white matter and cerebrospinal fluid to improve conspicuity of small structures and to facilitate segmentation of images. Third the scan time should be short (10-12 minutes) to facilitate quick and practical imaging in elderly or debilitated

subjects and allow extra time for further structural or functional sequences.

Since computational neuroanatomy involves a number of fully automated pre-processing steps to partition the brain into grey and white matter in stereotaxic space, the quality of the structural MRI is of major importance. Accordingly, the standard volumetric structural sequence (magnetization-prepared rapid gradient-echo imaging (MP-RAGE)) for our 2Tesla Siemens system was optimised to provide improved spatial resolution and T1 contrast facilitating excellent grey/white matter segmentation. The standard MP-RAGE sequence (Mugler, III and Brookeman 1990) comprises an inversion pulse, a delay (TI), followed by a single segment 3-D gradient echo (GRE), a further delay (TD) and a repetition of this process for the next segment. Usually each segment includes all partition-encoding gradients so the number of echoes acquired per segment equals the number of partitions, while the strength of the 2D-phase encoding gradient is different for each segment. The drawback of this sequence is a loss of contrast during segment acquisition due to relaxation effects, particularly when many partitions are selected. The contrast in GRE images depends on the order of the phase encoding (PE) because the image intensity is predominantly determined by the amount of longitudinal magnetisation available when the central k-space lines are acquired (Holsinger and Riederer 1990). When linear phase encoding is used, half of the segment acquisition time has already passed when the k-space lines are acquired, so notable relaxation has already occurred. Image contrast tends to be poor, particularly for a high number of phase encoding steps (Holsinger and Riederer 1990). It is possible to substantially increase contrast by ordering PE differently, such as centric PE, where the central k-space lines are acquired first. There is a drawback to this strategy; the relaxation during segment acquisition alters the magnetisation causing distortion of the point spread function (PSF) and blurring in one direction. A further drawback of centric PE is its vulnerability to RF inhomogeneity that occurs particularly at the periphery of the RF head coil. The optimised MR sequence for structural imaging developed in our laboratory (Deichmann *et al.* 2000a) (Deichmann *et al.* 2002b) uses centric PE to provide high tissue contrast and 100% improvement in contrast-to-noise. The deleterious effects on PSF are corrected by means of an appropriate k-space filter and RF coil inhomogeneities are corrected by the use of shaped excitation pulses. The new sequence provides high contrast-to-noise images of the whole brain with 1mm isotropic voxels and an acquisition time of 12 minutes. Importantly the new sequence allows markedly improved automatic segmentation of

images into grey and white matter.

MR image quality

The MR signal may be affected by many physical and physiological parameters. Artefacts arise from two main sources: the MR scanner (hardware and software) or the subject being scanned. Strict quality control of the MR scanner and local environment is essential to maintain a stable and homogeneous Bo magnetic field. Instability and/or inhomogeneity of the Bo magnetic field will result in variations in local Larmor frequencies, and misattribution of measured signal for a given coordinate. This may produce distortions of the reconstructed brain image. The homogeneity of the RF head coil falls off towards the edges. This causes B_1 inhomogeneities and signal loss in peripheral parts of the image unless specific compensation pulses are applied (as in the high resolution sequence used for our studies (Deichmann *et al.* 2000a; Deichmann *et al.* 2002b). For all of my experiments careful attention was paid to ensure that subjects' heads were positioned centrally within the head coil.

Gross head movement during scanning causes major problems for MRI and usually produces a markedly distorted image due to misattribution of signal for a coordinate that has moved. Some physiological movements such as blood vessel pulsations, or minor head movement during breathing and swallowing cannot be prevented, but these do not usually produce notable distortions. Before scanning each subject, I explained the importance of avoiding head motion and I made sure that they were relaxed and comfortable before starting the sequence. I also used foam pads to fix subjects heads centrally within the head coil. Most subjects tolerate a 12 minute structural scan well, but ill patients, especially those with dementia or movement disorders, and claustrophobic subjects have problems lying still for the duration of a scan. Usually after careful explanation and reassurance the scan can be repeated successfully.

SPM basic principles:

The statistic parametric mapping (SPM) framework and associated theory was originally developed for the routine statistical analysis of functional neuroimaging data (Friston *et al.* 1995). This software was made available to the emerging functional

imaging community in 1991, to promote collaboration and a common analysis scheme across brain imaging laboratories. This versatile framework incorporates the general linear model and the theory of Gaussian fields to analyse functional neuroimaging data. The value of each voxel in a functional statistical parametric map is a statistic that expresses evidence against the null hypothesis of no experimentally induced change at that voxel. There are 3 main steps in the formation of such maps (Friston 1997).

Spatial transformations

Images are initially realigned to remove movement-related variance, followed by spatial normalisation of images into standard stereotaxic space, using a combination of affine and non-linear transformations (Ashburner *et al.* 1997; Ashburner and Friston 1999; Ashburner *et al.* 2000). A smoothing step compensates for interindividual gyral variations.

Construction of an SPM

The experimental design and the model used to test for specific neurophysiological effects or neuroanatomical changes are embodied in a mathematical structure termed the design matrix. The design matrix partitions the scan data into effects of interest, confounds of no interest and an error term. This partitioning is based on the general linear model which in essence relates what one observes to what one expected to see, by expressing the observations as a linear combination of expected components and some residual error. The estimated contributions are known as parameter estimates. Regionally specific effects in the brain are framed in terms of differences amongst these parameter estimates and are specified using linear contrasts. The significance of each contrast is assessed with a statistic whose distribution has Student's t distribution under the null hypothesis. For each contrast a t statistic is computed for each voxel to form a SPM{t}.

Statistical inferences

Classical inference about parameters, or contrasts of the model parameters is made using conventional parametric statistics to provide P values pertaining to the maxima, spatial extent of voxel-clusters or number of clusters. These P values are used to reject the null hypothesis. The P values have to be adjusted to protect against

family-wise false-positives over the search volume (correction for multiple non-independent multiple comparisons) using distributional approximations from the theory of Gaussian fields (Friston *et al.* 1996; Friston 1997; Worsley *et al.* 1996). This is similar to the role of a Bonferroni correction for independent data.

Application of SPM to structure

With advancements in segmentation techniques from simple binary methods to more sophisticated segmentation methods encoding the probability of each voxel belonging to a particular tissue group, voxel-wise statistical analyses of brain structure are now possible. The SPM framework can be extended to the analysis of brain structure by considering local increases or decreases in the amount of grey (or white matter or CSF) instead of the presence or absence of functional activations. This framework forms the basis of computational neuroanatomy which comprises three interrelated techniques introduced in the first chapter, each of which informs about different aspects of brain structure: voxel-based morphometry (VBM), deformation-based morphometry (DBM) and tensor-based morphometry (TBM).

Voxel-based morphometry (VBM)

VBM was first introduced in 1995 (Wright *et al.* 1995a) as a technique to characterise regional cerebral grey and white matter density correlates of syndrome scores (distinct psychotic symptoms) in a group of 15 schizophrenic patients. At its simplest VBM involves the voxel-wise comparison of regional concentrations of grey (or white) matter between groups of subjects. The software is freely available (www.fil.ion.ucl.ac.uk/spm) and the procedure is fully automated and relatively straightforward. High-resolution 3D structural MR images are spatially normalised into the same stereotaxic space, segmented into grey and white matter and CSF compartments and smoothed with an isotropic Gaussian kernel. Voxel-wise parametric statistical tests are then performed on the smoothed grey matter segments employing the framework of the General Linear model.

Evolution in the pre-processing of structural data for VBM

In this section I will describe the evolution of the VBM methodology from its inception in 1995 to the current method. There are two major factors: Firstly SPM has

evolved since SPM94 which was the first major revision of the SPM software and the basis of the Wright et al., experiment (Wright *et al.* 1995a). SPM94 was written primarily by 1995 and has undergone further revisions: SPM 96, SPM99 and most recently SPM2 (2002). Secondly the VBM methodology has been refined and augmented (optimised technique). I will describe first the standard method of VBM. I then highlight the need for an optimised method and finally detail the various steps of the optimised method for grey and white matter.

Before pre-processing, all the structural images are checked for incidental pathology (lipoma of the corpus callosum) or anatomical variants (for example mega cisterna magna), technical quality and artefacts and the centre point is placed on the anterior commissure. Originally the technique used SPM95 pre-processing steps that involved segmentation, smoothing and spatial normalisation (affine only) to a symmetrical template in stereotaxic Talairach space. Following specific refinements to the segmentation and spatial normalisation pre-processing steps within SPM (Ashburner and Friston 1997), VBM was released as part of the freely available SPM 96 package (Wellcome Department of Imaging Neuroscience, ION, UCL, London). The sequence of the pre-processing steps was altered so that spatial normalisation preceded segmentation, the reason being that the segmentation of spatially normalised images is preferable since the procedure partitions the normalised images into grey and white matter (and CSF) segments based upon a priori knowledge from prior probability images which are themselves in stereotaxic space.

Standard VBM protocol

In simple terms, pre-processing for the simple VBM protocol involves:

1. Spatial normalisation of subject whole brain volumetric MR brain images to a whole brain template in stereotaxic space (e.g. the SPM T1 template)
2. Segmentation of normalised whole brain images into grey matter, white matter and CSF compartments
3. Smoothing with an isotropic Gaussian kernel

A design matrix is then created within the framework of the general linear model and statistical maps of grey matter (or white matter) concentration differences are generated (see Fig. 2.1).

Template

The standard SPM whole brain template is the ICBM 152 template (Montreal Neurological Institute) that is derived from 152 young normal subjects (mean age 24 (4.9), 59% male) and approximates the Talairach space.

Spatial normalisation

Structural MRI scans (in native space) are transformed to the same stereotaxic space by registering each of the images to the same template image, using the residual sum of squared differences as the matching criterion. Spatial normalisation consists of a combination of linear and relatively low dimensional non-linear transformations. The first step in spatial normalisation involves estimating the optimum twelve-parameter affine transformation to match images (Ashburner and Friston 1997). A Bayesian framework is used, whereby the maximum *a posteriori* (MAP) estimate of the spatial transformation is made using prior knowledge of the normal variability in brain size.

The second step accounts for global non-linear shape differences, which are modelled by a linear combination of smooth spatial basis functions (three dimensional discrete cosine transform basis functions) (Ashburner and Friston 1997; Ashburner and Friston 1999). The matching involves simultaneously minimising the membrane energies of the deformation fields and the residual squared differences between the image and template. The goal of these non-linear warps is to discount global brain shape differences (i.e., displacement of grey matter from its normal location), but not to match each gyrus and sulcus exactly. VBM thus allows the characterisation of regional differences at a local scale having discounted global shape differences. If the spatial normalisation were perfect (infinitely high dimensional warps), the normalised images would be identical and all the differences would be encoded in the deformation fields. TBM could then be used to characterise the deformation field differences with high precision. This idea is appealing; particularly for characterising subtle gyral and

sulcal differences, but at present the high dimensional warps are too computer intensive and time consuming, and thus impractical for large study groups.

A masking procedure is used to weight the normalisation to brain rather than non-brain tissue. The spatially normalised images are resliced with a final voxel size of approximately 1.5 x 1.5 x 1.5mm^3 (1 x 1 x 1 mm^3 if high-resolution 1mm isotropic voxel structural scans are used (Deichmann *et al.* 2000).

Segmentation

Scans are segmented into grey matter, white matter, CSF and other non-brain partitions. SPM segmentation employs a mixture model cluster analysis to identify voxel intensities matching particular tissue types (grey matter, white matter and CSF) combined with an *a priori* knowledge of the spatial distribution of these tissues in normal subjects, derived from prior probability maps.

Smoothing

The normalised, segmented images are smoothed with an isotropic Gaussian kernel. After smoothing, the intensity in each voxel is a locally weighted average from a region of surrounding voxels, the size of the region being defined by the size of the smoothing kernel (Ashburner and Friston 2000). Smoothing helps to compensate for the inexact nature of the relatively low dimensional non-linear spatial normalisation. Smoothing also conditions the data to conform more closely to the Gaussian field model underlying the statistical procedures used for making inferences about regionally specific effects. Prior to smoothing, the segmented images tend to have a highly non-normal density function with voxels having values close to the extremes of 0 and 1. This is because the voxel values correspond to a probability of a voxel being grey or white matter. The distribution of errors about any group mean also tends towards a similar non normal distribution. However it is generally assumed that errors are rendered normally distributed by spatial smoothing (according to the Central Limit Theorem). The size of the smoothing kernel should be a function of registration accuracy balanced with localisation accuracy and normality of the data. In practice smoothing kernels of 10-12mm are the best balance between compensating for registration inaccuracies, rendering the data more normally distributed and optimising the spatial resolution of the inferences. For most study designs, and in particular group comparisons, inferences are quite robust to violations of normality and remain valid

even with no smoothing (Salmond *et al.* 2002). I would however caution against the exclusion of smoothing, because the low dimensional non-linear warps do not provide precise gyral mapping. High-resolution differences in anatomy would generally be finessed with high dimensional warps and tensor based morphometry. Unbalanced designs, for example comparing a single subject to a normative group, are susceptible to violations of normality, and smoothing kernels in the order of 12mm are essential to avoid false positive results. (See Fig. 2.1).

Statistical analysis

The smoothed data are analysed using MATLAB 5 (MathWorks, Natick, Mass., USA) and SPM99 (Wellcome Dept. of Cognitive Neurology, ION, London) employing the framework of the General Linear Model. Global and regionally specific differences in grey (or white) matter or CSF between groups can be assessed statistically using 2 contrasts, namely testing for increases or decreases in grey (or white) matter or CSF (two tailed test). Normalisation for global differences in voxel intensity across scans is made by inclusion of the global mean grey matter (or white matter or CSF) voxel value as a confounding covariate in an analysis of covariance (ANCOVA) whilst preserving regional differences in grey (or white or CSF) matter. This provides information about regionally specific changes in a tissue over and above global tissue changes. Corrections for the size of the search volume (multiple comparison correction) are made using techniques based on Gaussian field theory to permit valid inference (Friston *et al.* 1996; Worsley *et al.* 1996)

Figure 2.1: Schema of the standard VBM protocol

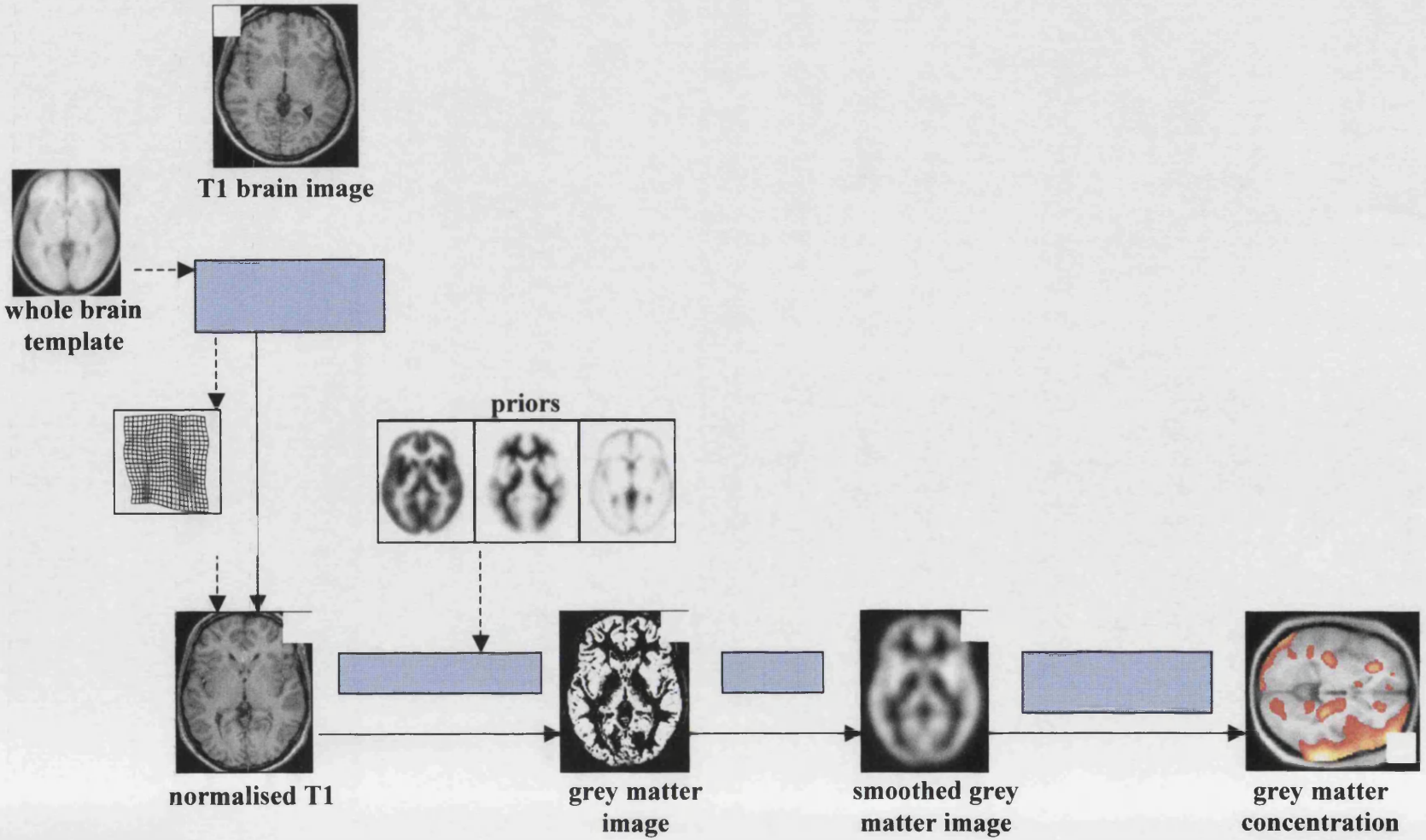

Motivation for Optimisation

Inspection of segmented images from the simple pre-processing procedure described above often shows several small areas of mis-segmented non-grey matter voxels. For example, on segmented grey matter images, voxels from the dural venous sinuses, scalp fat, petrous apices and diploic space are often mis-classified as grey matter (Fig. 2. 2). This has implications if there are systematic differences in skull size and shape or scalp thickness among study groups, especially if the groups are large, as in this study. For example, in a standard VBM analysis of sex effects on grey matter (see chapter 4), large clusters of significant voxels that are not ascribable to grey matter change can be seen along the course of the venous sinuses and outside the brain margins. This error is removed by the introduction of additional pre-processing steps to exclude non-brain voxels prior to normalisation and subsequent segmentation. New features of the optimised method include (1) a fully automatic brain extraction technique, (2) study-specific grey/white matter templates and (3) a modulation step to incorporate volume changes induced during normalisation into the analysis. This modulation procedure allows me to assess both regionally specific changes in grey/white matter volume and concentration (i.e. density).

Optimised structural volumetric image with high spatial and contrast resolution:

The structural MRI sequence has been optimised to produce volumetric scans with a high spatial resolution providing 1mm isotropic voxels and enhanced grey/white matter contrast to allow optimal segmentation (Deichmann *et al.* 2000; Deichmann *et al.* 2002).

Creation of a separate grey and white matter and CSF customised templates

An ideal brain template should consist of the average of a large number of MRI scans that have been registered to within the accuracy of the spatial normalisation technique. The best-matched templates are created from the study group itself so that the template is customised to the local scanner and subject population. This is relevant when studying disease groups, since diseased brains may differ substantially from a template based upon young normal subjects (e.g. the default SPM template). Customised population specific templates allow the spatial normalisation for diseased brains to be balanced to control brains, thus avoiding a systematic group difference in

spatial normalisation. Separate grey and white matter templates are created from the study group thereby providing templates that are customised to the MR scanner and to the demographics of the study population. Practically, I spatially normalise (affine registration and non-linear warps) all the study MRI scans to the SPM whole brain template, segment into grey and white matter and CSF compartments and smooth with an 8mm isotropic Gaussian kernel. Averaging the smoothed segments produces the grey and white matter and CSF templates.

Segmentation and extraction of a brain image

This is a fully automated procedure to remove scalp tissue, skull and dural venous sinus voxels. This procedure initially involves segmentation of the original structural MR images (in native space) into grey and white matter images, followed by a series of fully automated morphological operations for removing unconnected non-brain voxels from the segmented images (erosion followed by conditional dilation). The resulting images are extracted grey and white matter partitions in native space.

Normalisation of grey and white matter images

The extracted grey and white matter segments are pre-processed separately. The grey matter images are spatially normalised (affine and non-linear) to the customised grey matter template and the extracted white matter segments are spatially normalised to the customised white matter template. This method prevents any contribution of non-brain voxels and affords optimal spatial normalisation of grey/white matter. The 12 parameter affine registration has been made more robust by the inclusion of regularisation (a mathematical procedure for increasing stability by preventing overfitting of the data). The penalty for unlikely warps is now based on the matrix log of the affine transformation matrix (after removing rotation and translation components) being multivariate and normal. The non-linear warps have also been further refined with improved computation of derivatives of objective functions and the inclusion of regularisation. The bending energy of the warps is used to regularise the procedure, rather than the membrane energy, resulting in more realistic looking distortions (Ashburner and Friston 1999). There is however a caveat: the initial segmentation (implicit in the brain extraction step) is performed on affine-normalised images (in native space), but the probability maps which are used as Bayesian priors for segmentation, are in stereotaxic space. Segmentation of fully-normalised images is

therefore preferable. In order to facilitate an optimal segmentation, the optimised normalisation parameters (this is performed separately for grey and white matter) are re-applied to the original, whole brain structural images (in native space). Effectively this protocol employs a recursive version of segmentation, extraction and normalisation operators (see Fig. 2.7).

Figure 2.2: Error in the standard VBM protocol

Glass brain images of a grey matter VBM comparison of healthy males and females using the simple VBM method. The black arrows point to clusters of significant differences along the course of the dural venous sinuses. These erroneous differences are removed by the optimised VBM method.

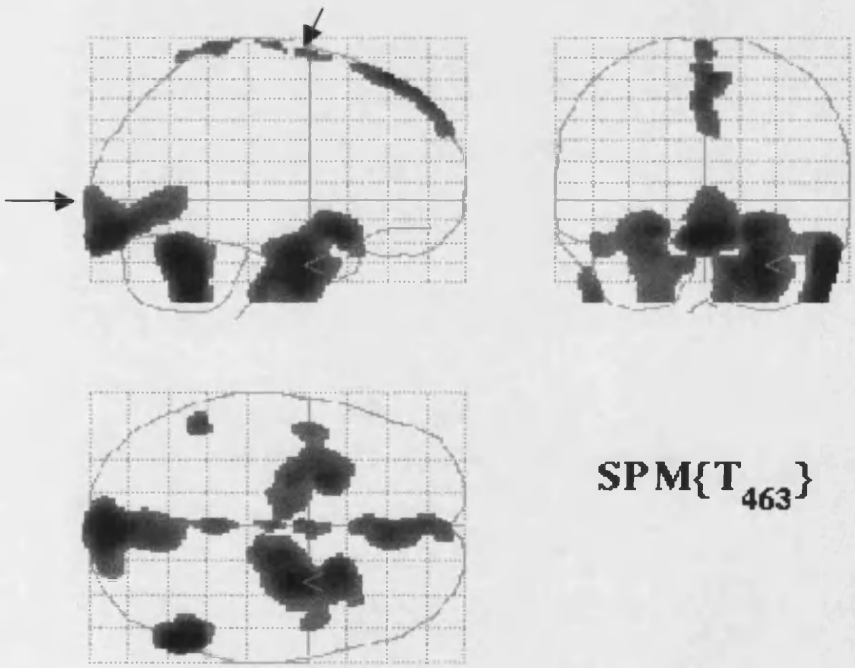

Optimised VBM protocol

Segmentation and extraction of normalised whole brain images

The optimally normalised whole brain structural images, which are now in stereotaxic space, are then segmented into grey and white matter, CSF and non-CSF partitions and subject to a second extraction of normalised segmented grey/white matter images. The segmentation step now includes an image intensity non-uniformity correction step which models intensity non-uniformity caused by different positions of cranial structures within the MRI head coil by a linear combination of smooth basis functions (Ashburner and Friston 2000). Figure 2.3 shows the improvements in segmentation from SPM 96 to SPM 99. The customised grey and white matter and CSF templates used for spatial normalisation can also be used as the prior probability maps for segmentation. Theoretically, prior probability maps from young normal subjects (the default SPM priors) are not optimal for diseased brains. In practice, visual inspection of segmented images shows little difference using customised disease specific priors and the default SPM priors in groups of patients with Alzheimer's disease and semantic dementia (see Chapter 5) (Good *et al.* 2002), however statistical parametric maps show a significant main effect of the choice of priors with improved registration of brainstem and cingulate voxels and higher T statistics using customised priors (see Chapter 5).

The brain extraction step is repeated at this stage because some non-brain voxels from scalp, skull or venous sinuses in the optimally normalised whole brain images could still remain outside the brain margins on segmented grey/white matter images (Fig. 2.4).

Figure 2.3: Evolution of the spatial normalisation and segmentation within SPM

The top row depicts the native structural image and normalised (ns) images using SPM 96, SPM 99 and SPM2 respectively. The bottom three rows depict differences in the normalised grey matter segments. Note particularly the improvement in the temporal lobe of normalised grey matter segments between SPM 96 and SPM 99 (red arrows)

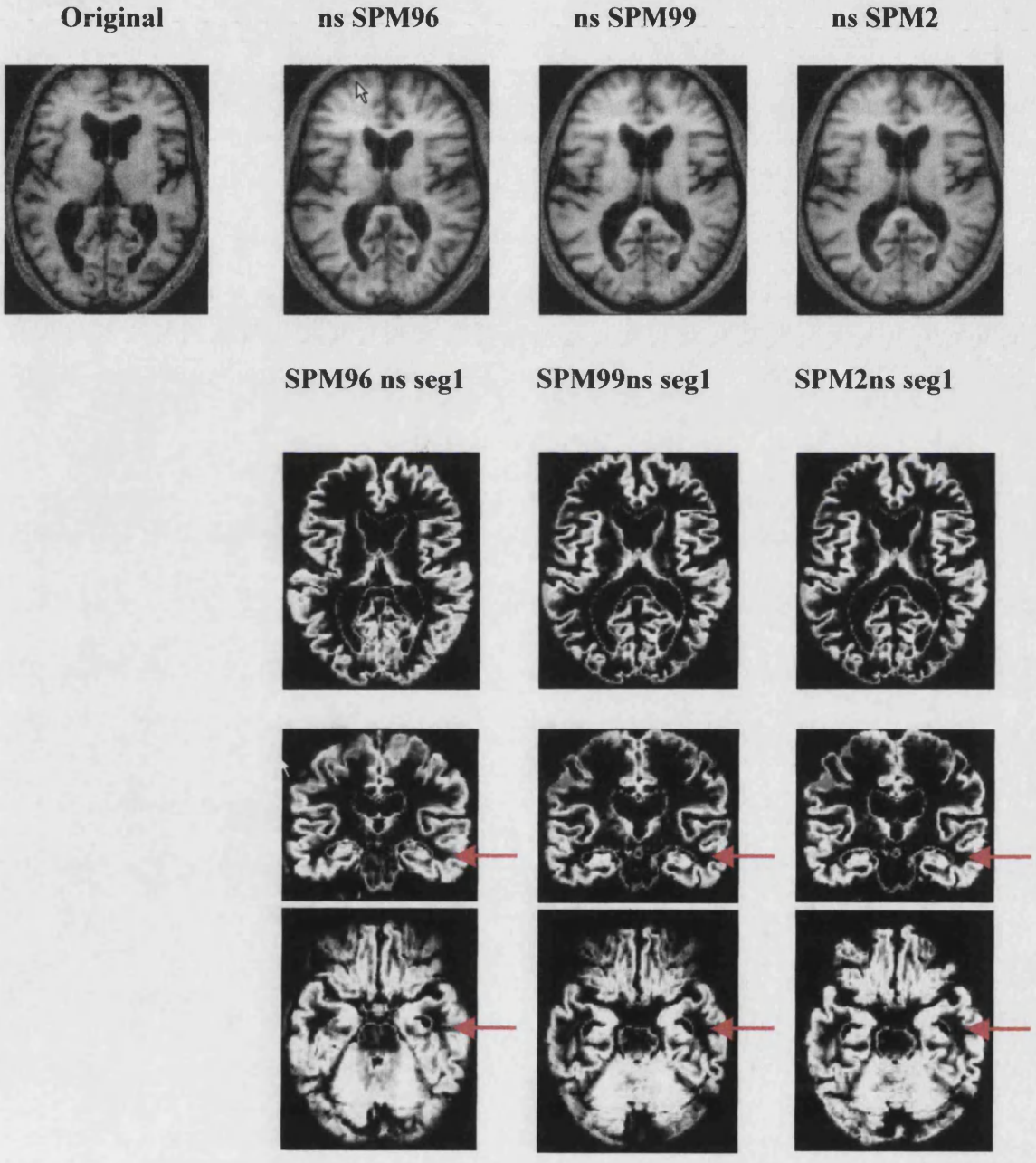

Figure 2.4: The effect of brain extraction

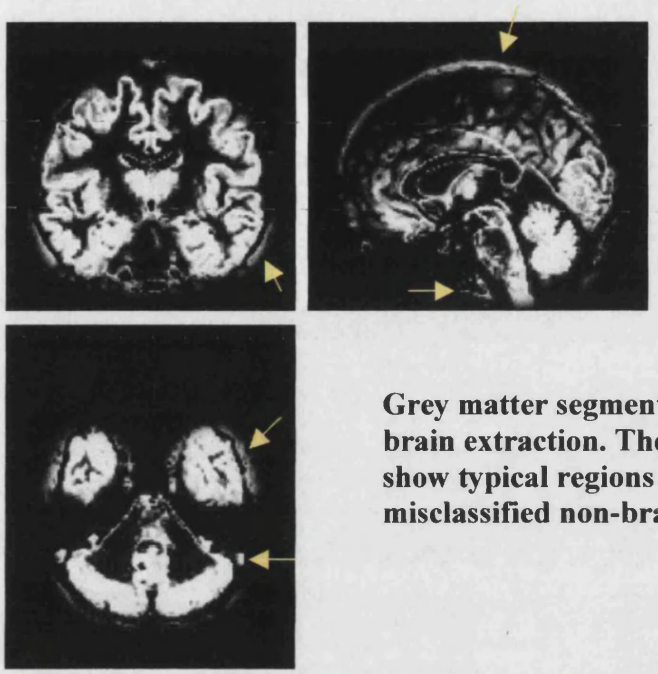

Grey matter segment before brain extraction. The arrows show typical regions of misclassified non-brain voxels.

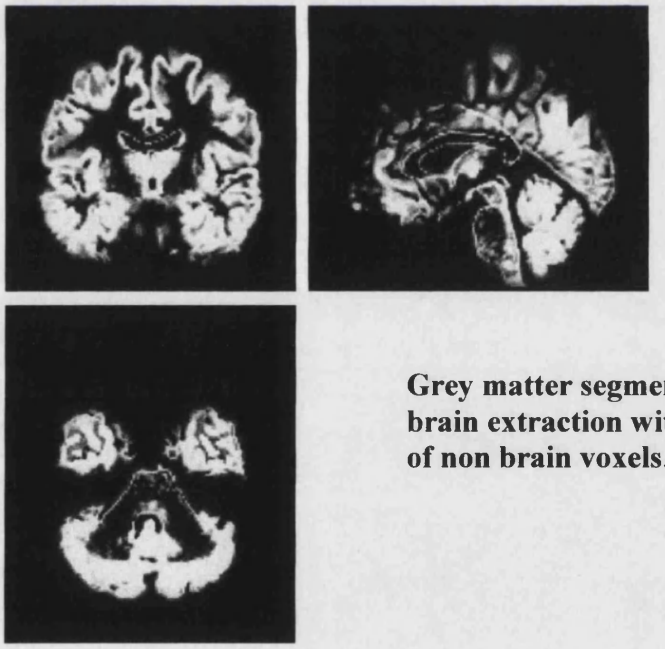

Grey matter segment after brain extraction with removal of non brain voxels.

Modulation

As a result of non-linear spatial normalisation the volumes of certain brain regions may grow, whereas others may shrink. In order to preserve the absolute amount of a particular tissue (grey or white matter) within a voxel, a further processing step is incorporated. This involves modulating voxel values by the Jacobian determinants derived from the spatial normalisation step (see Fig. 2.5) (Ashburner and Friston 2000; Ashburner and Friston 2001).

Figure 2.5: Modulation step

Cartoon to illustrate the effect of modulation. (**v**) represents the absolute amount of grey matter in a voxel before normalisation. During spatial normalisation the voxel may grow or shrink (volume change denoted by **x**) to match the corresponding voxel in the template while the concentration of grey matter is preserved. The modulation step corrects for this so that absolute volume of grey matter is preserved within the normalised voxel (the concentration will correspondingly be altered as demonstrated by the preserved size but altered colour of the voxel cartoon). A reslicing step follows to preserve isotropic voxels in the matrix.

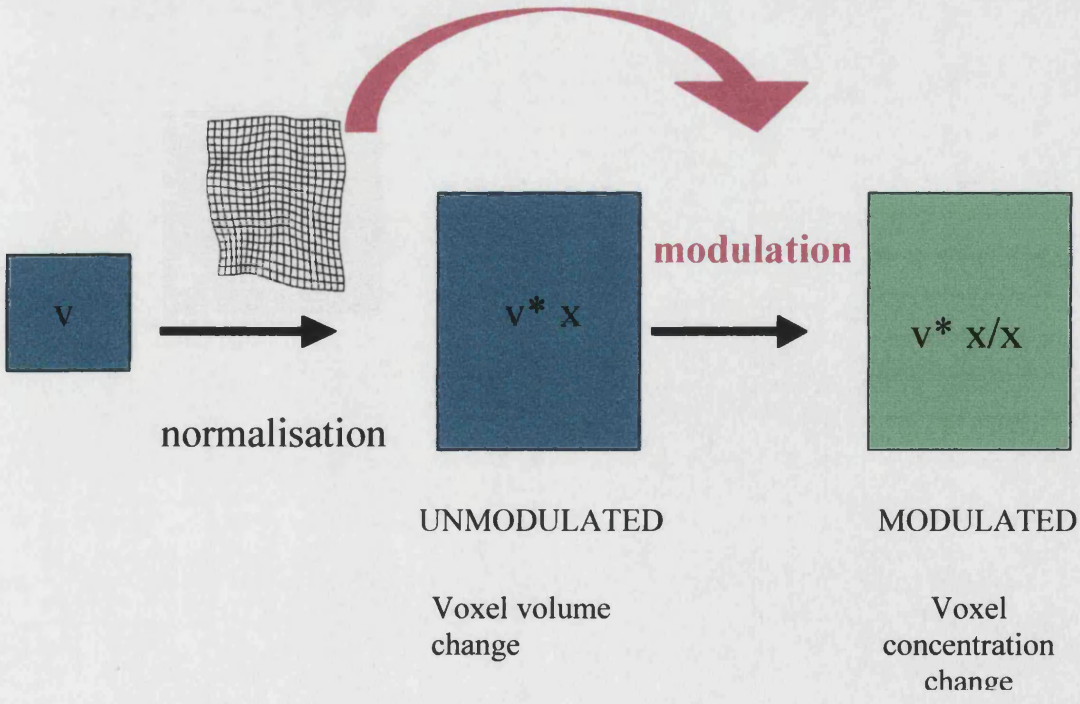

This augmented VBM can thus be considered a combination of VBM and TBM, where TBM employs testing of the Jacobian determinants themselves. In order to simplify this concept, it is helpful to compare VBM with an analysis using regions of interest. Each voxel in a smoothed grey matter image is the count of the grey matter voxels within the limits of a region defined by the smoothing kernel. After spatial normalisation, the voxels within the region defined by the smoothing kernel can be thought of as being projected onto the original anatomy, but in doing so their shapes and sizes will be distorted. Without modulation, the proportion of grey matter within each region of interest would be measured. Modulation effectively converts values of grey and white matter concentration into grey matter mass (i.e. rendering the inferences about the absolute amounts (volume) of grey matter in a voxel as opposed to the relative amounts (concentration)) (Ashburner and Friston 2000; Ashburner and Friston 2001; Davatzikos *et al.*, 2001). Analyses of modulated and unmodulated data are complementary and not exclusive. A practical illustration of the differences between the two can be seen in male: female comparisons (see Fig. 2.6). It is well known that males have larger brains than females, but more interesting is the detection of regionally specific differences (over and above global differences). VBM detects regions of increased grey matter volume in the anteromesial temporal lobes, but no regions of significantly increased concentration in males. In females, VBM detects diffusely increased grey matter concentration throughout the cortical mantle as well as regions of increased grey matter volume in the posterolateral temporal lobes (Good *et al.* 2001c). Another example where the two techniques show different and complementary results is gross cerebral atrophy such as in Alzheimers disease or semantic dementia. For studies of normal subjects of similar age groups (where the deformation maps from spatial normalisation are very similar) the modulated and unmodulated data show similar effects.

Smoothing

The normalised, modulated/unmodulated grey and white matter segments are smoothed using a 12mm FWHM isotropic Gaussian kernel (as in the standard method). The various steps of the optimised method are summarised in Fig. 2.7.

Figure 2.6: Practical effect of the modulation step

Sex differences in grey matter volume (modulated data) and concentration (unmodulated data), $p<0.05$ corrected.

(a) Grey matter volume (modulated)

males – females **females - males**

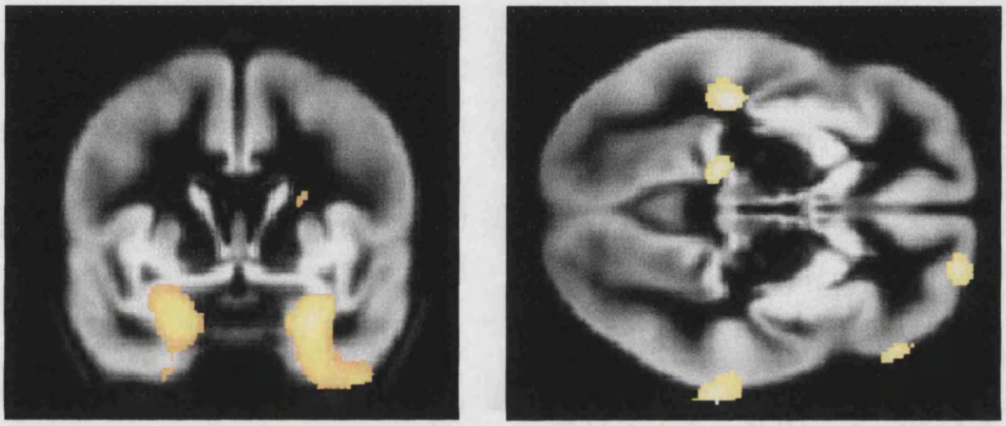

(b) Grey matter concentration (unmodulated)

males – females **females - males**

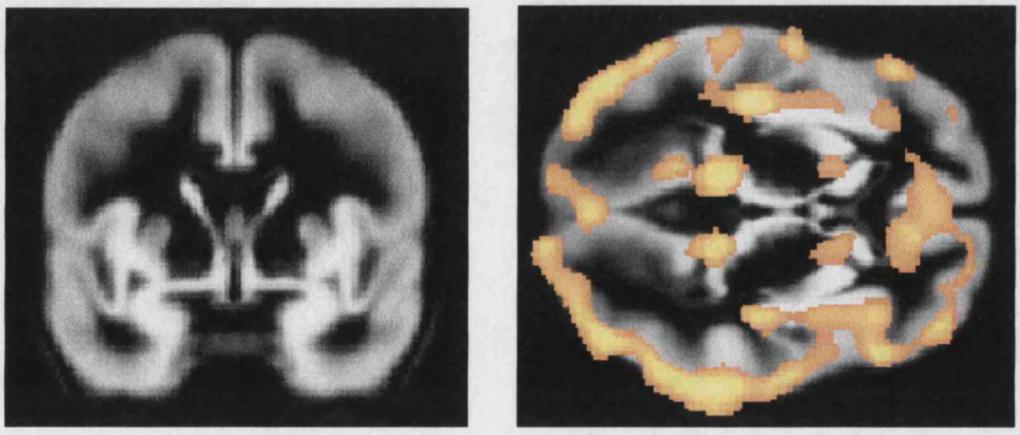

Statistical analysis

The unmodulated and modulated smoothed data are analysed separately using MATLAB 5 (MathWorks, Natick, Mass., USA) and SPM99 (Wellcome Dept. of Cognitive neurology, ION, London) employing the framework of the General Linear Model as in the standard method. Grey and white matter and CSF analyses are performed separately in order to provide a more complete characterisation of brain structure than grey matter analyses in isolation. This has relevance when making inferences about brainstem and deep grey matter structure since voxel classification into grey and white matter in these regions is less reliable because of intrinsic contrast properties. Global modelling proceeds according to the method described for the standard VBM protocol: the global mean grey voxel value is included as a confounding covariate for grey matter analyses and the global white voxel value is included as a confounding covariate for white matter analyses. This provides information about regionally specific changes within a tissue compartment, over and above global changes within that compartment. This is important if, for example, the detection of regionally specific differences between males and females is sought, given that there are marked global differences in brain volumes. In certain instances, such as in analyses of patients with dementia, it may be more appropriate to model total intracranial volume (TIV) as a confounding covariate, so that differences in head size are separately accounted for and the influence of this variable on the result is removed, while global grey matter changes are preserved (which is generally what ROI approaches measure). This only applies for modulated analyses that have incorporated a correction for volume changes during spatial normalisation. For unmodulated analyses, TIV would not need to be included, since the global differences have already been removed. In most cases, global and regional inferences are complementary. Corrections for the size of search volume (multiple comparison correction) are made to the p values using techniques based on Gaussian field theory (Friston *et al.* 1996; Worsley *et al.* 1996). In general a whole brain correction is applied, however this is stringent when one considers classical region of interest (ROI) based morphometric methods, which are limited to only a few metrics. Where prior hypotheses about putative regional structural change exist, sensitivity can be increased by using small volume corrections (SVC).

Validation of the optimised technique

Details on the evaluation of the VBM segmentation technique, including evaluation of the non-uniformity correction and stability with respect to mis-registration with *a priori* images can be obtained in Ashburner and Friston (2000). Evaluation of the assumptions about normal distribution of the data is also detailed in this reference. In order to determine scan-rescan differences in tissue classification, I scanned 10 healthy subjects twice on the same day. Each subject left the scanner room between scans, and the time interval between scans was approximately 15 minutes. For the standard VBM method, the coefficient of variation (100 × standard deviation of the differences/overall mean) for grey and white matter volumes, CSF volume and TIV were 0.45, 0.75, 1.07 and 0.16 respectively. For the optimised VBM method, the coefficients of variation for grey matter volume, white matter volumes, CSF volume and TIV were 0.41, 0.59, 1.07 and 0.17 respectively. These values show that tissue classification is highly reproducible using both standard and optimised VBM methods. Furthermore, a VBM statistical analysis using a paired t-test design matrix yielded no significant regional differences between first and second scans, even with reduced corrected thresholds of 0.5. The standard VBM technique has been validated with independent region of interest measurements (Maguire *et al.* 2000; Vargha-Khadem *et al.* 1998) and as detailed in Chapter 5, I validate the optimised VBM technique with an independent automated segmentation technique and region of interest measurements in groups of elderly healthy subjects and patients with Alzheimer's disease and semantic dementia (Good *et al.* 2002).

Since no gold standard exists against which in vivo measurements can be compared, and furthermore since variations in MRI protocols, normalisation and segmentation techniques can be expected to produce inconsistent data, reproducibility of a given technique is more important. In this regard the tissue classification technique used in VBM yields highly reproducible results.

Figure 2.7: Schema showing the steps implicit in the optimised protocol

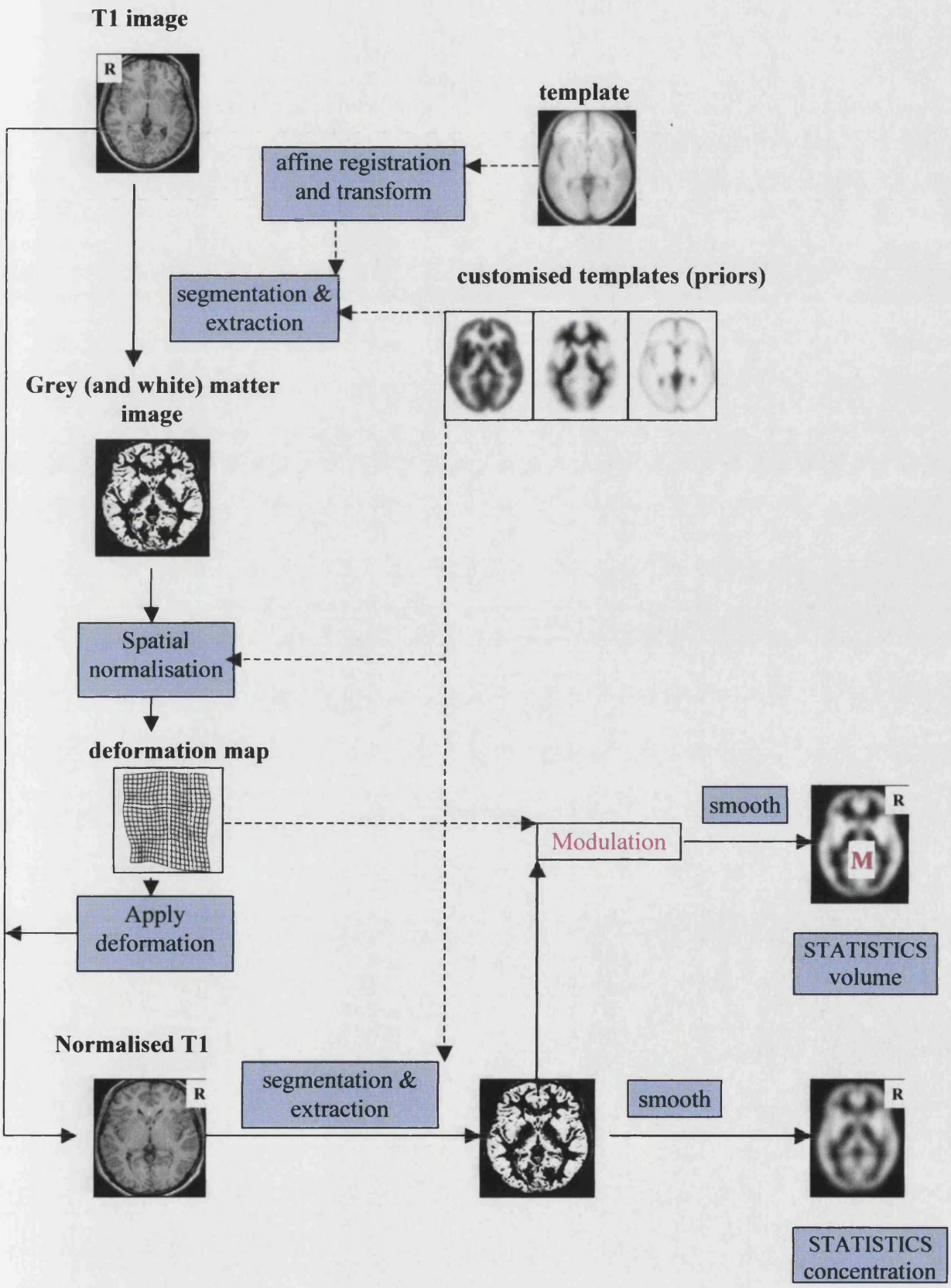

Deformation based morphometry (DBM)

Whereas VBM analyses the spatially normalised brain segments on a voxel-wise basis, DBM analyses differences in the deformation fields used to normalise brains into standard space. The deformation fields are defined by the affine and non-linear components of the spatial normalisation. The affine components relate to head position and size, which are not themselves interesting and can be modelled as confounds, whereas the non-linear components relate to head shape. Inferences about these global shape differences can be made using multivariate statistics.

Tensor Based Morphometry (TBM)

TBM characterises regional shape differences by interrogating the Jacobian matrices of the deformation fields. The Jacobian matrices encode information about local shearing, stretching and rotation of voxels when an image is spatially normalised to a template. Inferences about local shape differences can be made using multivariate statistics. A simpler form of TBM involves analysis of the Jacobian determinants with univariate statistics to provide information about local volume changes. As previously mentioned, the more accurate the spatial normalisation is, the more information is encoded in the deformation fields and the more appropriate TBM is for testing the differences. One can imagine a continuum with simple VBM being performed on images with relatively low-resolution spatial normalisation at one end of the spectrum and TBM being performed on the Jacobian determinants of high-resolution deformation fields at the other end of the spectrum. The augmented VBM (i.e. incorporating the modulation step) could be regarded as a combination of VBM and TBM, becoming more important with faster and more precise spatial normalisation techniques.

Summary

This chapter has firstly detailed the basic principles of MR imaging whilst expanding upon techniques to optimise structural brain images. Secondly, this chapter describes the application of SPM to structural analysis, introducing the concept of computational neuroanatomy. Special emphasis has been placed on the methodology implicit in voxel-based morphometry and in particular on optimisations I have introduced to the technique.

CHAPTER 3

NORMATIVE DATA

AGEING

Guide to Reader

An understanding of normal brain structure, and in particular, normal variability, is fundamental to the appreciation of patterns of pathologically induced structural change. The acquisition and characterisation of a large bank of normative data also provides a canonical framework against which future studies of disease can be compared. Chapter 3 addresses the physiological effects of ageing on brain structure and Chapter 4 characterises normal human brain asymmetries and the effects of gender and handedness on brain morphology

Summary

In this experiment VBM is used to characterise the global and regional effects of physiological ageing on brain structure in a large cross-sectional study of healthy subjects. Global grey matter declines linearly with age, with a significantly steeper decline in males compared to females. Local areas of accelerated grey matter loss are observed in the insula, superior parietal gyri, central sulci and cingulate sulci bilaterally. Areas exhibiting relatively little age effect (relative preservation) include the amygdala, hippocampi and entorhinal cortex bilaterally. Global white matter does not decline with age, but local areas of accelerated loss and relative preservation are seen. There is no evidence of an interaction of age with sex for regionally specific effects. The global results confirm previous autopsy and imaging data, while VBM introduces new data on the regional effects of ageing.

Introduction

There is compelling evidence from post mortem and *in vivo* studies that the brain shrinks with age, but accurate quantification of the specific patterns of age-related atrophy has proved elusive. It remains unclear whether there are predictable common patterns of ageing or whether individual human brains respond to the ageing process idiosyncratically. Post mortem analysis of mammalian brains suggest that there may be a gradient of ageing from the association areas to the primary sensory regions, with the former showing the most prominent correlations between age and atrophy (Flood and Coleman 1988). In ageing humans, autopsy studies consistently reveal age-related decreases in brain weight and brain volume (e.g. Dekaban 1978; Hubbard and Anderson 1981) with evidence of neuronal loss within the cerebral cortex, brainstem and basal ganglia (Brody 1992; Vijayashankar and Brody 1979; Bugiani *et al.* 1978). Despite the large autopsy literature, detailed characterisation of regionally specific age related changes is relatively scanty. This is predominantly due to the practical constraints of analysing vast numbers of pathological specimens. Furthermore, if brain weight is related to body height, the progressive increase in height over the past century may limit the applicability of conclusions from the significant fraction of post-mortem studies that were conducted in the last century (Miller and Corsellis 1977).

A number of *in vivo* imaging studies have attempted to quantify age-related change in whole brain volume, grey matter, white matter and CSF compartments using CT, 2D MRI and more recently high resolution MRI morphometry. Apart from the more obvious limitations of small cohort studies and earlier imaging techniques (e.g. Schwartz *et al.* 1985), as well as variability in reporting absolute or fractional volumes, the majority of these studies have been based on manual or semi-automated region of interest guided measurements (Filipek *et al.* 1994; Luft *et al.* 1999; Pfefferbaum *et al.* 1990; Pfefferbaum *et al.* 1994; Raz *et al.* 1992; Raz *et al.* 1997; Raz *et al.* 1998; Xu *et al.* 2000a) which may be inherently biased. This bias is introduced by the small number of regions and metrics used in classical morphometrics that are insensitive to changes elsewhere in the brain. Despite such constraints, CT and MRI consistently confirm global increases in CSF and global grey matter loss without significant global loss of white matter (e.g. Jernigan *et al.* 1991c).

With the improved resolution of structural MRI scans and emergence of a

number of unbiased whole brain morphometric techniques more accurate characterisation of the structural correlates of ageing is now possible. Relatively simple rigid body registration within subjects, shows minor global brain volume loss in aged normal subjects and accelerated loss in a small group of patients with Alzheimer's disease over a one year interval (e.g. Fox *et al.* 1996a). More sophisticated and less constrained non linear within subject registration confirms little change in a small group of elderly controls over a year using a fluid model (Freeborough and Fox 1998). Automated segmentation techniques have allowed the quantification of global effects of age on tissue compartments, but provide no information with regional specificity within these compartments (Guttmann *et al.* 1998a). More recently, researchers have used a combination of semi automated registration and segmentation techniques followed by region of interest measurements to characterise ageing changes in a few predefined brain regions. One group document disproportionate volume loss in the frontal lobes and hippocampus with white matter loss occurring later and ultimately more marked than grey matter loss (e.g. Jernigan *et al.* 1991a). Another group (Resnick *et al.* 2000) show disproportionately large age effects in the parietal lobes and sex differences most marked in the frontal and temporal lobes. They also reveal increases in ventricular volume over a one-year period but no detectable change in global or regional brain volumes.

The great variety of morphometry methodologies combined with the heterogeneity of study groups are probably the most relevant factors accounting for the conflicting literature on linear and non-linear patterns of tissue change, the effect of sex and the heterogeneic response of various compartments of the brain to ageing.

Despite the rapidly developing literature on various forms of unbiased whole brain methods allowing reproducible voxel-wise characterisation of brain structure (e.g. Ashburner *et al.* 1998; Ashburner and Friston 2000; Christensen *et al.* 1997; Davatzikos 1996; Davatzikos 1997b; Davatzikos *et al.* 2001b; Guimond *et al.* 2000; Thompson *et al.* 1996a; Thompson *et al.* 1996b; Thompson and Toga 1997), at the time of this research such methods had not yet been applied to large subject groups to characterise ageing effects. For this reason the following study applies VBM to a large group of normal adults (n= 465) in order to characterise and quantify age-related change in the human brain on a voxel-by-voxel basis. This facilitates not only the global assessment of separate brain compartments, namely grey and white matter and CSF, but more importantly regionally specific changes within these compartments.

Methods

Subjects

Approval for the study was obtained from the Local Research Ethics Committee of The National Hospital for Neurology and Neurosurgery (UCLH, NHS Trust) and the Institute of Neurology (UCL). The study group was selected from a population of 1761 normal volunteers who responded to advertisements and were scanned at the Wellcome Department of Cognitive Neurology between February 1998 and December 1999. All subjects with any neurological, medical, psychiatric condition or migraine were excluded. Inclusion criteria included: 1) Normal MRI brain as determined by an experienced neuroradiologist (myself). Any MRI scans with structural abnormalities, prominent normal variants (e.g. mega cisterna magna, cavum septum pellucidum) or technical artefacts were excluded. 2) No history of alcohol intake of more than 30 units/week or intake of more than 10 units within 48 hours prior to scanning (A unit of alcohol is equal to 10ml of pure alcohol and is roughly equivalent to a glass of wine (125ml) or a single measure of spirits (25ml). 3) No history of severe head trauma requiring medical attention. 4) No history of cognitive difficulties, 5) No history of treated hypertension. 465 subjects met all the inclusion criteria. They comprised 29 left- handed females (aged 18-75, median 31), 171 right-handed females (aged 18-79, median 28), 38 left- handed males (aged 20-59, median 33) and 227 right- handed males (aged 17-67, median 26).

Structural MRI scanning protocol

Magnetic resonance imaging was performed on a 2 Tesla Siemens MAGNETOM Vision scanner. A 3D structural MRI was acquired on each subject using a T-1 weighted MPRAGE sequence (TR/TE/TI/NEX: 9.7/4/ 600/1, flip angle 12°, matrix size 256 × 192, FOV 256 × 192, yielding 120 sagittal slices and a slice thickness of 1.5mm with in plane resolution of 1mm × 1mm).

Data analysis

Voxel based morphometry was performed using the optimised method, which is fully detailed in Chapter 2. Details pertinent to this study will be emphasised here.

Global effects of age were examined by multiple regression of summed voxel values of grey matter, white matter, CSF and total intracranial volume (TIV) in a

model including linear and quadratic expansions of age for both males and females. Significance levels for F statistics were set at $p<0.05$.

Regionally specific differences in grey (and white) matter and CSF between groups were assessed statistically using a two-tailed contrast, namely testing for an increased or decreased probability of a voxel being grey (or white) matter. I tested for volumetric changes in grey or white matter by incorporating the modulation of segmented data. Concentration changes were assessed using the segmented images directly (unmodulated data). Normalisation for global differences in voxel intensity across scans was effected by inclusion of the global mean voxel value (grey matter globals for the grey matter analysis and white matter globals for the white matter analysis) as a confounding covariate in an analysis of covariance (ANCOVA) whilst preserving regional differences in grey (and white) matter. Orthogonalised first, second and third order polynomial expansions of age were entered into the design matrix to determine the linear and non-linear effects of age. I assessed the goodness of fit of first, second and third order polynomial expansions using F maps or SPM{F} (Buchel *et al.* 1996; Friston 1997). Significance levels for the F statistics were set at $p<0.05$, corrected for multiple comparisons. Significance levels for one-sided T statistics were set at $p<0.025$, corrected.

Results

Grey matter

Global effects of age

There was a decline of global grey matter volume with age (Figure. 3.1a), overall R squared = 0.489. This involved cortical and deep grey matter structures and cerebellum diffusely, and a similar pattern was observed when TIV was included as a confounding covariate. The linear coefficient (b1) was significant for both males, b1 = -0.0039, $F(1,458) = 58.7$, $p<0.0001$, and females, b1 = -0.0026, $F(1,458) = 31.7$, $p<0.0001$. Both quadratic coefficients failed to reach significance ($F<1.06$, $p>0.30$). The rate of decline was greater in males than females, a trend that approached significance, $F(1,458) = 3.54$, $p<0.06$. The mean grey matter volume was significantly greater in males (0.829 litres) than females (0.747 litres), $F(1,458)=239.85$, $p<0.0001$. There was no effect of handedness on global grey matter

volume, F (1,458) <1. When absolute volumes were expressed as a fraction of TIV, a similar significant pattern of linear decline was noted for males ($p<0.001$) and females ($p<0.001$), although the increased decline in males was less marked, F (1,457) = 0.8, p = 0.17) The mean fractional volume of grey matter was significantly greater for males than females ($p<0.001$), although this was less pronounced than the absolute volume difference (Fig. 3.1b). The grey-white absolute volume ratio was 1.89 for females and 1.89 for males. The grey-white fractional volume ratio was 1.82 for females and 1.82 for males.

Regional effects of age

Local areas of relative accelerated loss of grey matter volume (modulated data) (i.e. regional loss more than the global loss) were observed bilaterally in the superior parietal gyri, pre- and post- central gyri, insula/frontal operculum, right cerebellum (posterior lobe) and anterior cingulate (Fig. 3.2). Areas of relative accelerated loss of grey matter concentration (unmodulated data) were observed in the left middle frontal gyrus (F2), transverse temporal (Heschl's) gyri bilaterally and left planum temporale (Fig. 3.3). Areas of relative preservation (i.e. less than the global loss) of grey matter volume were noted symmetrically in the lateral thalami, amygdala, hippocampi and entorhinal cortex (Fig. 3.4). Areas of relative preservation of grey matter concentration were seen more diffusely in the thalami (Fig. 3.5). Table 3.1 demonstrates the stereotaxic co-ordinates corrected p and Z scores for grey matter analyses. These local effects tended to be linear, with no improved fit to the data with inclusion of a second and/or third order polynomial term. There were no significant two or three way interactions with age, sex or handedness.

Figure 3.1: Global grey matter changes with age

465 normal subjects: males are depicted in blue and females in red. Absolute grey matter volume (a) and grey matter volume normalised to TIV (b). Note the linear pattern of grey matter loss with age with a significantly steeper decline in males.

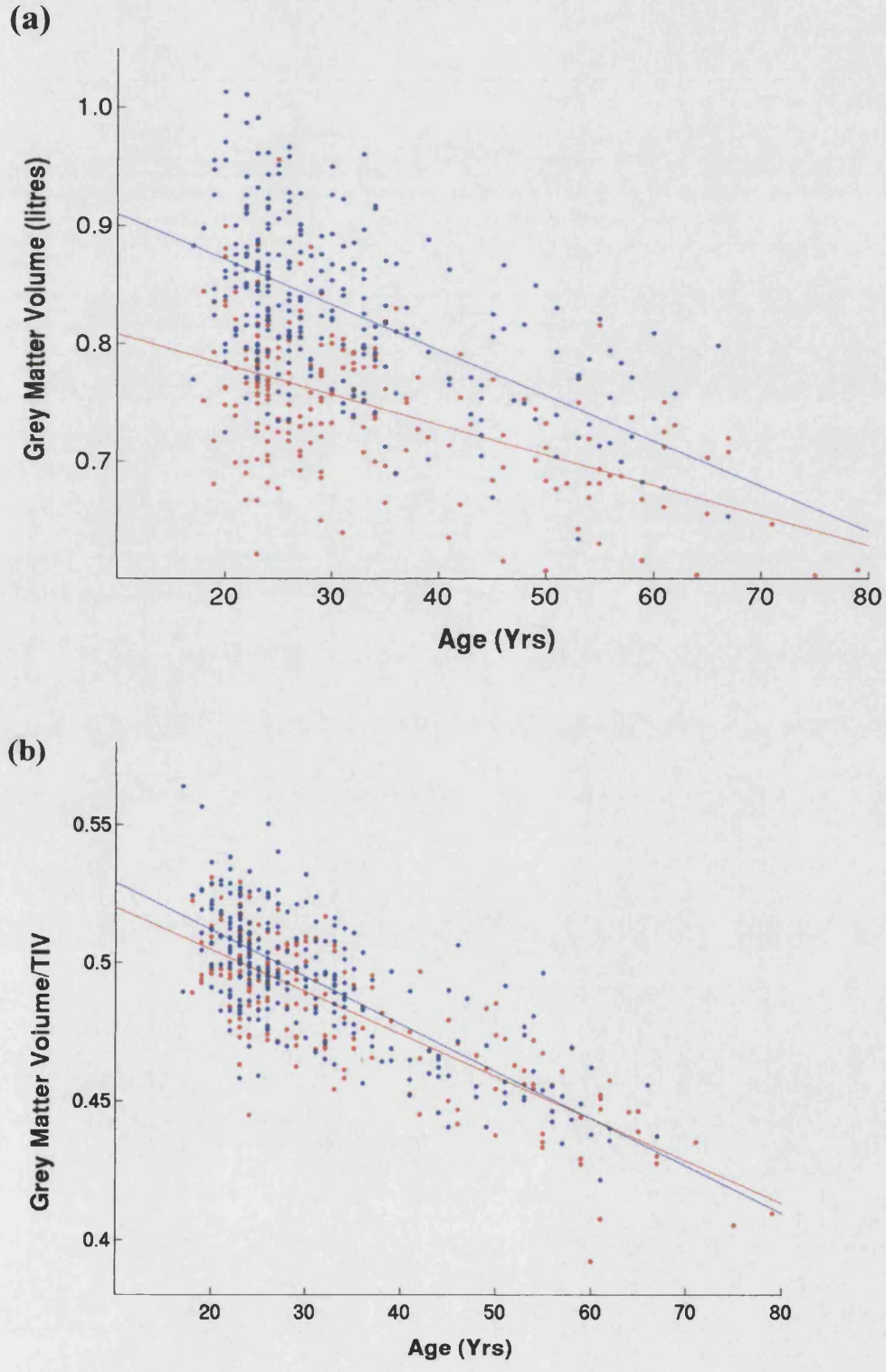

Figure 3.2: Grey matter volume (modulated): negative correlation with age

Regions of accelerated loss of grey matter volume from 465 healthy subjects superimposed on the normalised structural image. The colour bar represents the T score. Significant voxels ($p>0.025$, corrected) are shown in the anterior cingulate, bilateral pre- and post- central gyri and bilateral angular gyri (anterior insular and cerebellar voxels not shown).

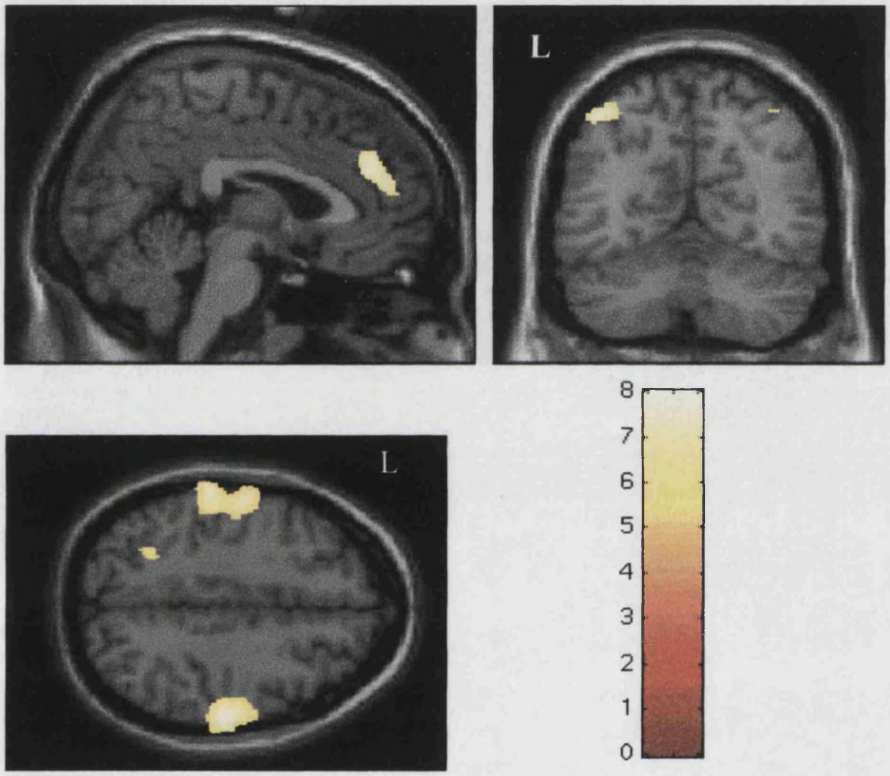

Figure 3.3: Grey matter concentration (unmodulated): negative correlation with age.

Regions of accelerated loss of grey matter concentration from 465 healthy subjects superimposed on the whole brain template derived from all subjects. The colour bar represents the T score. Significant voxels ($p<0.025$, corrected) are shown bilaterally in Heschl's gyri and the left planum temporale

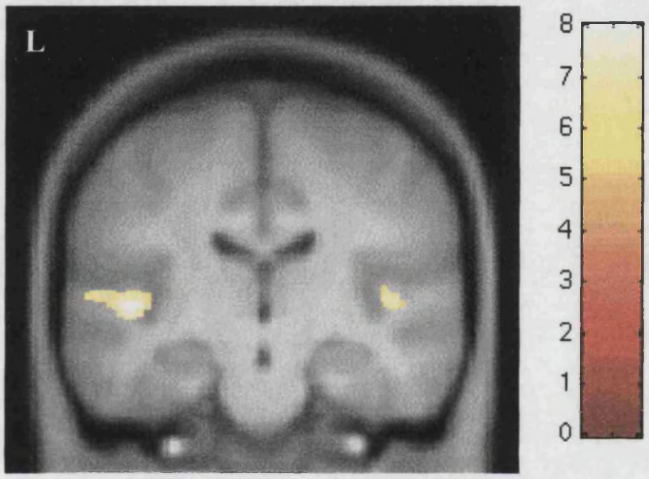

Figure 3.4: Grey matter volume (modulated): positive correlation with age.

Regions of relative preservation of grey matter volume in the mesial temporal lobes and lateral thalami ($p<0.025$, corrected) projected on the group template)

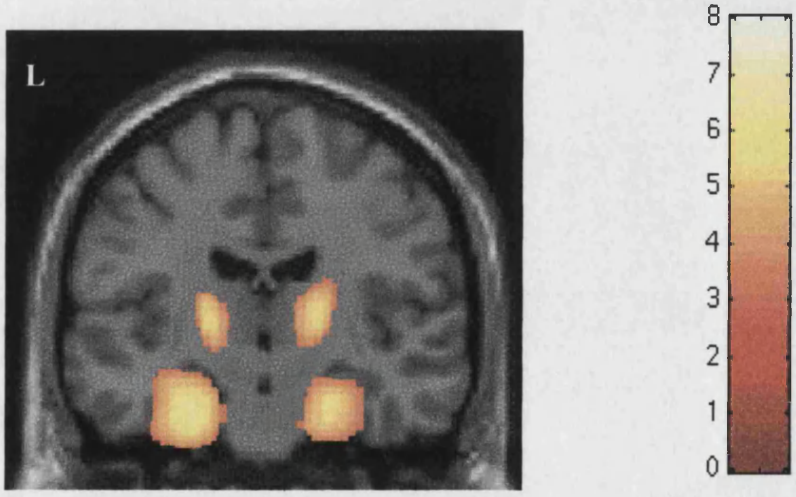

Figure 3.5: Grey matter concentration (unmodulated): positive correlation with age

Regions of relative preservation of grey matter concentration in the thalami bilaterally ($p<0.025$, corrected) projected on the group template

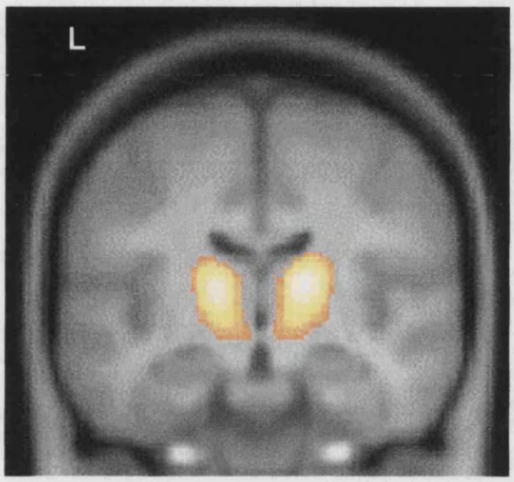

White matter

Global effects of age

There was no significant decline in white matter volume with age (Fig. 3.6a), overall R squared = 0.326. The linear coefficients were not significant ($F<1.05$, $p>0.30$), though the quadratic coefficient approached significance for females, b2 = 0.0004, $F(1,468) = 3.65$, $p<0.06$ (but not males, $F<1$). The mean white matter volume was significantly greater in males (0.454 litres) than females (0.395 litres), $F(1,458) = 218$, $p<0.0001$, but no other sex differences approached significance ($F<1.27$). There was no effect of handedness on global white matter volume $F(1,458) <1$. When white matter volume was expressed as a fraction of TIV, the quadratic coefficient was significant for females ($p<0.01$), but not for males (Fig. 3.6b)

Figure 3.6: Global white matter changes with age

(a)

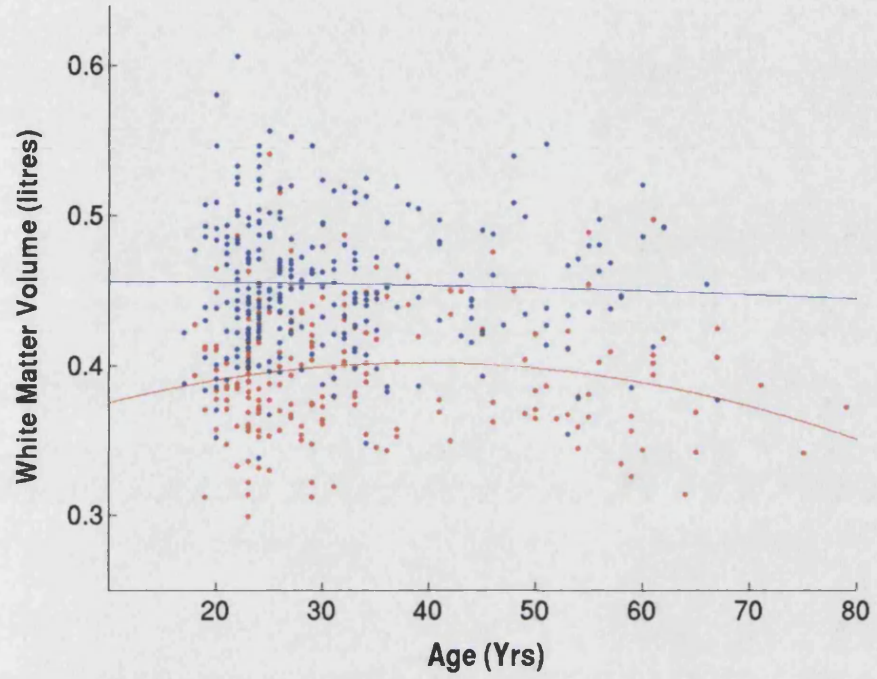

(b)

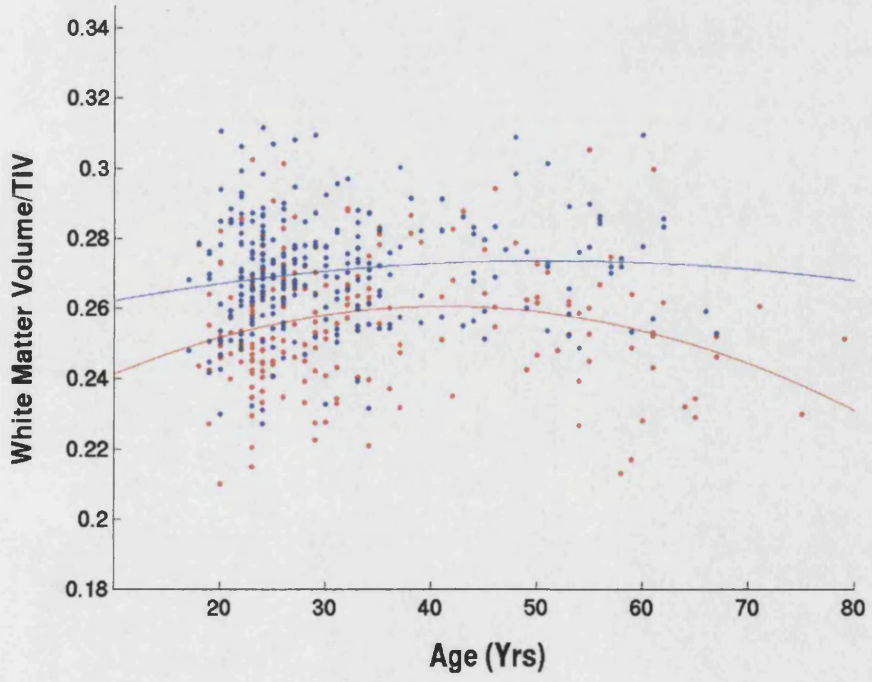

Regional effects of age

There were local areas of relatively accelerated loss of white matter volume bilaterally in frontal white matter, optic radiations (Fig.3.7) and posterior limbs of internal capsule, bordering on the ventrolateral thalamus. Local areas of accelerated decline of white matter concentration were seen bilaterally in posterior limbs of internal capsule, bordering on the lateral thalamus (Fig. 3.8). Inspection of white matter segmented images (from the optimised pre-processing method) shows some lateral thalamus voxels classified as white matter (see discussion). There were local areas of relative preservation of white matter volume bilaterally in the posterior frontal lobes (Fig.3.9), cerebellum and right temporal lobe. Relative preservation of white matter concentration was noted bilaterally in the internal capsules, frontal and posterior temporal/occipital white matter (Fig. 3.10). Table 3.2 demonstrates the stereotaxic co-ordinates of local maxima, corrected p and Z scores for the white matter analyses.

These local effects of age also tended to be linear, with no improved fit to the data with inclusion of second and/or third order terms, apart from two small foci of accelerated non-linear decline in white matter concentration at the anterior aspect of both internal capsules. There were no significant two or three way interactions with age and sex and handedness.

Figure 3.7: White matter volume (modulated): negative correlation with age

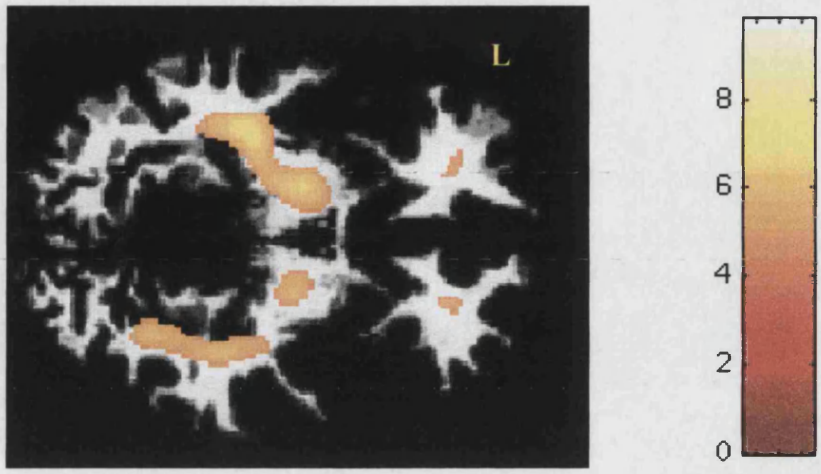

Figure 3.8: White matter concentration (unmodulated): negative correlation with age

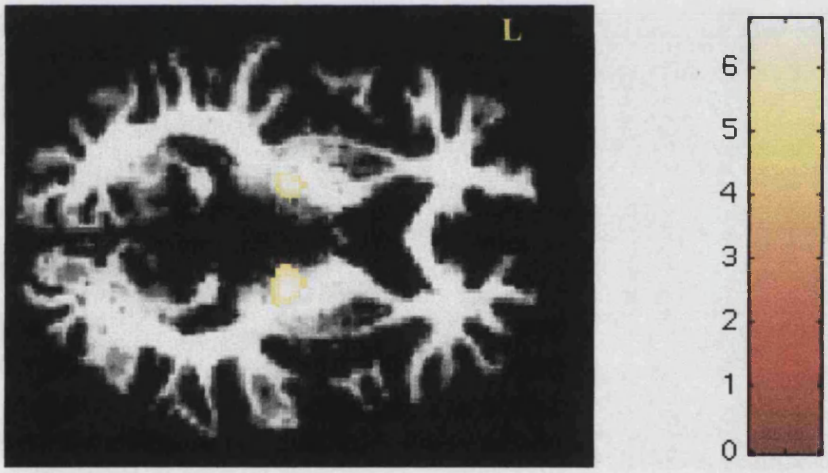

Figure 3.9: White matter volume (modulated): positive correlation with age

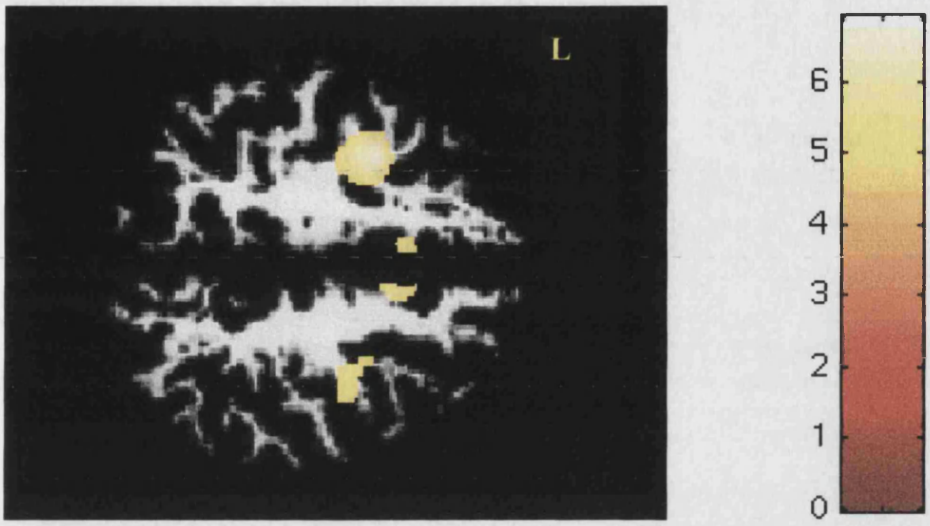

Figure 3.10:White matter concentration (unmodulated): positive correlation with age

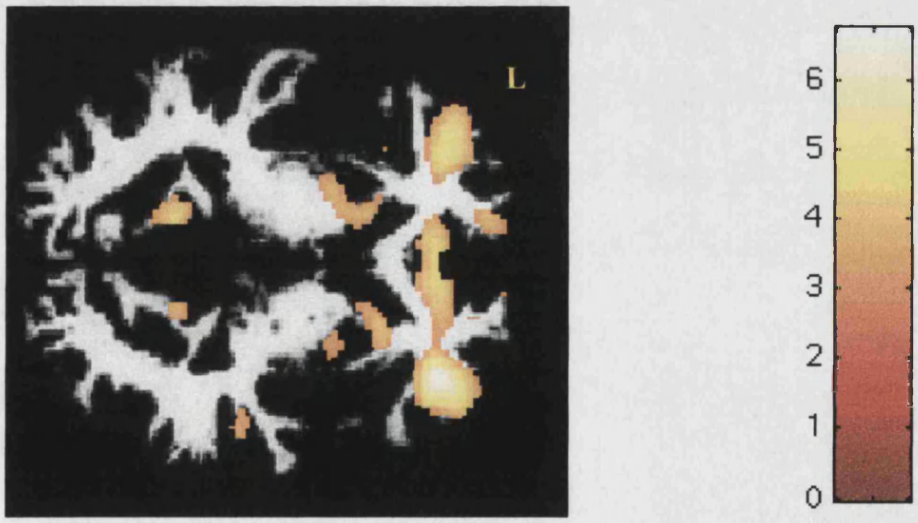

CSF

Global effects of age

There was a global increase in CSF volume with age (Fig. 3.11a), overall R squared = 0.377. This involved the entire CSF compartment including the ventricles and surface sulci. A similar pattern was observed when TIV was included as a confounding covariate. The linear coefficient was significant for both males, b1=0.0019, $F(1,458)=39.1$, $p<0.0001$, and females, b1 = 0.0018, $F(1,458) = 40.2$, $p<0.0001$. The quadratic coefficient was significant for females, b2 = 0.0003, $F(1,458) = 5.53$, $p<0.05$, but not males, $F<1$. The mean CSF volume did not differ significantly between males (0.397 litres) and females (0.401 litres), $F(1,458) = 1.91$, $p = 0.22$, and no other sex differences approached significance, $F<1.9$, $p>0.16$. There was no significant effect of handedness on CSF volume $F(1,458) <1$. When CSF was expressed as a fraction of TIV, the linear coefficients were significant for males ($p<0.001$) and females ($p<0.001$), and the quadratic coefficient was significant only for females ($p = 0.006$). There was also a significant difference in mean fractional volume of CSF, female fractional volume being greater than male ($p<0.001$)(Fig. 3.11b).

There was a slight but significant linear decline of TIV with age for males ($p = 0.008$) but not for females (p = 0,282). Both quadratic coefficients failed to reach significance. The rate of decline was greater in males than females, a trend that approached significance, $F (1,457) = 1.9$, $p = 0.08$. The mean TIV was significantly greater for males than females ($p<0.001$)

Figure 3.11: Global CSF volume change with age

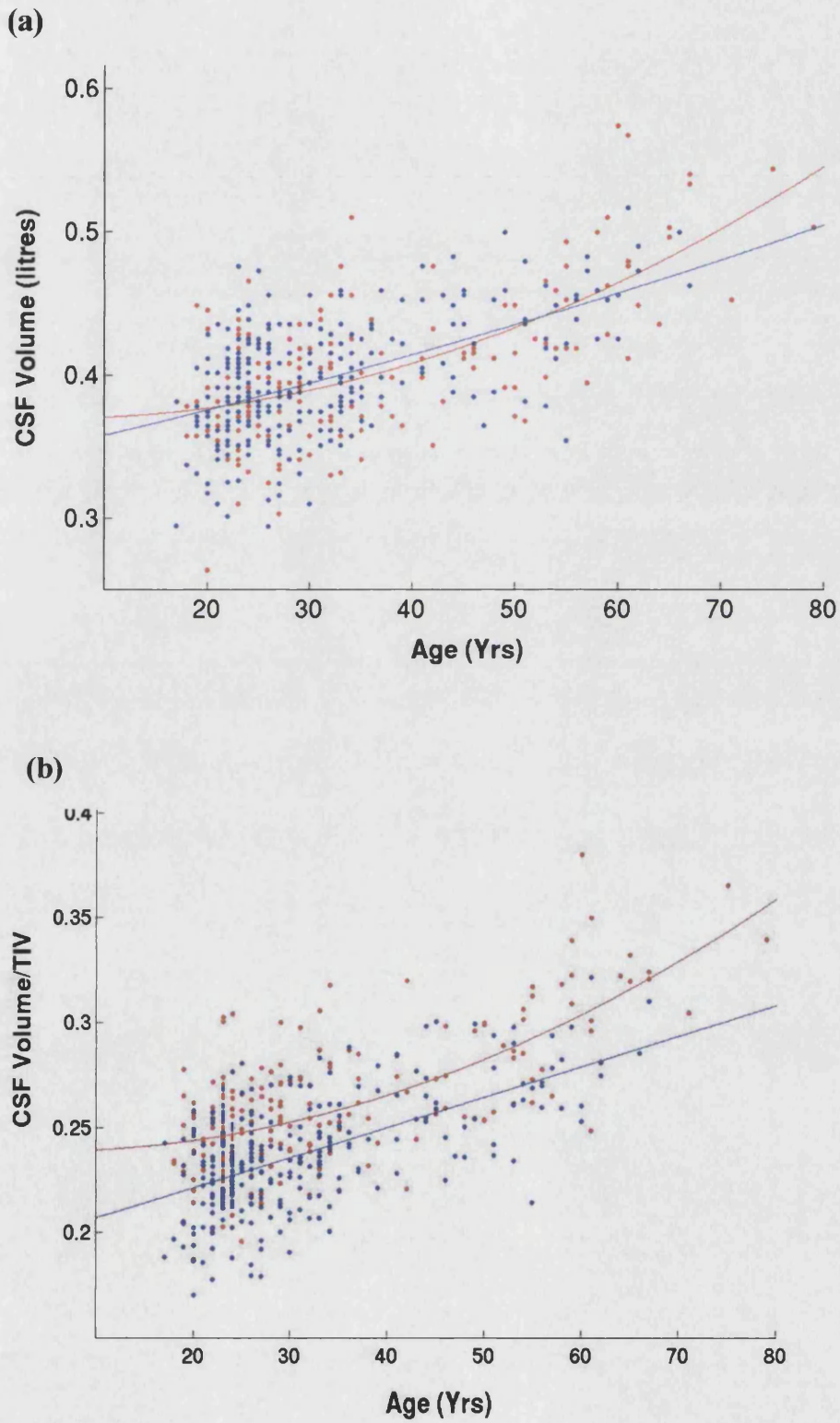

Regional effects of age

Relatively little enlargement of the CSF space with age (negative correlation with age) was seen in the pontine cistern, including its caudal extent around the medulla (Fig. 3.12). Areas of accelerated enlargement of the CSF space (positive correlation with age) were seen symmetrically in the chiasmatic and supracerebellar cisterns, cisterna magna, third ventricle and the Sylvian and interhemispheric fissures (Fig. 3.13). Regional effects of age tended to be linear with no improved fit of the data with inclusion of a second and/or third order polynomial expansion of age.

Figure 3.12: CSF volume (modulated): negative correlation with age

Relatively little or no increase in CSF with increasing age projected onto the mean normalised CSF image. The colour bar represents the T score. Significant voxels ($P<0.025$, corrected) are seen in the pontine cistern.

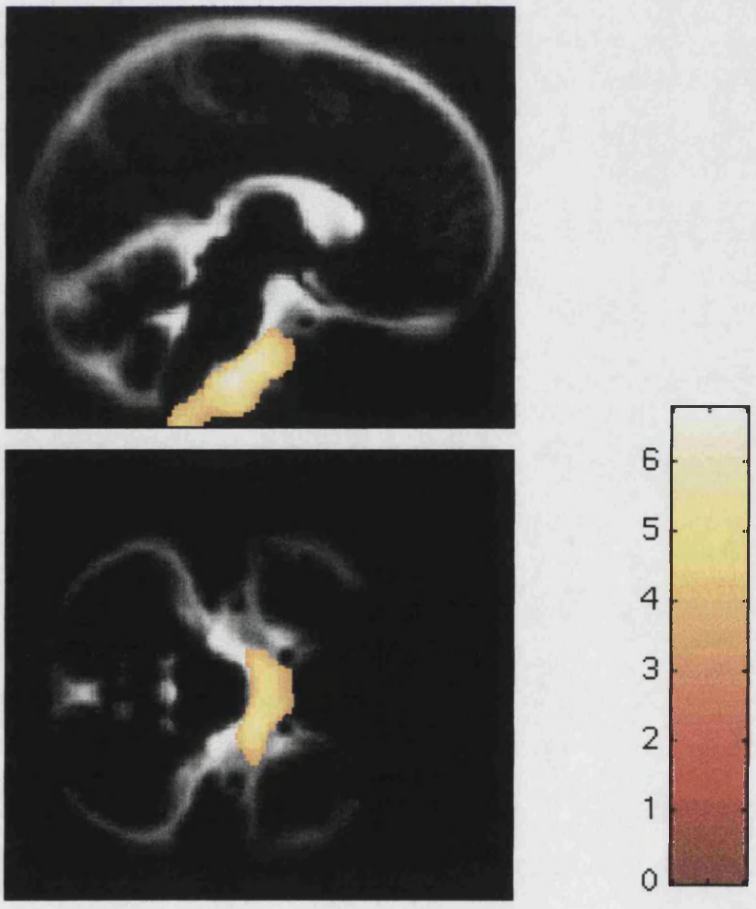

Figure 3.13: CSF volume (modulated): positive correlation with age

Accelerated enlargement of the CSF space with increasing age superimposed on the mean normalised CSF image. The colour bar represents the T score. Significant voxels ($P<0.025$, corrected) are seen in the Sylvian and interhemispheric fissures; chiasmatic and supracerebellar cisterns; cisterna magna and third ventricle.

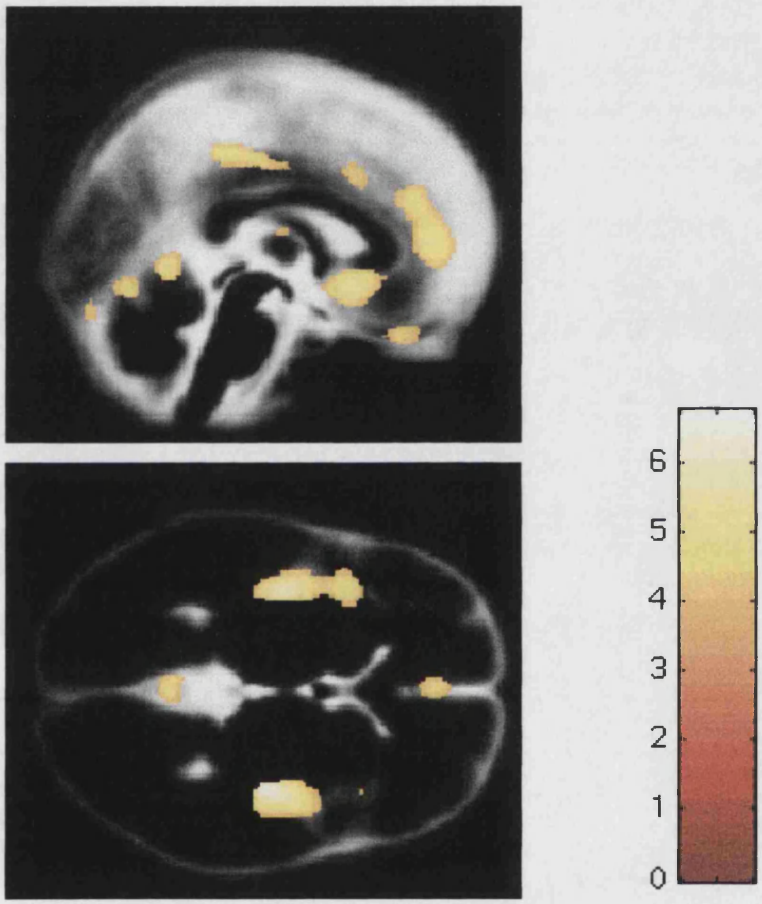

Discussion

Subject selection

This is a cross-sectional study in which structural age differences observed at a given time are used to make inferences about the ageing process. This approach has inherent limitations since there is potential for confounding age and cohort effects and in particular for secular bias, which can only be resolved by a longitudinal study. (Haug 1984) points out that an increase in height due to secular acceleration is in the

order of approximately 1mm per year, and as body weight increases, so does brain weight. There has been a trend in the literature to report brain volumes as percentages of body height or total intracranial volume. I have therefore provided data on absolute and fractional (as a fraction of TIV) brain volumes. It is worth noting that there are subtle differences between the two as demonstrated in the global ageing graphs, which further explains inconsistencies in the literature on ageing. The major drawback of a longitudinal study is the time it would take to acquire data from youth to senescence. It would also be practically impossible to maintain identical scanning parameters; thereby introducing systematic differences unassociated with ageing *per se*. Longitudinal studies thus tend to look at small time windows in the ageing process.

Another difficult issue is the question of what constitutes a "normal" ageing population? I recruited volunteers responding to advertisements distributed around the university and local community, and the vast majority of volunteers were of European extraction. Most young and middle aged subjects were students or professionals with higher degrees and the majority of elderly volunteers were motivated, high functioning individuals, many attending educational programs and thus probably not representative of the population at large. All volunteers with controlled hypertension were excluded, but since blood pressure rises with increasing age, "normal" elderly subjects may have been excluded and this is reflected in the relatively small numbers of subjects in the seventh to ninth decades. Formal cognitive tests were not performed on any subject, but subjects with any history of cognitive decline were excluded and all subjects completed a questionnaire as part of the recruitment process. If anything, this elderly population errs on the side of high cognitive functioning. Certainly further studies need to look longitudinally at a smaller cohort of elderly subjects with comprehensive cognitive testing, functional and structural imaging.

Silent brain lesions

Deep white matter lesions are seen on magnetic resonance imaging in approximately one-third of asymptomatic elderly subjects (Fein *et al.* 1990) and the significance of these remains unclear. Some reports have suggested an association between silent white matter lesions and coronary artery stenosis, hypertension and cognitive performance. A CT and MRI based study using relatively crude region of interest measurements reported an association between silent white matter lesions and brain atrophy (Yamano *et al.* 1997). The bulk of evidence suggests however, that they

are merely frequent incidental findings in the elderly, with no link to significant central nervous system pathological processes. A recent MRI study on the sex effects of age-related changes in brain structure (Xu *et al.* 2000a) specifically excluded all subjects with silent brain lesions, citing the CT study mentioned above. In this study, healthy subjects whose MRIs showed a few small hyperintense white matter foci were specifically not excluded, because these are probably a normal findings, and exclusion of such subjects would misrepresent the normal ageing population.

Global effects of age: Grey matter, white matter and CSF

Many neuropathological studies show that normal ageing is characterised by a substantial and extensive loss of neurons in the cerebral cortex, although this is controversial, with recent stereological investigations indicating little neuronal loss with normal ageing (e.g. Gomez-Isla *et al.* 1996; Peters *et al.* 1998). Some reports suggest that alterations in cerebral white matter and subcortical neuronal loss may be the predominant effect of age (Guttmann *et al.* 1998a). My data concur with those neuropathological and previous CT and MRI morphometry studies that suggest ageing predominantly and substantially affects the grey matter (Jernigan *et al.* 1991a; Lim *et al.* 1992; Pfefferbaum *et al.* 1990; Pfefferbaum *et al.* 1994; Schwartz *et al.* 1985; Hazlett *et al.* 1998). In particular, my data suggest a linear decline in grey matter in concordance with Pfefferbaum *et al.* (1994) and this pattern of decline is observed for absolute and fractional grey matter volumes. Others have suggested accelerated ageing in the later decades of life (Jernigan *et al.* 2001) and since my data included relatively few subjects over 65 years and furthermore my elderly subjects could be considered "super normal", a potential late non-linear trend may have been missed.

The majority of structural MRI data indicate that although significant microstructural changes are seen in cerebral white matter (Raz *et al.* 1997; Wahlund *et al.* 1990; Wahlund *et al.* 1996), significant total white matter volume loss is not found (Jernigan *et al.* 1991a; Pfefferbaum *et al.* 1986; Pfefferbaum *et al.* 1990; Pfefferbaum *et al.* 1994; Raz *et al.* 1997; Raz *et al.* 1998). My data are consistent with this finding. This phenomenon may be due to concomitant factors with opposing influence: the loss of myelin associated with ageing (Ansari and Loch 1975) may reduce white matter bulk, whereas the simultaneous expansion of the capillary network and swelling of perivascular spaces (Meier-Ruge *et al.* 1992; Ishiwata *et al.* 1998) may enlarge white matter bulk. In accordance with previous CT and MRI literature, my data show an

increase in the CSF compartment with age, best described by a linear function. A small but significant decline of TIV with age is noted in males and a smaller insignificant trend in females, which most probably reflects the secular trend of increasing head size over the last century. The mean absolute grey – white matter volume ratio was 1.89, and the mean fractional grey-white volume ratio was 1.82. Grey-white matter ratios vary widely in the literature, for example post mortem and in vivo studies, using a variety of methodologies, report ratios in a wide range from approximately 3 – 1.1, dependent on age (e.g. Caviness *et al.* 1996; Guttmann *et al.* 1998a; Pfefferbaum *et al.* 1994; Resnick *et al.* 2000).

Regional effects of age

These data support the theory of a heterogeneic response of various compartments of the brain to ageing. Accelerated loss of grey matter volume is noted symmetrically in parietal lobes (angular gyri), pre- and post- central gyri, insula and anterior cingulate cortex. Accelerated loss of grey matter concentration in noted in the left middle frontal gyrus, left planum temporale and transverse temporal gyri bilaterally. There is relative preservation of grey matter volume symmetrically in the amygdala, hippocampi, entorhinal cortices and lateral thalami, with relative preservation of grey matter concentration more diffusely in the thalami. This is in accordance with previous work showing a predominant age effect in the parietal lobes (Resnick *et al.* 2000) and prefrontal grey matter (Raz *et al.* 1997); a smaller effect in fusiform, inferior temporal and superior parietal cortices and minimal change in the hippocampal formation (Raz *et al.* 1997). The lack of a substantial age-related structural change in the amygdala/hippocampal regions demonstrated by my data and work by (Raz *et al.* 1997) also corresponds with recent evidence (unpublished data) of preserved regional cerebral blood flow in the mesial temporal lobes with age. Animal and human pathological studies have demonstrated age-related changes in the hippocampus (Kemper 1993; Landfield 1988; Desgranges *et al.* 1998; Insausti *et al.* 1998) as have previous structural imaging studies (Jernigan *et al.* 2001) and recent work using MR spectroscopy (Schuff *et al.* 1999). A possible explanation for this discrepancy could be the sampling methods used to assess the hippocampus: ROI techniques used in these previous studies may be observer dependent and subject to error due to the complex and variable shape of the hippocampus. It should be noted that VBM examines age-related changes in local tissue composition, deliberately

adjusting for macroscopic and shape differences that classical ROI-based morphometric approaches characterise. It is also worth emphasising that my data are reporting regionally specific changes within the grey matter compartment over and above global grey matter change, whereas most other studies report changes without covarying out global grey matter volume changes. A recent ROI and voxel-wise morphometry paper in young adults reported that the volume of the amygdala appeared to be independent of age and gender, whereas the hippocampi showed shrinkage with age in men but not in women (Pruessner *et al,* 2001). The statistical model used in this paper did not model the global amount of grey matter and the age range is substantially different, so it cannot be directly compared with my method.

Sex differences

The whole brain volume and grey and white matter partitions were larger in males compared to females in accordance with previous literature (Coffey *et al.* 1998; Gur *et al.* 1991; Murphy *et al.* 1996; Raz *et al.* 1997).

There was an interaction of sex with age-related global grey matter decline, with a steeper age-related decline in males, in accordance with previous reports (Coffey *et al.* 1998; Cowell *et al.* 1994; Gur *et al.* 1991; Murphy *et al.* 1996; Oguro *et al.* 1998; Xu *et al.* 2000a; Guttmann *et al.* 1998b), although this effect was not significant when global grey matter was expressed as a fraction of TIV. There was no interaction of sex with regional grey matter volume or concentration, contrary to a report from (Murphy *et al.* 1996) who showed greater age related loss in frontal and temporal lobes in males, and greater loss in hippocampus and parietal lobes in females. There was no significant interaction of sex with age for CSF or white matter change either globally or regionally. Some previous studies have found greater increases in CSF spaces in males compared with females (e.g. Coffey *et al.* 1998; Gur *et al.* 1991), although this has not been reproduced by others (Guttmann *et al.* 1998a).

Many previous reports have suggested regional sex differences in age-related decline, for example, Raz *et al.* (1997), demonstrated a steeper trend of ageing in the inferior temporal cortex in males. Xu *et al.* (2000a) showed significantly more atrophy in posterior right frontal lobe, right temporal lobe, left basal ganglia, parietal lobe and cerebellum in males, using semi-automated region of interest MR techniques in 331 subjects, but without partitioning the brain into grey and white matter compartments. Salat *et al.* (1997) showed sex differences in the corpus callosum with ageing, but no

atrophy of the pons or cerebellum. Gunning-Dixon *et al.* (1998) showed differential shrinkage of the globus pallidus in males. Murphy *et al.* (1996) reported sex differences in the ageing pattern of whole brain, frontal, temporal and parietal lobes and hippocampus. It is difficult to compare such results with my data, particularly since the majority of studies are confounded to a greater or lesser degree by methodological factors such as normalising for brain size, region of interest measurements, variable quality of structural images and the use of manual segmentation techniques.

Methodological issues

In order for VBM to be valid a number of assumptions need to hold. All raw original structural images need to be acquired on the same scanner with identical imaging parameters since different acquisitions can result in intensity and geometric variations. If such variations are systematic they can emerge erroneously as group differences. In this study all subjects were scanned on the same scanner using identical imaging parameters and the scanner was subject to strict quality control. The templates were created from a subset of the group, which matched the mean age, age-range and sex of the group in order to avoid bias during the spatial normalisation step. The non-linear spatial transformations used in this study were used to match global brain shape differences whilst preserving regionally specific effects of interest. Since this approach does not provide precise sulcal and gyral matching (see Chapter 2) a smoothing kernel is used to accommodate imperfect registration of variable structures. By applying the modulation step information from the deformation fields is incorporated and allows inferences about grey (and white) matter volume. While my approach cannot provide exact matches between small cortical or deep grey matter structures (which would require time consuming high dimensional warps), it provides additional information in a practical way for large subject cohorts.

The segmentation step needs to correctly identify grey and white matter and CSF partitions. In areas where grey/white matter differentiation is poor, for example in the brainstem and thalamus, voxels may be incorrectly classified, even when an optimal pre-processing method is used. This effect is demonstrated in the significant lateral thalamic differences detected on both the grey and white matter analyses. These age-related differences are real and significant but their cause cannot be attributed directly to grey or white matter changes, rather to the way the changes impact on the

classification of grey or white matter. This problem can be diminished by optimising the MR structural imaging sequence to provide better grey/white matter contrast and segmentation (Deichmann *et al.* 2000; Deichmann *et al.* 2002). Additional improvements can be made to the segmentation procedure by the creation of customised prior probability maps appropriate to the subject group of interest. This has particular relevance when studying patient populations whose brain structure differs greatly from young normal subjects. Elderly subjects with a few small white matter hyperintensities were deliberately included. In addition perivascular spaces enlarge with age and there may be subtle diffuse MRI T1 signal changes in the white matter of elderly subjects. These could potentially result in misclassification of CSF or grey matter, leading to a potential overestimation of CSF and grey matter and an underestimation of white matter. Since no age related global white matter atrophy was observed, one can conclude that perivascular spaces and small white matter lesions were predominantly classified as white matter. The inclusion or exclusion of the modulation step facilitates the assessment of *absolute amount* or *concentration* of a region of tissue. The latter does not however provide information about cytoarchitecture, neuronal packing density or cell morphometry; hence the term concentration is preferred to density.

The statistics I used to identify structural differences assume that the residuals after fitting the model are normally distributed and this is one of the reasons for using smoothing. If the data are not well behaved such as in unbalanced study designs (single subject versus group comparisons) or in diseased populations it may be appropriate to perform nonparametric statistical analyses (Ashburner & Friston, 2000, Holmes et al., 1996). The voxel-based extent statistic available within SPM, should not be used with VBM. This statistic is based upon the number of connected voxels in a cluster defined by a pre-specified threshold. In order to be valid, this test requires the smoothness of the residuals to be spatially invariant, but this is not the case with neuroanatomy which has a highly non-stationary nature and thus leads to inexact p values (Ashburner & Friston, 2000; Worsley et al, 1999).

There is a great deal of endogenous variability within and between brain regions, and in a recent paper the authors report that 80% of the total variance in gyral volume arises from individual and specific gyri, whilst only 10% of the total variance reflects uniform scaling to total neocortical volume (Kennedy *et al.* 1998). In addition there may be contributions from artifactual sources such as imperfections in the spatial

normalisation that themselves show regional specificity. These considerations have implications for the sensitivity of any morphometric technique to detect changes in regions of high variance. The VBM technique I have developed and used may be relatively insensitive to subtle age effects in regions of high variance whilst more sensitive to change in regions of low variance. However SPM employs a regionally specific estimate of variance that obviates some of these sources of error. Regional variance may well explain inconsistencies of the literature with regard to regionally specific age changes especially in small brain structures. The hippocampus, for example, is a relatively small structure with a complex architecture that often demonstrates a degree of variability between subjects on visual inspection. VBM has demonstrated subtle changes within the hippocampus in a group of taxi-drivers that corroborated independent and accurate ROI measurements (Maguire et al, 2000), suggesting that the technique can register and segment small structures with some degree of accuracy. There is more potential for error in patients, for example those with Alzheimer's disease, or indeed in normal elderly subjects, since the grey/white matter contrast is reduced and segmentation may be less accurate. As high dimensional warping techniques advance to the stage where they can provide accurate mapping of small gyri in large subject groups in a time efficient and practical way, then some of these sources of ambiguity will be more satisfactorily resolved.

Conclusion

My data provide evidence of specific patterns in the structural brain correlates of ageing, not only globally between grey and white matter compartments, but also locally within regions of the brain. The use of large numbers of subjects in this study permitted the examination of relatively subtle age-related effects, but also highlighted the need for a rigorous and optimal VBM method to avoid errors of interpretation caused by misclassification of non-brain voxels. Significantly the data have been obtained with a fully automated method that eschews observer bias and have been collected in life, eliminating post mortem and agonal changes. They also demonstrate that VBM is a suitable tool for detecting subtle structural brain changes in normal subjects.

CHAPTER 4

NORMATIVE DATA

BRAIN ASYMMETRIES AND EFFECTS OF SEX AND HANDEDNESS

Summary

In this experiment, VBM is used to characterise physiological brain asymmetries and the effects of sex and handedness on brain structure in a large group of normal subjects. VBM confirms the well-established lobar asymmetries whilst offering new insights into more subtle regional asymmetries, including an interaction of sex with asymmetry of Heschl's gyrus. VBM confirms the well known global differences in brain volume between the sexes whilst expanding upon regional sex differences in grey and white matter. Despite a prior expectation of an effect of handedness on brain structure, particularly in the central sulcus region, VBM does not detect any structural difference associated with left and right-handedness.

Introduction

The main and most consistently reported human brain asymmetries include the right frontal and left occipital lobar protuberances causing marked indentations of the inner table of the skull (the so called petalia) (Chiu and Damasio 1980; Gundara and Zivanovic 1968; LeMay 1986). Asymmetry of the Sylvian fissure is one of the earliest and most reproducible reported brain asymmetries. The trajectory of the Sylvian fissures is angled upwards (dorsally) more steeply in the right hemisphere (Cunningham 1892; cited in Geschwind and Levitsky 1968; Geschwind and Galaburda 1985a; Loftus *et al.* 1993; Ratcliff *et al.* 1980; Thompson *et al.* 1996a; Thompson *et al.* 1998; Westbury *et al.* 1999; Hochberg and Le May 1975). This trajectory asymmetry reflects another well-known posterior Sylvian asymmetry – namely asymmetry of the planum temporale that is more pronounced on the left side (Geschwind and Levitsky 1968; Geschwind and Galaburda 1985a; Steinmetz *et al.*

1989; Steinmetz 1996; Wada *et al.* 1975). This is associated with microscopic asymmetry of cytoarchitectonic area Tpt that is characteristically found in this region (Galaburda *et al.* 1978). Additional macroscopic asymmetry has been reported in Heschl's gyrus which houses primary auditory cortex and appears to be larger on the left side (Penhune *et al.* 1996; Rademacher *et al.* 1993; Rademacher *et al.* 2001). This difference has been ascribed to a larger volume of white matter than grey matter (Penhune *et al.* 1996). Several older and more recent studies confirm asymmetry of Broca's area (Brodmann areas 44 and 45) being larger in the left hemisphere (Amunts *et al.* 1996; Annett 1970; Falzi *et al.* 1982; Foundas *et al.* 1995; Foundas *et al.* 1996; Foundas *et al.* 1998a; Geschwind and Galaburda 1985a; Penhune *et al.* 1996). It is less clear from the literature what effect handedness and sex have on many of these asymmetries. One might for example expect functional lateralisation such as handedness and language to impact upon the structure of sensorimotor cortex and language regions respectively.

Certainly there are well-established sex differences in global brain size with males having approximately ten percent larger total brain volumes (Peters *et al.* 1996), but many post mortem and *in vivo* reports of regional sex differences conflict. Reports of regional sex effects include a larger left planum temporale (PT)/anterior Sylvian fissure in males (e.g. Kulynych *et al.* 1994); but see Foundas *et al.* (1999); cytoarchitectural dimorphism of the PT cortex, with significantly higher percentages of grey matter in females (Gur *et al.* 1999; Gur *et al.* 2002; Schlaepfer *et al.* 1995), which may possibly be explained by higher neuronal densities and neuronal number estimates in females (Witelson *et al.* 1995). Females have also been reported to have a larger anterior commissure (Allen and Gorski 1991; Allen and Gorski 1992) and a more bulbous posterior corpus callosum (Bishop and Wahlsten 1997; Habib *et al.* 1991; Steinmetz *et al.* 1992; Witelson 1985), although this latter finding has been refuted by others (Byne *et al.* 1988; Constant and Ruther 1996). Larger caudates have been observed in females (Giedd *et al.* 1996), although conversely there are also reports of smaller caudates in females (Filipek *et al.* 1994). Other reports of sexual dimorphism include leftward asymmetry of the inferior parietal lobule in males (Frederikse *et al.* 1999; Frederikse *et al.* 2000); a larger volume of one of the interstitial nuclei of the anterior hypothalamus in males (Byne *et al.* 1988) and larger globus pallidus and putamen volumes in males (Giedd *et al.* 1996). These conflicting reports in the literature of sex differences for regional structure not only reflect the different

measurement techniques but could also in part relate to inconsistent ways of de-trending differences in global brain volume from the data. There is a potential for global brain sex differences to masquerade as regional differences if substructure metrics depend nonlinearly on brain volume. For example, in an attempt to factor out effects of gross variations in brain size many earlier postmortem and neuroimaging studies expressed regional volumes as a ratio to global volume or weight. But such measures may be highly correlated with global measures. More recently linear statistical models such as analyses of covariance (ANCOVA) or multiple correlation analyses have been used to model global differences, but even these may be flawed since they do not model nonlinear correlations (Thompson *et al.* 2001a).

Handedness, as a habitual lifelong manual behaviour, may plausibly have structural correlates in the sensorimotor system. Melsbach *et al.* (1996) showed morphological asymmetries of motor neurons innervating upper extremities. More recently Amunts *et al.* (1996; 1997; 2000), reported deeper left central sulci in right-handed males and vice versa in left-handed males. This macrostructural asymmetry was associated with concordant leftward microstructural asymmetry of neuropil volume in Brodmann's area 4, suggesting that hand preference is associated with increased connectivity and an increased intra-sulcal surface of the precentral gyrus in the dominant hemisphere. White *et al.* (1994, 1997) examined the central sulcus of 42 post mortem brains in detail, and found a slight, but insignificant trend towards a longer left central sulcus and larger Brodmann areas 3 and 4 on the left side. Several studies have shown structural and functional asymmetries correlating with handedness. For example, Steinmetz (1996) reported decreased leftward asymmetry of the PT in left-handers (see also Geschwind and Galaburda 1985a). Others, however, have demonstrated that this finding may well be an artefact of the increased likelihood of atypical functional organisation in left-handers (Foundas *et al.* 1995; Moffat *et al.* 1998; Ratcliff *et al.* 1980). These researchers have found that, whereas subjects with left-hemisphere speech representation show a strong leftward asymmetry in the PT (regardless of handedness), subjects with right hemisphere speech representation do not show a consistent PT asymmetry. Moffat *et al.* (1998) also showed that left-handed subjects with left-hemisphere speech functions had a larger corpus callosum than either left-handed subjects with right-hemisphere speech representation or right-handed subjects. In addition, there have been reports of a handedness effect on frontal and occipital lobe asymmetry (Bear *et al.* 1986; Kertesz *et al.* 1990; Weinberger *et al.*

1982; Zilles *et al.* 1996).

In this study, VBM delivers a voxel-wise overview of regional physiological morphological effects in a large group of normal subjects to characterise and quantify human brain asymmetry and the effects of sex and handedness on macroscopic and mesoscopic brain structure.

Methods

Approval for the study was obtained from the Local Research Ethics Committee of the National Hospital for Neurology and Neurosurgery (UCLH, NHS Trust) and the Institute of Neurology (UCL). The study group was selected from a population of 1761 normal volunteers who responded to advertisements and were scanned at the Wellcome Department of Cognitive Neurology from February 1998-December 1999. All subjects with incomplete questionnaires, any neurological, medical, psychiatric condition or migraine were excluded. Inclusion criteria included: 1) Normal MRI brain as determined by an experienced neuroradiologist (myself). Any MRI scans with structural abnormalities, prominent normal variants (e.g. mega cisterna magna, cavum septum pellucidum) or technical artefacts were excluded. 2) No history of alcohol intake of more than 30 units/week or intake of more than 10 units within 48 hours prior to scanning. 3) No history of severe head trauma requiring medical attention. 4) No history of cognitive difficulties. Handedness was assessed by a simple questionnaire documenting which hand subjects wrote with, which foot they kicked with and whether or not they had been encouraged to change handedness as a young child. I only included subjects with a clear-cut hand preference, and no history of coercion to change handedness as a young child. In all, 465 subjects met the inclusion criteria. They comprised 29 left-handed females (aged 18-75, mean 38; 5 right-footed), 171 right-handed females (aged 18-79, mean 33; 3 left-footed, 4 equal-footed), 38 left- handed males (aged 20-59, mean 36; 9 right-footed) and 227 right- handed males (aged 17-67, mean 30, 10 left-footed, 3 equal- footed).

Structural MRI scanning protocol

Magnetic resonance imaging was performed on a 2 Tesla Siemens MAGNETOM Vision scanner. A 3D structural MRI was acquired on each subject using a T-1 weighted MPRAGE sequence (TR/TE/TI/NEX 9.7/4/ 600/1, flip angle

12°, matrix size 256 × 192, FOV 256 × 192, yielding 108 sagittal slices, slice thickness of 1.5mm and in plane resolution of 1mm × 1mm.

Data analysis

Data were analysed using the optimised VBM protocol as detailed in Chapter 2. Processing components pertinent to this study will be emphasised here.

Customised Templates

A whole brain template was created from 120 constituent images chosen pseudorandomly from the group, consisting of 60 males (30 left-handed) and 60 females (30 left-handed) matched for age, with a mean age corresponding to that of the whole group. Each image was normalised to the SPM T1 template, which approximates Talairach space. These normalised images were averaged and the resulting image was smoothed with an 8 mm Gaussian kernel to create a template in which the left side of the image represents the left hemisphere. Grey and white matter templates were derived separately by normalising all 465 images to the whole brain template, then segmenting, extracting, smoothing and finally averaging all the grey/white matter images to create separate grey/ white matter templates (details of each step to follow). Symmetric grey and white matter and whole brain templates were derived separately by averaging each template with its left-right flipped version. In these symmetrical templates, each side of the image represents an average of both hemispheres.

Normalisation for asymmetry analyses

The standard optimised normalisation protocol was followed using the symmetrical grey and white matter templates.

Normalisation for sex and handedness analyses

Exactly the same procedures were followed, but using non-symmetric (normal) grey and white matter templates.

Statistical design for analysis of brain asymmetry.

2 × 2 × 2 (flipped/unflipped by sex by handedness) factorial analyses were performed on modulated and unmodulated grey and white matter and CSF images respectively to assess brain asymmetry and the effects of sex and handedness. I

performed conjunction analyses to detect common asymmetry effects (for example, which asymmetries are found in both males and females).

Statistical analyses of sex and handedness effects

Global effects of sex and handedness were assessed by multiple regression analyses of voxel values of grey matter, white matter and CSF respectively in a model including linear and quadratic expansions of age. Regional effects were assessed by a factorial design of sex and handedness with linear and quadratic expansions of age and globals as confounding covariates. I applied this design separately to grey and white matter modulated and unmodulated data.

Handedness analysis

A separate handedness analysis was conducted using handedness as a factor, with sex and the first order effects of age as covariates. Effects of sex and handedness on global measures were assessed by multiple regression of summed voxel values from grey matter, white matter and CSF respectively in a model including linear and quadratic expansions of age.

Results

Grey matter

Asymmetry

Extensive grey matter asymmetries common to all groups (conjunction analysis) were observed, namely larger left occipital, right frontal and right temporal lobes (the petalia) (Fig. 4.1a). Furthermore, more focal leftward (left > right) asymmetry was seen in the transverse temporal (Heschl's) gyri, frontal operculum, in the depths of the superior and inferior frontal sulci, in the mesial temporal lobe (including amygdala and hippocampus), anterior cingulate sulcus, caudate head (Fig. 4.1a) and medial cerebellum (not illustrated). Focal rightward (right>left) asymmetry was seen in the lateral thalamus, around the calcarine sulcus, anterior cingulate (Fig. 4.1a) and in the lateral cerebellum (not shown). There was a significant interaction of sex with asymmetry at the medial end of Heschl's sulcus, at the junction with PT, with males having greater leftward asymmetry (Fig. 4.1b). There was no interaction of

handedness with asymmetry, even with reduced thresholds and small volume corrections for the left posterior temporal lobe (PT), central sulci and left occipital lobe (regions where handedness effects have previously been described).

Figure 4.1a: Grey matter: asymmetry common effects

Grey matter volume (modulated data) asymmetries common to all groups superimposed on the normalised symmetrical mean grey matter image. Significant voxels ($p<0.05$ corrected) represent ipsilateral side > contralateral side asymmetry (and thus also contralateral< ipsilateral asymmetry). The colour bar represents the T score. The right frontal and temporal and left occipital lobar asymmetries are shown (petalia). Focal left>right asymmetry is seen in the frontal operculum, posterior insula (extending into Heschl's gyrus and planum temporale (PT), not shown), in the depths of the superior and inferior frontal sulci, mesial temporal lobe (including amygdala and hippocampus), anterior cingulate sulcus and caudate head. Focal right>left asymmetry is seen in the lateral thalamus, around the calcarine sulcus and anterior cingulate. (Cerebellar asymmetries are not shown).

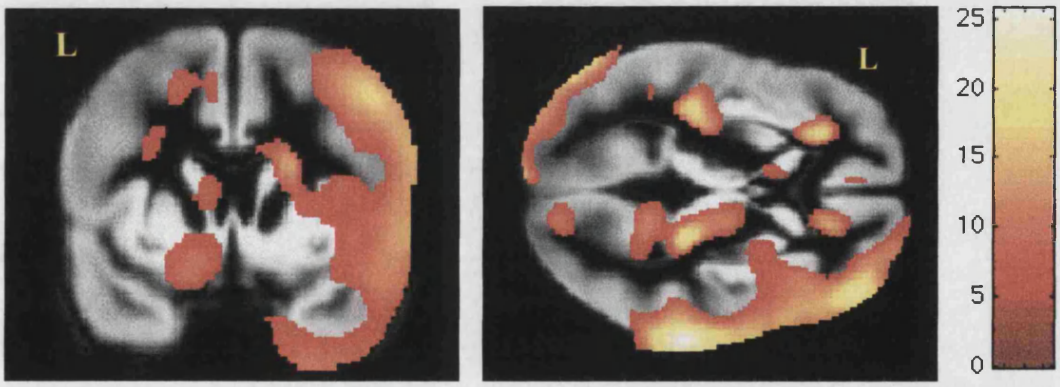

Figure 4.1b: Grey matter: increased asymmetry in males

Regions corresponding to an interaction of asymmetry with sex are superimposed on the normalised symmetrical mean grey matter image. The colour bar represents the T score. Significant voxels ($p<0.05$, corrected) are seen at the medial end of left Heschl's sulcus, at the junction with PT, with males having increased leftward asymmetry

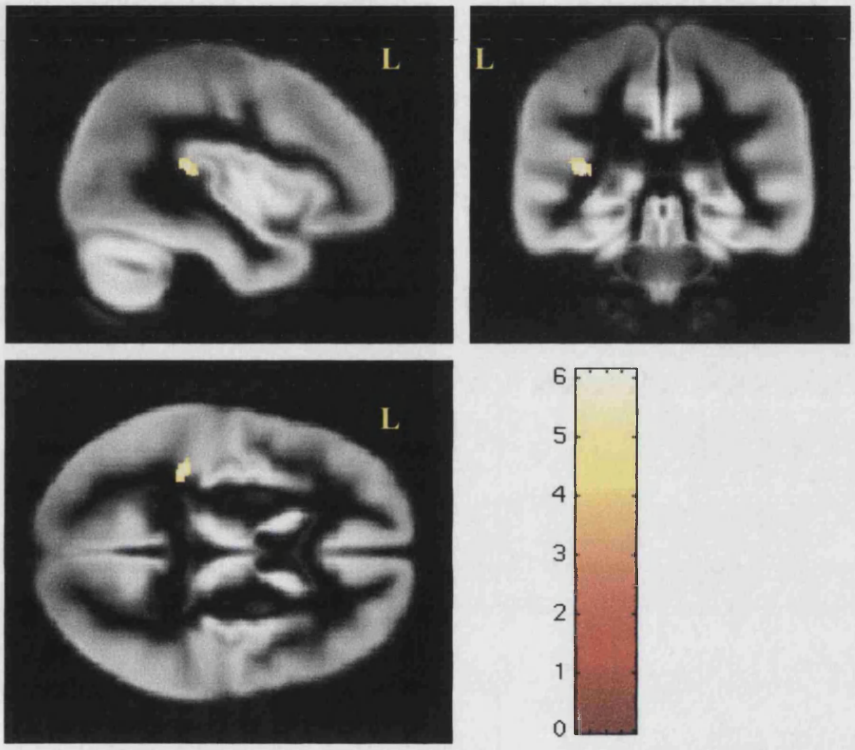

Global effects of sex

Although age was approximately matched between females and males (females 33.5 ± 13.6 years, males 30.9 ± 11.1 years), linear and quadratic expansions of age were included as covariates in the analysis since age has a marked effect on brain morphology (Good *et al.*, 2001). The mean grey matter *volume* was significantly greater in men (0.829 ± 0.069 litres) than in women (0.747 ± 0.064 litres), $F(1,458)=239.85$, $p<0.0001$) (Fig. 4.2). The mean fractional volume of grey matter (as a percentage of total intracranial volume) was also significantly greater for males than females ($p<0.0001$). The grey-white absolute volume ratio was 1.89 for females and 1.89 for males. The grey-white fractional volume ratio was 1.82 for females and 1.82 for males.

Figure 4.2: Main effect of sex on global brain tissue compartments

Box and whisker plots show the mean global volumes (modulated data) of grey matter (red), white matter (green) and CSF (blue) in females (n=200) and males (n=265). The box represents the interquartile range and the whiskers the 95% confidence intervals. The wide spread of data reflects the wide age range. Global grey matter and white matter volumes are increased in males compared with females.

Regional effects of sex

There were no interactions between sex and handedness. There was a significant main effect of sex. Males have significantly increased grey matter *volume* bilaterally in the amygdala, hippocampi, entorhinal and perirhinal cortex, in the anterior lobes of cerebellum and in the left anterior superior temporal gyrus (Fig. 4.3a (i and ii)). I did not detect any regions of significantly increased grey matter *concentration* in males. Females have significantly increased grey matter *volume* in the right middle temporal, lateral orbital and left parahippocampal gyri (Fig. 4.3b(i)), in the right transverse temporal (Heschl's) and both inferior frontal gyri (not illustrated), in right planum temporale (PT) and within the right inferior parietal and cingulate gyri (Fig. 4.3b(ii)). There was also increased grey matter *volume* in the banks of the left superior temporal sulcus and the banks of both central sulci (Fig. 4.3b(iii)). Females have significantly increased grey matter *concentration* extensively and relatively symmetrically in the frontal, posterior temporal and parietal cortical mantle, parahippocampal gyri, adjacent to the caudate heads and within the banks of the cingulate and calcarine sulci (Fig. 4.3c (i and ii)).

These regional main effects of sex were also observed as individual simple effects for right and left-handers. The stereotaxic coordinates of the maxima and corresponding p and T values are tabulated in Table 4.1

Table 4.1: Main effect of sex on grey matter.

x	y	z	p (corrected)	T statistic	location
Grey matter volume: modulated females > males					
-42	-30	-4	p<0.0001	6.16	L superior temporal sulcus
72	-14	10	p<0.0001	5.99	R planum temporale/Heschl's g
57	40	-9	p<0.0001	5.94	R lateral orbital gyrus
24	64	-8	p<0.0001	5.90	R frontomarginal gyrus
-15	-34	-4	p<0.0001	5.85	L parahippocampal gyrus
-39	-32	34	p<0.0001	5.79	L central sulcus
76	-34	-4	p<0.0001	5.61	R middle temporal gyrus
36	-26	36	p=0.002	5.37	R central sulcus
2	-22	50	p=0.001	5.54	Posterior cingulate
52	36	21	p=0.003	5.24	R inferior frontal gyrus
-58	34	9	p=0.005	5.16	L inferior frontal gyrus
-32	-88	34	p=0.002	5.35	L angular gyrus
66	-19.5	27	p=0.002	5.25	R inferior parietal gyrus
Grey matter volume: modulated males > females					
27	-2	-28	p<0.0001	7.29	R amygdala/hippocampus
-20	-3	-24	p<0.0001	7.24	L amygdala/hippocampus
-45	28	-26	p<0.0001	6.18	L anterior superior temporal g
-27	-60	-22	p=0.001	5.53	L cerebellum
-33	-58	-22	p=0.001	5.50	R cerebellum

Figure 4.3a: Grey matter volume: regional increases in males vs. females

Regions of increased grey matter volume (modulated data) are superimposed on a normalised symmetrical grey matter mean image (i) and a normalised single subject structural image (ii). The colour bar represents the T score. Significant voxels ($p<0.05$ corrected) are seen symmetrically in the mesial temporal lobes, in amygdaloid hippocampal complexes, entorhinal and perirhinal cortex, in the anterior lobes of the cerebellum, and in the left anterior superior temporal gyrus (ii). A few voxels can be seen at the junction of the superior edge of the right putamen and internal capsule (i), which may be misclassified.

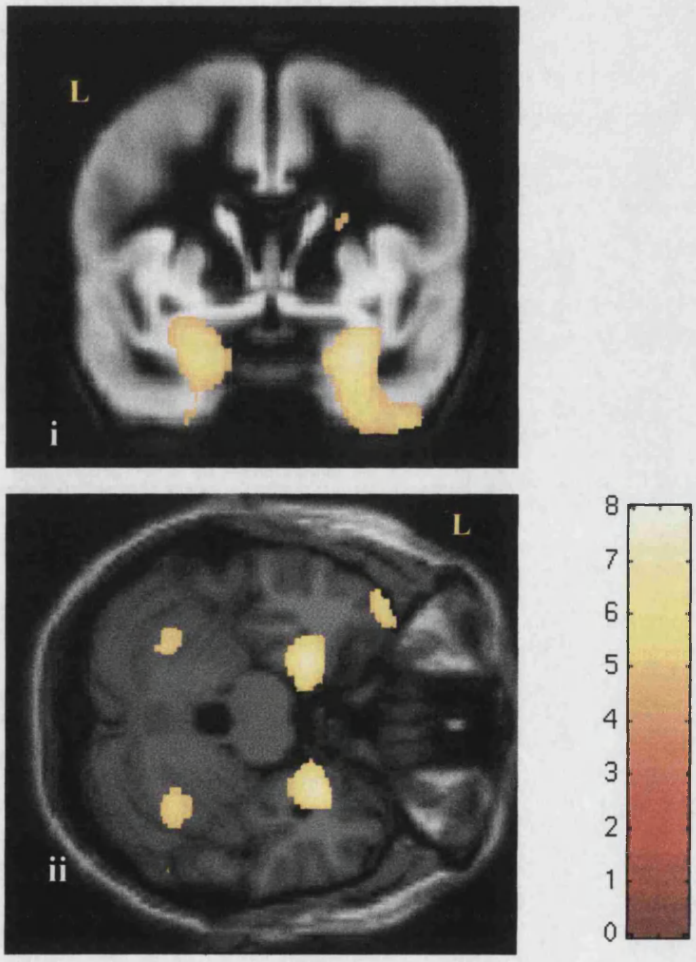

Figure 4.3b: Grey matter volume: regional increases in females vs. males

Regions of increased grey matter volume (modulated data) are superimposed on a normalised mean grey matter image (i, ii) and a normalised single subject whole brain image (iii). The colour bar represents the T score. Significant voxels ($p<0.05$ corrected) are seen in the right middle temporal gyrus, left parahippocampal gyrus, right lateral orbital and frontomarginal gyri (i); in the right inferior parietal gyrus, cingulate gyrus and right transverse temporal gyri (Heschl's) gyri/ planum temporale (PT)(ii), and within the banks of the left superior temporal and both central sulci (iii). (Significant voxels in the inferior frontal gyri are not shown).

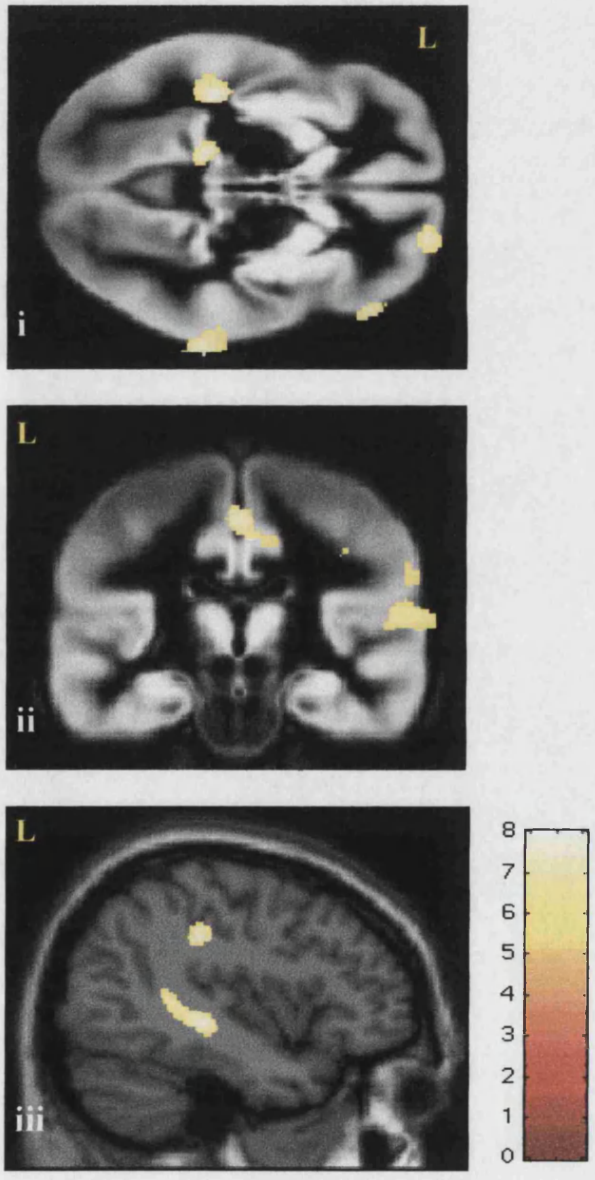

Figure 4.3c: Grey matter concentration: regional increases in females vs. males

Regions of increased grey matter concentration (unmodulated data) are superimposed on a normalised single subject image (i) and the normalised symmetrical grey matter mean image (ii). The colour bar represents the T score. Significant voxels are seen diffusely in the cortical mantle, parahippocampal gyri and in the banks of the cingulate and calcarine sulci. Significant voxels are also seen around the anterior limbs of the internal capsules, possibly reflecting caudate/lentiform nucleus changes, but probably also misclassification of voxels into grey/white matter.

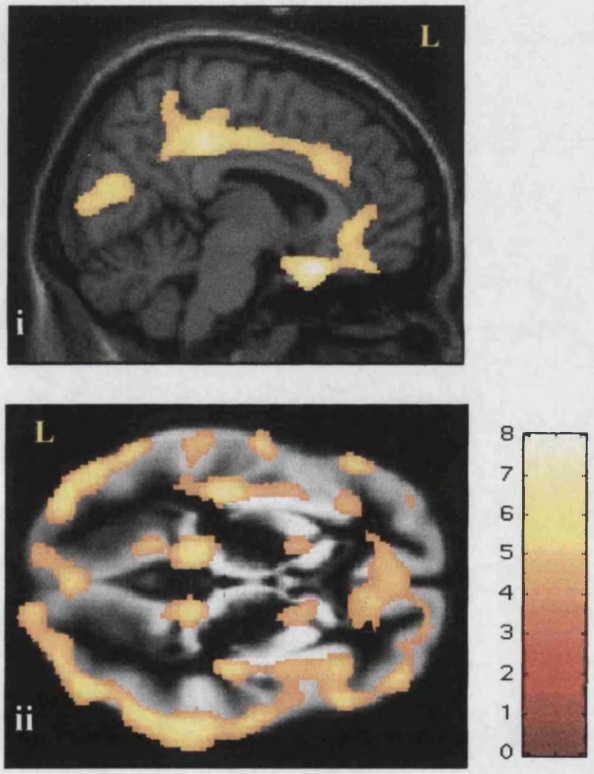

Global effects of handedness

The mean age of left and right-handers differed significantly ($p<0.001$), left handers (36.8 ±13.9 years) and right-handers (31.2 ± 11.8 years). When linear and quadratic effects of age were covaried out, there was no significant difference in global grey matter *volume* between left and right-handers, $F(1,458)<1$.

Regional effects of handedness

There was no significant difference in grey matter *volume* or *concentration* between right and left-handers on any of the handedness analyses. Furthermore, I did not detect regional differences, even with lowered thresholds and small volume corrections for primary motor and sensory cortex (particularly in the hand area) according to my prior hypothesis.

White matter

Asymmetry

Extensive white matter asymmetries common to all groups (conjunction analysis) were detected adjacent to areas of grey matter asymmetry (Fig. 4.4). There was a significant interaction of sex with asymmetry with increased leftward asymmetry adjacent to Heschl's gyrus/PT (Fig. 4.5).

Figure 4.4: White matter asymmetries

Regional areas of asymmetry common to the whole group are superimposed on the normalised symmetrical white matter mean image. The colour bar represents the T score. Significant voxels are seen adjacent to the regions of grey matter asymmetry

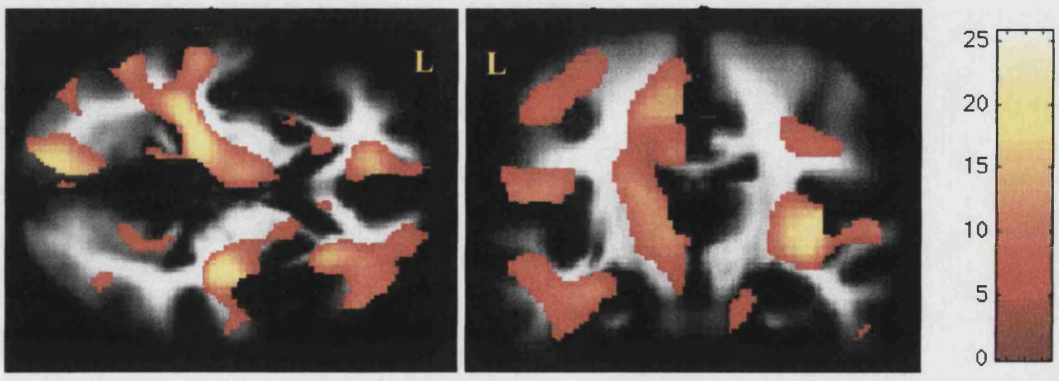

Figure 4.5: White matter: Interaction of sex with asymmetry

Regions corresponding to an interaction of asymmetry with sex are superimposed on the normalised symmetrical white matter mean image. The colour bar represents the T score. Significant voxels are seen adjacent to the medial end of left Heschl's gyrus and PT, with males having increased leftward asymmetry

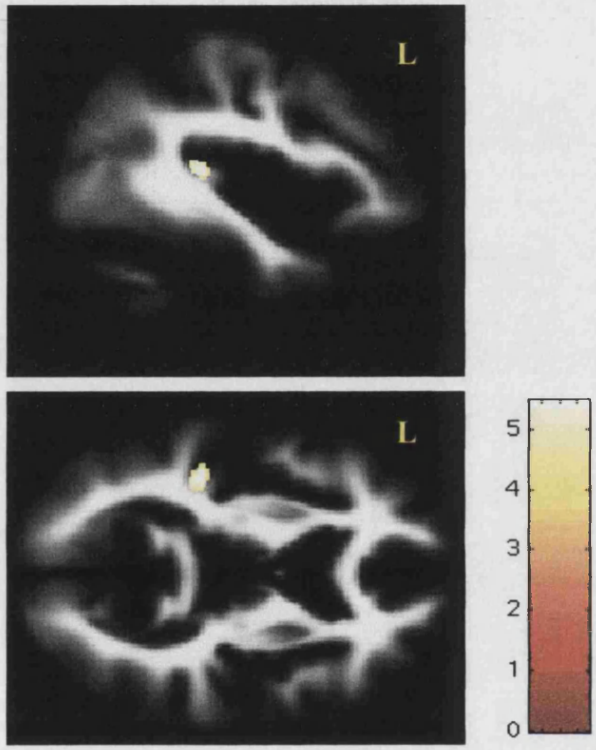

Global effects of sex

The mean white matter *volume* was significantly greater in men (0.454 ± 0.044 litres) than in women (0.395 ± 0.041 litres), F (1,458)=209.33, p<0.0001 (Fig. 4.2).

Regional effects of sex

There were no interactions between sex and handedness. There was a significant main effect of sex. Males had significantly increased white matter *volume* bilaterally in the anterior temporal white matter extending into the internal capsules (temporal stems)(Fig. 4.6a), and significantly increased white matter concentration bilaterally in the anterior temporal and posterior frontal lobes (Fig. 4.6b). Females had significantly increased white matter *volume* bilaterally in posterior frontal lobes and in

the left temporal stem/optic radiation (Fig. 4.7a). Females had significantly increased white matter *concentration* bilaterally in the internal and external capsules and optic radiations (Fig.4.7b). These changes were also observed as individual simple effects in right and left-handers. No corpus callosum differences were observed.

Figure 4.6a: White matter volume: increases in males vs. females

Regions of increased white matter volume (modulated data) are superimposed on a normalised mean white matter image. Significant voxels are seen in both temporal lobes, extending upwards into the temporal stems and internal capsules.

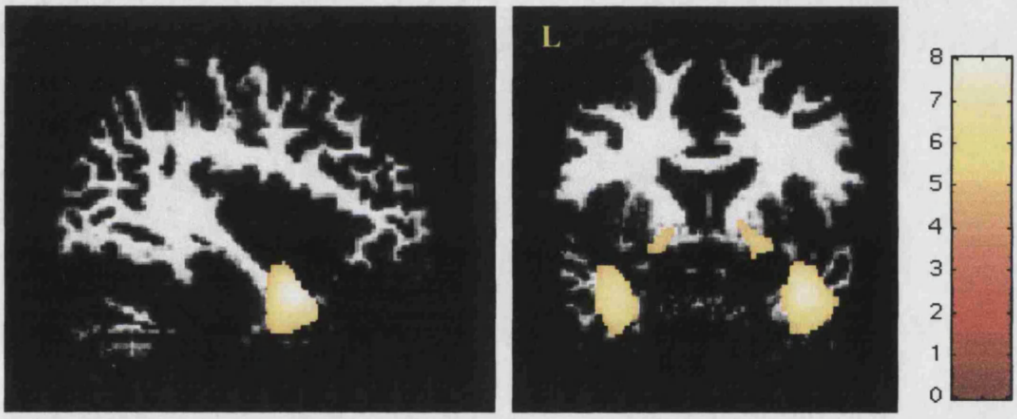

Figure 4.6b: White matter concentration: increases in males vs. females

Regions of increased white matter concentration (unmodulated data) are superimposed on the normalised mean white matter image. Significant voxels are seen bilaterally in anterior temporal white matter, and adjacent to the central sulcus.

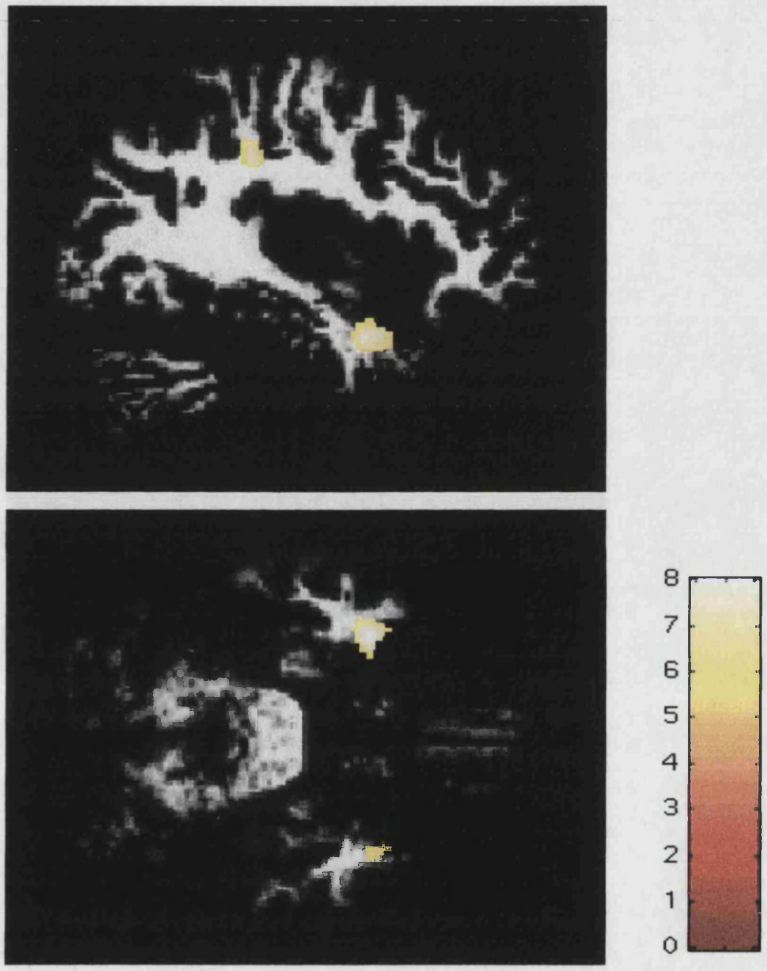

Figure 4.7a: White matter volume: increases in females vs. males.

Regions of increased white matter volume (modulated data) are superimposed on the normalised mean white matter image. Significant voxels are seen bilaterally in posterior frontal white matter, left temporal stem and optic radiation.

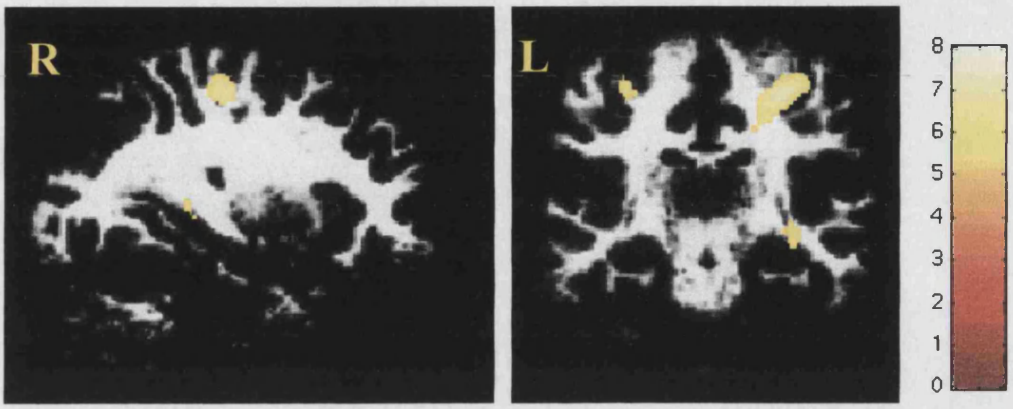

Figure 4.7b: White matter concentration: increases in females vs. males.

Regions of increased white matter concentration (unmodulated data) are superimposed on the normalised mean white matter image. Significant voxels are seen bilaterally in internal and external capsules and optic radiations. A number of voxels are also seen in globus pallidus and putamen on both sides, and are probably misclassified voxels owing to poor tissue contrast in these regions.

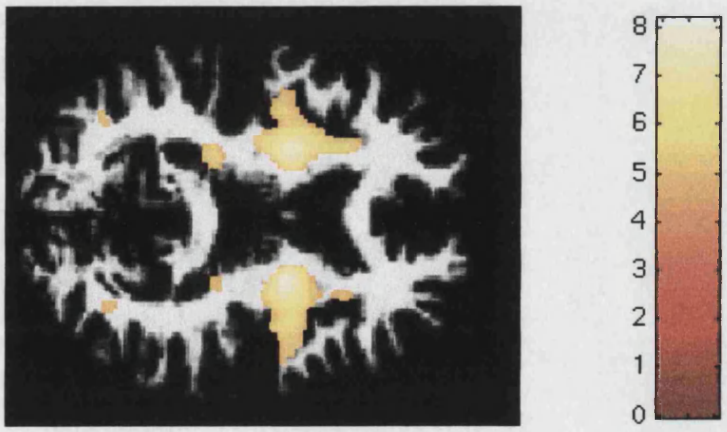

Global effects of handedness

There was no significant difference in global white matter volume between left and right-handers

Regional effects of handedness

Neither white matter *volume* nor *concentration* differed between right and left-handers. In order to prevent potential type 2 error owing to stringent whole brain correction, thresholds were reduced (down to 0.05 uncorrected) and small volume corrections performed on regions where I had a prior hypothesis for differences (such as hand/foot primary motor and sensory cortex). But still no structural difference was evident.

CSF

Asymmetry:

CSF asymmetry was noted around the regions of grey matter asymmetry, particularly in the right hemisphere and most prominently in the right Sylvian fissure

Global effects of sex and handedness:

The mean CSF *volume* did not differ significantly between males (0.397 ± 0.040 litres) and females (0.401 ± 0.048 litres), $F(1,458)=1.91$, $p=0.22$). There was no significant effect of handedness on CSF *volume* $F(1,458)<1$ (Fig. 2).

Regional effects of sex and handedness

There was no interaction between sex and handedness and no main effect of handedness. There was a significant main effect of sex. Females had increased CSF volume in the lateral ventricles. Males had increased CSF volume in the peri-mesencephalic cistern, anterior and superior interhemispheric fissure.

Discussion

Brain asymmetry, and interactions with sex and handedness

My data confirm larger left occipital and right frontal lobes, consistent with

previous reports (e.g., Chiu and Damasio 1980; Geschwind and Galaburda 1985a; Gundara and Zivanovic 1968; Kennedy *et al.* 1999; LeMay 1986). The right frontal asymmetry extended into central and even temporoparietal regions, although the reasons for this are unclear. Focal asymmetric enlargement of grey matter was seen at the posteromedial edge of the anterior transverse temporal (Heschl's) gyrus on the left, adjacent to the planum temporale, corroborating recent studies using accurate cortical mapping techniques (Thompson *et al.* 1998; Thompson *et al.* 2001a) and post mortem data (e.g. Geschwind and Levitsky 1968; Geschwind and Galaburda 1985a). In males this leftward asymmetry was more pronounced, and was observed in both grey and white matter. These data are consistent, in part, with those of Penhune *et al.* (1996), who found a greater volume of white matter (but not grey matter) in left Heschl's gyrus, but did not observe an interaction with sex. The discrepant results could reflect the smaller sample size in the Penhune study, or the local nature of the sex effect: Penhune's analyses were conducted on measurements of the whole of Heschl's gyrus. The observation of increased leftward asymmetry in males also concur with Kulynych *et al.* (1994) and Kansaku *et al.* (2000), who localised the leftward asymmetry to PT, and Witelson and Kigar (1992) who showed increased asymmetry of the horizontal segment of the Sylvian fissure (an indirect index of PT) in males. A recent study using accurate cortical mapping techniques corroborated these findings (Thompson *et al.* 2001a) and also reported superior and inferior temporal sulcal asymmetries (left anterior to right) and post-central cortex asymmetries (further anterior on the right). Voxel-based morphometry demonstrated additional temporal lobe asymmetries, namely, increased grey matter in the right lateral temporal lobe and left mesial temporal lobe, as well as caudate and cerebellar asymmetries.

Asymmetric white matter changes were observed predominantly adjacent to respective grey matter changes. Biologically, it seems plausible that regional cortical change is associated with corresponding change in the adjacent white matter connections. This observation may however in part reflect an edge effect, for example, if the interface of one tissue compartment is displaced the difference might be reflected in both compartments. A recent post mortem study ascribed leftward PT asymmetry to larger white matter volumes and axons with thicker myelin sheaths, and not to proliferation of glia or the density of cortical to cortical projections of neurons. These data confirm leftward asymmetry of white matter adjacent to the left PT, although, many other regions of white matter asymmetry were also detected.

Sex differences

These data concur with well-established findings of increased global brain volumes in males. The mean absolute and relative grey-white volume ratios were 1.89 and 1.82 respectively with no difference between males and females. Grey-white matter ratios vary widely in the literature, for example *post mortem* and *in vivo* studies, using a variety of techniques, report ratios in a wide range between approximately 1 and 3 (see Good *et al.* 2001c). Furthermore VBM reveals increased grey matter *concentration* extensively in the cortical mantle in females, corroborating previous histopathological reports of increased neuronal density and number in female temporal cortex (Witelson *et al.* 1995). More recent histopathological data from adolescent brains show the reverse, with larger neuronal density in 60 cortical loci in males (Rabinowicz *et al.* 1996; Rabinowicz *et al.* 1999), although clearly, such data cannot simply be projected to the adult population in view of continued brain maturation into adolescence that can vary between the sexes (Giedd *et al.* 1996; Lange *et al.* 1997). More interestingly, VBM reveals a significant main effect of sex on regional brain tissue composition. Grey matter *volume* is increased bilaterally and symmetrically in the amygdala/hippocampal complexes including entorhinal and perirhinal cortex and superior cerebellum, as well as in the left anterior temporal pole in males. In females, several relatively asymmetric foci of increased grey matter *volume* can be seen in the posterior temporal lobes, including right Heschl's gyri and PT; in the right orbital gyri; adjacent to the depths of the central sulci and in the inferior frontal gyri bilaterally and in left angular gyrus. As in the analyses for asymmetry, sex-related white matter changes were in most cases observed adjacent to respective grey matter changes. Precise interpretation of these regional structural differences is difficult giving the paucity and inconsistency of prior reports in the literature. It is beyond the scope of this manuscript to relate these findings to interpretations of brain function. Rather the aim is to present archival data in a large normal sample that will serve as a framework against which further structural and functional studies can be compared.

Handedness

VBM did not show any main effects of handedness on brain morphology, not even in the sensorimotor regions, as I had predicted. This was surprising, considering the large study group and the sensitivity of VBM to detect subtle asymmetry and sex effects and furthermore its ability to demonstrate subtle changes in the hippocampus

(Maguire *et al.* 2000), brainstem (Krams *et al.* 1999) and hypothalamus (May *et al.* 1999a) in substantially smaller study groups. But there is the possibility of insufficient power in this study to detect handedness effects. Given that many of the reported handedness effects have been found in sulcal topography (e.g., Amunts *et al.* 2000; White *et al.* 1997), it is plausible that VBM, in its current state of development is not sensitive enough to detect subtle sulcal differences. Furthermore, it is well known that there is a great degree of gyral and sulcal variation not only between individuals but also between brain regions (Kennedy *et al.* 1998). The data of White *et al.* (1997) suggest that the preferred use of the right hand in humans occurs without gross lateral asymmetry of the primary sensorimotor system. If indeed volumetric differences do occur in areas 3 and 4, then they are, at most, subtle. More importantly, White et al (1997) noted large interindividual differences in the overall extent of areas 3 and 4. Another explanation for my negative result could be an inadequate assessment of handedness and thus relative heterogeneity of the right-handed groups: time constraints made it impractical to administer a comprehensive handedness/footedness questionnaire, such as the Waterloo Handedness and Footedness Questionnaire (Elias *et al.* 1998), Annett's handedness questionnaire (Annett 1970) or the Edinburgh Handedness Inventory (Oldfield 1971). Nevertheless, hand used for writing correlates substantially (in Western populations) with laterality scores, "foot used to kick ball" was largely consistent with handedness self-reports and furthermore I excluded subjects who were not spontaneously right handed.

Conclusion

These data replicate many well established post mortem and in vivo findings of human brain structural asymmetry, whilst expanding on the regional details. The use of large numbers of subjects in this study permitted the examination of relatively subtle asymmetry and sex effects, although surprisingly, I did not detect any brain structural correlate of handedness. Significantly, these data have been characterised with a fully automated whole brain technique that avoids the subjectivity of region of interest approaches. VBM is thus emerging as a powerful unbiased technique for evaluating human brain structure in life, with important implications for the exploration of structural correlates of normality and disease.

CHAPTER 5

CLINICAL GROUPS

DEMENTIA

Guide to Reader

In this study voxel-based morphometry (VBM) is compared rigorously with the current "gold standard" morphometric technique namely independent accurate region of interest (ROI) measurements in order to validate VBM in the clinical setting. I have chosen two distinct forms of dementia that have been characterised extensively in the histopathological and neuroimaging literature so that VBM can be compared with "established" knowledge. In this sense VBM findings can be judged for biological plausibility and construct validity (comparison with the most commonly used morphometric method) in two forms of neurodegeneration exhibiting different patterns of cortical and deep grey matter atrophy.

Introduction

The gold standard for *in vivo* quantitative assessment of patterns of brain atrophy in health and disease is currently ROI-based. However, ROI measurements are laborious and time consuming. They do not accommodate changes at sites distant to the ROI and thus may be inherently biased (in spatial terms). In addition, ROI measurement errors are likely to be greater for smaller structures with complex architectures, particularly if anatomical borders are defined by arbitrary criteria. These assessments may thus be subject to wide inter- rater and intra- rater variability unless performed by dedicated experts where reproducibility is in the order of 5% (Chan *et al.* 2001). For these reasons, ROI-based morphometrics cannot provide comprehensive structural assessments of the entire brain and results are difficult to replicate and compare between laboratories. A fully automated whole brain technique such as voxel-based morphometry (VBM) avoids many of the constraints of ROI analyses, but it incorporates a series of pre-processing steps that may potentially complicate the simple

interpretation of regional changes in terms of grey matter loss. VBM therefore needs to be rigorously assessed and compared with the best techniques currently available.

In this study VBM is compared with accurate and reproducible region of interest (ROI) morphometrics (Chan *et al.* 2001) in two groups of patients with clinically and neuroradiologically distinct features. Alzheimer's disease (AD) is a diffuse neurodegenerative process characterised by the insidious onset of episodic memory impairment, gradually progressing to global cognitive impairment. In the early stages of the disease, imaging reveals predominantly mesial temporal atrophy (de Leon *et al.* 1993; de Leon *et al.* 1995; Fox *et al.* 1996c; Fox *et al.* 1996b; Killiany *et al.* 1993) as shown in two earlier VBM studies (Baron *et al.* 2001; Rombouts *et al.* 2000), progressing to generalised cortical atrophy in the advanced stages (Chan *et al.* 2001). Frontotemporal lobar degeneration (FTLD) is associated with three syndromic variants: frontotemporal dementia, semantic dementia (SD) and progressive non-fluent aphasia. Semantic dementia presents with semantic memory impairment in the context of preserved episodic memory (Snowden and Goulding 1989; Warrington 1975). Typically SD patients have fluent speech with normal articulation and prosody and relative preservation of syntax. Other features include surface dyslexia, dysgraphia and impaired object recognition. In contrast to AD, neuroimaging in SD reveals striking asymmetric temporal lobe atrophy, more marked on the left (dominant) side with particular involvement of the anteroinferior and anteromedial temporal structures.

The aims of this study were firstly to compare VBM with the best available equivalent of a gold standard, namely reproducible ROI measurements of temporal lobe structures (Chan *et al.* 2001) in these disease groups; and secondly to report the overall patterns of grey and white matter atrophy as detected by VBM in these two distinct disease groups. Ideally I would have liked to compare gyrus for gyrus across the whole brain and not limit comparisons to arbitrarily defined temporal regions of interest, but the practical limitations of obtaining accurate reproducible independent ROI measurements constrained my study design. In order to confirm the exact reproducibility of the VBM method with different operators, VBM was performed independently in two different imaging laboratories.

Methods

Subjects

Patients were recruited from the Cognitive Disorders Clinic at the National Hospital for Neurology and Neurosurgery, London. Ten moderately affected patients with probable sporadic Alzheimer's disease (AD), diagnosed according to NINCDS-ADRDA criteria (McKhann *et al.* 1984) were included in the study. The second patient group consisted of ten subjects who fulfilled criteria for the diagnosis of semantic dementia (Hodges *et al.* 1992; Hodges *et al.* 1998; Neary *et al.* 1998). In addition to comprehensive neuropsychological assessment by the Dementia Unit (ION, UCL), all patients underwent routine laboratory investigations for dementia. The two patient groups were matched for severity according to the Mini Mental State Examination (Folstein *et al.* 1975). An age and sex-matched group of ten individuals who had undergone MRI and neuropsychological assessments were selected from our group of normal controls.

The demographics of the subject groups are provided in Table 1. All subjects gave consent both for the MRI scan, and for participation in longitudinal research studies, which had the approval of the Local Research Ethics Committee of the National Hospital for Neurology and Neurosurgery (NHS Trust) and the Institute of Neurology (UCL).

Brain Imaging

T1-weighted, volumetric SPGR MRI scans were performed on a 1.5 Tesla Signa unit (General Electric, Milwaukee) yielding 124 contiguous 1.5 mm coronal slices through the head with a 256 × 128 image matrix (acquisition parameters: FOV/TR/TE/NEX/FLIP – 24/35/5/1/35°). Axial dual-echo sequences (T2- and proton density-weighted) were also acquired for diagnostic neuroradiological evaluation.

Voxel based morphometry

VBM was replicated independently by two researchers on two sites (myself and RS) using the optimised method as detailed in Chapter 2. Processing components pertinent to this study will be emphasised here.

Customised templates

Customised grey and white matter and CSF templates were created from the study group (30 subjects). This involved spatially normalising all the structural scans to the SPM T1 template, segmenting each normalised image into grey and white matter and CSF compartments and smoothing each grey and white matter segment with an 8mm FWHM smoothing kernel. Finally all the smoothed segments were averaged to create grey and white matter and CSF templates respectively.

Segmentation

Scan-rescan reproducibility for the optimised VBM segmentation technique yields coefficients of variation (100*sd/mean) of 0.41%, 0.59%, 1.07% and 0.17% for grey matter, white matter, CSF and total intracranial volume (TIV) respectively, scanning 10 subjects twice on the same day (Good *et al.*, 2001). In order to facilitate optimal segmentation of elderly patient and control MRI scans, I used our customised grey and white matter and CSF templates as prior probability maps (priors). I then compared segmentation with the customised priors versus default priors, which are based upon MRI brain scans from young healthy subjects.

Smoothing

All segments were smoothed with a 10mm FWHM isotropic Gaussian kernel. After smoothing, each voxel represents the local average amount of grey (or white) matter in the surrounding region, the size of which is defined by the size of the smoothing kernel.

Global volume statistical analysis

Global volumes of grey matter, white matter, CSF and whole brain (grey plus white matter) were normalised to the TIV and entered into an analysis of variance (ANOVA) between the three subject groups. In addition, Tukey posthoc analysis was employed to determine the significance of mean differences between group pairs, using SPSS version 9.0 (SPSS Inc., Chicago, Illinois, USA).

VBM statistical analysis:

The smoothed data were analysed using MATLAB 5.3 (MathWorks, Natick, Mass., USA) and statistical parametric mapping (SPM99) employing the framework of the General Linear Model. Regionally specific differences in grey and white matter

were assessed statistically using a two-tailed test, namely testing for increases or decreases in grey (or white) matter. In order to match the ROI analyses more closely (ROI analyses measured only temporal lobe structures), significance levels for temporal lobe structures were set at $p<0.05$, corrected for temporal lobe volume which was chosen arbitrarily as a rectangle of dimensions 40mm × 60mm × 40mm, providing a volume of 0.1 litre (a generous estimate of temporal lobe volume - ROI analyses measured the left and right temporal lobe volumes as approximately 0.07 litres each (Chan *et al.* 2001)). Significance levels for extra-temporal structures were set at $p<0.05$ corrected for the whole brain volume.

Voxel-wise analyses of grey and white matter were performed separately using three group effects (AD, SD and controls) with age and sex as confounding covariates. VBM analyses aim to find regionally specific changes that cannot be explained by global or distributed changes. To characterise the dependency of our changes on the global effect analyses were replicated three times using three methods of global modelling (i) total grey (or white) matter (TGWM) as a confounding covariate, (ii) TIV as a confounding covariate and (iii) no global confounding covariate. Clearly the TGWM and TIV reflect different aspects of global difference. TIV was calculated before spatial normalisation.

In order to compare VBM statistical parametric maps generated from images segmented with customised and default priors I constructed a separate design matrix. Conditions included 1) controls (default priors), 2) controls (customised priors), 3 AD (default priors) and 4) AD (customised priors). Global grey matter, age and sex were modelled as confounding covariates.

Comparison of ROI and VBM methods

The T statistics from the two techniques were correlated, providing plots and correlation coefficients.

Region of interest volumetric measurements

Medical Image Display and Analysis Software (MIDAS) was used for segmentation and volumetric analysis (Freeborough *et al.* 1997). The reproducibility error for ROI measurements was expressed as a coefficient of variation (100*sd/mean) for repeat measurements performed by the same rater at different times.

Whole brain and total intracranial volume

Whole brain segmentation (MIDAS) was performed using a semi-automated procedure that applies thresholding and a series of erosions and dilations to delineate brain tissue. TIV was used as an estimate of maximum pre-morbid brain size. TIV was measured using T2-weighted scans according to the technique described by (Jenkins *et al.* 2000) with a coefficient of variation of less than 1%.

Regions of interest (ROI)

ROI measurements were performed by Dennis Chan and Rachael Scahill (Dementia Research Unit, ION) according to previously described techniques and anatomical landmarks (Chan *et al.* 2001). The regions included whole temporal lobe, amygdala, hippocampus, entorhinal cortex, fusiform gyrus, parahippocampal gyrus, superior temporal gyrus and the combination of inferior and middle temporal gyri. The coefficients of variation (100*sd/mean) were 1.9%, 2.9%, 2.1%, 4.1%, 2.5%, 3%, 1.7% and 4.3% respectively. The entorhinal cortex (EC) region did not include the medial bank of the collateral sulcus owing to the interindividual variation in the position of the lateral border of the EC. Apart from the EC region, which contained only grey matter, all other regions contained a combination of grey and white matter. All volumetric measurements were corrected for head size by normalising to TIV.

Results

Global differences in whole brain, grey and white matter

ANOVA (summarised in Table 5.1) revealed significant differences in normalised global volumes (relative to TIV) of whole brain ($p<0.001$), grey matter ($p<0.001$) and CSF ($p<0.001$) across the three groups, but not for white matter. *Post hoc* analysis revealed significant decreases ($p<0.001$) in normalised global grey matter and whole brain volumes in SD and AD compared with controls. There was no significant difference in normalised global grey matter, white matter or whole brain volumes between SD and AD. There was no significant difference in normalised global white matter volume in SD or AD compared with controls. There were differences in the absolute and normalised measurements of whole brain volume between the fully automated VBM and semi-automated MIDAS techniques, but only minimal differences in ANOVA and *post hoc* probabilities (Table 5.1).

Table 5.1: Global volumes

	Control	AD	SD	ANOVA
Male/female	5/5	6/4	6/4	
Handedness	9/1	9/1	9/1	
MMSE score (max = 30)	29.8 (0.4)	21.2 (5.0)	21.8 (4.9)	
Age	60(6)	63(6)	60(8)	0.420
Global grey matter (VBM)	0.685 (0.060)	0.610 (0.075)	0.588 (0.049)	0.005
%TIV	49%	44%	45%	<0.001[1,2]
Global white matter (VBM)	0.406 (0.051)	0.412 (0.053)	0.383 (0.066)	0.66
%TIV	29%	30%	29%	0.38
CSF (VBM)	0.293 (0.038)	0.362 (0.050)	0.347 (0.059)	0.014
%TIV	21%	26%	26%	<0.001[1,2]
TIV (VBM)	1.385 (0.136)	1.384 (0.166)	1.318 (0.164)	0.56
TIV (MIDAS)	1.427 (0.182)	1.411 (0.182)	1.368 (0.148)	0.62
Whole Brain (VBM)	1.091 (0.106)	1.022 (0.123)	0.971(0.110)	0.078
%TIV	79%	74%	74%	<0.001[1,2]
Whole Brain (MIDAS)	1.190 (0.117)	1.096 (0.135)	1.064 (0.133)	0.096
%TIV	84%	78%	78%	0.003[1,2]

All volume measurements in litres (mean (SD)) TIV= total intracranial volume

MIDAS= Medical Image Display and Analysis Software

ANOVA= analysis of variance

Posthoc analysis: [1] significant difference between control and AD, $p<0.001$

[2] significant differences between control and SD, $p< 0.001$

Temporal lobe structures: a comparison of VBM and ROI

Tables 5.2 and 5.3 summarise VBM and ROI comparisons of temporal lobe structures for AD and SD respectively. Figure 5.1 (a, b) demonstrates VBM detected atrophy, having covaried out changes in TIV, in AD and SD projected onto a mean normalised image.

In AD, VBM detected most significant grey matter reduction in the right middle temporal gyrus, followed by relatively symmetrical reduction along the lengths of both hippocampi, right fusiform gyrus, left middle temporal gyrus, left superior temporal gyrus, right superior temporal gyrus and left fusiform gyrus (Figs 5.1a and 5.7a (in red)). Only the right middle temporal gyrus voxels were significant at $p<0.05$, corrected. The remainder did not survive correction for multiple comparisons. VBM detected least significant grey matter reduction in the entorhinal cortices, amygdalae and the anterior temporal poles. These findings differed from the ROI analyses, which detected most significant volume reductions in the amygdalae, right middle and inferior temporal gyrus, entorhinal cortices and left posterior hippocampus, all of which survived Bonferroni correction (see Table 5.2 for p values and T statistics).

In SD, VBM detected most significant grey matter reduction in the left amygdala followed by left anterior and middle hippocampus and left entorhinal cortex (Figs. 5.1b and 5.7b (in red)). The pattern of grey matter loss was strikingly different from the AD pattern. There was an anteroposterior gradient of grey matter reduction in the left and to a lesser extent right hippocampus. The right-sided structures were less reduced than the left, and the most severely affected right-sided structure was the amygdala. VBM detected a greater significance of grey matter loss in all temporal lobe structures, apart from the right middle temporal gyrus, in SD than AD.

ROI analyses showed a very similar pattern of volume loss, with most significant volume reduction in the left amygdala, followed by the left middle and inferior temporal gyri, left entorhinal cortex and right amygdala (see Table 5.3).

A comparison of ROI and VBM detected volume reductions in the anterior, mid and posterior hippocampus are plotted in Figure 5.2 and entorhinal cortex in Figure 5.3. The correlation coefficients (and their significance) for anterior, mid and posterior hippocampus were 0.28 ($p=0.1$), 0.574 ($p=0.001$) and 0.286 ($p=0.125$) respectively. Qualitatively, VBM shows slightly better separation of hippocampal data between the groups compared to ROI. For the left and right entorhinal cortices, the

correlation coefficients and their significance were 0.724 ($p<0.001$) and 0.490 ($p=0.06$) respectively.

Table 5.2: Alzheimer's disease

	Alzheimer's Disease			
	VBM (grey matter)		ROI (total volume)	
Location	**T (1,26)**	**p**	**T (1,26)**	**p**
R MTG/MITG	5.3	0.000*	3.5	0.001*
L hippocampus (♦total vol)			4.0	0.001*
anterior	4.1	0.000	0.6	0.262
mid	4.4	0.000	3.0	0.004
posterior	4.2	0.000	3.4	0.002*
R hippocampus (♦total vol)			3.4	0.004*
anterior	4.0	0.000	2.8	0.006
mid	4.3	0.000	1.4	0.085
posterior	3.1	0.002	1.6	0.064
R fusiform	4.1	0.000	0.7	0.255
L MTG/MITG	3.8	0.000	2.3	0.018
LSTG (lateral)	3.8	0.000	1.1	0.139
R STG (lateral)	3.6	0.001	0.5	0.317
L fusiform	3.4	0.001	1.4	0.086
R entorhinal	3.1	0.002	3.4	0.002*
L entorhinal	3.0	0.003	3.4	0.002*
R ITG	3.0	0.003	*not measured*	
L ITG	3.0	0.003	*not measured*	
L anterior temporal pole (anterior STG)	2.2	0.019	*not measured*	
R amygdala	2.32	0.014	3.6	0.001*
L amygdala	2.12	0.022	3.9	0.001*
R anterior temporal pole (anterior STG)	--	--	*not measured*	

* significant, $p<0.05$, corrected for temporal lobe volume (VBM) or Bonferroni corrected (ROI)

ITG= inferior temporal gyrus (VBM only)

MTG/MITG = middle temporal gyrus (VBM)/middle and inferior temporal gyri (ROI)

STG = superior temporal gyrus (♦total volume): ROI measured total volume of hippocampus anatomically, and sub-regions as anterior, middle and posterior thirds.

Table 5.3: Semantic dementia

	Semantic Dementia			
	VBM		ROI	
	T	p	T	p
L amygdala	13.3	0.000*♦	13.1	0.000*♦
L hippocampus (♠total vol)			5.8	0.000*♦
anterior	12.3	0.000*♦	1.8	0.047♦
mid	10.2	0.000*♦	3.7	0.001*♦
posterior	7.7	0.000*♦	1.6	0.065♦
L entorhinal	9.5	0.000*♦	10.6	0.000*♦
L fusiform	7.9	0.000*♦	6.7	0.000*♦
R amygdala	7.7	0.000*♦	8.4	0.000*♦
L ITG	7.1	0.000*♦		
L anterior temporal pole (anterior STG)	6.44	0.000*♦	*not measured*	
R hippocampus (♠total vol.)			3.9	0.001
anterior	6.42	0.000*♦	3.1	0.003
mid	5.41	0.000*♦	0.8	0.203
posterior	5.04	0.000*♦	0.4	0.360
L MTG/MITG	6.37	0.000*♦	10.9	0.000*♦
L STG (lateral)	6.2	0.000*♦	6.1	0.000*♦
R fusiform	4.5	0.000	2.7	0.007
R MTG/MITG	4.31	0.000	4.5	0.000*
R ITG	_		*not measured*	
R entorhinal	4.0	0.000	5.9	0.000*
R STG (lateral)	3.8	0.000	4.1	0.000*♦
R anterior temporal pole (anterior STG)	3.6	0.001♦	*not measured*	

* significant, $p<0.05$ corrected for temporal lobe volume (VBM) or Bonferroni corrected (ROI)

♦ significantly more atrophy in SD than AD, $p<0.05$ corrected

ITG= inferior temporal gyrus (VBM only)

MTG/MITG = middle temporal gyrus (VBM)/middle and inferior temporal gyri (ROI)

STG = superior temporal gyrus

(♠total volume): ROI measured total volume of hippocampus anatomically, and sub-regions as anterior, middle and posterior thirds

Figure 5.1a: Grey matter atrophy in AD

VBM detected regions of temporal grey matter loss in AD (threshold T> 2 for illustrative purposes only) projected over coronal slices of the normalised group mean image. TIV was included as a confounding covariate.

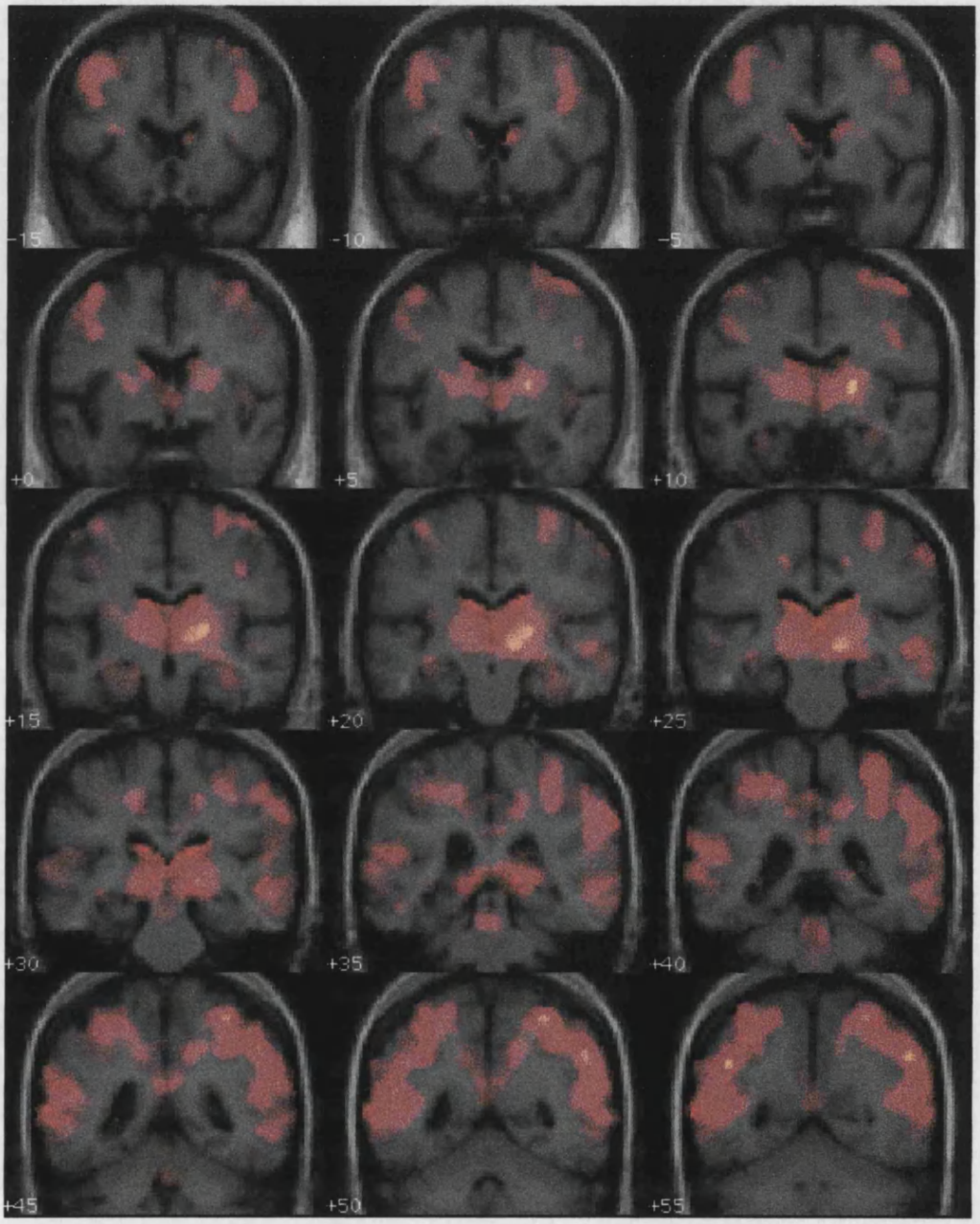

Figure 5.1b: Grey matter atrophy in SD

VBM detected regions of temporal grey matter loss in SD (threshold T> 2 for illustrative purposes only) projected over coronal slices of the normalised group mean image. TIV was included as a confounding covariate.

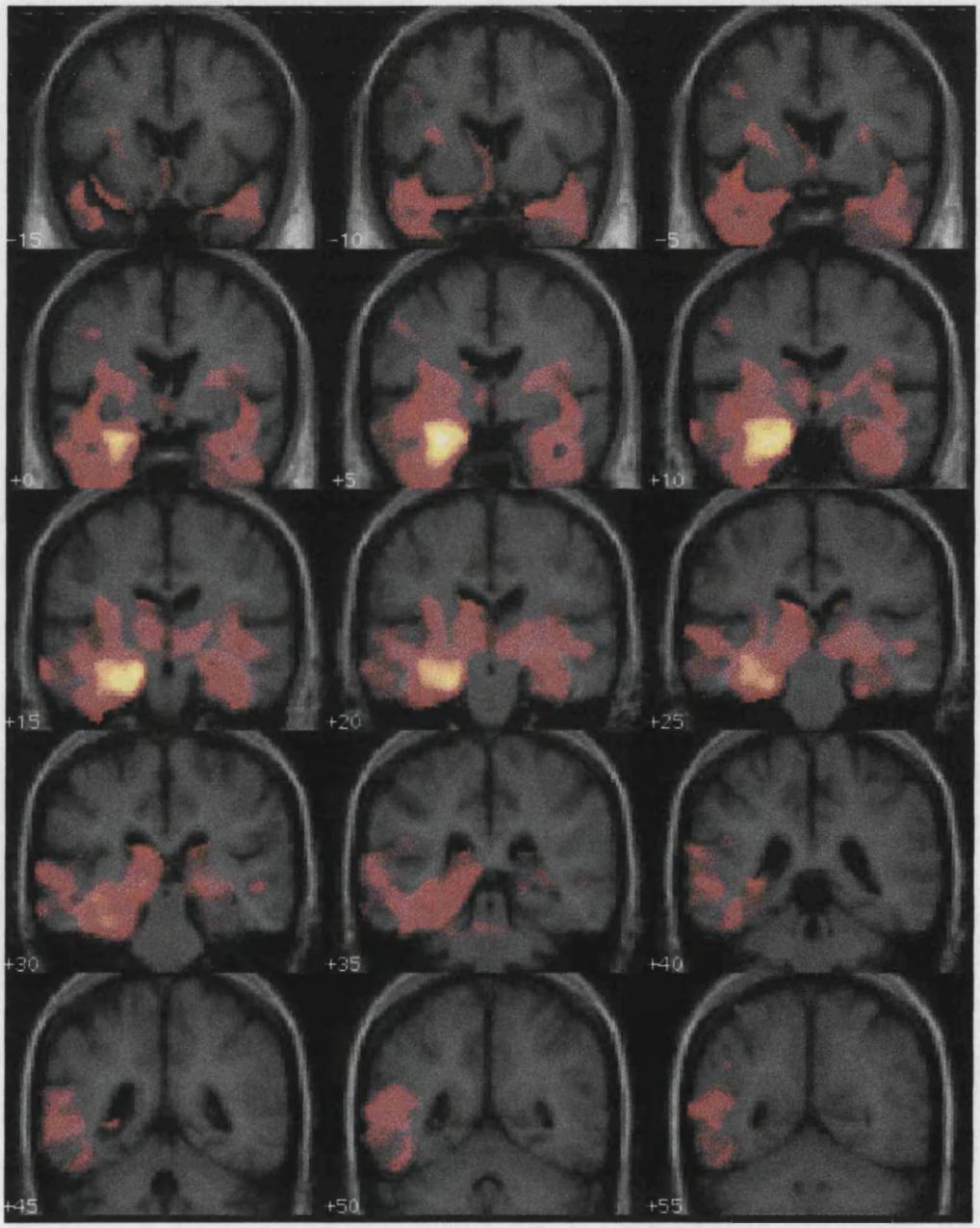

Figure 5.2: Hippocampal volumes

Scatter plots of left anterior (a), middle (b) and posterior (c) hippocampal volume detected by ROI on the y-axis and VBM on the x-axis. VBM measures grey matter volume (mm^3) within a single voxel ($1.5mm^3$) placed in the left anterior, middle and posterior hippocampus respectively. ROI measures total volume (predominantly grey matter) for each section of the hippocampus normalised to TIV. The groups are colour coded: blue (SD), green (AD) and red (controls). Volume loss is most marked in SD and the separation of the groups appears best with VBM.

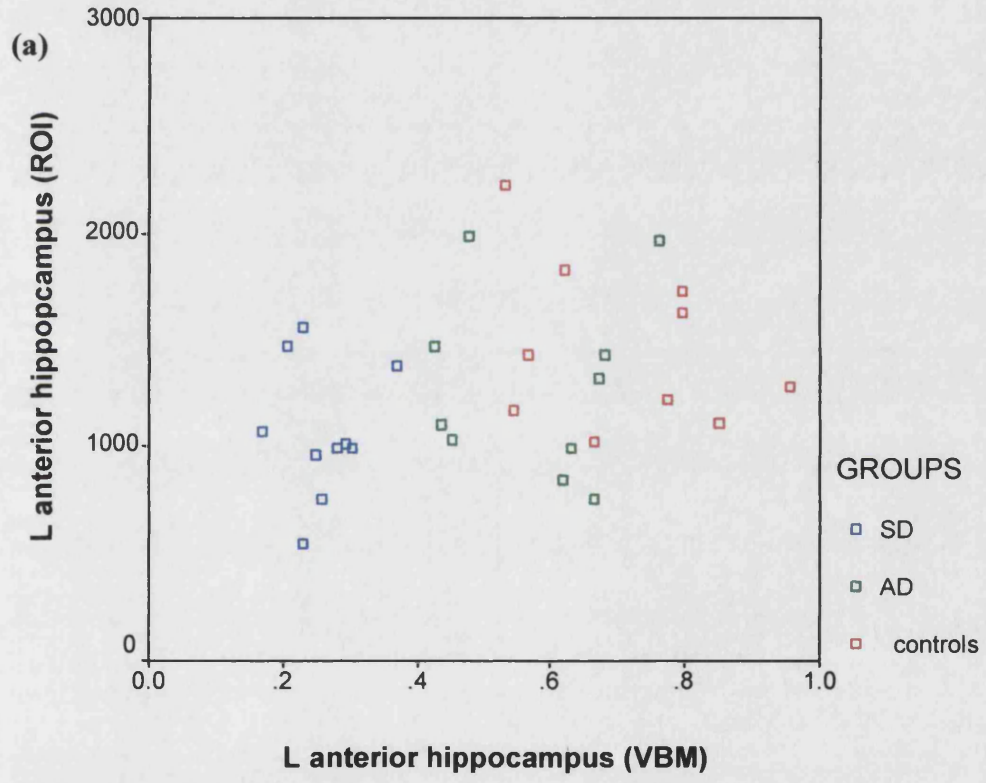

(b)

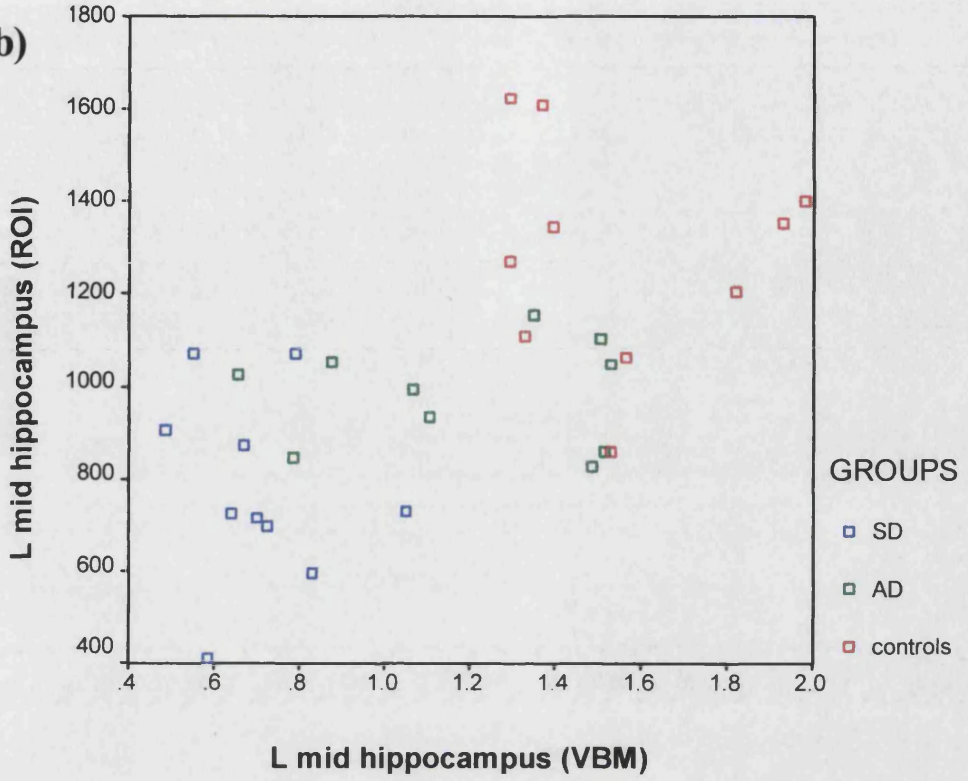
1800
1600
1400
1200
1000
800
600
400
L mid hippocampus (ROI)
.4
.6
.8
1.0
1.2
1.4
1.6
1.8
2.0
L mid hippocampus (VBM)
GROUPS
SD
AD
controls

(c)

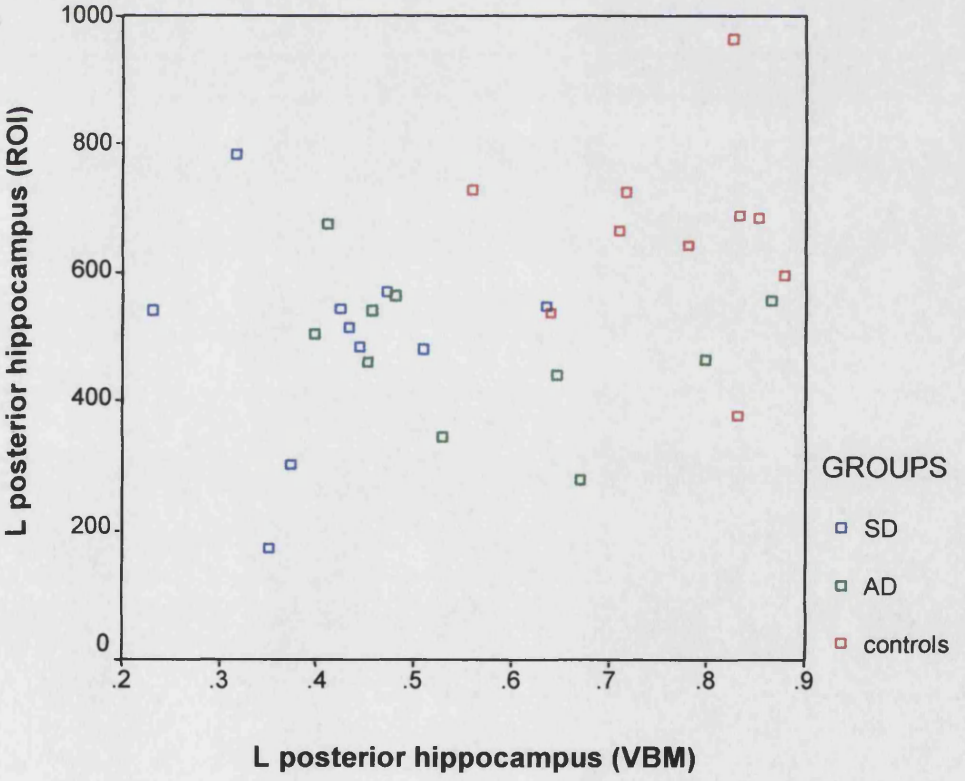
1000
800
600
400
200
0
L posterior hippocampus (ROI)
.2
.3
.4
.5
.6
.7
.8
.9
L posterior hippocampus (VBM)
GROUPS
SD
AD
controls

Figure 5.3: Entorhinal cortex volume

Scatter plots of right (a) and left (b) entorhinal cortex volume detected by ROI on the y-axis and VBM on the x-axis. VBM measures grey matter volume (mm^3) within a single voxel ($1.5mm^3$) placed in the right and left entorhinal cortex respectively. ROI measures total volume (predominantly grey matter) for right and left entorhinal cortex normalised to TIV. The groups are colour coded: blue (SD), green (AD) and red (controls). Volume loss is most marked in SD.

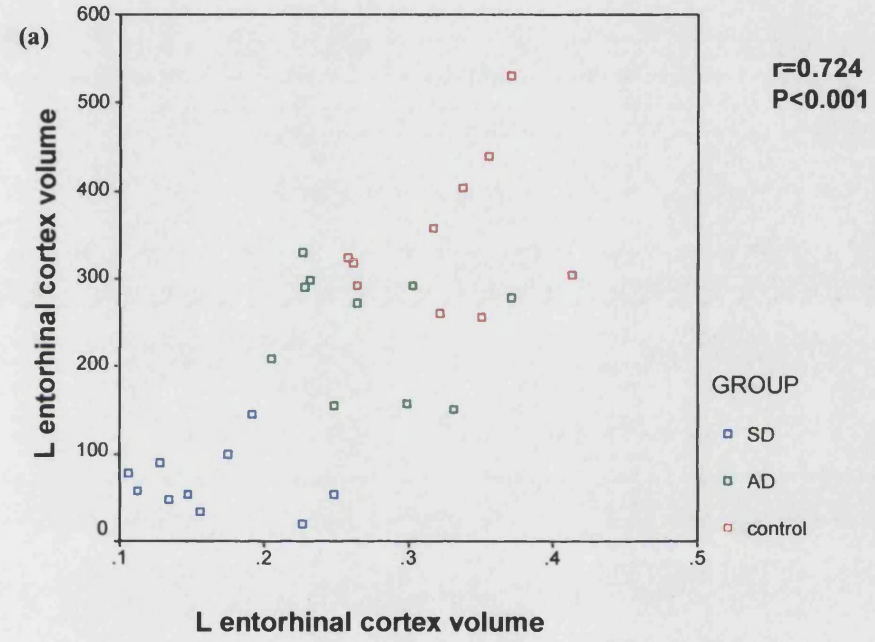

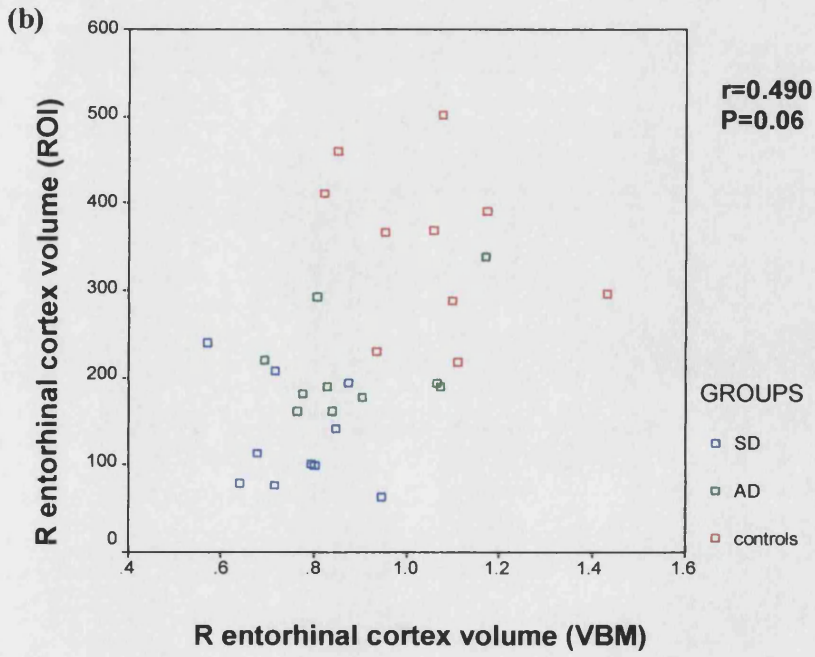

In order to more formally compare the automated technique with the accepted gold standard, I plotted the T statistics for ROI and VBM measurements of temporal lobe structures (Fig. 5.4). In AD, ROI measurements appear more sensitive for the volume loss in the amygdala, whereas VBM measurements appear more sensitive for volume loss in both superior and right middle temporal gyri, both fusiform gyri and regional hippocampal volumes (right mid and posterior hippocampus, left anterior hippocampus). The correlation between the two techniques was not significant ($r = -0.25$ ($p=0.341$)) In SD; ROI measurements appear more sensitive for volume loss in the left MITG whereas VBM appears more sensitive to regional hippocampal atrophy. The correlation between the two techniques was good apart from the hippocampal differences, which reflect in the correlation coefficient ($r=0.28$ ($p=0.29$)). It is worth noting that the correlation appears higher for higher T statistics (as in SD) and lower for lower T statistics (as in AD).

Figure 5.4: Correlation of T statistics for ROI and VBM

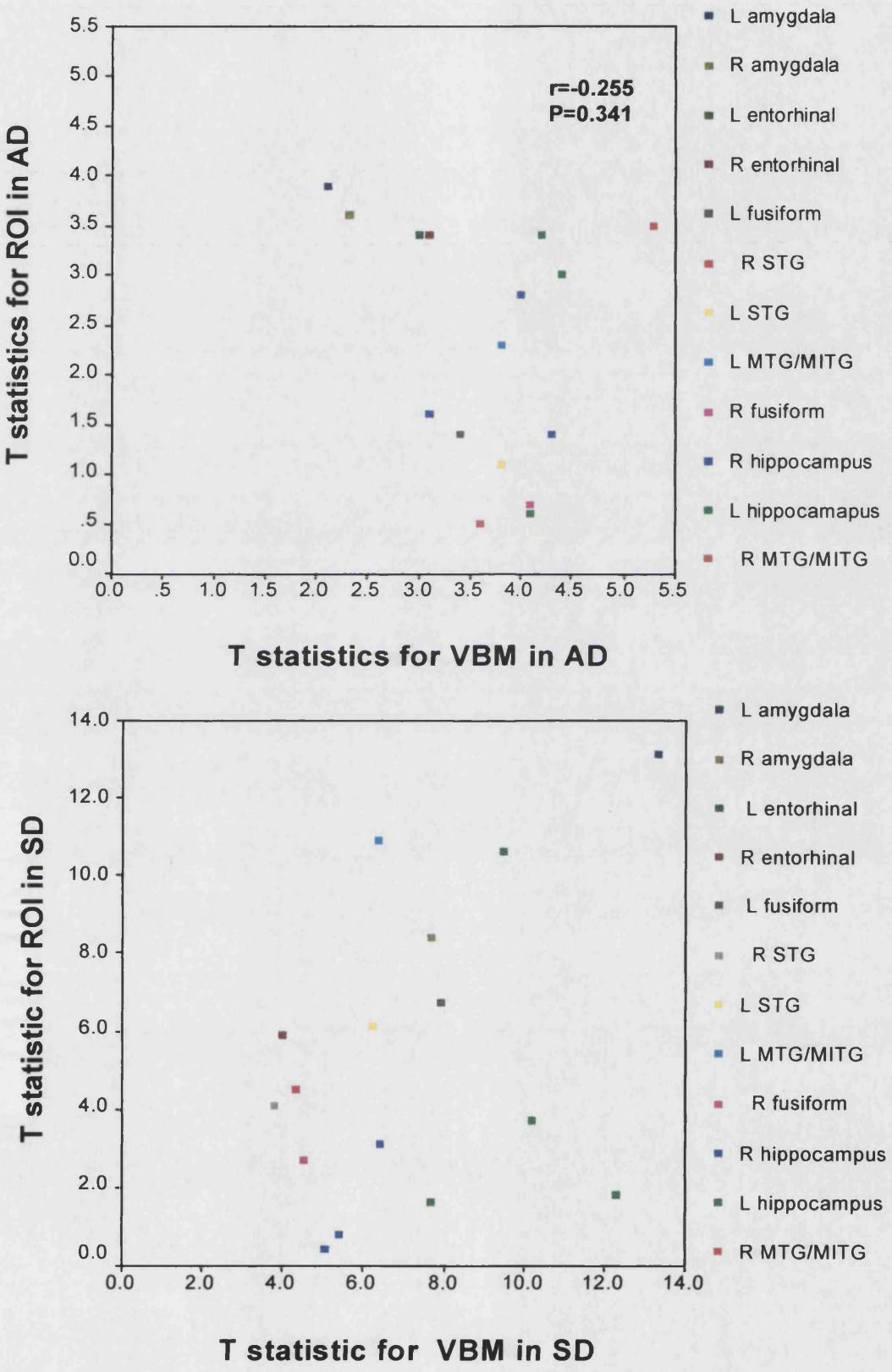

Comparison of segmentation using customised priors and default priors

A qualitative comparison of grey matter segments derived from segmentation using customised versus default priors revealed only minor differences with no clear improvement using customised priors. Inspection also revealed sub optimal classification of grey and white matter in the mesial temporal lobes in one elderly control, one patient with SD and three patients with AD. Figure 5.5 demonstrates segmented grey matter images derived from the standard SPM priors (a) and the customised priors (b) in one of the AD patients with sub optimal classification of grey and white matter in the anteromesial temporal lobe.

Formal VBM statistical comparison revealed no interaction between the choice of priors and differences between controls and AD patients, but did reveal a significant main effect of priors that was seen separately in the control and AD groups. In a comparison of default priors - customised priors there was a large cluster of significant voxels within the pons (Fig. 5.6a) ($p<0.05$, corrected) and additional voxels extended throughout the cingulate gyrus at a lower threshold ($p<0.001$, uncorrected) (Fig. 5.6b). Conversely, there were no significant voxels in the customised priors – default priors contrast for either control or AD groups (Fig. 5.6b). There were also subtle differences in the T scores of the maxima when looking at SPMs of control – AD groups for customised and default priors with customised priors yielding higher T scores (Table 5.4). These findings suggest that customised priors allow more precise classification and registration of voxels within healthy and diseased subjects.

Table 5.4: Maxima for control – AD

		Customized priors		Default priors	
Location	**Coordinates**	**T**	**p, corrected**	**T**	**p, corrected**
L parietal	-56 -66 33	8.08	<0.000	7.00	<0.000
Post cingulate	-2 -58 28	7.14	<0.000	7.17	<0.000
R parietal	58 -60 36	6.85	<0.000	6.245	<0.000

Figure 5.5: Effect of priors on segmentation

Segmented grey matter image derived from a) default SPM prior probability maps and b) customised disease-, age- and sex-matched prior probability maps. There is little qualitative difference in tissue classification between the two methods despite the theoretical advantage offered by customised priors.

Default SPM priors

Customised disease and age matched priors

Figure 5.6ab: Statistical comparison of customised and default priors.

Main effect of priors within the control group: default priors – customised priors. Significant voxels ($P<0.05$, corrected (a) within the pons and $p<0.001$, uncorrected (b) extending along the cingulate gyrus are projected over a single scan in stereotaxic space. The crosshairs represent the maximum and the colour bar represents the T score. Conversely in the comparison customised priors – default priors no significant voxels were detected

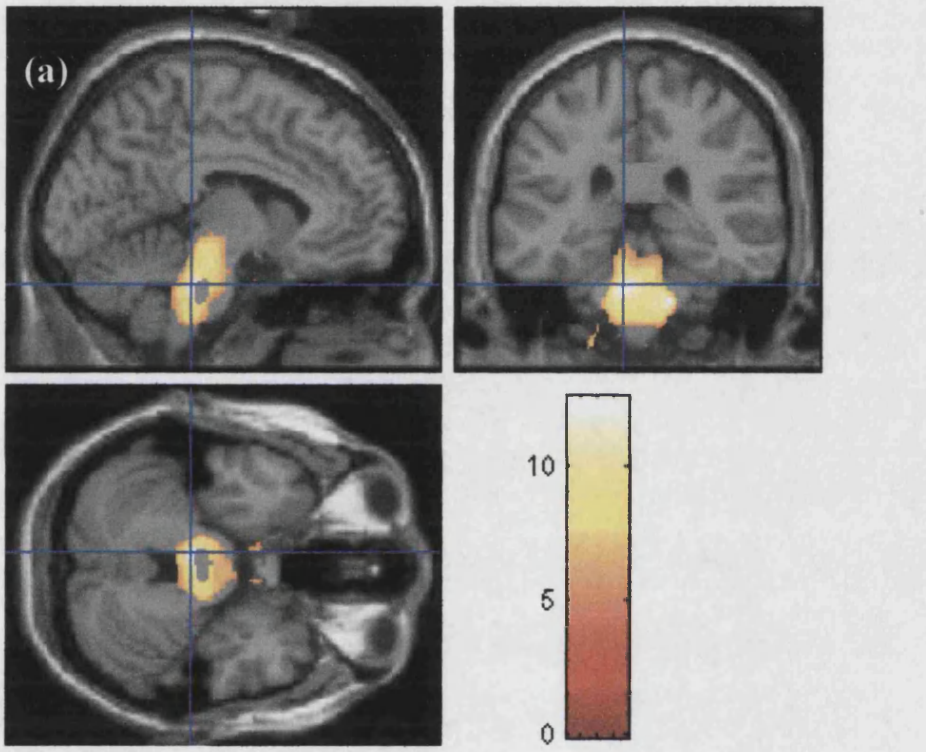

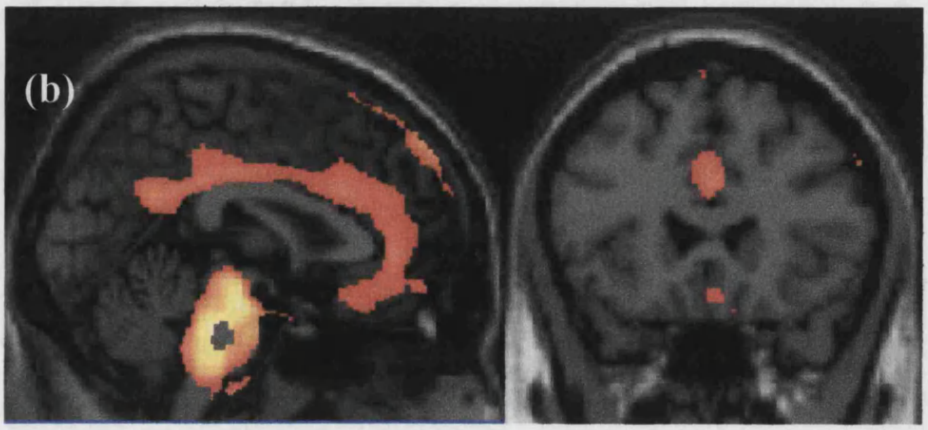

Additional VBM findings not assessed in the ROI analysis

Extra-temporal grey matter

Figures 5.7 and 5.8 show the VBM detected patterns of grey matter reduction in AD and SD and highlight the differences between the grey matter analyses with no global covariate (5.7a, 5.8a), TIV as a covariate (5.7b, 5.8b) and grey matter mean global volume as a covariate (5.7c, 5.8c).

In AD, VBM detected a relatively diffuse and symmetrical pattern of grey matter loss, most prominent in the parietal lobes and posterior cingulate cortex. When the mean global grey matter was modelled as a confounding covariate in order to determine regionally specific patterns of loss within the grey matter compartment itself, significant atrophy was seen in the parietal lobes, posterior cingulate cortex, caudate nuclei and thalami and not in the anteromesial temporal structures (Fig. 5.7c).

Figure 5. 7a: C-AD (no global covariate)

VBM detected grey matter atrophy in AD. With no global covariate there is distributed volume loss in the temporal, parietal and frontal lobes

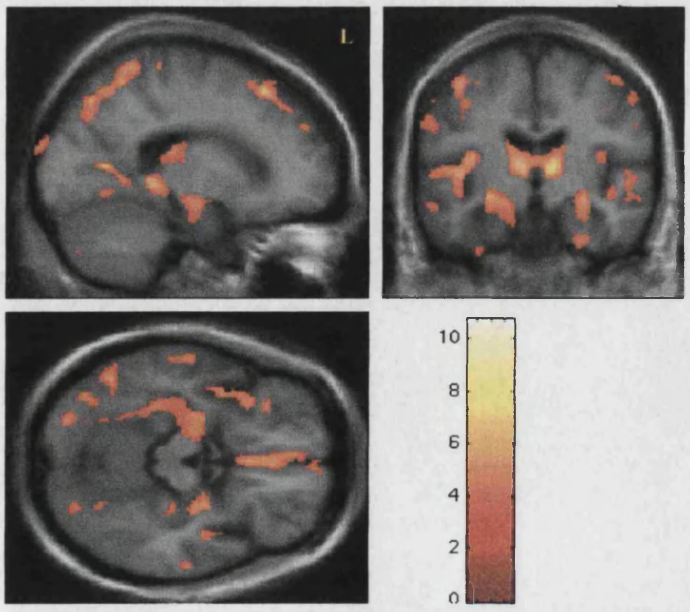

Figure 5.7b:C-AD (TIV)

VBM detected atrophy in AD. With TIV as a covariate to remove any head size differences, there is a similar pattern of atrophy to Fig. 5.7a with distributed volume loss in the temporal, parietal and frontal lobes (see Table 5.2 for full details)

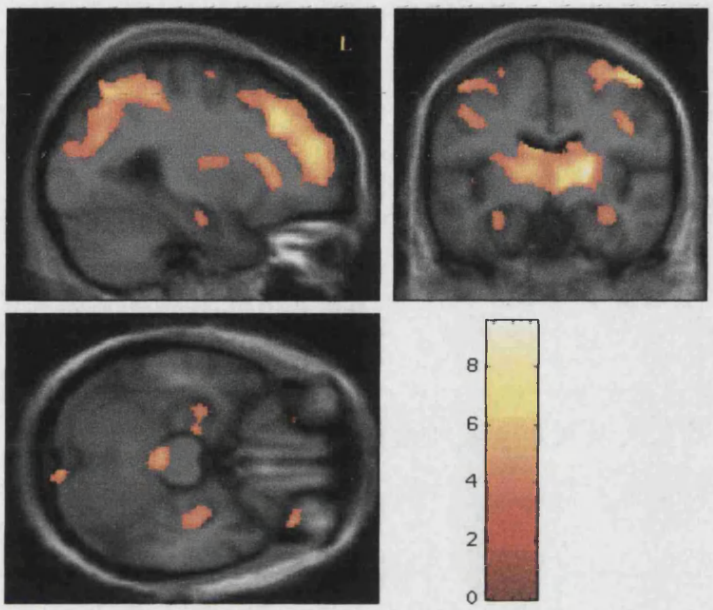

Figure 5.7c: C-AD (grey matter globals)

VBM detected atrophy in AD. With global grey matter volume as a covariate, areas of volume loss more than global loss are being detected. Here, most significant volume loss is seen in the parietal cortices and posterior cingulate

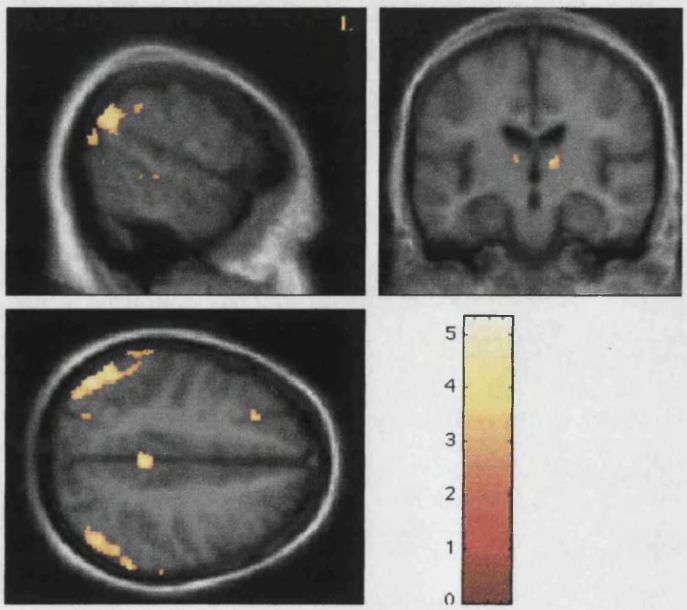

In SD, VBM detected asymmetric regional temporal lobe atrophy, with only minimal atrophy in frontal cortex. The pattern of grey matter reduction was similar, irrespective of the inclusion or exclusion of a global covariate (TIV or mean global grey matter), the main difference being the detection of perisylvian grey matter and cingulate reduction when no global covariate was included.

There were no significant regional increases of grey and white matter in AD and SD relative to controls.

Figure 5.8a: C-SD (no global covariate)

VBM detected grey matter atrophy in SD. With no global covariate there is asymmetric regional volume loss in the temporal lobes, particularly on the left side. Volume loss is also noted in the anterior cingulate, left thalamus and caudate nucleus.

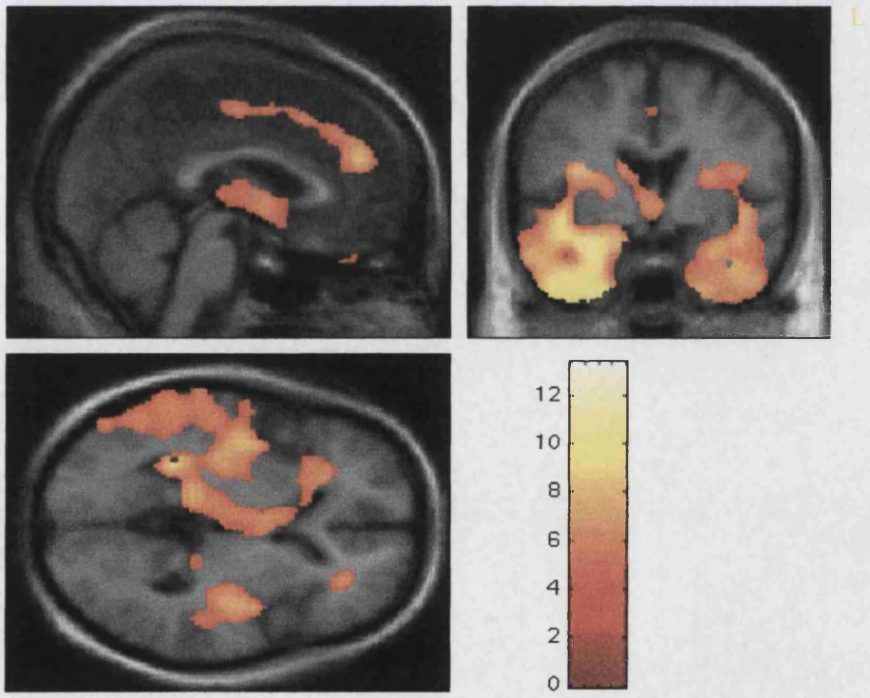

Figure 5.8b:C-SD (TIV)

VBM detected atrophy in SD. With TIV as a covariate, head size differences have been removed. The pattern of atrophy is similar to Fig. 5.8a with atrophy most pronounced in the temporal lobes (L>R)

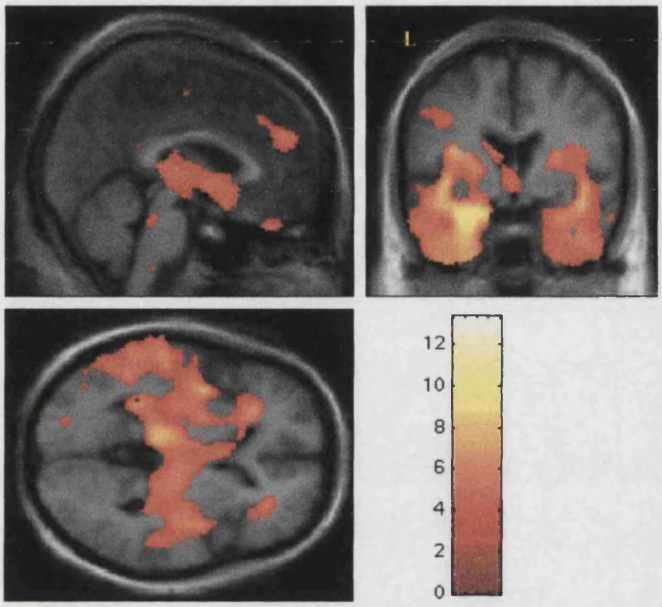

Figure 5.8c: C-SD (grey matter globals)

VBM detected atrophy in SD. With global grey matter volume as a covariate areas of volume loss more than global loss are being detected. The pattern of atrophy remains most pronounced in the temporal lobes (L>R)

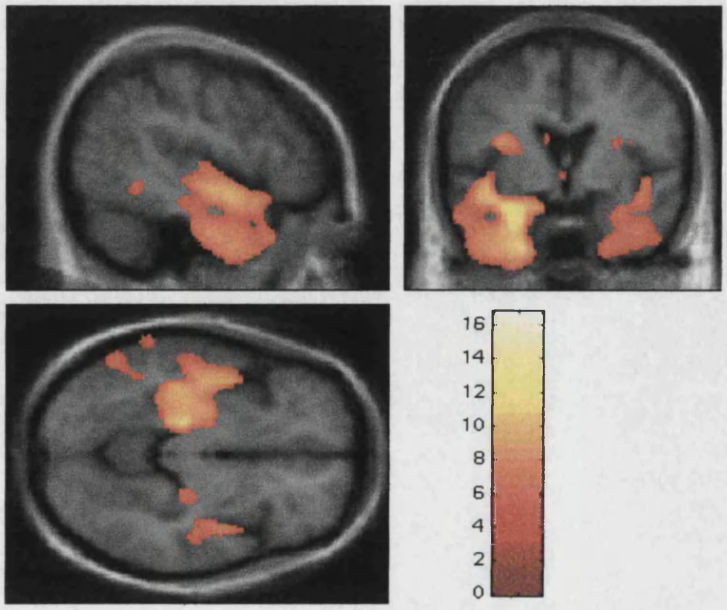

White matter reduction

In AD, VBM (with TIV as a covariate) detected a relatively symmetric pattern of white matter reduction (in the subcortical white matter around the insula, in the parietal lobes, in the peritrigonal white matter and in the columns of the fornix. Regionally specific white matter reduction (after covarying out global white matter changes) was observed in the periventricular white matter, especially around the lateral ventricles and diffusely within the corpus callosum. VBM detected apparent increases in white matter in misclassified thalamic and caudate voxels (see discussion). In SD, VBM (with TIV as a covariate) detected asymmetric regional reduction in the temporal white matter, particularly on the left side (Fig. 5.9b in blue) and asymmetric atrophy of the periventricular white matter and corpus callosum, particularly on the left side. Similar changes were observed after covarying out global white matter changes.

CSF change

In AD, VBM detected increased CSF in the Sylvian fissures (Fig. 5.9a in green), interhemispheric fissures, lateral ventricles and collateral sulci (right more than left). There were no regions of decreased CSF.

In SD, VBM detected asymmetric (left > right) increased CSF in the Sylvian fissures, collateral sulci, temporal horn and hippocampal fissure, around the temporal poles, in the body of the left lateral ventricle and in the interhemispheric fissure (Fig. 5.9b in green). There were no regions of decreased CSF.

As expected with an automated technique, the VBM analyses performed independently by the different researchers on different sites gave identical results.

Figure 5.9: Atrophy patterns in AD and SD

A comparison of patterns of atrophy in AD (a) and SD (b) projected over a single temporal coronal slice. Grey matter atrophy is depicted in red, white matter atrophy in blue and CSF enlargement in green ($p<0.001$ uncorrected)

a) AD **b) SD**

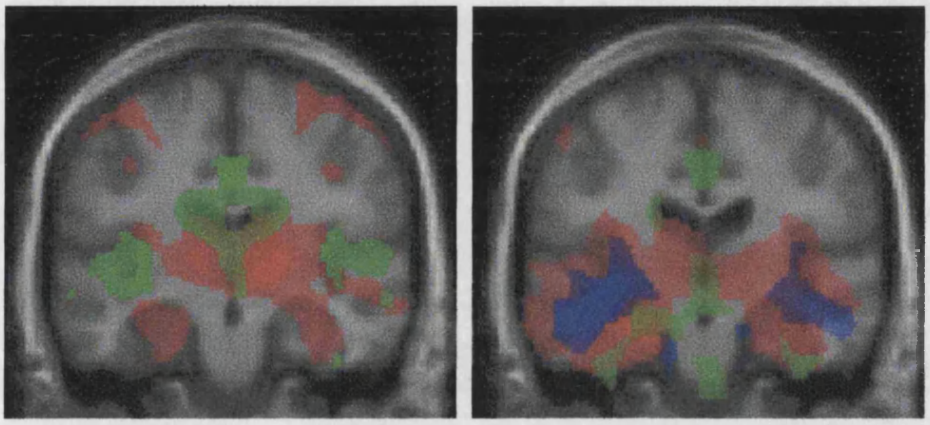

Discussion

Comparison of VBM and independent ROI data for temporal lobe structures

While ROI volumetric analyses and VBM are not directly comparable, this paper attempts to validate the automated VBM method against manual volumetric measurements of temporal lobe regions in two diseases with very different patterns of atrophy. The ROI analyses measured differences in regional volume of brain structures (normalised to TIV) in the temporal lobes only whereas VBM detected regional differences in grey and white matter on a voxel by voxel basis throughout the brain. The atrophy outside the temporal lobes detected with VBM could not be directly related to the ROI analyses, which only measured temporal lobe structures. The TIV and whole brain volumes were slightly smaller when measured with VBM compared with MIDAS. These differences were not unexpected and probably relate to partial volume corrected labelling based upon prior probabilities and the explicit removal of non-brain voxels in the former and intensity thresholding with whole voxel inclusion/exclusion in the latter. It is well known that measurements of segmented brain volumes can vary quite considerably depending upon the segmentation technique

used. What is more important is that they are reproducible, as is the case for both the MIDAS and SPM segmentation techniques.

Looking specifically at temporal lobe atrophy, there were similarities and differences between the VBM and ROI results. In AD, the difference between the two morphometry techniques was most marked for ranking atrophy severity. ROI analyses appeared more sensitive to volume loss in the amygdalae whereas VBM analyses appeared more sensitive to right middle temporal gyrus and regional hippocampal volume loss. The T scores were generally higher for VBM than ROI, but the stringent correction for multiple comparisons in the less constrained VBM produced less significant corrected p values. This is not a failing of VBM, rather it emphasises the need to examine the data under less stringent correction thresholds.In AD, where the T scores were generally lower than SD, VBM only detected significant (corrected) volume loss in the right MTG whereas ROI analyses showed significant (corrected) volume loss in many more temporal structures (the amygdalae, right middle and inferior temporal gyri, entorhinal cortices, total hippocampi and left posterior hippocampus). In SD, the T scores were generally higher than in AD and there was relatively good correlation between the two techniques, but there were slight differences in the relative significance of changes. ROI analyses appeared more sensitive to left middle and inferior temporal gyrus volume loss whereas VBM appeared more sensitive to regional hippocampal volume loss. The areas of consistency between the two techniques are reassuring. For areas of inconsistency the questions therefore are: which is the more accurate measurement, and why? There is no simple answer to these questions, but an understanding of how temporal lobe structures were measured by each technique, will identify potential sources of discrepancy.

VBM measurements

VBM consists of a number of automated morphological operations, thus the cause of regionally significant differences can potentially enter at each step. Although these operations are complicated they render the data more directly related to the anatomical metric of interest (e.g. grey matter volume). It is important to realise, however, that changes in local grey matter volume can have a number of causes that include (i) loss of grey matter (e.g. cortical atrophy), (ii) disproportionate increases in brain volume (e.g. hydrocephalus) and (iii) displacement of grey matter from its

normal location (e.g. tumour). To attribute significant results to atrophy, other potential causes must be discounted by considering their interaction with spatial normalisation and segmentation.

Spatial normalisation

The spatial normalisation step aims to map each structural MRI to a template in standard stereotaxic space. The customised templates were created from all the patients and controls in order to minimise the degree of non-linear warping required. The non-linear spatial transformations used in this study do not attempt to match every gyrus in the brain exactly; rather the goal is to discount global brain shape differences (i.e. displacement of grey matter from its normal location). A number of potential systematic differences can arise from misregistration during the spatial normalisation step. For example, the patient group may have systematic differences in the relative intensity of grey matter voxels compared to white matter, or may be subject to more motion artefact. Differences in spatial normalisation accuracy have not yet been formally studied, and certainly there is the potential for greater errors in the patient group leading to non-sphericity problems, although these can be corrected. It is important to note that inaccuracies in spatial normalisation cannot introduce bias or false positives *per se*. Even if there are brain structures that are difficult to normalise, any differences detected by VBM must be caused by systematic differences in the anatomy of these structures. By using more accurate spatial normalisation, VBM detected differences between patients and controls could be more directly attributed to volumetric differences in grey matter however, a method with enough freedom to warp one image perfectly to another is not necessarily a better option. More degrees of freedom incur more potential local minima, so that while the images may be globally well matched, gyral and sulcal correspondence is not necessarily precise (Ashburner and Friston 1999; Ashburner and Friston 2000; de Leon *et al.* 1993; de Leon *et al.* 1995).

Small structures such as the amygdala, hippocampus and entorhinal cortex, not only have a complex architecture, but may also be highly variable between subjects on visual inspection, particularly in elderly and diseased subjects. This regional variance has implications for the sensitivity of any morphometric technique to detect changes. VBM may be relatively insensitive to subtle atrophy in regions of high variance in the studied population whilst more sensitive to atrophy in regions of low variance.

However, SPM employs a voxel-wise estimate of variance. VBM has previously demonstrated subtle changes within the anterior and posterior hippocampus in a group of taxi-drivers, that corroborated independent accurate ROI measurements and functional data (Maguire *et al.* 2000), suggesting that this technique can register and segment small structures with some degree of accuracy in normal subjects. Furthermore, VBM detected anteromesial temporal lobe atrophy, including the hippocampi, amygdalae and entorhinal cortex in early Alzheimer's disease (Baron *et al.* 2001; Rombouts *et al.* 2000), bilateral hippocampal atrophy in children with hypoxic ischaemic damage (Salmond *et al.* 2000) and reductions in left hippocampal grey matter density in chronic unipolar depression, that correlated with verbal memory scores (Shah *et al.* 1998). More importantly VBM can separate normals from subjects with mild cognitive impairment (Chetelat *et al.,* 2002) who show grey matter loss in the hippocampi and cingulate gyrus.

By incorporating a modulation step to the VBM analysis (Ashburner and Friston 2000; Ashburner and Friston 2001) information is added from the deformation fields generated during spatial normalisation themselves to render the VBM analyses more similar to ROI analyses. This is because each voxel in a modulated smoothed segment of tissue contains a count of absolute amount of grey matter in a "region of interest" defined by the smoothing kernel. Since I have incorporated this correction for volume change induced by spatial normalisation, it is appropriate to include TIV as a confounding covariate to remove any variance due to differences in head size. Without the modulation step, spatial normalisation removes differences in head size and thus TIV does not need to be included as a confounding covariate.

Segmentation

Diseased brains are a challenge for any automated or manual segmentation technique. In AD and SD and to a lesser extent elderly controls, there are two particular problems. Firstly the brains are atrophic. In regions of atrophy, there is more potential for partial volume effect between grey matter and CSF, and consequently voxels may be misclassified. However this does not matter in terms of inferring regional change, it only affects the attribution of change in terms of the tissue class affected. Misclassification can be reduced by using high-resolution scans with small voxel size, preferably isotropic $1mm^3$. In this study the voxels were anisotropic: 1mm×1mm×1.5mm. Secondly, and probably more importantly, pathology (and to a

lesser extent ageing) may be associated with signal change and a reduction in the grey/white matter contrast, and this was particularly true for the temporal lobes in AD and SD: In AD I observed apparent increases of white matter in the thalami and caudate nuclei. This may in part reflect misclassification of grey matter voxels, which can be seen on inspection of grey and white matter segmented images. The default SPM prior probability maps are based on MRIs from young normal subjects, which differ quite markedly from MRIs of elderly and diseased subjects. I therefore used customised age and disease matched priors and demonstrate that these allow improved classification of voxels, particularly in the brainstem and cingulate gyrus and higher T scores for statistical inferences compared with default priors.

Smoothing

The final step of VBM pre-processing is smoothing with an isotropic Gaussian kernel. This makes the subsequent voxel-wise analysis comparable to a region of interest approach, since each voxel in a smoothed, normalised, modulated grey matter image contains the average amount of grey matter within a region (defined by the smoothing kernel) surrounding that voxel. The size of the smoothing kernel should be comparable to the size of the expected regional differences between groups, but there is a trade-off between localisation accuracy and the number of independent comparisons between the resulting 'resolution elements' (RESELS) performed. If the objective is to increase sensitivity so that correction for multiple comparisons is less severe, then more smoothing must be used. If the objective is for localisation accuracy a smaller smoothing kernel should be used, although this will provide less compensation for inexact spatial normalisation. I used a 10mm smoothing kernel as the best compromise. I also tested the data with a 6mm smoothing kernel, and obtained almost identical results. In small adjacent brain regions such as the amygdala and entorhinal cortex, localisation accuracy may become an issue: a voxel may reflect a composite average from both regions which could explain why expertly defined ROI measurements are more sensitive than VBM in these small structures in AD.

Regional changes due to displacement of tissue

VBM detects changes in grey, white and CSF compartments. If the interfaces between compartments move due to mass effect or volume loss, the changes can be reflected in both compartments. For example, in conditions associated with ventricular

enlargement (physiological such as ageing, or pathological such as AD and SD), VBM shows changes in the CSF and white matter compartments. This does not necessarily imply white matter atrophy, and inspection of the original structural images, as well as the segmented images will help determine whether a structure is truly altered in volume, or merely displaced. It is therefore helpful to the interpretation of VBM results to perform analyses of all three tissue compartments. In AD and SD I observed apparent decreases in white matter volume in the corpus callosum and periventricular regions. Inspection of the structural images shows ventricular enlargement, and in many cases thinning of the corpus callosum. I conclude, that in this patient group, some of the white matter changes are real, but some could reflect ventricular enlargement. A similar effect is noted in the white matter adjacent to the enlarged Sylvian fissures, which probably reflects a boundary shift.

ROI Measurements

ROI measurements were manually defined on a segmented brain image (having removed CSF with a threshold at 60% of mean brain intensity) using a mouse driven cursor. Regions were defined and edited in real time in three planes with a reproducibility error of 1.9-4.3%. Most temporal regions included grey and white matter so it is more appropriate to refer to volume reductions of these structures rather than grey matter atrophy. The entorhinal cortex ROI only included grey matter, but the medial portion of entorhinal cortex along the collateral sulcus was excluded due to the variance of this structure. In addition, the middle and inferior temporal gyri were included in the same ROI, making direct regional comparisons with VBM difficult. Furthermore, ROI measurements of total hippocampal volume (which excluded the hippocampal tail) cannot be directly compared with VBM measurements, rather the measurements of anterior, middle and posterior thirds are more comparable (see tables 2&3). As with VBM there are potential sources of volume changes not directly related to atrophy. Firstly, in these elderly patients with cerebral atrophy, partial volume artefact can occur between brain/CSF interfaces leading to misclassification of voxels. Secondly, with reduced grey/white contrast, the borders of complex anatomical structures are difficult to define accurately by visual inspection. Thirdly, by excluding part of the entorhinal cortex, namely the part with greatest variance, the ROI data are not a true reflection of the state of the whole entorhinal cortex.

Previous morphometry studies

Little information is available on the whole brain patterns of atrophy in moderate or severe AD, although within subject longitudinal data suggest global cortical atrophy in more advanced stages (Fox *et al.* 1996a; Fox and Freeborough 1997; Scahill *et al.* 2002). Most previous quantitative morphometrics have focussed only on temporal lobe measurements making comparisons with our VBM data difficult. In early AD, previous VBM (Baron *et al.* 2001; Rombouts *et al.* 2000) and ROI-based MR morphometry studies (e.g. Chan *et al.* 2001; de Leon *et al.* 1993; de Leon *et al.* 1995; Fox *et al.* 1996c; Frisoni *et al.* 1999; Jack, Jr. *et al.* 1997; Jack, Jr. *et al.* 1998; Juottonen *et al.* 1998; Juottonen *et al.* 1999; Killiany *et al.* 1993; Laakso *et al.* 1998; Laakso *et al.* 2000) have documented predominant anteromesial temporal lobe atrophy. Opinions differ on whether or not the hippocampi or entorhinal cortex are more severely affected. Juottonen *et al.* (1999) suggest that entorhinal cortex is preferentially atrophied however Laakso *et al.* (2000) showed more atrophy in the right hippocampus and lesser but equivalent atrophy in the left hippocampus and both entorhinal cortices in AD. Xu *et al.* (2000b) noted that despite the expectation of preferential entorhinal atrophy in early AD based on pathological data, MR data showed equivalent measurements for entorhinal cortex and hippocampus. They surmised this was due to anatomic ambiguity of the borders of the entorhinal cortex, image artefact, or both, and suggested that hippocampal measurements may be more useful for differentiating AD from normality. A recent morphometry study using a temporal rating scale (validated with ROI measurements) with good inter-rater and intra-rater variability studied 30 mild-moderate AD and 17 SD patients and 18 control subjects (Galton *et al.* 2001). The study showed hippocampal atrophy in 50% of AD patients but no significant differences in entorhinal cortex, parahippocampal gyrus, or other temporal areas relative to controls, although it should be noted that entorhinal cortex was not explicitly defined and was included as part of a parahippocampal gyrus region. Direct comparisons of their data with the ROI data of this study are therefore not possible.

In SD, Galton *et al.* (2001) showed significantly more atrophy than AD in all temporal lobe structures (except the right hippocampus). A previous VBM study of six patients with SD showed asymmetric temporal lobe atrophy, more pronounced on the left side but did not find significant atrophy in the hippocampus and entorhinal cortex

(Mummery *et al.* 2000). These data differ in part from ours, since I detected most significant atrophy in the left amygdala, hippocampus and entorhinal cortex. This discrepancy reflects in part the evolution of VBM techniques, in particular optimisations of spatial normalisation and segmentation that have been recently introduced (Good *et al.* 2001c; Good *et al.* 2001b). My method, in contrast to that of (Mummery *et al.* 2000) included updated SPM software, an automated brain extraction step, customised templates, a modulation step to incorporate information from deformation fields and statistical analyses modelling TIV as well as global grey matter.

Histopathological data

In AD, histopathological data suggest early entorhinal cortex involvement (Braak and Braak 1991) with subsequent spread to the hippocampus proper, other temporal gyri, parietal and posterior cingulate cortices (Braak and Braak 1996; Braak *et al.* 1998). In SD, there is a spectrum of non-Alzheimer pathological findings identical to those reported in the frontal variant of FTLD, but with most pathology in the temporal lobes, particularly anteriorly (Hodges *et al.* 1998), either with or without specific neuronal inclusions (tau or ubiquitin positive). There are few pathological data on entorhinal cortex involvement in FTLD, and the literature on hippocampal atrophy is conflicting, most reports suggesting only minor atrophy.

VBM data for extra-temporal structures

Unfortunately these results cannot be corroborated with ROI analyses, since it is impractical to collect ROI data for each and every cortical structure. In AD, VBM detected most significant atrophy in the parietal and posterior cingulate cortices, with sparing of occipital and sensorimotor cortex. Interestingly, when the global amount of grey matter was modelled as a confounding covariate, no atrophy greater than that found generally was detected in the hippocampus, or elsewhere in the temporal lobes. This suggests that the degree of hippocampal atrophy does not exceed that for grey matter in general in patients with moderately severe AD. This was contrary to a prior expectation of increased mesial temporal lobe atrophy, over and above distributed changes. One might speculate that early on in AD atrophy is most marked in anteromesial temporal structures as has been suggested by a number of previous structural imaging studies (e.g. de Leon *et al.* 1993; de Leon *et al.* 1995; Fox *et al.* 1996c; Jack, Jr. *et al.* 1997; Juottonen *et al.* 1998; Juottonen *et al.* 1999; Killiany *et al.*

1993), but as the disease progresses to the moderate and severe stages, atrophy becomes more generalised. In this study all the AD patients were impaired, with global impairment in 6 out of 10 patients. Impairment was moderately severe, with scores between the first and fifth percentiles of performance on both verbal and visual subtests, so it is not surprising that VBM detected global cortical atrophy. Furthermore, the pattern of posterior atrophy detected by VBM matches the parietal and posterior cingulate distribution of oxygen and glucose hypometabolism on PET studies (Baron *et al.* 2001; Foster *et al.* 1983; Frackowiak *et al.* 1981). Interestingly PET data suggest that these regions appear to be affected earlier than the mesial temporal regions in AD (Minoshima *et al.* 1997; Small *et al.* 2000) although this is contrary to histopathological evidence of the hierarchical spread of neurofibrillary tangles in AD (Braak and Braak 1996; Braak *et al.* 1998; Delacourte *et al.* 1999). Recent work by Thompson *et al.* (2001a) using an accurate cortical mapping technique and voxel-wise assessment of grey matter also show a pattern of temporo parietal atrophy in AD. It is worth noting that two recent VBM studies detected predominant mesial temporal lobe atrophy (anterior hippocampus, amygdala and entorhinal cortex) in patients with early Alzheimer's disease (Baron *et al.* 2001; Rombouts *et al.* 2000).

In SD, VBM detected a regional pattern of temporal lobe atrophy in all analyses, corroborating previous imaging data (Baron *et al.* 2001; Frisoni *et al.* 1999; Laakso *et al.* 2000).

Callosal atrophy has been documented in AD, FTLD and other degenerative conditions and has been found to be associated with cognitive impairment and cerebral cortical hypometabolism, probably reflecting cortical disconnection and axonal degeneration (Hampel *et al.* 1998; Teipel *et al.* 1999; Yamauchi *et al.* 1993; Yamauchi *et al.* 2000). In my study VBM showed white matter volume loss in the region of the left side of the corpus callosum in the SD group. As mentioned earlier, this probably reflects an interface shift due to the adjacent enlarged lateral ventricle, since asymmetric atrophy of callosal white matter tracts would seem anatomically implausible. The changes in the caudate nucleus and thalamus are more difficult to interpret. Atrophy of the caudate nucleus has been observed in a previous VBM study (Rombouts *et al.* 2000) and histopathological changes have been observed in the striata of AD brains (Braak and Braak 1990). Atrophy of the thalamus has been associated with poor verbal learning in Alzheimer's disease (Stout *et al.* 1999), although there is little further corroborating evidence from previous MRI studies to confirm or refute

these findings. Some of these VBM detected thalamic and caudate changes may reflect misclassified voxels and interface shifts due to ventricular enlargement, and should thus be interpreted with some caution. There are clearly differences in these regions but a simple attribution to grey matter atrophy may be premature.

Conclusion

In this study VBM is compared with the best available approximation to a gold standard for measurements of temporal lobe atrophy in AD and SD. The agreements and differences between VBM and classical ROI-based analyses are highlighted and the different measurement techniques and potential sources of misattribution are discussed. The results from the automated and manual methods are not expected to be identical, just as the ROI based approach would not produce the same results if a different parcellation scheme were adopted. The principal requirement is that the two approaches should show the same general trends. VBM produces comparable results to a time consuming manual technique that requires brain structures to be expertly labelled but provides far more additional detail. In several regions VBM is more sensitive than ROI measurements, furthermore VBM has the distinct advantage of showing changes throughout the brain on a voxel-wise basis and the versatility of the SPM framework allows global and regional changes to be finessed. This allows biologically important changes outside the temporal lobe to be highlighted rather than be ignored (as in so many ROI based studies). Significantly VBM avoids the subjectivity of ROI approaches introduced by observer bias, and results are thus comparable between laboratories. With ever increasing improvements in image acquisition and computational power there will be greater value in automated unbiased whole brain techniques such as VBM. I would however caution users of automated techniques such as VBM for disease based studies to carefully inspect each stage of image pre-processing in order to improve interpretation.

CHAPTER 6

CLINICAL GROUPS

TEMPORAL LOBE EPILEPSY

Guide to Reader

A previous study using VBM in its earliest form of development failed to detect focal hippocampal atrophy in a small group of patients with histologically proven mesial temporal sclerosis and temporal lobe epilepsy (Woermann *et al.* 1999b) raising concerns about the validity and sensitivity of the technique. In order to further establish the clinical validity of the optimised method of VBM, I test here whether VBM can identify and characterise ipsilateral hippocampal atrophy in groups of patients with temporal lobe epilepsy, histologically proven unilateral mesial temporal sclerosis and reduced unilateral hippocampal volume on ROI morphometry. I also test whether preoperative ROI morphometry and VBM can predict clinical outcome after temporal lobectomy.

Introduction

The high prevalence and morbidity of epilepsy along with the development of new medical and surgical therapies have stimulated major advances in morphometric techniques of the brain. In many instances a patient is severely debilitated with epilepsy, but the MRI appears normal and functional tests may be contradictory. VBM may offer some hope for detecting occult epileptogenic foci and is currently being introduced in the research setting. In patients with malformations of cortical development, for example, VBM detects anatomical abnormalities that correlate with benzodiazepine receptor density and functional imaging changes. Importantly, these anatomical changes were invisible on high resolution MRI and missed by independent blinded region of interest measurements (Richardson *et al.* 1997). This study implemented voxel-wise comparisons of structural and functional data for the first time, which may have great potential for future studies if the methodological challenges can be met. VBM has been applied also to other forms of epilepsy: in 20

patients with juvenile myoclonic epilepsy and normal diagnostic MRI, VBM detects increased grey matter in the mesial frontal lobes (Woermann *et al.* 1999b). Paradoxically in another study by the same group, VBM (using a very early form) did not detect hippocampal atrophy in 10 patients with histologically proven mesial temporal sclerosis (MTS) (Woermann *et al.* 1999a) raising concerns about the technique.

Approximately thirty percent of patients with refractory mesial temporal epilepsy (mTLE) and hippocampal sclerosis (HS) experience persistent seizures after appropriate temporal lobe surgery. Unilateral hippocampal volume loss and increased T2 signal on preoperative magnetic resonance imaging (MRI) are favourable factors, but some patients with histological proven HS and apparently complete resections do not become seizure free (Berkovic *et al.* 1991; Berkovic *et al.* 1995). Not all pathologies are visible on MRI and there may be subtle abnormalities in addition to visible changes of HS on preoperative MRI.

MRI post-processing techniques can identify extra-hippocampal abnormalities that are not apparent on visual inspection (Sisodiya *et al.* 1996). A quantitative analysis of mesial and lateral temporal lobe volumes in mTLE patients revealed atrophy in all mesial and lateral temporal lobe structures examined except the amygdala, for which reliable identification of boundaries was difficult (Moran *et al.* 1999; Moran *et al.* 2001). The presence of extra-hippocampal abnormalities of cerebral configuration, identified quantitatively on visually normal-appearing brain MRI, was associated with a reduced chance of a good outcome in patients with HS (Sisodiya *et al.* 1997). These methods employed large ROIs and therefore did not allow detection of subtle regional changes within the ROI nor changes outside the ROI. Clearly a whole brain morphometric technique such as VBM that allows unbiased whole brain voxel-wise assessment of grey and white matter differences offers distinct advantages, but equally would need to be proved valid.

The aims of this study were firstly to determine whether VBM could reliably detect regional grey matter (GM) abnormalities on pre-operative structural MR images in patients with mTLE (in light of the early VBM study which did not reliably detect mTLE in 10 patients either as a group effect or within individual subjects). Secondly to determine whether there were differences in the distribution of atrophy between left and right mTLE. Thirdly to determine whether there were differences between groups who were either seizure-free or who continued to have seizures following temporal

lobe resection.

Methods:

Subjects

The study group comprised thirty patients (19 female, median age 32 years, range 20 to 49 years) with left mTLE and twenty-two patients (14 female, median age 33, range 22-56) with right mTLE who were evaluated for epilepsy surgery at the National Hospital for Neurology and neurosurgery, UCLH and Charlfont Centre for Epilepsy. All patients had a clear MRI diagnosis of hippocampal sclerosis (HS) according to accepted qualitative and quantitative MRI criteria with unilaterally reduced hippocampal volumes corrected for intracranial volume, abnormal hippocampal volume asymmetry indices, and increased hippocampal T2 times. Thirty patients underwent standardized anterior temporal resections performed by Mr William Harkness, with removal of the affected hippocampus, part of the amygdala, and anterior 3 cm of lateral temporal neocortex. The MRI finding of HS was histologically verified in the excised mesial temporal structures in all patients.

Thirty neurologically normal control subjects (18 female, median age 30 years, range 16 to 46 years) were scanned for comparison. Written informed consent was obtained in all cases according to the Declaration of Helsinki, and approval for the study was obtained from the Local Research Ethics Committee of the National Hospital for Neurology and Neurosurgery (UCLH, NHS Trust) and the Institute of Neurology (UCL).

Outcome

All patients had a minimum duration of follow-up of 2 years after surgery. Outcome was assessed using a strict interpretation of Engel's scale (Engel *et al.* 1993) in that patients were considered to be seizure free only if they had not had any seizures or auras for a continuous period of at least 2 years up to the last follow-up.

MRI scanning

Preoperative MRI images were obtained at the Chalfont Centre for Epilepsy on a 1.5T GE Signa scanner (GE Medical Systems, Milwaukee, Wis., USA) using a T1-weighted inversion-recovery prepared volume acquisition [IRSPGE: T1/TR/TE/flip =

450/15/4.2/20; 124 x 1.5mm thick contiguous coronal slices; matrix 256 x 192, 24 cm x 18 cm FOV (field of view)(T1 = inversion time; TR = repetition time; TE = echo time]. All images were reviewed by an experienced neuroradiologist focusing particularly on abnormalities outside the affected hippocampus.

Image processing

The optimised method of VBM was followed (see Chapter 2) using the SPM apriori grey and white matter templates for grey and white matter analyses respectively.

VBM statistical analysis

The smoothed modulated and unmodulated data were analysed. Significance levels were set at $p<0.05$, corrected for whole brain volume, and in addition temporolimbic voxels were small volume corrected (SVC) using a mask covering temporo-limbic structures, including hippocampus, amygdala, parahippocampal gyrus and orbitofrontal cortex bilaterally. The aim was to assess the effect of post-operative seizure outcome when comparing mTLE patients versus controls. For this purpose regions showing a difference between patients and controls were further assessed for differences between seizure-free patients and patients suffering from seizures post-operatively (using inclusive masking). Duration of epilepsy was defined as a covariate of interest in a separate parametric analysis with age and gender as confounding covariates.

Results

Comparison of pre-operative mTLE patients versus controls

Voxel-based comparison of patients and controls revealed a group main effect of grey matter volume (modulated data) and concentration (unmodulated data) with decreases in the patient population in the ipsilateral hippocampus (x=-30, y=-15,z=-20; Z=6.13, $p<0.001$), amygdala (Z=5.59, $p<0.001$), dorsal mid thalamic region (x=-8, y=-33,z=6; Z=5.26, $p<0.005$) and superior temporal gyrus (x=-36, y=28,z=-30; Z=4.94, $p<0.05$) (Figs. 6.1and 6.2).

Comparing patients with left and right MTS, VBM detected grey matter volume (and concentration) loss was asymmetric, with more extensive grey matter loss

being observed in left MTS (Fig. 6.2)

Figure 6.1: Grey matter concentration loss in temporal lobe epilepsy

Reduced grey matter concentration in 30 left TLE patients compared to 30 controls, displayed on a single normalised T1 volume MRI image thresholded at $p<0.001$ uncorrected for display. The colour bar represents the T score

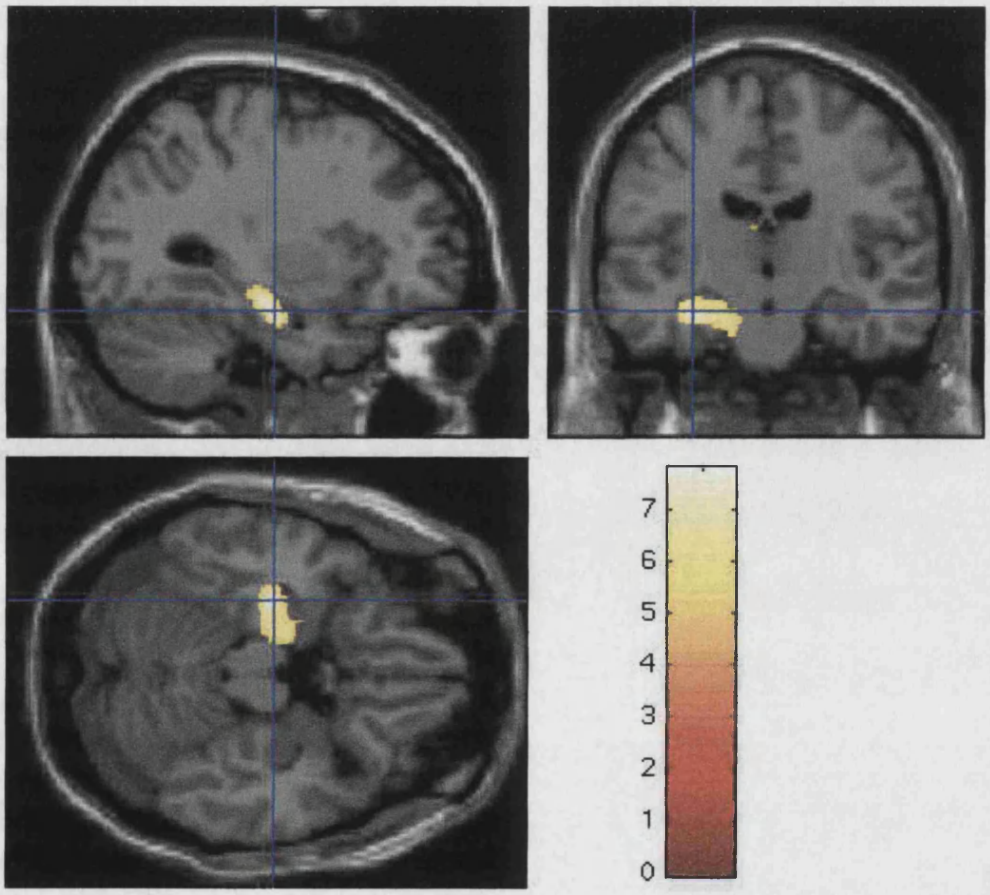

Figure 6.2: Asymmetry of MTS atrophy

VBM detected grey matter volume loss in left mesial temporal sclerosis (MTS) (in red) and right MTS (in green) projected over the group mean normalised image. Atrophy is asymmetric, with more extensive grey matter loss being observed in left MTS.

- left sided mesial temporal sclerosis (pre-operative)
- right sided mesial temporal sclerosis (pre-operative)

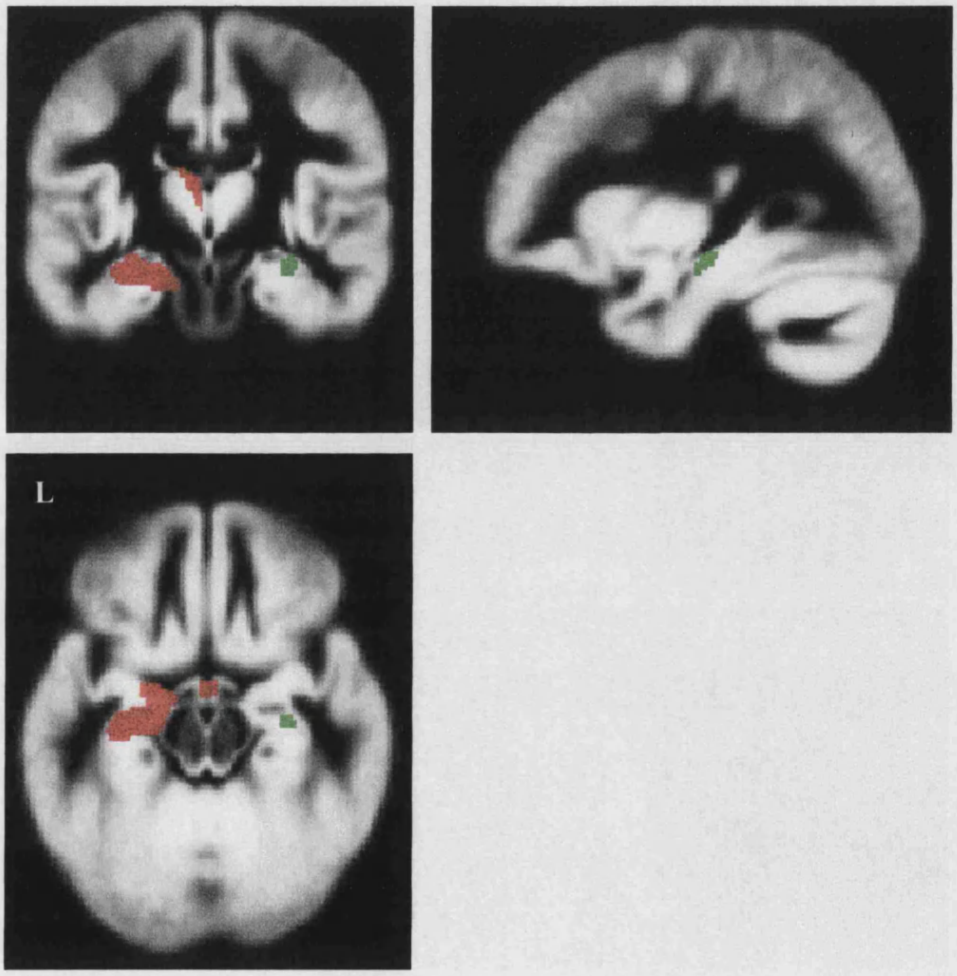

Comparison of postoperative seizure-free left mTLE patients versus patients with post-operative seizures

16 patients (10 female, median age 33 years, range 28 to 48 years) with a median follow-up of 48 months (range: 24 – 60 months) remained seizure-free postoperatively and 14 patients (8 female, median age 31 years, range 20 to 49 years) with a median follow-up: 36 months (range: 24 – 60 months) continued to experience seizures after surgery. There were no differences in quantitative ROI hippocampal volume measurements between these two groups.

VBM group-comparison showed significantly larger grey matter reductions in the ipsilateral mesial temporal lobe and orbitofrontal cortex (x=-18, y=2,z=-14; Z=4.33, $p < 0.005$) in patients who continued to have seizures after temporal lobe surgery, compared with those who remained seizure free post operatively (Fig. 6.3, 6.4). In those patients that remained seizure free, grey matter loss was more pronounced in the anterior hippocampus (x= -30, y = -15,z=-20; Z=6.31, $p<0.001$) and inferior temporal gyrus (x=-32, y=18, z=-30, Z=4.94, $p<0.05$) (Fig. 6.5). Furthermore, VBM also shows more extensive white matter loss in patients with postoperative seizures.

Figure 6.3: Unfavourable post-operative outcome and grey matter concentration

Decreases in grey matter concentration in 14 left TLE patients with post-operative seizures compared to 16 left TLE post-operatively seizure-free patients, masked inclusively with grey matter reduction in left TLE versus controls. Significantly larger grey matter reductions are seen in the ipsilateral orbitofrontal cortex (x=-18, y=2,z=-14; Z=4.33, p <0.005) and mesial temporal lobe (not shown) in patients who continued to have seizures

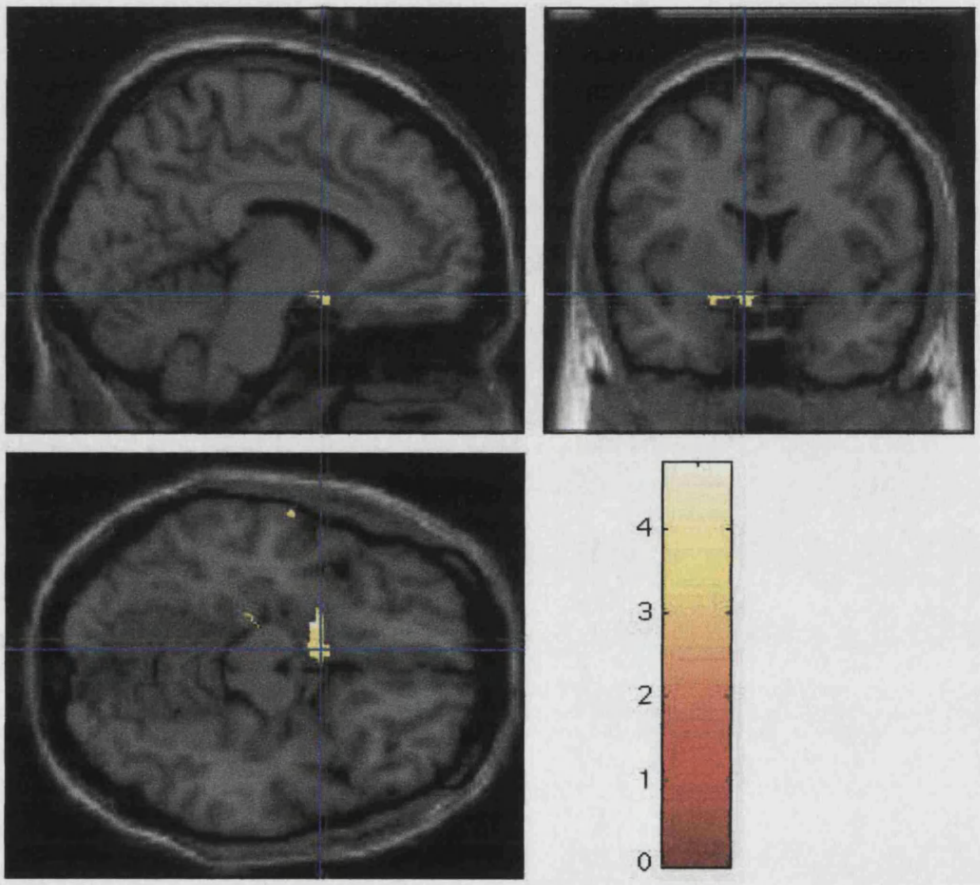

Figure 6.4: Post-operative outcome and grey matter volume

- Grey matter volume loss in patients with left MTS who continued to have seizures after left temporal lobectomy

- Grey matter volume loss in patients with left MTS who remained seizure free following left temporal lobectomy

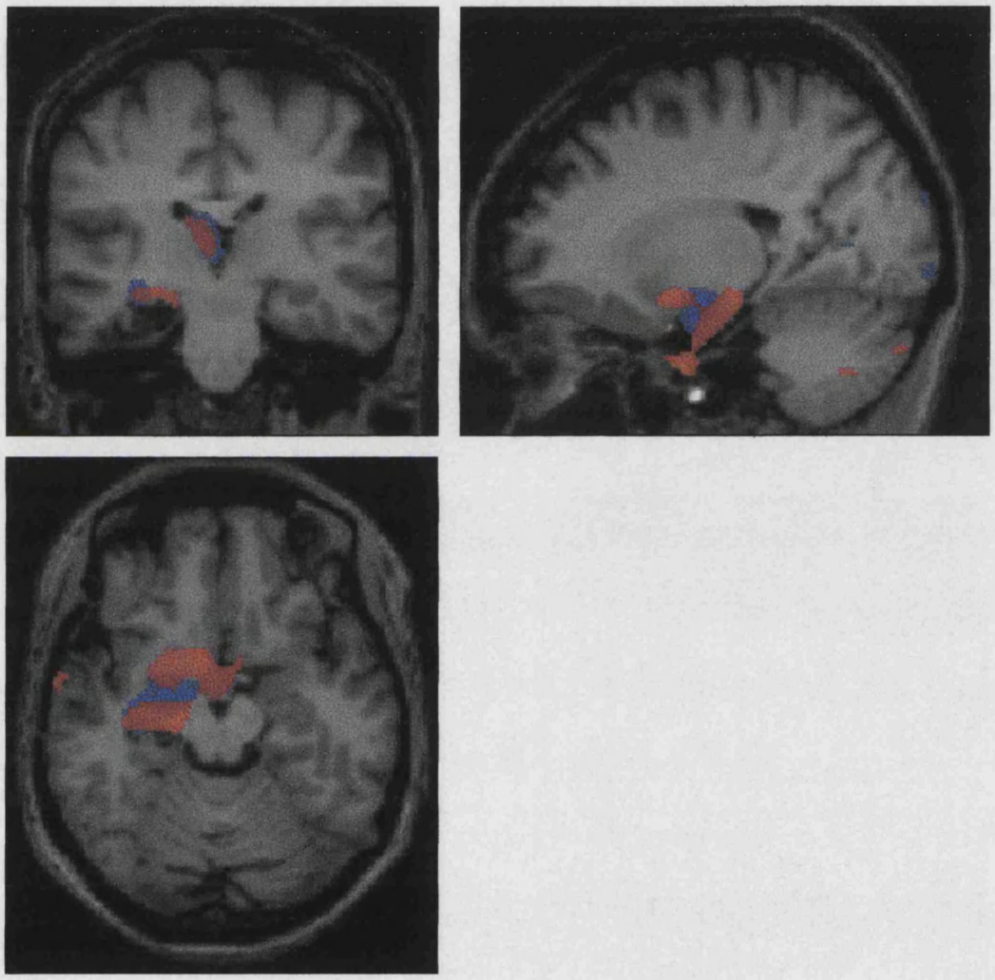

Figure 6.5: Favourable post-operative outcome and grey matter concentration

Decreases in grey matter concentration in 16 post-operative left TLE patients who remained seizure-free compared to 14 left TLE patients with persistent post-operative seizures, masked inclusively with the grey matter reductions in left TLE versus controls. The colour bar represents the Z score. Grey matter loss is more pronounced in the anterior hippocampus (x= -30, y = -15,z=-20; Z=6.31, $p<0.001$) and inferior temporal gyrus (not shown) (x=-32, y=18, z=-30, Z=4.94, $p<0.05$)

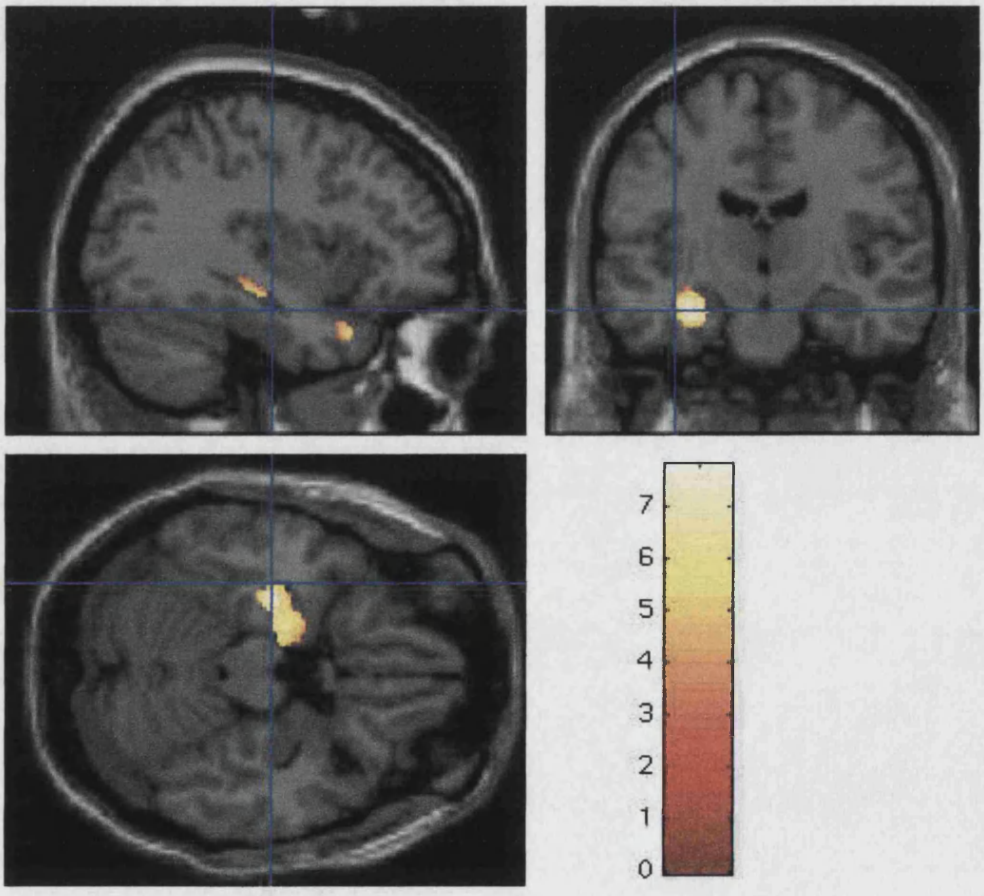

Covariate analysis: duration of epilepsy

There was no correlation between duration of epilepsy and grey matter concentration or volume in the hippocampus or elsewhere in the brain.

Discussion

These in-vivo MRI findings confirm numerous observations of pathology in mTLE beyond the sclerotic hippocampus in the adjacent regions of the amygdala, entorhinal cortex, and thalamus (DeCarli *et al.* 1998; Moran *et al.* 2001). The advantage of VBM over region-based approaches is that it is a fully automated whole brain technique and thus is not biased to a subjectively chosen region. This study confirms that the optimised method of VBM is sensitive to regional hippocampal atrophy due to mesial temporal sclerosis, refuting concerns generated by the early VBM study of 10 patients with MTS (Woermann *et al* 1999). VBM shows a clear difference in the extent of atrophy in right and left MTS, with more extensive atrophy in left MTS. More importantly VBM is sensitive to subtle regional structural changes within the hippocampal GM that were undetectable on standard imaging methods. This finding suggests differences in the distribution of hippocampal atrophy and that volume profiles of the hippocampus may be more important than total hippocampal volumes in predicting seizure outcome. If pathology is confined to the surgical resection site, the patient is more likely to be seizure-free post-operatively.

Using VBM I confirm previous reports of extra-hippocampal damage in patients with poor outcome (Lieb *et al.* 1991) and localise these changes to the posterior orbitofrontal cortex around the anterior perforated space, a region of strong reciprocal connections with the hippocampus (Lieb *et al.* 1991). VBM detected focal ipsilateral grey matter reduction in the mid dorsal thalamus of patients with poor outcome. As I have mentioned earlier, it is important to exclude boundary shift in this region, but none of the patients showed asymmetrical enlargement of the body of the lateral ventricle, so it is likely that the thalamic volume loss is real. These findings concur with previous ROI volumetric measurements of thalamic atrophy in MTS (DeCarli *et al.* 1998; Dreifuss *et al.* 2001). The hippocampal formation receives substantial innervation from a number of thalamic nuclei with widespread, mostly

reciprocal connections of the medial dorsal thalamic nucleus with mesial temporal structures (Lieb *et al.* 1991). Although these reports cannot define the basis for macroscopic morphological changes within the thalamus or the functional consequences of such changes, they do suggest a potential role of the thalamus in TLE.

Conclusion

This study confirms that VBM is a useful technique for characterising the pattern of atrophy in patients with mTLE. Moreover, VBM detects changes that are occult on expert visual appraisal of MRI. These data confirm evidence of widespread pathology in mTLE beyond the sclerotic hippocampus (DeCarli *et al.* 1998; Dreifuss *et al.* 2001; Keller *et al.* 2002; Lieb *et al.* 1991; Moran *et al.* 1999; Moran *et al.* 2001; Sisodiya *et al.* 1997). In addition, the group of patients with a favourable post-operative outcome have structural MRI abnormalities detectable by VBM and not ROI morphometry that are confined to the resected temporal lobe with the anterior hippocampus being most affected, whereas those patients with an unfavourable outcome have structural abnormalities extending outside the resection zone, in particular into the orbitofrontal cortex.

CHAPTER 7

CLINICAL GROUPS

MIGRAINE

Guide to Reader

Migraine is a common, disabling form of headache that has generally been attributed to primary pathophysiology within the cranial vasculature. More recently a number of functional imaging studies of primary headache have demonstrated activations within generic pain regions such as cingulate cortex and insulae and more specific activation of the dorsal pons suggesting that migraine may be based fundamentally on focal brain dysfunction. Conventional neuroimaging may reveal evanescent white matter foci, but no consistent structural abnormality has yet been identified. In light of an early VBM study showing hypothalamic grey matter changes in patients with cluster headache exactly matching a region of hyperactivation on functional imaging, I test here whether VBM can reveal a putative structural correlate to the dorsal pontine activations seen in migraine patients.

Introduction

Migraine, an episodic pain condition with associated features, is a common clinical problem that affects approximately 15% of the population (Lipton *et al.* 2003; Stewart *et al.* 1992; Menken *et al.* 2000). This form of episodic primary neurovascular headache is likely to be based fundamentally on dysfunction within the brain. Recent advances in the underlying pathophysiological mechanisms of migraine and new therapeutic strategies have provided considerable insights into the problem. Since migraine is a form of primary headache (Headache Classification Committee of the International Headache Society 1988) it is generally hypothesized that the underlying problem is biochemical or biophysical in nature and consequently macroscopic brain structure should be normal.

Recent developments in functional brain imaging have allowed improved understanding of many aspects of neurophysiology. For example, focal activations in brain areas known to be associated with pain, such as cingulate cortex and insulae, have been demonstrated in patients with primary headaches such as migraine (Bahra *et al.* 2001; Weiller *et al.* 1995) and cluster headache (May *et al.* 1998a; May *et al.* 2000; May and Goadsby 2001). These areas are similarly activated when pain is induced by injection of capsaicin into the forehead of volunteers (May *et al.* 1998b). In addition to these generic pain areas, activations can be seen in specific brain regions in migraine and cluster headache that are not observed when the first (ophthalmic) division pain pathways are activated by the capsaicin injections. For example, brainstem areas are activated in migraine (Weiller *et al.* 1995), which have recently been localised to the dorsal pons (Bahra *et al.* 2001). In contrast the posterior hypothalamic grey matter is uniquely activated in cluster headache and SUNCT (short-lasting unilateral neuralgiform with conjunctival injection and tearing) (May *et al.* 1999c).

An early VBM study has suggested that there is a correlation between the brain area specifically activated in acute cluster headache (May *et al.* 1998a), the posterior hypothalamic grey matter and some macroscopic change in grey matter in the same region (May *et al.* 1999b). This finding needs careful evaluation on its own merits, but does stimulate the question as to whether other primary headaches, particularly migraine, show similar functional-structural correlations. In this study I use VBM to investigate whether there are structural changes associated with previously documented activations in the brainstem, in particular the dorsal pons and/or hypothalamus of migraine sufferers.

Methods

Subjects

Approval for the study was obtained from the Local Research Ethics Committee of the National Hospital for Neurology and Neurosurgery (UCLH, NHS Trust) and the Institute of Neurology (UCL). Patients with migraine were recruited from patients attending the Hospital and patient support groups by Professor Goadsby's clinical team, in particular Dr Manjit Matharu. The study group comprised 11 patients with migraine with aura (10 females, 1 male: 23-52 years, mean 31); 11 controls (10 females, 1 male: 23-52, mean 31); 17 patients with migraine without aura

(16 females,1 male: 24-57, mean 34); 17 controls (16 females, 1 male: 24-57, mean 34).

Structural MRI scanning protocol

High-resolution magnetic resonance imaging was performed on a 2 Tesla Siemens MAGNETOM Vision scanner. A 3D structural MRI was acquired on each subject using a T-1 weighted MPRAGE sequence TR/TE/TI/NEX 9.7/4/ 600/1, flip angle 12°, matrix size 256 × 192, FOV 256 × 192, yielding 108 sagittal slices, slice thickness of 1.5mm and in plane resolution of 1mm × 1mm.

Data Pre-processing and analysis

The optimised voxel-based morphometry protocol was used for image pre-processing (see Chapter 2 for details).

I used customised grey and white matter templates for spatial normalisation, which were created from a separate group of 180 normal subjects with no history of migraine (168 females and 12 males; 18-70 years, mean 32 years), imaged on the same scanner with identical parameters in order to remove any scanner dependent bias.

VBM statistical analysis

Separate analyses were performed for grey and white matter using modulated and unmodulated data. 4 conditions were assigned, namely migraine with aura, migraine without aura and 2 age and sex matched control groups. Since patients with migraine and their respective controls were exactly age and sex matched, no age or sex confounds were included. I controlled for global differences in voxel intensity across scans by proportionally scaling the global mean voxel intensity value. I also included analyses with no global modelling. Significance levels were initially set at $p<0.05$, corrected for multiple comparisons. In order to improve sensitivity (and minimize the possibility of false negatives), the data were subjected to further scrutiny as follows: since the dorsal pons and hypothalamus had been identified *a priori* as possible candidates for structural change, the analysis was repeated with more liberal significance levels set at $p<0.005$ uncorrected for multiple comparisons (the intention being to use small volume correction if any pontine or hypothalamic changes were observed). I arbitrarily chose spheres of 20 and 10mm diameter as conservative estimates of dorsal pons and hypothalamus volume, respectively.

Results

Global grey matter

There was no significant difference in global grey matter volume between either patients with migraine and controls ($F<1$), or patients with aura and without aura ($F<1$).

Regional grey matter

VBM detected no significant difference in grey matter volume or concentration between patients and their respective control groups, or a common difference between patients with migraine (with and without aura) and both control groups (Fig. 7.1).

Global white matter volume

There was no significant difference in global white matter volume between either patients with migraine and controls ($F<1$), or patients with aura and without aura ($F<1$).

Regional white matter

VBM detected no significant difference in white matter volume or concentration between patients and their respective control groups, or a common difference between patients with migraine (with and without aura) and both control groups.

Figure 7.1: No structural difference between migraineurs and controls

Glass brain image on the left showing no significant voxels for the contrast migraine - controls. Design matrix on the right. Column 1 represents controls for migraine with aura patients; Column 2 represents migraine with aura patients; Column 3 represents controls for migraine without aura patients; Column 4 represents migraine without aura patients and Column 6 represents the global mean grey matter value. Each row represents an individual subject.

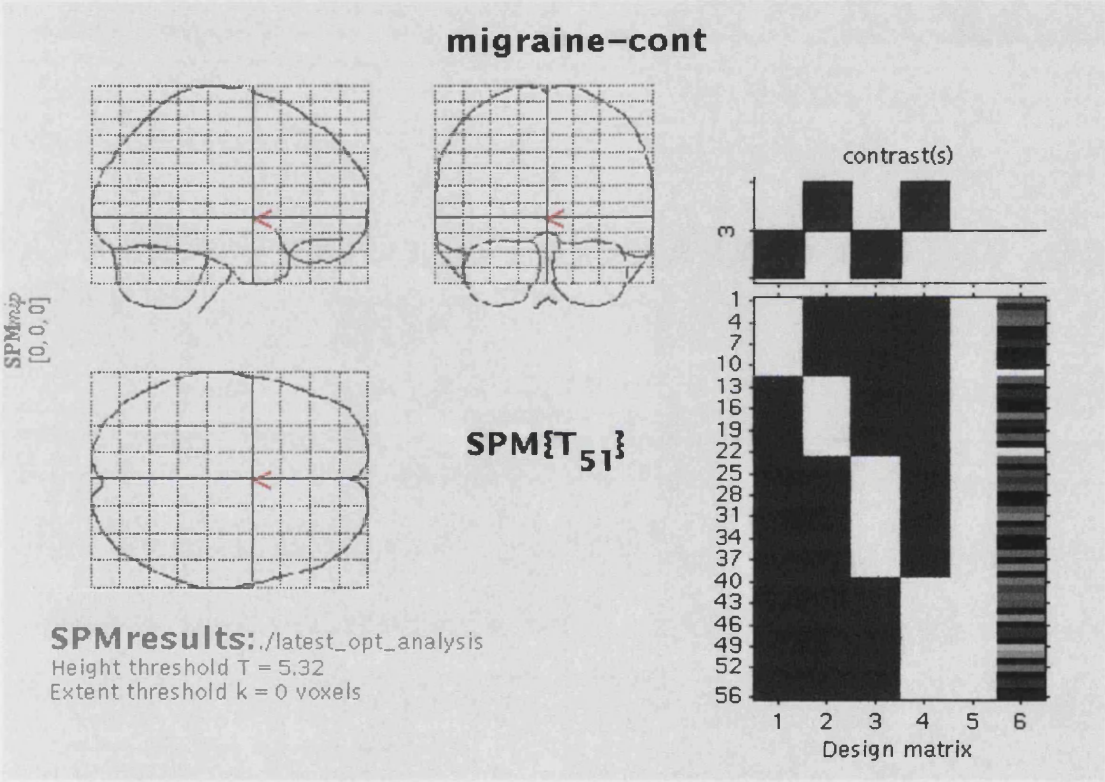

Discussion

In this study I have employed VBM to compare the brains of migraine sufferers with healthy non-headache controls. Migraine patients were sub-classified according to their dominant phenotype namely migraine with aura or migraine without aura, in line with the International Headache Society classification guidelines (Headache Classification Committee of the International Headache Society 1988). I observed no difference in either group when compared to appropriate distinct age and sex matched control groups. These results suggest that either migraine sufferers do not have consistent macroscopic structural brain changes in regions known to be functionally

implicated, or that any putative changes may vary with some biological trait other than simply headache phenotype.

I have shown in previous chapters that the optimised method of VBM replicates established pathological and neuroimaging findings in normal subjects (Chapters 3 and 4), patients with distinct forms of dementia (Chapter 5) and temporal lobe epilepsy (Chapter 6). I have also shown (Chapter 6) and will show (Chapters 8,9,11) that VBM is sensitive to subtle regional structural changes in grey and white matter that are undetectable on standard imaging methods (see also Abell *et al.* 1999; Krams *et al.* 1999; May *et al.* 1999a; Salmond *et al.* 2000; Richardson *et al.* 1997; Woermann *et al.* 1999c; Woermann *et al.* 1999a). Furthermore, an early VBM study has shown macroscopic grey matter changes matching PET activation in the posterior hypothalamus of patients with acute cluster headache. It follows therefore that VBM, particularly the optimised form, should be able to detect consistent macroscopic changes if they are indeed present in patients with migraine. VBM cannot inform about microstructural details such as cytoarchitectonics or histochemistry, rather it can detect differences in tissue volume and concentration on a voxel-wise macroscopic or mesoscopic level.

Focal evanescent white matter lesions have been previously described in migraineurs (Igarashi *et al.* 1991; Soges *et al.* 1988). I would not expect them to be detected by VBM since they occur in variable locations within the white matter, and would thus not be seen as a consistent structural difference between groups. VBM aims to detect consistent structural differences between groups of subjects that can be related to functional correlates and thus further our understanding of disease pathophysiology.

The absence of macroscopic structural change in migraine concurs with current views of the condition (Olesen *et al.* 2000). If indeed migraine is primarily a biochemical/biophysical disorder it is not surprising that the brain structure is normal. This would be the simplest explanation for my negative results. However, it is appropriate to consider some alternative possibilities. This study used the simplest division of migraine into patients with and without aura. One could argue that this may not be the ideal way to classify the patients for this type of study. For example there was no subdivision into laterality of headache or aura. Migraine has a strong genetic component, in terms of predisposition to the disorder (Ferrari 1998) and it seems most likely that this genetic tendency will be heterogenous. Definite genetic links have been

found with specific forms of migraine. For example, familial hemiplegic migraine, a rare well characterised autosomal dominant form of migraine with a prolonged aura, was first genetically characterised with mis-sense mutations in the chromosome 19 located gene for the $\alpha_1 2.1$ sub-unit of the P/Q voltage gated calcium channel (Ophoff *et al.* 1997). This accounts for about 55% of affected families (33), while some families appear to map to chromosome 1 (Ducros *et al.* 1997; Gardner *et al.* 1997) and still others have defects that map to a third, or perhaps more sites. It is possible that structural neuroimaging studies of a genetically heterogenous condition, such as migraine, may miss subtle changes that might segregate with a more homogenous genotype. In order to further examine this possibility I have applied VBM to a specific kindred with a homogeneous genotype (see Chapter 12)

Another consideration is the relationship between migraine headache and aura. It can be argued that migraine aura is a parallel process to the headache (Goadsby 2001). Aura typically precedes headache but may also occur with headache, after headache or indeed without headache. The relationship between a predisposition to aura and any putative structural change related to the headache is unknown. On a positive note, although migraine with aura has a small association with an increased risk for stroke (Tzourio *et al.* 2000), the brains of patients with aura show no consistent loss of either grey or white matter. Furthermore, if there are indeed structural changes to be found in migraine that are of a causal nature to the basic disorder, based on PET studies, one would expect them to be in the diencephalon and brainstem (Bahra *et al.* 2001; Weiller *et al.* 1995) which are challenging areas to compare owing to poor tissue contrast. Perhaps more homogenous populations and even more refined methods may be required to detect such changes.

Conclusion

There is no evidence of consistent macroscopic structural change in the brains of migraine sufferers with or without aura using VBM. These data suggest that migraine is a biochemical/biophysical problem without macroscopic structural consequences. Since the migraine phenotype is heterogeneous, if putative structural changes do exist further studies will probably need to carefully divide patients based on genotype or response to treatment, rather than simply on headache phenotype.

CHAPTER 8

CLINICAL GROUPS

SCHIZOPHRENIA

Guide to Reader

The morphological literature on schizophrenia is large and conflicting owing to a wide variety of study designs and predominantly region of interest based measurement techniques. The most consistent structural alterations in schizophrenia include ventricular enlargement and distributed grey matter loss. Less consistent findings are reports of regional abnormalities such as selective reductions in thalamic volume. In this study I use VBM to characterise the structural brain alterations in a group of 20 schizophrenic patients. I test firstly whether VBM reproduces the most consistent imaging findings and secondly if it reveals new findings in biologically plausible locations that match functional imaging abnormalities.

Introduction

Schizophrenia is a complex mental illness with a worldwide prevalence of approximately 1%. This condition is characterised in acute phases by hallucinations, delusions and disordered thinking, and chronically by flat affect, apathy and social withdrawal. "Negative" cognitive symptoms are common.

Despite extensive research, the underlying pathophysiology of schizophrenia remains poorly understood. Many propose an underlying neurodegenerative process but histological evidence for this is limited by a relative paucity of autopsy studies and methodological inconsistencies. High resolution *in vivo* neuroimaging offers the potential of detecting altered brain morphology that might provide insight into underlying functional and biological processes. Although the neuroimaging literature on schizophrenia is large it is for the most part inconsistent and conflicting. Study sample sizes are often small and most reports are based upon region of interest methods that vary widely across laboratories. In addition, groups of schizophrenic patients tend to be phenotypically heterogeneous with no consistent genotype. For

these reasons, meta-analyses are being increasingly employed to assist interpretation of the literature. The most consistent imaging findings in schizophrenia include reduction in global brain volume, increased CSF volume and regional volume reductions in the amygdala/hippocampal formations (e.g. Weinberger 1984; Weinberger *et al.* 1979b; Weinberger *et al.* 1979a; Fannon *et al.* 2000; Harvey *et al.* 1993; Lim *et al.* 1996; Wright *et al.* 1999; Wright *et al.* 2000a). Observations of localised morphometric abnormalities are generally variable across studies. In a meta-analysis of 58 morphometric studies of schizophrenia, the majority employing manual ROI metrics, volume reductions in medial temporal lobe structures were the most frequent observation (Wright *et al.* 2000a). Morphometric abnormalities in the thalamus have also been reported (Andreasen *et al.* 1994; Gilbert *et al.* 2001; Konick and Friedman 2001) particularly within the mediodorsal thalamic nucleus and pulvinar (Byne *et al.* 2001; Byne *et al.* 2002). Such findings support the theory that thalamic dysfunction, potentially leading to impaired sensory filtering and gating mechanisms, underlies the psychological abnormalities of schizophrenia (Andreasen *et al.* 1996; Andreasen 1997; Frith *et al.* 1995; Schultz and Andreasen 1999).

In schizophrenia, the first application of VBM demonstrated reduced grey matter density in insula, prefrontal and lateral temporal cortices (Wright *et al.* 1995b). A more recent VBM study of childhood-onset schizophrenia reported structural abnormalities of thalamus, posterior cingulate, basal ganglia and ventricular volume (Sowell *et al.* 2000). Voxel-wise assessment of magnetic transfer imaging, an MRI technique sensitive to subtle changes in regional macromolecular integrity, provides additional information about the underlying pathology of schizophrenia (Foong *et al.* 2001). Schizophrenic patients demonstrate frontotemporal abnormalities that correlate with severity of negative symptoms reflecting abnormal integrity of medial prefrontal and adjacent anterior cingulate cortices. It therefore seems likely that schizophrenia is characterised by a combination of widespread grey matter atrophy and more localised frontotemporal changes, perhaps selectively involving thalamocortical circuitry.

Methods

Subjects

Twenty patients with a clinical diagnosis of schizophrenia (ICD-10R) were recruited from the inpatient and outpatient departments of the Royal Free and

associated hospitals by Dr H Ananth and Dr I Popescu. All patients gave informed consent to participate in the study. Ethical approval was granted by the National Hospital for Neurology and Neurosurgery and Institute of Neurology Joint Research Ethics Committee. Controls were recruited from healthy volunteers who were matched closely with the patients on the basis of age, gender, social class and ethnicity (mean ± S.D., controls versus schizophrenic patients; age (years), 38.6 ± 9.7 versus 37.8 ± 9.5; 10 males and 10 females in each group). Detailed clinical data of patients were obtained from medical notes and corroborated by clinical interview on the day of scanning. All schizophrenic patients had a history of treatment with antipsychotic medication (mean treatment duration was 15 ± 9 years) and were clinically stable at the time of scanning. No subjects had a history of additional neurological or systemic illness, head injury or excessive drug and/or alcohol misuse.

MR scanning

Subjects were scanned on a 2 Tesla Siemens MAGNETOM Vision scanner by Dr Hugo Critchley. A 3-dimensional structural MR scan was acquired on each subject using a T-1 weighted MPRAGE sequence (TR/TE/TI/NEX 9.7/4/ 600/1, flip angle 12°, matrix size 256 × 192, FOV 256 × 192, yielding 120 sagittal slices and a slice thickness of 1.5mm with in plane resolution of 1mm × 1mm).

Data pre-processing for voxel-based morphometry

Data pre-processing and analysis was performed by myself using the optimised method of VBM (see Chapter 2 for full details). Customised grey and white matter templates were created from the study group according to previously described methods.

Statistical Analysis

Firstly, I tested global volume measures of grey matter, white matter and CSF calculated from the non-normalised segmented images for group differences in overall tissue compartment volumes. Secondly, for each tissue compartment, I constructed separate design matrices to test for regional group differences in grey and white matter between schizophrenic patients and control subjects. Age, gender and total intracranial volume (TIV, derived from sum of the global measures of compartmental volumes) were entered into each analysis as confounding covariates.

Thirdly, I tested for morphometric changes across the schizophrenic patient group correlating with individual variables that are putative influences on psychosis. These included age of illness onset, handedness, level of educational achievement, family history of psychosis, past substance abuse, age and gender. Regressors were constructed for each of these factors and entered into correlation analyses. Clinical details were obtained from patient notes and confirmed by direct interview with the subjects and carer (Dr H Ananth and Dr I Popescu). Educational achievement was rated on a 3-point scale, 0 indicating no academic qualifications and 3 indicating attainment of a degree or equivalent. Family history of psychosis was scored as; 0: no family history, 1: a second-degree relative and 2: a first-degree relative. Past substance abuse was scored clinically as 0: no significant history to 3: past diagnosis of dependence syndrome, poly-substance abuse or dual diagnosis (a score of 3 excluded the subject from the study).

Statistical parametric maps were constructed to test for morphological differences between schizophrenics and controls (main effects), and for correlations between contextual variables within the schizophrenic group. The distribution of morphological differences across the whole brain was initially assessed using a liberal threshold of $p<0.001$, uncorrected for multiple comparisons, however inferences are centred on differences that achieved significance at $p<0.05$, corrected for whole brain volume.

Results

Global differences

There was no significant between-group difference in a measure of total intracranial volume (TIV) ($F(38) = 0.05$, $p=0.8$). Patients with schizophrenia had significantly lower global cerebral grey matter than controls (absolute volume (ml), controls vs. patients, mean ± S.D.; 516 ± 50 vs. 453 ± 48, $F(38) = 15.4$, $p<0.01$), but there were no significant differences in overall white matter or CSF volumes (controls vs. patients, white matter, 441± 51 vs. 415 ± 56, $F(38) = 2.6$; CSF, 321± 45 vs. 331 ± 54, $F(38) = 1.15$) (Fig. 8.1a). Finally, there were no between group differences in the *relative* proportions of grey and white matter and CSF, by controlling for TIV. Schizophrenic patients showed a reduction in the relative amount of grey matter (controls versus patients; 51.6% versus 48.9%, $p<0.001$) and increased relative CSF

volume (controls versus patients; 20.6% versus 23.6%, $p<0.05$) compared to controls. No difference in between-group proportion of white matter was observed (controls versus patients; 27.7% versus 27.5%, $p=0.7$).

Figure 8.1a: Global tissue compartment volumes

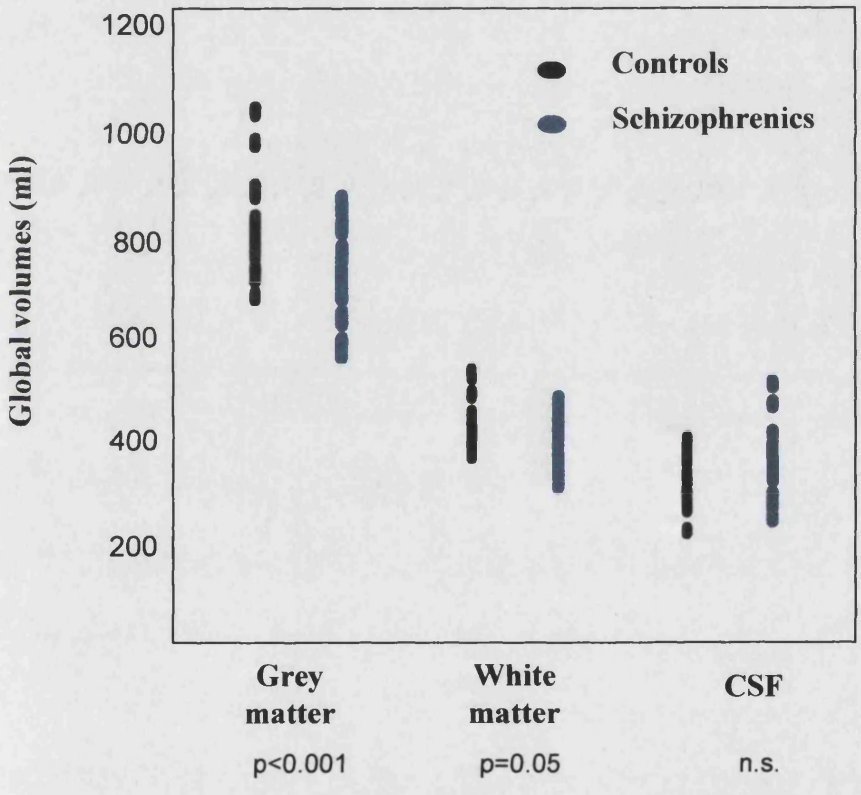

Figure 8.1b: Grey matter volume loss in schizophrenia

The figure shows the location and statistical magnitude (colour bar of T-score) of between-group differences in grey matter volume across the whole brain, to illustrate the widespread distribution of grey matter loss in schizophrenic subjects

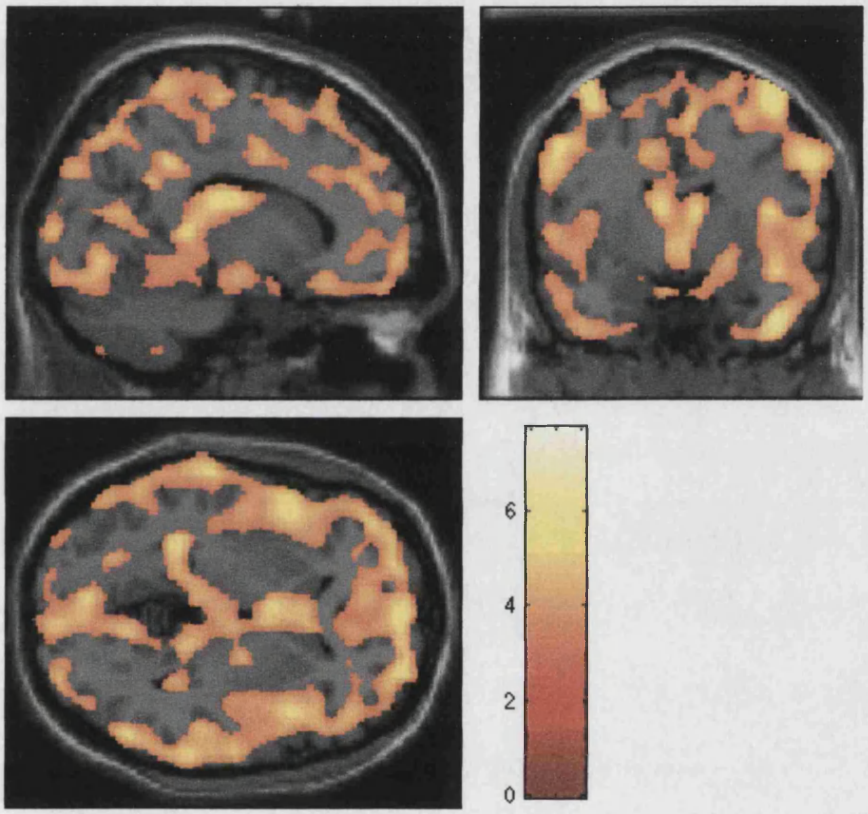

Regional differences

To test for regionally selective differences in cerebral morphology associated with schizophrenia, voxel-wise comparisons of segmented grey matter, white matter and CSF images were performed, using global grey and white matter volumes as confounding covariates. At a low threshold ($p<0.001$,uncorrected), widespread grey matter reductions were observed in cortical and subcortical regions in schizophrenic patients compared to controls (Fig. 8.2). Many brain areas remained significant after a stringent correction for multiple comparisons across whole brain ($p<0.05$, corrected)

(Table 8.1), with the most robust difference in regional grey matter volume being observed in mediodorsal thalamus, especially on the left (Fig. 8.2). Other regional reductions were observed in occipitoparietal cortex, premotor, medial and orbital prefrontal cortices and inferolateral temporal lobe (Table 8.1, Figure 8.3). There were no regions of significantly increased grey matter volume in the schizophrenic group, even without correction for multiple comparisons. Only one region showed a between-group difference in regional white matter volume, the right optic radiation in occipital cortex, which was significantly reduced in the schizophrenic patients ($p<0.05$, corrected). Schizophrenic patients did not show any localised increases in white matter.

Figure 8.2: Regional grey matter decreases in schizophrenic patients.

Most significant grey matter reduction in the mediodorsal thalamus ($p<0.05$ corrected) projected on parasagittal and coronal sections of the normalized unsmoothed template

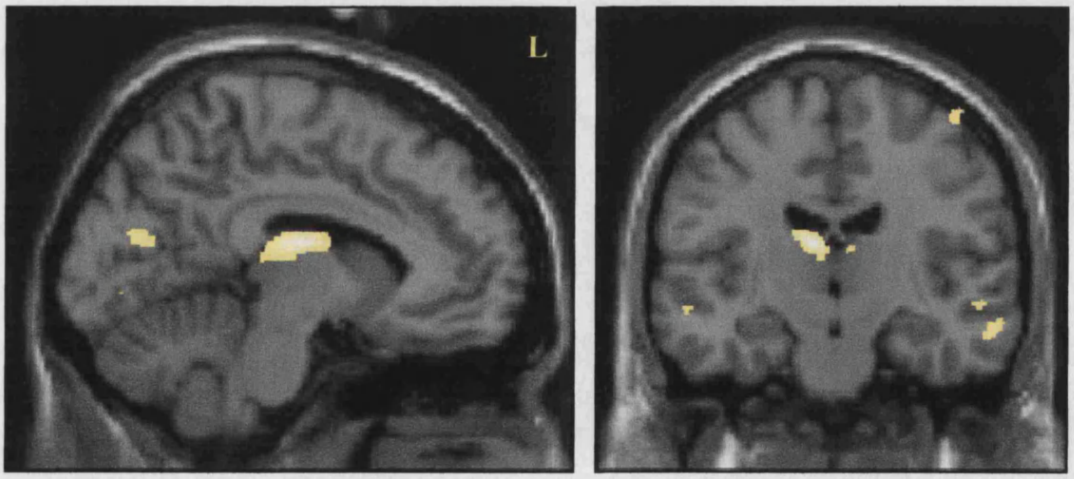

Table 8.1: Grey matter reductions in schizophrenia

Location (x,y,z coordinates of peak difference)	**Side**	**T-score** ($p<0.05$, corrected)
Mediodorsal thalamus (-8,-15,17)	L	7.70
Fusiform gyrus (-23,-74,-9)	L	6.92
Peristriate visual cortex (-6,-75,18)	L	6.75
Inferior frontal gyrus (-45,15,36)	L	6.61
Precentral gyrus (-39,-5,68)	L	6.61
Medial frontal pole (2,63,14)	L&R	7.32
Middle occipital gyrus (45,-74,18)	R	7.52
Premotor/motor cortex (42,-5,65)	R	7.04
Inferior temporal gyrus (66,-35,-6)	R	7.03
Postcentral gyrus (47,-20,68)	R	6.68
Superior frontal gyrus (23,38,53)	R	6.62
Inferior parietal lobule (51,-69,38)	R	6.61
Orbitofrontal cortex (30,33,-9)	R	6.50

Figure 8.3: Regional reductions in grey matter volume in schizophrenia.

Orbitofrontal cortex (1), medial frontal pole (2), inferolateral temporal lobe (3), mediodorsal thalamus (4), insula (5) and occipitoparietal cortex (6).

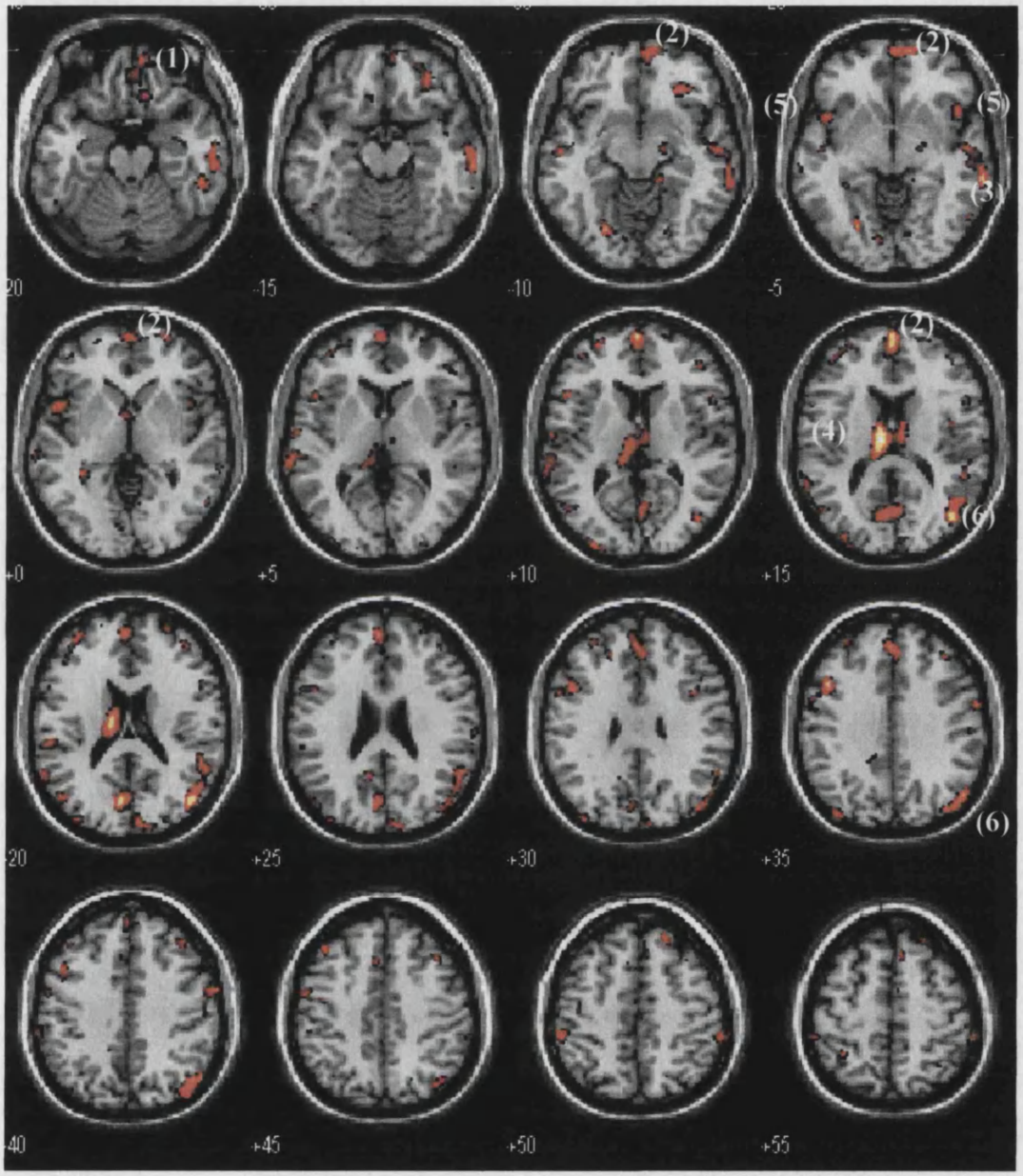

Correlations within patient group

In order to gain further insight into the pathoaetiological associations of detected morphological abnormalities in patients with schizophrenia additional analyses tested for correlations between reductions in grey matter volume and variables that may influence psychosis (handedness, substance misuse and level of educational achievement) and more specific illness-related factors, i.e. age, family history of psychosis and illness-onset. There was a significant negative correlation between global grey matter volume and age of schizophrenic patients ($R=-0.66$, $p<0.01$). Moreover, preservation of (mediodorsal) thalamic grey matter was associated with greater educational achievement (Pearson $R= 0.48$, $p=0.04$, 2-tailed). Regression analyses of regional grey matter revealed a relationship between thalamic grey matter loss and age (0.55, $p=0.01$). A region of ventromedial prefrontal cortex showed a significant relationship with family history of schizophrenia (Fig. 8.4).

Figure 8.4: Effect of family history of schizophrenia

Correlation of medial prefrontal cortex volume (18 40.6 7.6) and a positive family history of schizophrenia / psychosis ($p<0.001$, uncorrected). On the top, group data is projected on the unsmoothed template. On the bottom, adjusted raw data plotted against a regressor for family history of schizophrenia.

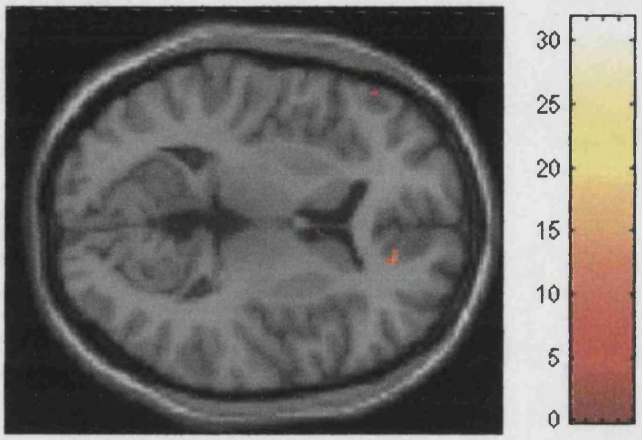

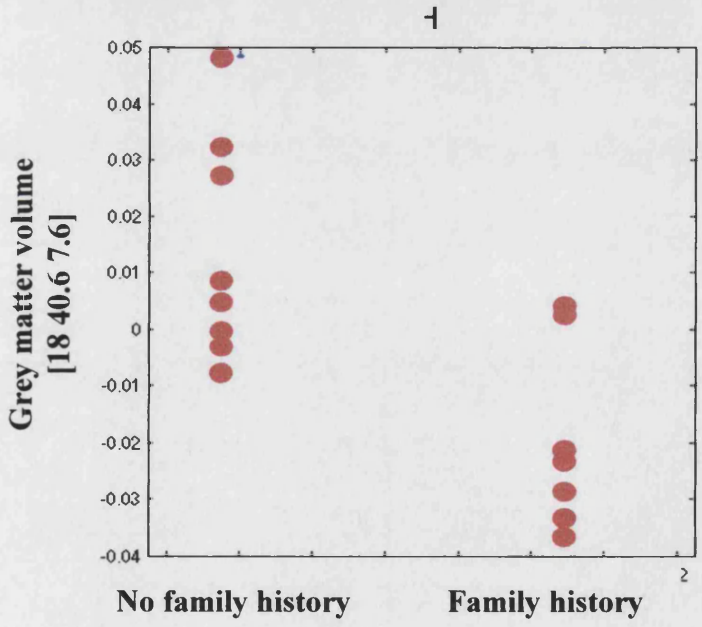

Discussion

In this study VBM confirms the most consistent previous reports of reductions in global grey matter and increases in cerebrospinal fluid in schizophrenic patients (Wright *et al.* 2000b). In addition to widespread frontal, temporal, parietal and occipital cortical involvement, there are also regionally specific cortical morphological changes. The most significant local effect is selective thalamic grey matter loss in schizophrenic subjects relative to controls. This observation, together with a significant correlation of both global and thalamic grey matter loss with age, provide insight into underlying pathoaetiological mechanisms implicit in the schizophrenia phenotype.

Autopsy studies of schizophrenics have confirmed marked neuronal loss in the thalamus, with greatest cell depletion in medial / mediodorsal thalamus (Pakkenberg 1990; Popken *et al.* 2000). This region of thalamus projects to prefrontal cortex, which has been implicated in a variety of cognitive deficits and symptom patterns associated with schizophrenia (Barch *et al.* 2001; Callicott *et al.* 2000; Dolan *et al.* 1993; Liddle and Morris 1991; Weinberger 1988). Previous neuroimaging studies have also observed thalamic structural abnormalities in chronic schizophrenics (Andreasen *et al.* 1994; Buchsbaum *et al.* 1996; Byne *et al.* 2001), untreated schizophrenics (Gur *et al.* 1998), childhood-onset schizophrenics (Dasari *et al.* 1999; Sowell *et al.* 2000), relatives of schizophrenics (Staal *et al.* 1998; Lawrie *et al.* 1999) and schizotypal individuals (Hazlett *et al.* 1999). Meta-analysis of schizophrenia studies (Wright *et al.* 2000b; Konick and Friedman 2001) reveals a mean thalamic volume loss of approximately 4%. In contrast, other studies have not reported any differences in thalamic volumes between schizophrenic patients and controls (Arciniegas *et al.* 1999; Portas *et al.* 1998) though psychotic symptoms have been shown to be related to thalamic volume (Portas *et al.* 1998).

These data add to the weight of evidence for altered thalamic structure in schizophrenia. The combination of local thalamic and more widespread global grey matter loss, suggests that functional alteration of thalamocortical connectivity may be a key feature of schizophrenia, consistent with theoretical models of cognitive integration and dysfunction in schizophrenia (Andreasen *et al.* 1996; Tononi and Edelman 2000). Anatomically, the thalamus is a crucial relay between sensory

pathways and cortex and also between sensory cortices and association areas, acting possibly as a sensory filter (Andreasen *et al.* 1996; Andreasen 1997; Andreasen *et al.* 1998).

There is strong empirical support for a deficit in thalamocortical function in schizophrenia. Functional imaging studies of schizophrenia have shown abnormal thalamic activity at rest (Buchsbaum *et al.* 1996), during auditory hallucinations (Shergill *et al.* 2000; Silbersweig *et al.* 1995) and during a variety of cognitive tasks (Andreasen *et al.* 1995; Heckers *et al.* 2000; Rubia *et al.* 2001; Russell *et al.* 2000). Clinical studies also suggest dysfunction within this system. Schizophrenic patients demonstrate abnormalities in sensory experience and attribution, neuropsychological deficits and abnormalities in motor coordination and execution (Diforio *et al.* 2000; Walker *et al.* 1999; Neumann and Walker 1999). These clinical features suggest an underlying disorder in the coordinated regulation of sensory, motor and cognitive function in schizophrenia. The structural data from this study add further evidence of a thalamocortical basis to schizophrenia.

An important observation in this study was the correlation between regional differences in grey matter and clinical variables across the schizophrenic patients. In particular the significant correlation between global grey matter loss and subject age, suggesting progressive neuronal loss in schizophrenic subjects distributed across cortical and subcortical regions. Additionally, when global volume differences were accounted for, grey matter loss within the thalamus also correlated with age, but was relatively preserved in those patients with higher level of educational achievement. These observations, in the context of a lack of correlation between the age of illness onset or years of neuroleptic treatment, suggest that primary thalamic dysfunction may result in progressive involution within thalamus with secondary neuronal depletion within distributed cortical areas to which the thalamus is connected. In support of this proposal are the observed thalamic structural changes in individuals predisposed to schizophrenia or who have never received treatment (Gur *et al.* 1998; Lawrie *et al.* 1999; Staal *et al.* 1998; Hazlett *et al.* 1999). The finding of most marked volume loss in the mediodorsal thalamic nucleus, which connects reciprocally with prefrontal regions concurs with earlier reports (Pakkenberg 1990; Popken *et al.* 2000). Furthermore prefrontal cortical regions demonstrated the strongest association with a positive family history of schizophrenia suggesting that altered thalamofrontal connectivity may selectively increase vulnerability to schizophrenia. Educational

achievement may reflect delayed or less fulminant pathology within thalamocortical circuits. Correspondingly, good premorbid functioning (suggested by educational achievement) is associated with reduced negative symptomatology and a more positive outcome in schizophrenia (Johnstone *et al.* 1995).

Conclusion

VBM confirms the most consistent neuroimaging reports from the schizophrenic literature of distributed cortical changes while revealing more specific thalamocortical grey matter depletion in schizophrenia. Furthermore prefrontal cortical regions demonstrated the strongest correlation with a positive family history of schizophrenia suggesting that thalamofrontal dysconnectivity may selectively increase vulnerability to schizophrenia. These data add further weight to the theory of an underlying thalamocortical basis to schizophrenia.

CHAPTER 9

CLINICAL GROUPS

PURE AUTONOMIC FAILURE

Guide to Reader

Pure autonomic failure (PAF) is an acquired disease characterised by selective, peripheral denervation of the autonomic nervous system. In response to physical or cognitive effort patients with PAF fail to generate bodily states of arousal via the autonomic nervous system. Previous functional imaging studies have implicated a number of brain regions in the generation and representation of states of arousal including the anterior cingulate, insula, medial prefrontal cortex and pons, however conventional neuroimaging studies have failed to demonstrate any structural correlates. In this study I use VBM to test the hypothesis that longstanding absence of peripheral autonomic responses in PAF patients is accompanied by structural alteration of brain regions known to be involved in autonomic control.

Introduction

Animal studies of cerebral autonomic control have focused predominantly on hypothalamic, brainstem and cerebellar mechanisms of autoregulatory homoeostatic control (Spyer 1999) with less emphasis on the role of higher brain regions. There is however experimental evidence that autonomic responses can be modulated by specific neocortical, limbic and subcortical structures (Butcher and Cechetto 1995; Kaada 1951). In humans, direct stimulation of cingulate (Pool and Ransohoff 1949), insula (Oppenheimer *et al.* 1992) and medial temporal lobe (Fish *et al.* 1993) induces distinct autonomic responses. Furthermore lesions of the anterior cingulate, ventromedial prefrontal cortex, insula and medial temporal lobe diminish autonomic responsiveness (Tokgozoglu *et al.* 1999; Tranel and Damasio 1994; Tranel 2000). Functional imaging studies have demonstrated involvement of anterior cingulate, insula and pons in generation and representation of cardiovascular arousal (Critchley *et al.* 2000a), medial prefrontal cortex and anterior insula during variation of

electrodermal activity (an index of sympathetic arousal) (Critchley *et al.* 2000b) and anterior cingulate during states of autonomic arousal with anticipation (Critchley *et al.* 2000a).

PAF patients cannot modulate their bodily state via the autonomic nervous system but demonstrate no other sensory or motor neurological deficit. As a result there is no integrated central feedback of information about the autonomic changes that normally accompany behaviour (Mathias 2000). A cardinal feature of PAF is the failure of neurogenic control of circulation, and in particular orthostatic hypotension due to an inability to vasoconstrict during orthostatic challenges (Mathias *et al.* 1999; Mathias and Bannister 1999; Mathias 2000). PAF patients do not generate increases in heart rate and blood pressure when performing stressor tasks such as effortful exercise or mental arithmetic (Mathias *et al.* 1999) and do not increase circulating catecholamines during physical or emotional challenges (Mathias *et al.* 1999). These patients also show absent sympathetic skin conductance responses to emotive and orienting stimuli (Magnifico *et al.* 1998) and diminished pupillary reflexes (Clark and Ewing 1988). Histologically there is evidence of Lewy bodies in peripheral autonomic ganglia (Matthews 1999), but the precise underlying pathophysiology remains unclear.

PAF can be clinically differentiated from central neurodegenerative causes of autonomic failure such as multiple system atrophy (MSA) or Parkinson's disease by absent clinical and hormonal indicators of central neurological degeneration and normal life expectancy (Kimber *et al.* 1997; Mathias *et al.* 1999; Mathias and Bannister 1999; Mathias 2000). Functional abnormalities have been observed in PAF patients in the pons, insula and somatosensory cortices associated with homeostatic regulation of bodily states. Changes in cingulate activity have been associated with context-dependent changes in bodily arousal (Critchley *et al.* 2000b; Critchley *et al.* 2001b). During fear-conditioning, the absence of peripheral arousal in response to a learnt threat-stimulus is associated with reduced activity in amygdalar and insular regions (Critchley *et al.* 2002). Such findings provide strong evidence that the cingulate, insula, pons and amygdala are involved in autonomic control and highlight the importance of afferent feedback in influencing central representations of autonomic responses.

Qualitative assessment of brain imaging in PAF patients is characteristically normal. In this study, VBM is used to reveal subtle structural changes within regions known to be functionally involved in autonomic arousal, but as yet undetected by

conventional imaging appraisal. The hypothesis being that chronic absence of peripheral autonomic responses would result in regional morphometric differences in specific brain areas functionally implicated in central autonomic control and representation namely cingulate, insulae, pons and amygdalae.

Methods

Subjects

Fifteen patients (9F, 6M; mean age ± S.D. 62yrs ± 8) with an established diagnosis of PAF (greater than 5 years of symptoms of orthostatic hypotension and dysautonomia, without clinical evidence of non-autonomic pathology or central neurological degeneration (cerebellar signs, parkinsonism)) were recruited by Dr Hugo Critchley. All patients underwent full clinical assessment by Professor Mathias' team. In addition 15 healthy right-handed age and sex- matched controls were recruited (9F, 6M; mean age ± S.D. 62yrs ± 9). Diagnostic axial dual-echo MRI scans for each PAF subject were examined by an experienced neuroradiologist to exclude patients with MRI evidence of additional pathology, in particular neurodegenerative syndromes such as multiple system atrophy. All subjects gave full, informed, written consent (Declaration of Helsinki, 1991) and approval for the study was obtained from the Local Research Ethics Committee of the National Hospital for Neurology and Neurosurgery (UCLH, NHS Trust) and the Institute of Neurology (UCL). Details of the PAF patients are listed in Table 9.1.

Table 9.1: Pure autonomic failure patient details

Gender	Age (years)	Duration of symptoms (years)[1]	ADL score[2]
Male	69	7	3
Male	42	8	1
Male	63	9	1
Male	55	11	9
Male	65	14	7
Male	66	15	10
Female	63	7	7
Female	61	8	1
Female	65	8	9
Female	64	8	10
Female	54	12	15
Female	61	13	10
Female	79	13	12
Female	64	14	7
Female	64	15	10

[1]Symptom duration was estimated retrospectively from clinical interview with patients (Professor Mathias' team)
[2]ADL = Activities of Daily Living (Katz et al., 1965), a general questionnaire scoring levels of disability in daily life. Variability in ADL score may reflect in part efficacy of treatment with hypertensive agents.

Structural MR scanning

Subjects were scanned on a 2 Tesla Siemens MAGNETOM Vision scanner. A 3D structural MRI was acquired on each subject using a T-1 weighted MPRAGE sequence (TR/TE/TI/NEX 9.7/4/ 600/1, flip angle 12°, matrix size 256 × 192, FOV 256 × 192, yielding 120 sagittal slices and a slice thickness of 1.5mm with in plane resolution of 1mm × 1mm).

Data pre-processing for voxel-based morphometry

The optimised VBM protocol was followed (see Chapter 2 for full details). Processing components pertinent to this study will be emphasized here. Customised grey and white matter templates were created from the study group according to previously described methods.

Statistical Analysis

Modulated and unmodulated data were analysed separately. Firstly, regionally specific group differences in grey and white matter volume and concentration were assessed by constructing separate design matrices using global (grey or white matter) voxel intensity, age and gender of subjects as confounding covariates. Secondly, across the PAF patient group, regression analyses tested for morphometric changes correlating with duration of autonomic symptoms and severity of disability (scored using the Activities of Daily Living (ADL) Questionnaire (Katz *et al.* 1965), with age and gender as confounding covariates. Differences were reported if significance reached $p < 0.05$, corrected for whole brain, or when corrected for small volume of identified *a priori* regions of interest from human functional neuroimaging evidence, specifically published studies of autonomic control in healthy controls and PAF patients. The regions of interest were (1) anterior cingulate /medial prefrontal cortex (Critchley *et al.* 2000b; Critchley *et al.* 2000a; Critchley *et al.* 2001a; Critchley *et al.* 2001b); (2) insulae (Critchley *et al.* 2000b; Critchley *et al.* 2001b; Critchley *et al.* 2002), (3) amygdalae (Critchley *et al.* 2002) and (4) pons (Critchley *et al.* 2000a; Critchley *et al.* 2001b). Anatomical regions of interest were delineated bilaterally on the unsmoothed customised template (average normalized brain image derived from all 30 subjects in the study) using MRIcro on a MS-Windows platform (http://www.psychology.nottingham.ac.uk/staff/cr1/mricro.html). MRIcro enables the manual delineation of volumes of interest in three planes. The anatomical boundaries

of the amygdalae, anterior cingulate and insular cortices were traced manually in three planes with reference to the anatomical atlas of (Duvernoy 1999). The delineated volumes were smoothed (4mm FWHM) then saved to produce mask images that reflected regional spatial extent and underlying anatomy of the a priori regions of interest and enabled simultaneous testing of contralateral areas. The bilateral anterior cingulate mask was 20392 voxels; insulae mask, 14612 voxels; amygdala mask, 1268 voxels; and the pontine mask was 7400 voxels where voxel size was 1.5 x 1.5 x 1.5 mm^3. These masks were applied individually for small volume significance correction of regional effects.

Results

Global structural differences

No between group differences (PAF patients and controls) were observed for total brain volume ($t(28) = 0.5$, $p= 0.5$) or concentration. There were no significant between-group differences in global volumes of grey matter, $t(28) = 0.82$, $p = 0.4$; white matter, $t(28) = 0.13$, $p = 0.9$ or CSF, $t(28) = 0.53$, $p = 0.6$, suggesting that there is no systematic or generalized atrophy associated with PAF (Fig. 9.1).

Regional grey matter structural differences

PAF subjects had significant reductions in grey matter volume and concentration in the left anterior cingulate (peak coordinates: volume, -11,38,27; concentration, -9,35,27; $p < 0.05$, corrected for bilateral anterior cingulate) (Fig. 9.2), and right anterior insula / frontal operculum (48,14,10; 46,21,0, $p < 0.05$, corrected for insular mask), extending to right inferior prefrontal gyrus (57,18,9, $p = 0.08$). Reductions in grey matter concentration were observed at an uncorrected level in dorsal and ventral pons of PAF subjects, but did not reach $p < 0.05$, corrected for the whole pontine region (–17,-30,-29, $p = 0.08$, corrected; and 3,-15,-26, $p = 0.12$, corrected). VBM detected no significant reduction of grey matter volume or concentration in the amygdalae of PAF subjects (Table 9.2). There were no significant regional increases in grey matter in PAF subjects relative to controls.

Figure 9.1: Global brain volume differences

No significant between-group differences in global volumes of grey matter, $t(28) = 0.82$, $p = 0.4$; white matter, $t(28) = 0.13$, $p = 0.9$ or CSF, $t(28) = 0.53$, $p = 0.6$.

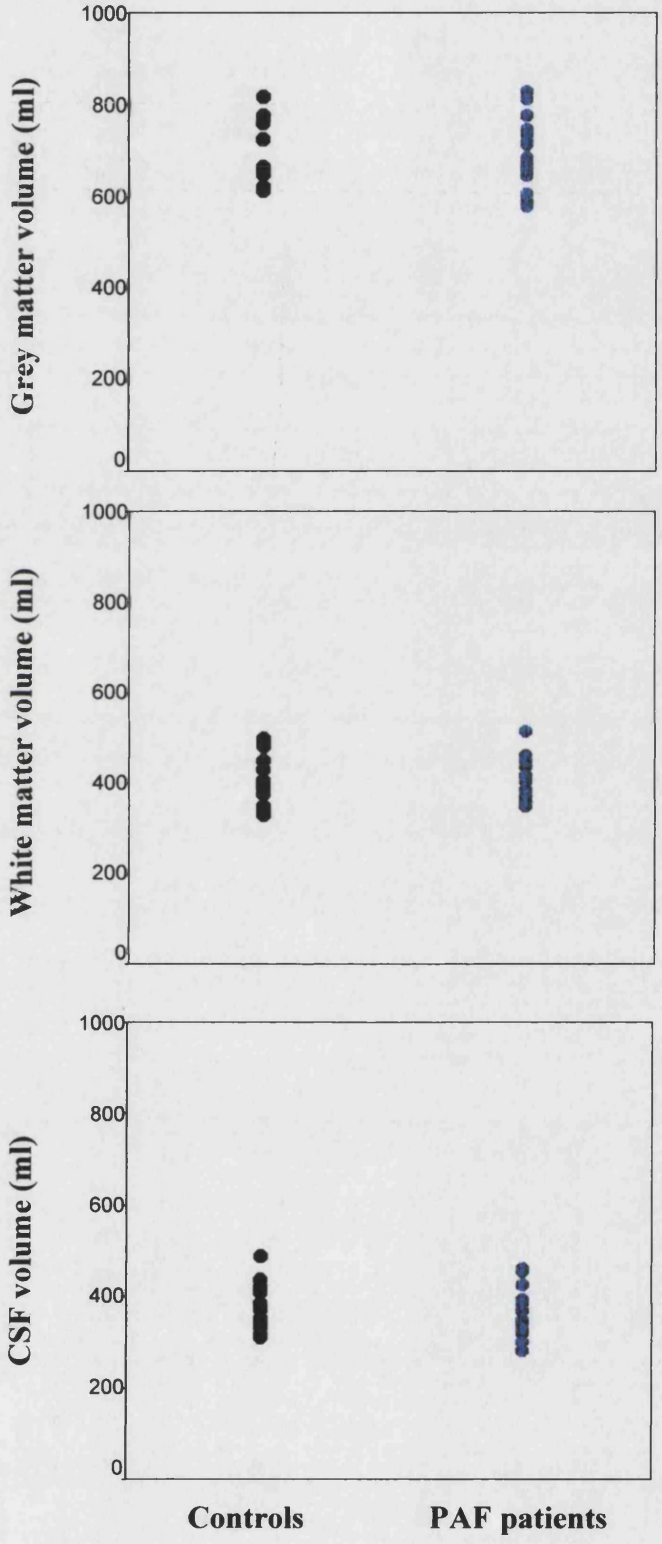

Table 9.2: Regional grey matter differences between PAF patients and controls

Location	Grey matter volume			Grey matter concentration		
	Side	*Coordinates*	*T value*	*Side*	*Coordinates*	*T value*
Anterior cingulate	L	-11,38,27	5.45*	L	-9,35,27	5.02*
	L	-9,2,36	4.09			
Subgenual cingulate	-	-	-	L	-6,51,-8	3.95
Anterior insula	R	57,18,9	5.46*	R	54,18,6	4.47
extending to inferior frontal gyrus	R	48,14,10	4.19*	R	48,21,0	4.60*
Pons -dorsal	-	-	-	L	-17,-30,-29	3.94
-ventral					3,-15,-26	3.76

*Significant $p < 0.05$, corrected for full extent of bilateral anatomical structure

Regional white matter structural differences

No significant between-group differences were observed in regional volume or concentration of white matter.

Within-group correlations of grey matter reductions

VBM assessed whether observed morphometric differences in grey matter were influenced by the duration of autonomic symptoms or degree of disability. Age and gender were treated as confounding covariates. There was no significant regional change of grey matter volume or concentration related to the duration and severity of disability across whole brain or in regions of *a priori* interest in regression analyses confined to the 15 PAF patients. The adjusted data for grey matter changes in left anterior cingulate in PAF patients, observed in the group comparison with control subjects, correlated negatively with the ADL score of the patients (Pearson $R = -0.65$, $p < 0.05$). This observation suggests that increasing severity of the symptoms of peripheral autonomic failure is associated with increased morphological change within an anterior cingulate region known to be implicated in autonomic control.

Figure 9.2: Regional grey matter reduction in PAF

Above, significant anterior cingulate reduction in grey matter volume projected on the template. Below, the effect size for grey matter volume differences in the peak voxel for this contrast for each PAF and control subject is plotted.

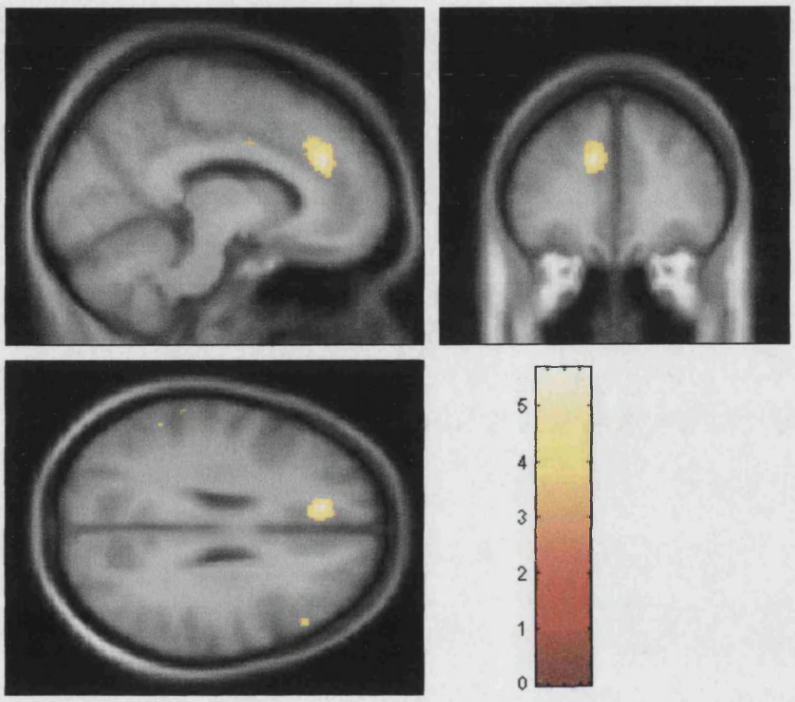

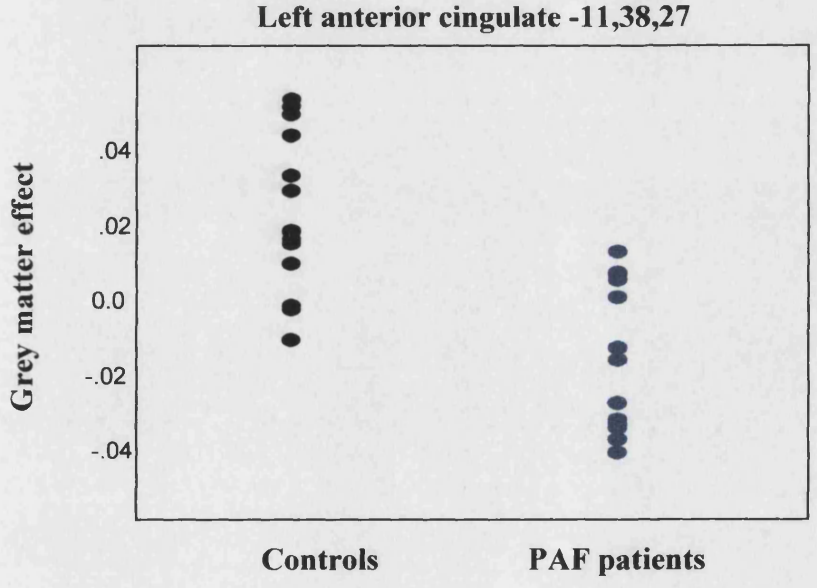

Discussion

Previous conventional neuroimaging studies have not shown any structural alterations in the brains of patients with pure autonomic failure (PAF). Here, using a sensitive whole brain technique, guided by strong prior hypotheses for regions known to be functionally implicated in autonomic control, biologically plausible structural alterations are now revealed. Clinical and pathological evidence suggest that PAF is a peripheral disorder with selective compromise of postganglionic autonomic responses (Mathias and Bannister 1999; Mathias 2000). In this group of PAF patients VBM shows regional reductions in cortical grey matter in distinct brain regions known to be involved in the generation and representation of autonomic responses. Moreover a correlation is observed between anterior cingulate cortex morphology and severity of physical symptoms, suggesting that selective loss of cortical grey matter is a consequence of longstanding absence of afferent feedback from autonomic responses. There was no significant correlation between observed morphometric changes and illness duration. There could be a number of reasons for this. The insidious onset and overlap of autonomic symptoms with a range of other physical and psychological disorders may delay their recognition by patients and clinicians. Furthermore, compensatory physiological, postural and behavioural mechanisms in the early stages of autonomic failure may confound retrospective dating of symptom onset, and clinical severity scores such as ADL may be influenced by therapeutic interventions (Mathias *et al.* 1999; Mathias 2000). These factors, coupled with the small patient group and stringent analytical methods of VBM may explain the absence of a correlation between regional morphological changes and symptom duration.

Although some single post-mortem studies have reported Lewy bodies in the brainstem of PAF patients there has been no previous clinical or radiological evidence for an underlying central pathology. Lewy bodies in PAF are characteristically confined to peripheral autonomic ganglia, and this condition remains clinically and prognostically different from more pernicious diseases such as Multiple System Atrophy (MSA, Shy-Drager syndrome) (Mathias 2000). Importantly, VBM reveals no group differences in global measures of grey and white matter and CSF suggesting normal global cerebral integrity. The regionally specific morphometric differences in PAF subjects are therefore more likely to arise as a direct consequence of longstanding *peripheral* autonomic failure.

VBM reveals local grey matter reductions within anterior cingulate and insula/inferior prefrontal cortex in PAF patients relative to controls. These areas are known to be involved in generation and representation of autonomic states of bodily arousal. Anterior cingulate plays a role in autonomic arousal. Functional imaging studies in healthy subjects have shown a correlation between right anterior cingulate activity and measures of cardiovascular arousal, such as blood pressure (Critchley *et al.* 2000b). Bilateral anterior cingulate activity is modulated by the degree of anticipatory arousal (Critchley *et al.* 2001a; Critchley *et al.* 2001b) and increased anterior cingulate activity, particularly in the left hemisphere is associated with the intention to decrease sympathetic tone during biofeedback relaxation exercises (Critchley *et al.* 2001c). Evidence from PAF patients also indicates that anterior cingulate contributes to generation of autonomic states of arousal. PAF patients show enhanced right anterior cingulate activity while performing effortful tasks that normally engender cardiovascular arousal in healthy subjects (Critchley *et al.* 2001b; Critchley *et al.* 2001a). A possible explanation for anterior cingulate grey matter loss is that poverty of afferent information results in reduced functional representation of autonomic states and subsequent morphological adaptation. In accordance with this theory is anatomical evidence of direct afferent and efferent connections between anterior cingulate, insula and pontine nuclei that are implicated in control of central and peripheral arousal (Porrino and Goldman-Rakic 1982).

Insula cortices play an important role in the representation of somatic states and bodily responses. Functional imaging studies show insula activity during a variety of conditions that elicit or reflect a modulation of visceral state such as micturition (Nour et al., 2000), oesophageal distension (Aziz *et al.* 2000), respiratory challenge (Corfield *et al.* 1995), thermosensory stimulation (Craig *et al.* 2000), cardiovascular arousal (Critchley *et al.* 2000a) and electrodermal activity (Critchley *et al.* 2000b). In PAF, functional imaging shows decreases in insula activity relative to controls (Critchley *et al.* 2001b). The observed grey matter reductions within anterior insula cortex of PAF patients would also be consistent with involutional adaptation in response to loss of integrated feedback of autonomic responses. In this study the volume reductions extended into prefrontal operculum and inferior prefrontal gyrus which have both been implicated in error detection (Menon *et al.* 2001).

Local decreases in grey matter concentration were observed in the dorsal and ventral pons of PAF patients, but did not survive corrected significance. Functional

imaging of PAF patients shows context-independent increases in dorsal pons activity (Critchley *et al.* 2001b). Brain stem regions including the pons support homoeostatic and effector mechanisms for control of autonomic responses (Spyer 1999) and have been proposed as a site of first-order representation of bodily states (Damasio 1999). The absence of marked morphometric differences in the pons of PAF subjects may reflect sub optimal segmentation of pontine tissue into grey and white matter compartments owing to poor intrinsic contrast of this region, but since I performed grey and white matter analyses any systematic group difference would have been revealed. Another possibility is that increased functional activity results in a relative preservation of grey matter that maximizes residual autonomic responses during the early stages of autonomic failure. However, it is possible that morphometric adaptations to absent autonomic responses preferentially impact only on cortical regions involved in integrating bodily representations with behavioural experience, rather than regions involved primarily in autoregulation. It was surprising that no morphometric differences were apparent in the amygdalae since these are known to be involved in generation of emotional autonomic responses and also mediate memory-enhancement of salient material perhaps through arousal mechanisms. Functional imaging in PAF shows markedly reduced amygdalar responses to threat stimuli in association with absent peripheral autonomic responses (Critchley *et al.* 2002). There is no clear explanation why the morphology of some autonomic brain regions is differentially affected.

Conclusion

VBM reveals previously occult structural changes in PAF patients corresponding to regions that are known to be functionally implicated in both autonomic control and emotional behaviour. PAF patients show significant reductions of grey matter concentration and volume within anterior cingulate and insula cortices and more subtle changes within the pons. Furthermore, VBM demonstrates a relationship between anterior cingulate cortex structure and severity of physical symptoms in PAF patients. These data add weight to evidence from functional imaging studies of central control of autonomic responses in humans and provides empirical evidence for adaptive changes in the adult human brain consequent to peripheral autonomic dysfunction.

CHAPTER 10

GENOTYPE-PHENOTYPE MAPPING

VBM MAPPING OF THE X CHROMOSOME

Guide to Reader

Major advances in molecular imaging now allow precise localization of genes and an almost complete map of the human genome. As a result of the human genome project, new disease genes are discovered almost weekly. Recent important discoveries include genes for prostate cancer, breast cancer, holoprosencephaly and Alzheimer's disease. Genotype-phenotype correlations allow insight into illness at a molecular level. Over time, this can lead to the development of treatments, prevention strategies and accurate diagnostic tests, which in some instances can be life saving. Since VBM has been shown to be sensitive to subtle changes in brain morphology, and previous studies of Alzheimer's disease for example, have demonstrated morphological changes that precede the onset of clinical symptoms, it follows that the structural brain phenotype may correlate more closely with genotype than the clinical phenotype. In this study, I test whether VBM is a useful tool to characterise the relationship between genotype, structural brain phenotype and cognitive phenotype in patients with deletions of one X chromosome. Using the versatility of the General Linear Model, I employ a gene deletion mapping strategy to identify regions on the short arm of the X chromosome containing putative candidate genes coding for specific structural brain phenotypes.

Introduction

A fundamental role for the X chromosome in neurodevelopment is suggested by reports of altered cognitive profiles in those with sex chromosome aneuploidies. The evolution of the sex chromosomes has given rise to unique mechanisms of regulation so as to equalise gene expression between the sexes (Disteche 1999). In normal females one of the two X chromosomes is inactivated at random in order to ensure equal expression of X-linked genes in male and female mammals (Lyon 1961). Genes that escape X inactivation are found at the tips of the X and Y chromosome arms, the so called pseudo-autosomal regions, where the equivalent nucleotide sequence is identical in both sex chromosomes, thus allowing meiotic recombination to take place. Surprisingly, many genes are now known to escape X inactivation elsewhere on the X chromosome. These are non-randomly distributed, lie mostly on the short arm and do not necessarily have expressed Y homologues (Carrel *et al.* 1999; Carrel and Willard 1999). Persistence of dosage imbalance in such genes between males (46,XY) and females (46,XX) may be important for sex specific functions (Disteche 1999). Turner syndrome (TS) offers a convenient natural experiment to study genotype-phenotype correlations of the X chromosome. This sporadic genetic disorder of human females is associated with complete or partial absence of one X chromosome and is associated with a characteristic neurocognitive and psychosocial profile. I suggest that it should be possible to identify the effects of dosage sensitive loci on brain development by studying TS females and that this would constitute a proof-of-principle study attempting to assess genotype-phenotype correlations of the human brain in life.

TS has a prevalence of 1 per 2500 live female births, in which typically all (45,X or X-monosomy) or a substantial part of one X chromosome is missing due to nondisjunction or chromosome lost during early cleavage of the zygote. In 70% of monosomic (45,X) TS the single X is maternally inherited (Jacobs *et al.* 1997), the remainder are paternally inherited. In monosomic TS the single X chromosome is never inactivated, whereas in normal females (46,XX) one of the two X chromosomes is inactivated at random during the blastocyst stage of development (Boumil and Lee 2001). Dosage-sensitive genes that escape X inactivation may contribute to the TS phenotype if haploinsufficient in X monosomy. For example, SHOX (Blaschke and Rappold 2001) is now known to contribute to the short stature of the syndrome, and is

normally expressed from the pseudo-autosomal region (PAR1) of both X and Y chromosomes.

Most cases of TS syndrome show normal verbal abilities but almost all have poor visuospatial skills (Temple and Carney 1993; Temple and Carney 1996). Impairments in social skills and affective discrimination affect the majority, who may be socially isolated with a poor concept of self (McCauley *et al.* 1987; Ross *et al.* 2000; Ross *et al.* 2002). Recent evidence shows that the condition is associated with a substantially increased risk of autism (at least 200 fold) (Creswell and Skuse 1999). Milder autistic features of behaviour such as failure to understand non verbal social cues and poor maintenance of eye contact are much more common affecting up to 30% of 45,X females (Lawrence *et al.* 2003). Phenotypic features of the syndrome relating to neuronal dysfunction are due in large part to haploinsufficiency for X linked gene products that are normally expressed in two copies from genes that normally escape X inactivation in normal 46, XX females (Ross *et al.* 2002). Males are also potentially haploinsufficient for these gene products, because few X linked genes that escape X inactivation outside the pseudo-autosomal regions at the tips of the X chromosome have expressed Y homologues (Disteche 1999). Accordingly one could reason that it should be possible, through a study of individuals with X chromosome anomalies, to map dosage sensitive genes that influence sexually dimorphic cognitive abilities. This hypothesis has received considerable recent support in terms of both theory (Zechner *et al.* 2001) and empirical evidence from other species (Xu *et al.* 2002). Owing to the predisposition of 45,X females to show autistic features, one could also hypothesise that dosage sensitive genes that contribute to this aspect of the TS phenotype may also explain male vulnerability to develop disorders of social cognition.

No genes have yet been identified that contribute to the cognitive or behavioural disorders of TS. Deficits in social cognition in particular are highly variable in X monosomy when measured by conventional rating scales or interviews. I thought that the structural brain phenotype might be more consistently abnormal than cognitive deficits in 45,X females relative to normal 46, XX females. In this investigation, I aimed to firstly characterise the structural brain phenotype of monosomic X females (45,X) and secondly to identify dosage sensitive X linked loci that influence the structure and function of neural systems affecting social-cognitive development. I used a deletion mapping strategy, based on a study of brain structural and cognitive phenotypes in females with variably sized deletions of the X

chromosome.

Methods

This study, which had the approval of the Local Research Ethics Committee of The National Hospital for Neurology and Neurosurgery (UCLH, NHS Trust) and the Institute of Neurology (UCL), involved 64 females with X-chromosome anomalies (51 TS 45,X, ages 15- 44 yr. and 13 partial X chromosome deletions (46,XXp-); ages 9 to 52 yr.). All were selected on the basis that they had no significant learning difficulties. 40% had participated in some form of higher education and 20% had attended university. Subjects' consent was obtained according to the declaration of Helsinki (BMJ, 1991; 302: 1194).

Karyotyping

Karyotypes were determined in the Wessex regional genetics laboratory by N. Simon Thomas by analysis of G banded metaphase chromosomes harvested from peripheral blood. DNA for molecular studies was extracted by salt precipitation. Parental origin of the normal X chromosome was determined using the polymerase chain reaction (PCR) to amplify DNA polymorphisms from each proband and their parents. Deletion breakpoints (James *et al.* 1998) were also mapped by PCR using a panel of short tandem repeat polymorphisms spanning the X chromosome short arm. Standard PCR conditions were used throughout and all primer sequences are available through the Genome Database. The X inactivation status of a deleted X chromosome was determined at the androgen receptor locus. In deletions 5 to 13 the abnormal X was unilaterally inactivated. In order to detect possible mosaicism a minimum of 50 cells per individual, and usually 100 cells, were analysed cytogenetically. All 45,X females were apparently non-mosaic in peripheral blood, although this does not exclude the presence of an additional cell line in the brain. Among the deletion carriers, a 45,X cell line was also present in three cases: in number 1 (10% of cells), number 7 (46% of cells) and in number 12 (45% of cells). Thus these three cases have an X chromosome complement intermediate between monosomic 45,X females and normal females.

Subjects

Clinical subjects were selected from a national survey of TS and from the

records of the Wessex Regional Genetics Laboratory and assessed by Professor D Skuse in the Behavioural and Brain Sciences Unit, Institute of Child Health. The mean age of the 45,X females was 25.1 years (s.d. 7.1), and that of the 46,XXp- females was 26.4 years (s.d. 13.2). Mean Verbal IQ of the 45,X and 46,XXp- females was similar (96.9 s.d. 13.3 vs. 101.6 s.d. 12.3) as was their Performance IQ (90.3 s.d. 16.0 vs. 91.0 s.d. 17.6). All subjects were healthy with no significant neurological disease. All 45,X women had been receiving sex steroid replacement therapy since early adolescence. The comparison group of 45 normal 46,XX women was matched to the 45,X group in terms of mean age (24.1 yr., s.d., 4.6) and Verbal IQ (Wechsler, 1986)(100.9, s.d., 11.7). Their mean Performance IQ of 108.1 (s.d., 14.4) was significantly greater than that of 45,X females, ($p<0.001$), as expected (Temple and Carney 1993; Temple and Carney 1996). I imaged 21 apparently non-mosaic Turner syndrome females with a 45X karyotype (45,X), 17 age and verbal IQ matched control females (25 yr. ± 9.0) and 25 age matched normal males (27.1 yr. ± 8.1). Eleven had a single X-chromosome of maternal origin ($45,X^m$) (mean age 24.3 yr. ± 7.5) and 10 of paternal origin ($45,X^p$) (22.3 yr. 6.4).

MR scanning and imaging analysis

High resolution volumetric MR imaging was performed on a Siemens 2T Magnetom scanner using an optimised MPRAGE sequence which affords enhanced grey /white matter contrast and segmentation (Deichmann *et al.* 2000; Deichmann *et al.* 2002). The acquisition parameters included: TR/TE/TI 11/4/1000, flip angle 12, matrix 256 × 224, FOV 256 × 224mm; 176 sagittal slices, 1mm isotropic voxels. The optimised method of voxel-based morphometry was used (see Chapter 2). A customized grey matter template was derived from all the Turner syndrome patients and control subjects in order to avoid any bias during the spatial normalisation step.

Assessment of fear recognition

Based on a hypothesis that characteristic social adjustment problems of TS (McCauley *et al.* 1987) could be linked to amygdala dysfunction, subjects were tested by Professor D. Skuse using Ekman pictures of facial affect (Ekman 1976). Subjects were shown sixty pictures of male and female faces and had to decide which emotion was being conveyed by the particular facial expression; happiness, sadness, fear, surprise, anger or disgust. Fifty-one 45,X individuals were compared to forty-five

normal 46,XX females matched for age and verbal IQ.

Statistical analyses

Regionally specific structural differences were assessed statistically using a two-tailed test, testing for increased or decreased grey matter. Corrections for the search volume, and implicit multiple comparisons, were made to the p values using Gaussian random field theory. Significance levels were set at $p<0.05$, corrected for whole brain volume. Because the amygdala had been identified a priori as a possible candidate for structural change, amygdala changes were small volume corrected using a sphere of 40mm diameter as a generous estimate of total amygdala volume. The design matrix modelled the control group, the 45,X group (divided according to the maternal or paternal origin of the single X chromosome), and individual partial deletions arranged in order of the number of megabases missing from the short arm of the X chromosome (Fig.10.1). The mean global grey matter intensity was modelled as a covariate in order to facilitate the detection of regionally specific structural changes having discounted global differences. Age was included as a confounding covariate. In a separate analysis I compared normal males, normal females and 45,X females with mean global grey matter and age as covariates.

A separate analysis tested for fear recognition differences between Turner syndrome (45,X) and normal females (46,XX). Scores for the 6 emotions were entered into a MANOVA, covarying for Performance IQ, with Bonferroni corrections.

Figure 10.1: Design matrix for gene deletion mapping

Columns 1-14 represent the different genotypes: column 1 representing normal females (46,XX), columns 2-12 representing partial deletions arranged in order of increasing size of deletion, columns 13 and 14 represent Turner females with a single X chromosome (45,X) divided according to their maternal (13) or paternal (14) origin. Age and global voxel intensity are modelled as confounding covariates. In column 3, 2 subjects (mother and daughter) had the same partial deletion size).

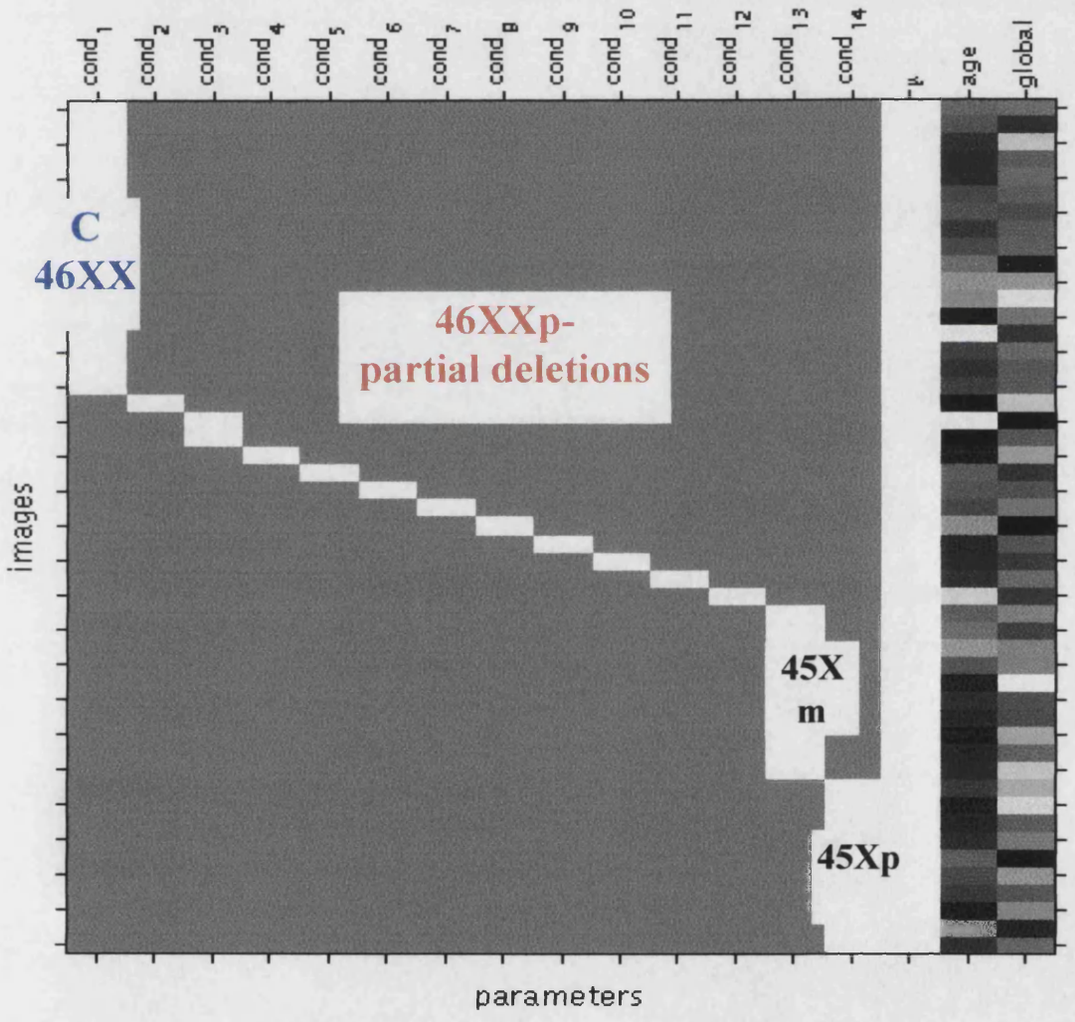

Results

VBM detected an altered brain structural phenotype in X-monosomic females (45,X) with significantly increased grey matter volumes of the amygdalae with local extension into the hippocampal heads and entorhinal cortices (local maxima: -37 -12 -22; -12 -18 -21; 21-10 -24) (Fig. 10.2a) and orbitofrontal cortex bilaterally involving posterior and lateral orbital gyri and gyri recti (local maxima: -4.5 22 -27; -39 36 -20; ±31 -82 -21) (Fig. 10.3). In Chapter 4, I showed that VBM reveals a remarkably similar pattern of gender difference in the amygdala structure of normal subjects; males (46,XY) have increased grey matter compared with females (over and above the global grey matter differences between the sexes)(Fig. 10.2b)(Good et al., 2001a;Murphy et al., 1993). In this study, matched samples of normal males with 46,XX and 45,X females revealed that, although males did have larger amygdalae than normal females ($p<0.001$ uncorrected), those of 45,X females were larger still ($p<0.05$ corrected). These findings suggest a dose-response relationship between the expression of one or more X-linked genes that escape inactivation (and which lack Y-homologues) and the structural development of the amygdala. In Chapter 4, I detected no physiological gender difference (46XX vs 46XY) in orbitofrontal cortex grey matter volume or concentration, suggesting that separate processes influence the development of this brain region.

Figure 10.2: The Turner brain phenotype.

Similarities between the Turner brain phenotype and physiological male-female differences (see Chapter 4) with regionally specific increases in amygdala volume in Turner females and normal males compared to normal females. (Coronal images through y =1 for each contrast for illustrative purposes)

(a) 45,X – 46,XX

Turner – normal females

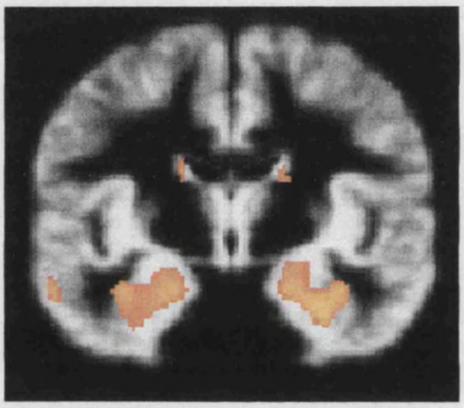

(b) 46,XY – 46,XX

normal males - females

Figure 10.3: VBM detected brain structural phenotype in Turner syndrome.

Regionally specific bilateral grey matter volume increases within orbitofrontal cortex centred on posterior and lateral orbital gyri and gyri recti, $p<0.05$, corrected) in Turner females (45,X) compared with normal females (45,XX) projected onto a normalised image from a single Turner subject (a) (-39 33 –21) and the smoothed customised template (b) (-4.5 22.5 25.5). The colour bar represents the T score for (a).

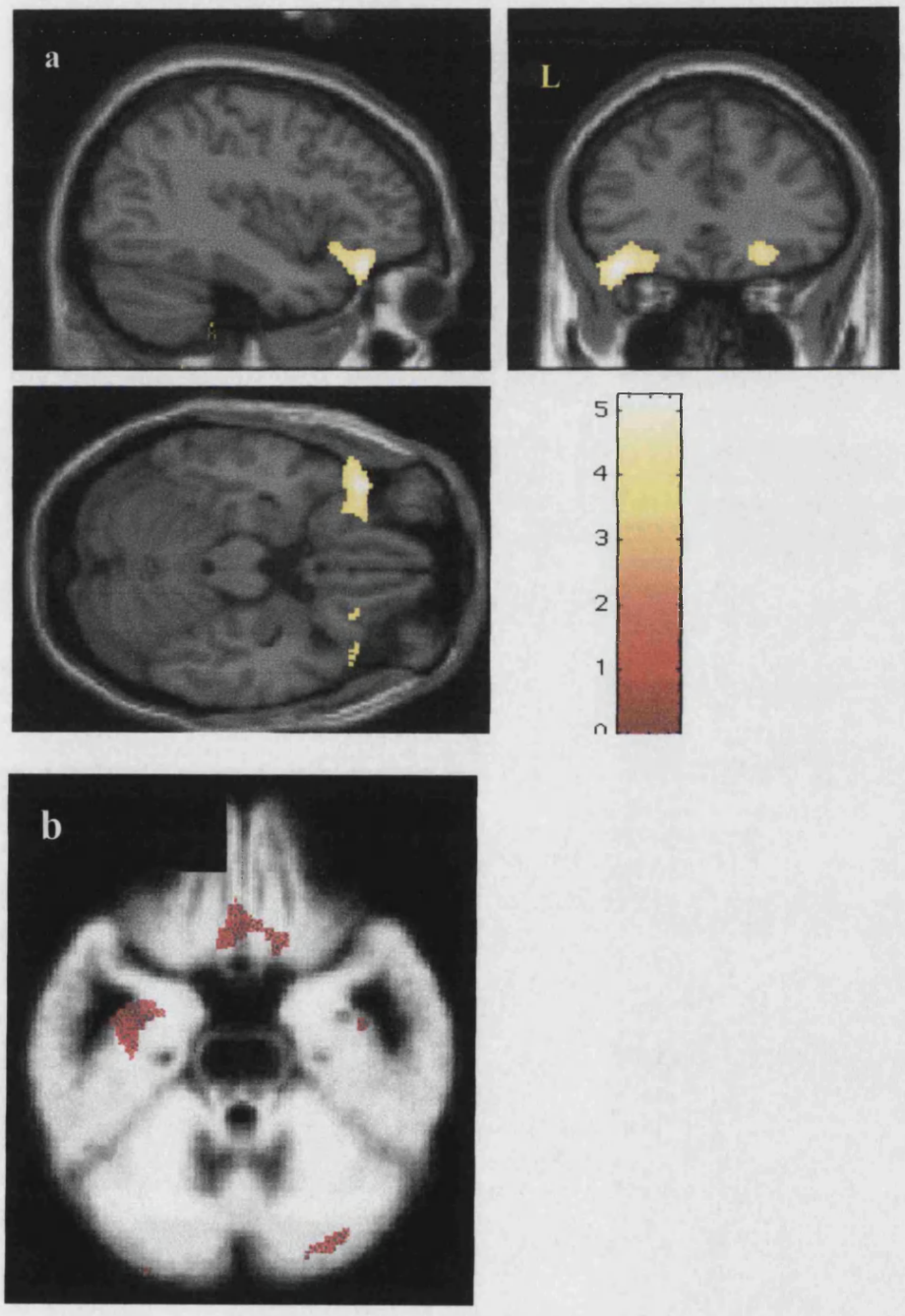

45,X females were substantially impaired at recognizing fear ($p < .0001$, effect size = 1.3) and anger ($p < .006$, effect size = 1.0) relative to 46,XX females (Fig. 10.4), but they were unimpaired in the recognition of other facial emotions. None was aware of their perceptual deficit. They could provide plausible situations in which fear or anger might be experienced, but many could not recount times when they themselves had experienced these emotions. Face emotion perception was similar in normal females and an age and IQ matched sample of 16 normal males. Males lacked the fear recognition deficit of 45,X TS, despite their single X-chromosome and relatively larger amygdalae than 46,XX females. This dissociation suggests that the increased grey matter I observed in the orbitofrontal cortex (OFC) of 45,X females, which was not seen in normal males (compared to normal females), was associated with compromised functional integrity of an emotion processing neural circuit in the 45,X group. Face-selective neurons can be identified in the primate orbitofrontal cortex (Scalaidhe *et al.* 1999)and ventral frontal lobe damage in humans impairs the identification of face expression, but not of face identity (Hornak *et al.* 1996). The orbitofrontal cortex (OFC) receives inputs of the same general type as the amygdala, and is certainly connected intimately with it (Rolls 2003).

Figure 10.4. Recognition of fear in facial expressions.

Mean ratings of fear recognition for subject groups presented as standard deviation scores below population norms. Bars indicate 2 standard errors. There is no significant difference in the fear recognition skills of 46,XX females (n=17) and 46,XXp- females with small deletions extending no further than DXS1058 (cases 4-8 in Figure 2). 45,X Turner syndrome females (n=51) and 46,XXp- females with larger deletions extending beyond DXS8083 (cases 10-13 in Figure 2) demonstrate significantly less accurate fear recognition than 46,XX controls ($p<.005$, effect size = 1.5). Patient DR (who underwent bilateral amygdalectomy) was tested on the same fear recognition task.

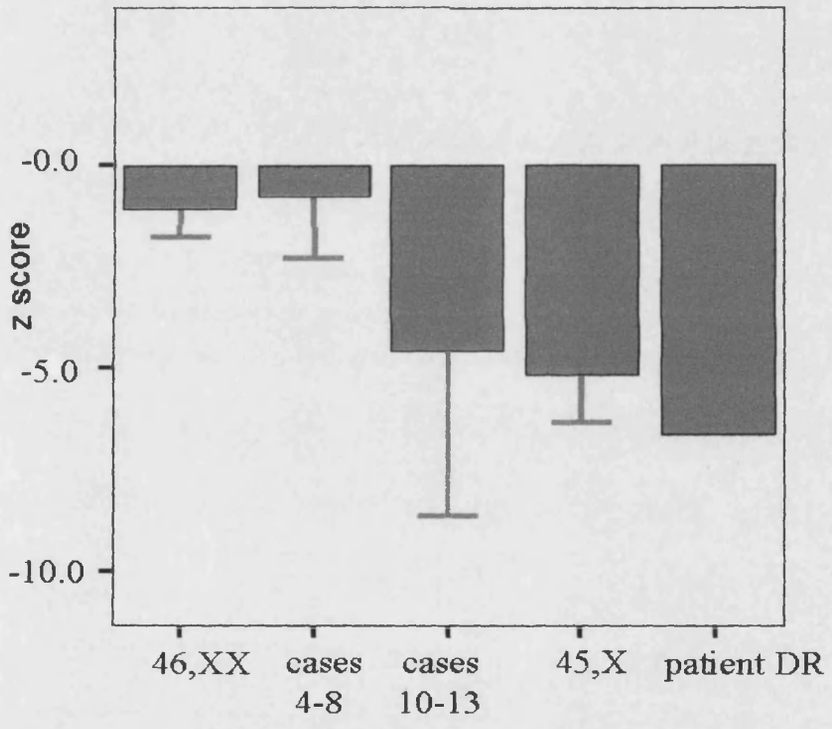

Using the subjects with partial deletions of the short arm of the X chromosome (46,XXp-), I then employed a gene deletion mapping strategy to attempt to identify a putative dosage-sensitive locus coding for the structural brain phenotype. This sample of 13 females had variably sized breakpoints, all but one terminal, which ranged in size from 5Mb to 55Mb from the telomere. For the purpose of analysis they have been numbered 1-13 in increasing size of deletion (Fig. 10.1). Subjects with breakpoints

including or proximal to the locus DXS8083 (44.07 Mb from Xpter) were phenotypically similar to 45,X, with significantly increased grey matter in the amygdala and orbitofrontal cortex (Fig. 10.5 and 10.6). In contrast, these brain structures were indistinguishable from normal in 46,XXp- females with breakpoints distal to the locus DXS1368 (39.11 Mb from Xpter). Partially deleted subjects had fear recognition skills that closely mirrored their brain phenotypes (Fig. 10.4). No other aspect of cognitive or somatic phenotype differentiated those with deletions that extended beyond the critical region from the remainder.

These findings suggest that a dosage-sensitive locus, influencing both amygdala and orbitofrontal cortex development in 45,X females, lies in the interval between 39.11 and 44.07 Mb from the telomere of the short arm. This critical region is defined by loci DXS1368 (distally) and DXS8083 (proximally) (Fig. 10.7) and must contain one or more genes which escape X inactivation, and are thus needed in two copies in 46,XX females for normal development to occur. Genes escaping X-inactivation tend to exist in clusters and, significantly, at least one cluster maps within the DXS1368 - DXS8083 interval (Carrel *et al.* 1999; Carrel and Willard 1999; Disteche 1999; Sudbrack R 2001). Within this 4.96 Mb interval there are 25 known genes and also 12 putative genes with potential open reading frames. However, the sequence between DXS1368 and DXS8083 contains seven large gaps of unknown size and therefore there are likely to be additional genes to those already described. There is a block of homology between this region of the X chromosome corresponding to cytogenetic bands Xp11.4 and Xp11.3 and a non-recombining part of the Y chromosome, Yp11.2. Of the 20 X-linked genes within this critical region that are known to escape inactivation, or whose inactivation status is uncertain, only three (USP9X, DDX3 and UTX) have functional Y-homologues. Completion of the Human Genome sequencing project and more extensive gene annotation may identify additional X/Y gene pairs.

Figure 10.5: VBM mapping of partial deletions of the X chromosome

Subjects with breakpoints including or proximal to the locus DXS8083 (44.07 Mb from Xpter) were phenotypically similar to 45,X, with significantly increased grey matter in the amygdala and orbitofrontal cortex (depicted in red). In contrast, these brain structures were indistinguishable from normal in 46,XXp- females with breakpoints distal to the locus DXS1368 (39.11 Mb from Xpter).

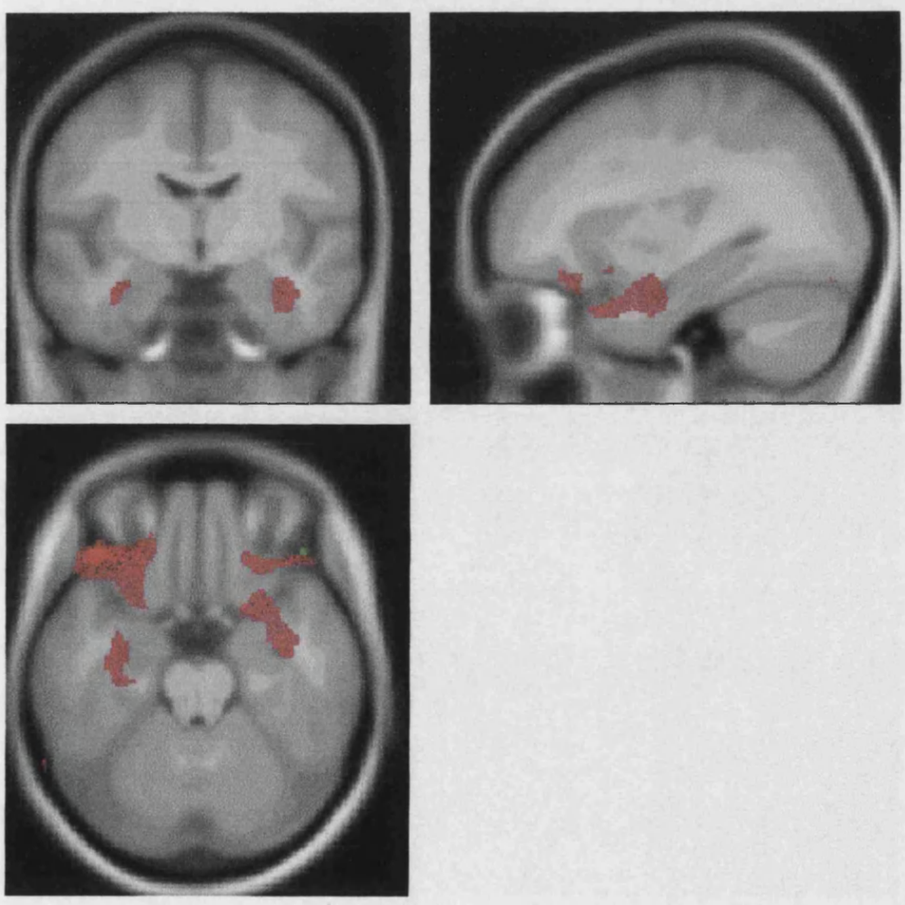

Figure 10.6: Gene deletion mapping of the X chromosome

Parameter estimates for VBM detected percentage volume change of the amygdala (a) and orbitofrontal cortex (b). The coordinates (x.y.z) at the voxel of maximal effect are shown on the vertical axis. Mean values (± 2 standard errors) are given, relative to the grand mean, for 17 46,XX females, at position 1, 11 45,X^m females at position 14 and 10 45,X^p females at position 15. At positions 2-13 data for 13 individual Xp deletion subjects are given in order of increasing size of deletion from the telomere. (There are two individuals at position 3 with identical deletions- a mother and daughter). Grey matter volume changes occur between subjects 8 and 9 at both locations.

(a): Left amygdala maximum

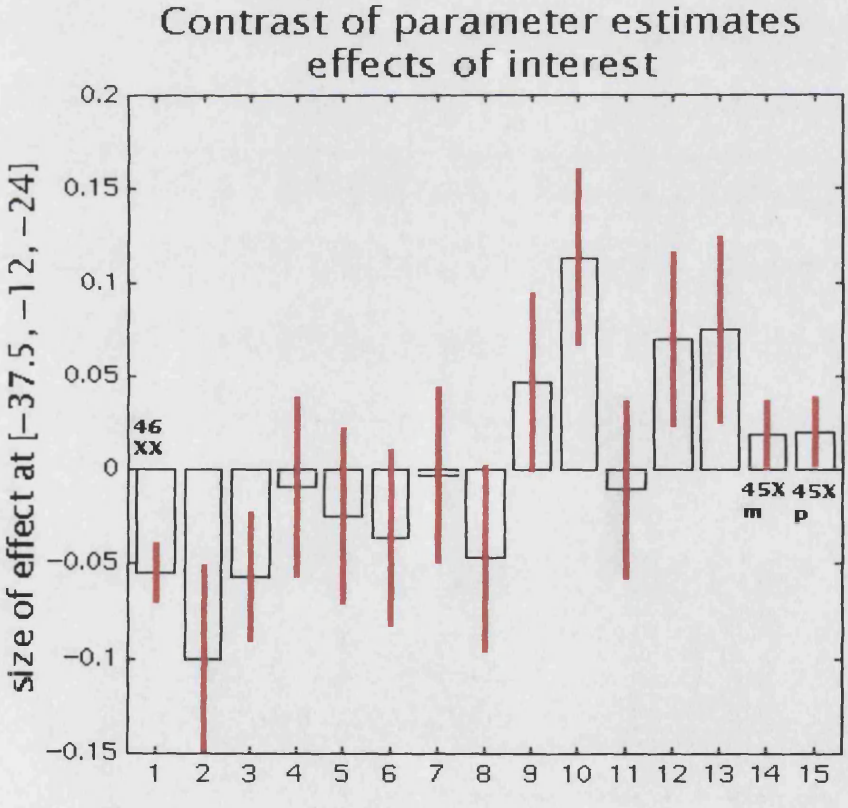

(b): Left orbitofrontal cortex maximum

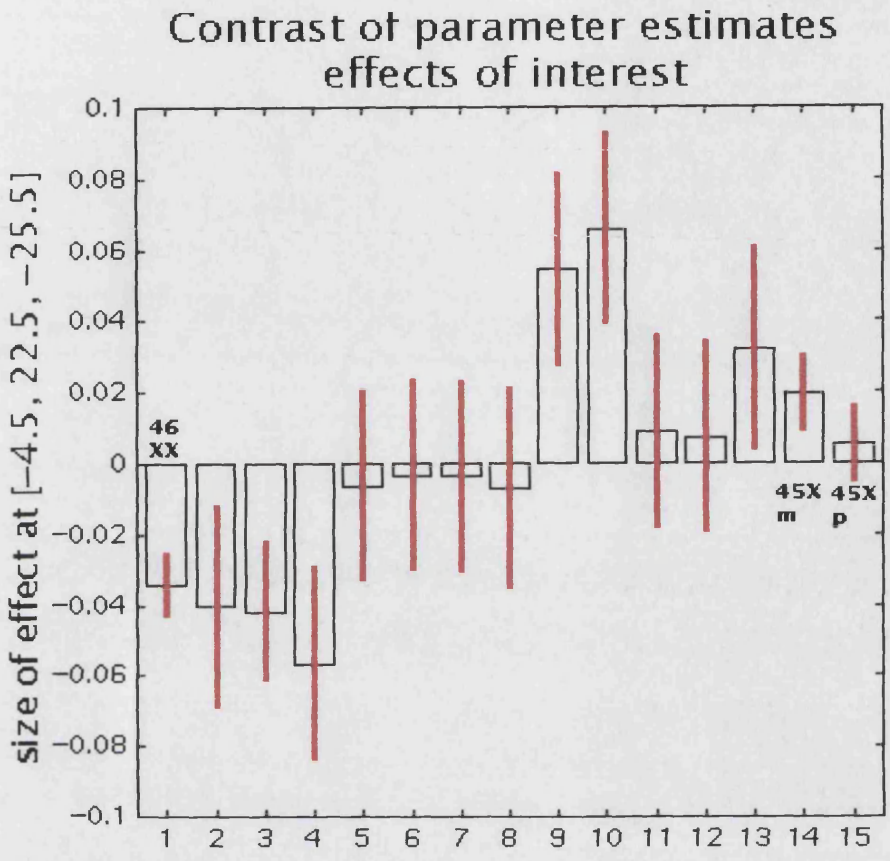

Among the genes in this critical region lie the monoamine oxidases A & B. These are nuclear encoded mitochondrial isoenzymes which catalyse the oxidative deamination of a number of biogenic amines including the neurotransmitters serotonin (5-HT), norepinephrine (NE), and dopamine (DA) as well as the neuromodulator phenylethylamine (PEA). Both enzymes have been implicated in predisposition to a range of psychiatric disorders (Shih and Thompson 1999) and both genes are expressed in human amygdala. MAOB is also expressed in platelets, in which activity levels are believed to reflect genotypic variation. Methylation analysis of the MAOB 5' CpG island has shown that all CpG dinucleotides tested in DNA extracted from lymphocytes were unmethylated on both the active (Xa) and inactive (Xi) X chromosomes (Chen *et al.* 1992). This suggests the gene is expressed from both X-chromosomes in normal females, and is not subject to X inactivation. There is no

functional Y-homologue of MAOB (males in whom it is deleted have no measurable MAOB activity). Accordingly, males and 45,X females could be haploinsufficient for the gene products, relative to normal females, if up-regulation of their single copy does not occur, and 45,X females will show male-typical levels of activity. Work in Professor Skuse's laboratory confirmed prior evidence that the platelet activity of MAOB is sexually dimorphic (e.g. Harro *et al.* 2001), levels in males being approximately 30% lower than levels in normal females. He also showed, in a preliminary investigation of MAOB activity in non-smokers, mean male levels and mean TS (45,X) levels were almost identical. In contrast, mean normal female levels were significantly higher ($p=0.05$).

Discussion

The increased amygdala volumes of 45,X subjects is consistent with previous studies that have found an inverse correlation of amygdala volume with the number of X-chromosomes, irrespective of sex. Two studies (Goldstein *et al.* 2001; Good *et al.* 2001b) have reported larger volumes in normal males 46,XY compared with normal females 46,XX. 47,XXY males have amygdalae of similar volume to 46,XX females, whereas the amygdalae of 47,XXX females are significantly smaller than either group (Patwardhan *et al.* 2002). Individual nuclei within the amygdala subserve different functions but I was unable, with the scanning resolution available, to distinguish whether these substructures were differentially affected.

The amygdala is a critical component of the social cognition circuitry in primates. Modular cognitive processes are committed to making social judgments, in particular the perception of facial expressions plays a critical role in social intelligence (Adolphs *et al.* 1999; Winston *et al.* 2002). An influential neurobiological model of social cognition (Brothers 1997) postulates that socially relevant information processed by sensory and association cortices is imbued with emotional significance by the amygdala and orbitofrontal cortex. This model has received widespread support from research in both primates and humans (Amaral 2002). Lesion and functional imaging studies in humans have demonstrated the amygdala's role in identifying emotions in others. Humans and primates with complete bilateral amygdala damage have difficulty recognizing fear (and anger) in facial expressions and they demonstrate subtle

abnormalities of normal social responsiveness (Adolphs *et al.* 1999; Young *et al.* 1995; Young *et al.* 1996).

Within the critical region mapped in this investigation of females with partial deletions of the short arm of the X-chromosome, the monoamine oxidase genes are clearly contenders for a potential influence upon amygdala development. A recent study showed that three of four members of a family of G protein-coupled receptors that are activated by trace amines, such as beta-phenylethylamine, are expressed exclusively in the human amygdala (Borowsky et al., 2001). Trace amines are exceptionally sensitive to the deaminergic actions of MAO genes (in the case of phenylethylamine it is especially MAOB (Grimsby *et al.* 1997)). Accordingly, relatively low levels of MAOB activity due to haploinsufficiency in males and 45,X females, may produce male-typical patterns of amygdala responsiveness, such as in the context of emotional learning (Canli *et al.* 2002).

Genes that are subject to X-inactivation do not have functional Y-homologues, and since expression is from a single X-chromosome in males and females, dosage is likely to be equivalent in both sexes. Furthermore, because in Turner syndrome (45,X) the single X-chromosome is invariably active it is unlikely that such genes contribute in any significant way to the Turner phenotype. In contrast to MAOB, methylation analysis of the MAOA CpG island has suggested the gene might be subject to inactivation (Hendriks et al., 1992). Although expression of MAOA has not been detected from Xi in cDNA from cloned human cell lines, the approach used - reverse transcription of intronic polymorphisms (Hendriks *et al.* 1992)– has limited sensitivity. Heterogeneous expression from Xi has been demonstrated for some X-linked genes, indicating variability of inactivation between tissues and even between individual females (Carrel and Willard 1999). Testing of somatic cell hybrids suggests some 5-15% of X-linked genes behave this way (Carrel *et al.* 1999). It is thus possible that MAOA escapes X-inactivation in some tissues. If so, activity would be relatively lower in 45,X than 46,XX females, as well as being potentially sexually dimorphic with lower activity in males. Such a mechanism could exacerbate sex differences in vulnerability to disorders affecting predominantly males (e.g. Caspi *et al.* 2002).

Figure 10.7: Putative candidate genes in the VBM detected locus on the short arm of X chromosome

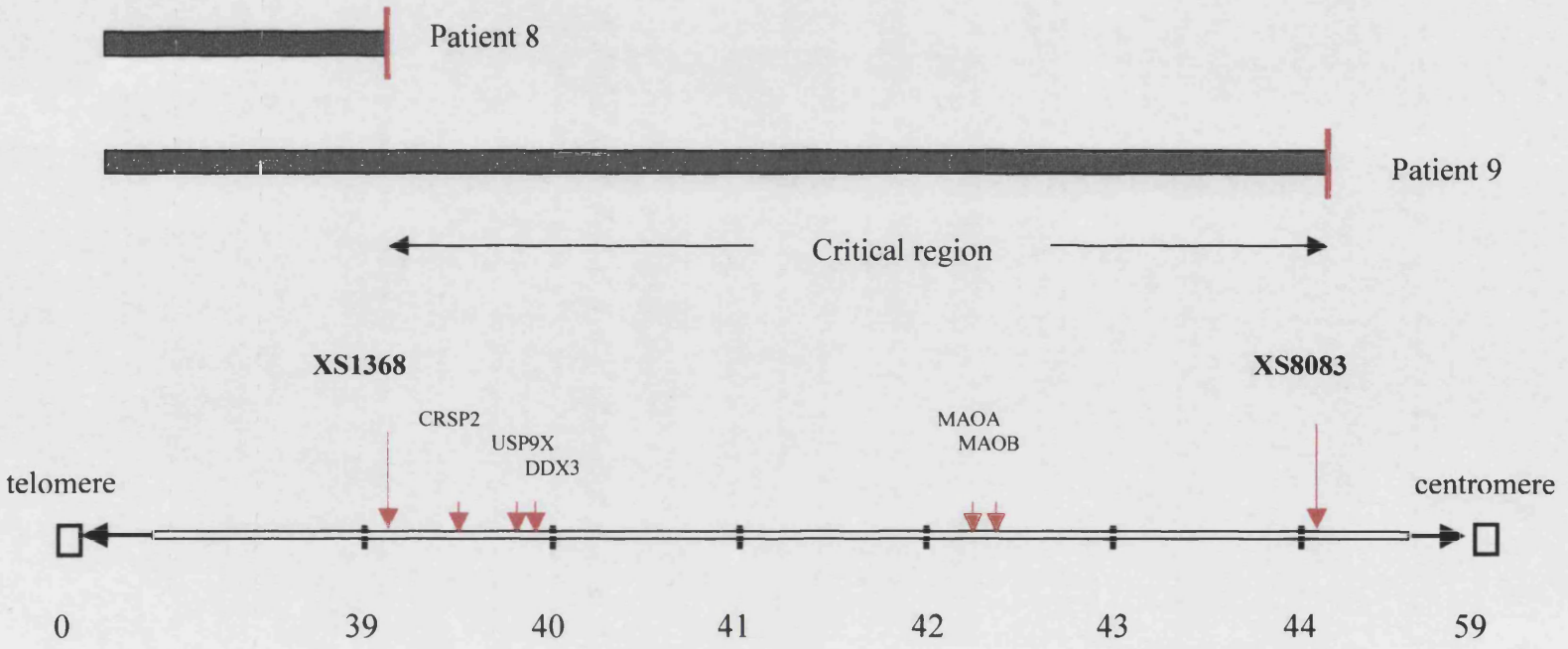

Haplo-insufficiency for genes at a dosage-sensitive X-linked locus is not the only possible explanation for the structural and cognitive characteristics of brains of 45,X females. One contributory factor that cannot be discounted by this experiment is an interaction between sex steroid abnormalities and neurodevelopment. In 45,X TS there is typically ovarian dysgenesis and failure of endogenous oestrogen production. Oestrogen receptors are widely expressed in the forebrain, with highest concentrations of the alpha-subtype in the amygdala and certain hypothalamic nuclei in both primates and humans (Osterlund and Hurd 2001). However, no correlation existed between menstrual history and amygdala structure or fear recognition skills in these partial deletion subjects. The 46,XXp- female deleted to DXS8083, subject 9, had conceived spontaneously and two subjects with larger deletions (subjects 10 and 11) had normal menstrual histories. Consequently, oestrogen deficiency is unlikely to be directly responsible for abnormalities of brain structure and function, among the 46,XXp- sample. It is also possible that environmental influences, perhaps a disadvantage relating to short stature, could systematically have affected brain development of the 45,X relative to 46,XX females. This explanation could not account for the within-group differences in brain phenotype of our 46,XXp- subjects, who were all of short stature.

It has been shown previously (Skuse *et al.* 1997) that the social adjustment of 45,X females is influenced by the parental origin of their single X-chromosome. It is therefore possible that there is an X linked imprinted locus that is preferentially expressed only from the paternally derived X-chromosome -X^p (normally found only in 46,XX females). In this investigation of 45,X TS females there were no significant differences in the structure of the amygdala or the orbitofrontal cortex nor in the deficit in fear recognition according to the parental origin of the single X-chromosome (X^p or X^m). However, there are preliminary data showing that an X-linked imprinted locus may nevertheless influence the process of emotional learning. A strong correlation has been found between accuracy of fear detection from facial features and facial recognition memory in normal females (Campbell *et al.* 2002) and in unpublished work in 45,X^p Turner syndrome subjects. There is no significant correlation between these variables in normal males, or in 45,X^m Turner syndrome subjects who are similar to males in their possession of a single maternally derived X-chromosome.

The findings could have relevance to the aetiology of male susceptibility to

disorders that are associated with social cognitive impairment, such as autism. This condition is at least four times as common in males as females. Among subjects whose IQ is in the normal range (full scale >70) the ratio is substantially greater. No explanation has yet been found for this discrepancy in prevalence, but one possibility is that the phenotypic penetrance of genetic susceptibility due to autosomal loci is decreased in females, because they possess two X-chromosomes (Folstein and Rosen-Sheidley 2001).

Converging strands of evidence suggest the amygdala is functionally and also structurally abnormal in autistic individuals (Grelotti *et al.* 2002). They show a lack of amygdala activation in fMRI studies of exposure to facial expressions that would normally evoke a response, and poor cognitive performance on tasks that involve neural processing by this structure. Specifically, amygdala-related cognitive deficits include poor facial recognition memory (Davies *et al.* 1994), a failure to recognize specific facial emotions, especially fear (Howard *et al.* 2000) and a lack of interest in and failure to follow normally eye gaze (Baron-Cohen *et al.* 1997). The data I report show that each one of these deficits is characteristic of females with 45,X Turner syndrome (Elgar *et al.* 2002).

X-monosomic females also display high levels of autistic symptomatology (Creswell and Skuse 1999) which may reflect the developmental consequences of failing to acquire normal expertise with faces due to amygdala (and OFC) dysfunction. Serotonin (5-hydroxytryptamine, 5-HT) blood levels have often been reported elevated in platelets in about one third of autistic subjects and their first-degree relatives (Betancur *et al.* 2002). More than 99% of blood 5-HT is in the platelet fraction and normal levels of platelet 5-HT are higher in males than females. So far no explanation for the excessively high level in autism has been found, but a lack of MAOB activity, which is associated with relatively impaired aminergic degradation, is one possibility.

In summary, my data suggest that one or more non-inactivated X-linked genes (within a 4.96Mb interval at Xp11.3-Xp11.4) is involved in the development of a neural system that influences social cognitive processing, in which the amygdala plays a critical role. If that neural system should become dysfunctional for whatever reason, the resultant phenotype would be expected to be sexually dimorphic because of amygdala recruitment. My findings suggest that the critical gene is expressed in two copies in normal 46,XX females, and that full dosage compensation does not occur in 46,XY males, or in 45,X- monosomy. Sexual dimorphism in the expression patterns of

one or more genes at this locus is therefore predicted. MAOB is proposed as a candidate gene, with an important contributory role in the structural development of the amygdala.

Conclusion

High-resolution structural brain imaging and a deletion mapping strategy have been used to identify a dosage-sensitive locus on the X chromosome that plays an important role in the development and function of the amygdala. This is the first time that a scientific methodology has mapped genetic structure and brain morphology at a molecular level. The consequences of haplo-insufficiency for this locus are that 45,X0 females are socially poorly adjusted and have a predisposition to autistic-like behaviours. The finding of sexually dimorphic amygdala structure and function in social learning has relevance for the male preponderance of social communication problems and indeed autism, suggesting why males find social learning from emotional experience more difficult.

CHAPTER 11

GENOTYPE-PHENOTYPE MAPPING PRE-SYMPTOMATIC HUNTINGTON'S DISEASE

Guide to Reader

This study represents a collaboration with colleagues in Sydney, Australia who made available a set of MRI images from a unique population of families with members suffering from Huntington's disease (HD). I analysed these from the perspective of my interest in genotype-phenotype correlations using the techniques described in Chapter 2.

The use of putative neuroprotective agents in HD may be optimised if the drugs can be given before brain pathology becomes manifest clinically. If these agents are to be tested in clinical trials, a reliable surrogate marker of the burden and rate of progression of pathologic change in a pre-clinical group is needed (Hughes, 2001). In this study, I use VBM to identify early structural changes in pre-symptomatic patients with the HD genotype. I ask whether the HD genotype is associated with regional differences in brain structure, in particular, differences that could not be predicted from clinical or neuropsychologic assessment. A secondary aim is to seek indirect evidence of pathological progression, in the form of changes in local tissue volume with age, specifically in those with the HD genotype.

Introduction

Since the discovery that the HD phenotype results from a specific genotype, namely an expanded CAG trinucleotide repeat within the *IT15* gene located on chromosome 4 (Huntington's Disease Collaborative Research Group 1993), there have been rapid advances towards an understanding of the underlying histopathological processes implicit in HD. The mutant gene product huntingtin (Htt) is expressed throughout the brain in HD (Aronin *et al.* 1995) and there is evidence to suggest that differential instability of the CAG mutation causes polyglutamine load differences between tissues (Kennedy and Shelbourne 2000). Proteolysis of mutant Htt within the

cytoplasm allows translocation to the nucleus, where the toxic effects are likely to be exerted (Sieradzan and Mann 2001). Htt fragments aggregate into neuronal intranuclear inclusions (NII) (Davies *et al.* 1997; DiFiglia *et al.* 1997) which are widely distributed in the cerebral cortex (Becher *et al.* 1998) particularly in insular and cingulate regions (Gutekunst *et al.* 1999). Cortical NII can only be demonstrated in symptomatic cases (DiFiglia *et al.* 1997; Gutekunst *et al.* 1999) where their density correlates with CAG repeat number (Becher *et al.* 1998; Sieradzan and Mann 1997). Furthermore reversal of NII accumulation is associated with resolution of neurological signs in a murine model (Yamamoto *et al.* 2000). Relatively few NII can be found within the striatum (Gutekunst *et al.* 1999) where the classical histopathological changes of HD (neuronal loss and reactive astrocytosis) are prominent (Vonsattel *et al.* 1985; Vonsattel and DiFiglia 1998), suggesting that other factors are involved (Sieradzan and Mann 2001). Diffuse intranuclear accumulation of polyglutamine stretches is pronounced within the striatum (Yamada *et al.* 2000), which may be more vulnerable to the effects of accumulating mutant Htt than other tissues. Researchers have proposed that the abnormal gene product unmasks regional developmental susceptibility to normally non-lethal stressors such as excitotoxins (Mehler and Gokhan 2000) and impairment of mitochondrial function, which manifests as elevated striatal lactate evident on magnetic resonance spectroscopy (Jenkins *et al.* 1998). This susceptibility might allow glutamatergic cortical afferents to trigger oxidative stress and ultimately neuronal death (Calabresi *et al.* 20032; Petersen *et al.* 1999).

Neuroimaging studies have consistently demonstrated striatal volume reductions in HD, and there are reports of volume loss in the thalamus and inferior cortical areas, especially in mesial temporal lobe structures (Jernigan *et al.* 1991b). Many researchers have attempted to correlate the pattern of striatal neuronal loss with clinical stage of HD. Involuntary movement disorder and 'frontal' dementia (Watkins *et al.* 2000) are generally attributed to interruption of motor and cognitive basal ganglia loops in the putamen and caudate (Alexander and DeLong 1986). Atrophy of other components in this pathway, including globus pallidus externa (Halliday *et al.* 1998; Vonsattel *et al.* 1985; Vonsattel and DiFiglia 1998) and subthalamic nucleus (Lange *et al.* 1976) is thought to be secondary to striatal neuronal loss. Vonsattel and DiFiglia (1998) suggest that the striatal degeneration appears to move in caudo-rostral and dorso-ventral/medio-lateral directions with disease progression. In pre-symptomatic cases basal ganglia volume loss can be seen (Aylward *et al.* 1994; Harris

et al. 1999), suggesting that striatal neuronal loss occurs early in the clinical course. However, in symptomatic subjects, progressive motor and cognitive impairment are perhaps better explained by white matter volume loss (Aylward *et al.* 1997; Aylward *et al.* 1998), reflected in enlargement of the frontal horns of the lateral ventricles (De la Monte *et al.* 1988; Harris *et al.* 1999). Although striatal volume declines at a greater rate in younger symptomatic subjects (Aylward *et al.* 1997; De la Monte *et al.* 1988), it appears that white matter loss particularly around the lateral ventricles best predicts the duration of chorea (Halliday *et al.* 1998).

Several focal cognitive and neurological features in early HD are difficult to explain purely on the basis of striatal dysfunction. Firstly, there is a specific deficit in the recognition of facial expression of disgust in symptomatic (Sprengelmeyer *et al.* 1996) and pre-symptomatic (Gray *et al.* 1997) HD. This might reflect more general limitation of the experience of disgust and may also relate to the specific loss of olfactory experience in HD (Hamilton *et al.* 1999; Moberg and Doty 1997; Nordin *et al.* 1995). Such deficits could be explained by striatal interruption of a ventral basal ganglia loop with inputs from orbitofrontal cortex and outputs via the medio-dorsal thalamus (Alexander and DeLong 1986; Gray *et al.* 1997; Hamilton *et al.* 1999; Lawrence *et al.* 2000; Moberg and Doty 1997). However, recent neuroimaging studies suggest that focal damage to insular cortex might provide a simpler explanation. Bilateral insular activation upon presentation of 'disgust' faces can be demonstrated in normal subjects with functional MRI (Phillips *et al.* 1997). Moreover, an isolated focal lesion of the left insula results in an identical deficit in disgust recognition to HD (Calder *et al.* 2000).

Additionally there is evidence for midbrain involvement in HD. Aminergic neurons in the locus coeruleus are reduced (Zweig *et al.* 1992) and striatal monoaminergic terminals are decreased (Bohnen *et al.* 2000). Studies of oculomotor physiology reveal increased latency of the pupillary light reflex attributed to involvement of the pre-tectal and Edinger-Westphal nuclei and intercalated neurons in the rostral midbrain (Den Heijer *et al.* 1988). There is slowing of oculomotor saccades in the vertical plane (Leigh *et al.* 1983; Leigh *et al.* 1985) even early in disease (Kirkwood *et al.* 2000), possibly related to loss of burst neurons in the rostral interstitial nucleus of the medial longitudinal fasciculus (riMLF) (Leigh *et al.* 1983; Leigh *et al.* 1985) or perhaps in the nucleus pontis centralis caudalis (Koeppen 1989). In addition, all levels of the dorsal brainstem show prominent diffuse intranuclear

accumulation of polyglutamine stretches (Yamada *et al.* 2000).

The oculomotor deficit in HD also includes increased latency in saccadic initiation, particularly apparent on an anti-saccade task, where errors are also frequent (Zasker and Zee 1997). Recent functional imaging data suggest that anti-saccades activate an inferior parietal network centred in the intra-parietal sulcus, involved in covert attention (Connolly *et al.* 2000). Notably, attentional shifts are impaired in early HD (Lawrence *et al.* 2000). Visuospatial deficits are also noted in early HD (Lawrence *et al.* 2000), particularly an inability to perform spatial transformations on fragmented figures (Gómez-Tortosa *et al.* 1996). Furthermore striking loss of pyramidal neurons has been demonstrated in the adjacent angular gyrus of HD patients (McDonald *et al.* 1997).

All these studies reinforce the notion that HD is indeed a multifocal process (Lange *et al.* 1976), and therefore any imaging analysis technique constrained to a small number of structures and metrics will fail to characterise the distribution of pathology appropriately. Accordingly in this study, I use VBM to provide whole brain assessment of HD patients in order to locate regionally specific structural differences in grey and white matter within and between gene-status groups, previously identified by predictive testing. Statistical analysis within the flexible General Linear Model framework allows effects to be partitioned between several explanatory variables in a principled manner (see Chapter 2). In particular, to address questions of relevance to future clinical trials: whether changes in structural imaging in early HD can be predicted from detailed clinical and neuropsychological assessment; whether there are changes in local tissue volume that have a non-linear relationship to CAG repeat number; and whether there are progressive structural changes over time, specific to the HD genotype.

Methods

This study was a collaboration between the Wellcome Dept of Imaging Neuroscience, UCL, London and the departments of Neurology, Radiology and Clinical Genetics, Westmead Hospital, New South Wales, Australia. The patients were recruited and assessed in Australia and I performed all imaging analysis in London. The Western Sydney Area Health Service ethics committee and the Local Research Ethics Committee of the National Hospital for Neurology and Neurosurgery (UCLH,

NHS Trust) and the Institute of Neurology (UCL) approved the project.

Subjects

The disease and control groups were selected from a population that had undergone predictive genetic testing with the NSW genetics service. According to standard guidelines (International Huntington's Association (IHA) and the World Federation of Neurology (WFN) Research group on Huntington's Chorea. 1994) all predictive tests followed a neurological assessment by a specialist neurologist confirming no clinical evidence of HD. The study was publicised by the NSW HD Association and by the social worker of the genetic service who remained in contact with affected families following predictive testing. Selected subjects were at 50% risk of HD prior to genetic testing on the basis of a single affected parent and remained asymptomatic at the time of the current study. Exclusion criteria included symptoms suggesting HD onset, history of other neurological or psychological illness, alcohol intake of more than 4 units daily or head trauma associated with loss of consciousness. The disease group comprised 34 subjects, 16 had less than 36 CAG repeats in the longest allele (mean repeat number 20.38, standard deviation 3.70) and were classified gene-negative (Rubinsztein, 1996; McNeil, 1997). 12 subjects had 40 or more CAG repeats and 5 had between 36 and 39 CAG repeats (at risk of HD but with reduced penetrance). In 1 subject, the exact number of repeats could not be determined for technical reasons, but was nevertheless greater than 35. For the purposes of analysis, all those subjects with 36 or more CAG repeats were classified gene-positive (mean repeat number of longest allele 41.06, standard deviation 2.70). In total, there were 18 subjects in the gene-positive group. The range of repeat lengths within this group (38-46) is consistent with other studies of adult predictive test populations. Age, sex and handedness details of the groups, and the estimated parental age of onset and inheritance pattern, are given in Table 11.1. Since age and sex were not exactly matched across groups, potential confounding effects were accommodated in the clinical and imaging statistical analyses.

Table 11.1: Subject demographics

	Number *(n)*	**Mean age** *(SD)*	**Sex** *(M:F)*	**Handedness** *(L:R)*	**Inheritance** *(paternal: maternal)*	**Parental age of onset** *(SD)*
All subjects	34	41(12)	19:15	1:4	1:1	47(13)
Gene-negative	16	38(11)	5:3	1:6	4:3	45(13)
Gene-positive	18	43(12)	1:1	1:3	4:5	48(13)

Clinical assessment

Each subject underwent formal motor examination by 1 of 3 neurologists experienced in the clinical assessment of HD who were blinded to genetic status. In addition subjects underwent more rigorous assessment for subtle chorea, given the importance of the identification of this sign in the diagnosis of early HD (McCusker et. al., 2000). For this assessment, a video recording of foot movement was made while subjects were stressed using a mental distraction task. Two clinicians independently assessed the video for chorea, without being able to identify the subject featured. Scores from the two observers were then combined. On the basis of all of these assessments, subjects were scored according to the motor component of the United Huntington's Disease Rating Scale (UHDRS). This is a standardised test of motor function that includes quantification of chorea, bradykinesia, rigidity, motor impersistence, motor sequencing, ocular movements and gait. Scores range from 0 to 128, higher scores representing greater motor impairment. When applied to the whole spectrum of gene-positive subjects, the scale is internally consistent, has inter-observer reliability and is useful for tracking progression of disease (Huntington Study Group 1996).

Cognitive function was assessed according to UHDRS specifications by a Phonetic Verbal Fluency Test, Symbol Digit Modalities Test, Stroop Word, Stroop Colour and Stroop Interference Tests (Huntington Study Group 1996). Results from the six scores (one motor and five cognitive) were expected to be closely correlated.

MR Imaging

Whole brain structural MRI was performed on all subjects on the same 1.5 Tesla scanner (Siemens Magnetom Vision, Erlangen, The Netherlands). Images were acquired in the sagittal plane, with isotropic $1mm^3$ voxel size. A high-resolution 3-D T1-weighted MP-RAGE sequence was chosen with the following parameters: T1/TE/TI/NEX: 9.5/4/600/1, flip angle 20°, matrix 256 x 256, FOV 256 mm^2. The optimised VBM protocol was used for data analysis as detailed in Chapter 2.

Statistical analyses

Firstly to test whether the UHDRS motor score was significantly higher and cognitive scores were significantly lower in the genotype positive group a design matrix was constructed with gene status conditions, clinical scores as covariates of interest and age, sex and education as confounding covariates.

Secondly to test whether structural changes in HD always have a clinical correlate evident on thorough clinical testing, a single 'optimal clinical score' that best discriminated the gene positive and gene negative subjects was generated using linear discriminant analysis. This was entered as a confounding covariate in the image analysis to determine whether there was a residual significant main effect of HD gene status alone on structural integrity. The optimal clinical score was also used as a covariate of interest in a parametric design in order to test for the effect of clinical stage on structural change within the gene positive group.

Statistical threshold was set at $p \leq 0.05$, corrected for multiple comparisons across the whole brain. Where a prior hypothesis about regional pathology existed (see introduction) correction was limited to a small volume around this region (the radius of a sphere used for the small volume correction is given in Table 11.2).

The simplest analyses tested for the main effect of gene status (Fig. 11.2) on grey and white matter and CSF. Here, genetic predisposition was treated as a categorical variable: variability of genotype within the gene positive group was neglected. Analyses were performed both with and without global voxel intensity as a confounding covariate, to assess whether significant local effects reflected changes in global tissue quantities. Analyses were also performed with and without an optimal clinical score confounding covariate, to test the pre-clinical pathology hypothesis. Age and sex were included as confounding covariates was based on my findings in

Chapters 3 and 4. Inheritance (paternal or maternal) was not explicitly modelled since there is evidence that anticipation of the HD phenotype with paternal inheritance is directly attributable to CAG repeat expansion (Kremer *et al.* 1005; Ranen *et al.* 1995).

The potential dependence of brain structure on differences in repeat number within the gene positive and negative categories was investigated with an extension of the basic design to include longest allele repeat length covariates for each gene status condition, corrected for condition mean. The shorter allele repeat length was included as an extra confounding covariate. Contrasts tested for greater loss of grey or white matter tissue volume with increasing repeats in the gene-positive relative to the gene-negative group. Classification into gene-status categories was also derived from the repeat number, so this condition-by-covariate interaction effectively tested for a non-linear parametric effect of genetic load on brain structure.

Although this study was not designed to investigate progression over time within subjects, among the gene-positive group a subject's age may be considered to be an indicator of duration of the pathologic process. Regional loss of grey and white matter volume with age has been demonstrated in normal subjects (Chapter 3) so it was necessary to test for an interaction of age with gene status. The design matrix in this analysis was similar to the repeats analysis described above, with age covariates for each gene status condition, and sex and global voxel intensities as confounding covariates.

In addition to the repeat and age interaction designs mentioned above, gene positive and gene negative groups were also analysed separately in analyses that included both age and repeat number as covariates of interest.

Figure 11.1: Design matrix for the grey matter gene status analysis.

Rows correspond to individual subjects, arranged according to gene status. Cond 0 represents gene negative and Cond 1 represents gene positive subjects. Age, sex and global grey matter voxel intensity are modelled as confounding covariates. μ is a column of ones which models the mean of the data across subjects.

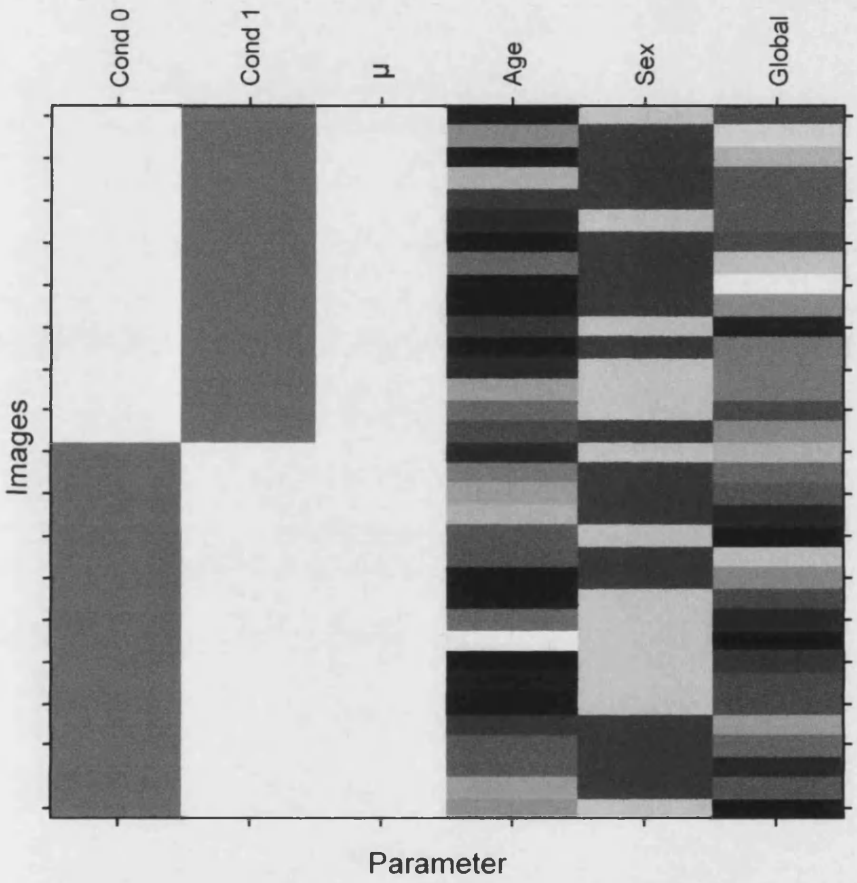

Results

Controlling for potential confounding effects of age, sex and education, the HD genotype is associated with a significantly higher UHDRS motor score ($p \leq 0.016$) and a significantly lower Stroop word score ($p \leq 0.009$). There is a non-significant trend toward lower scores in the HD genotype on the other cognitive tests. The distribution of grey matter volume loss in HD gene positive subjects is shown in Figure 11.2. Local maxima for the main effect of gene status are tabulated in Table

11.2. Significant grey matter volume loss was seen in the left head and body of caudate, putamen and globus pallidus. Ventrally, this extended into nucleus accumbens and orbito-frontal cortex, particularly the left olfactory sulcus. Right caudate volume loss reached only borderline significance. Grey matter volume loss was also seen in the midbrain tectum on the left extending into medio-dorsal thalamic nucleus. Volume loss in the dorsal medulla and pons did not survive whole brain correction and in the absence of a specific prior hypothesis further inference about these regions was impossible.

Table 11.2: VBM results

Analysis	**x**	**y**	**z**	**Z score**	**P corrected (SVCmm)**	**Location**
Grey matter						
Gene status	-12	12	3	4.08	0.003(10)	L caudate head
	-15	9	14	3.44	0.026(10)	L caudate body
	-22	9	0	3.81	0.009(10)	L putamen
	18	-2	22	3.06	0.070(10)	R caudate body
	-4	-28	-3	3.69	0.003(5)	L midbrain tectum
	30	-72	27	4.57	0.004(20)	R intraparietal sulcus
	38	-8	-4	3.37	0.032(10)	R insula
	-30	-12	-8	3.76	0.010(10)	L insula
	-9	33	-24	3.39	0.030(10)	L olfactory sulcus
Gene status, cognitive	-12	12	3	4.08	0.030(10)	L caudate head
CAG repeat x gene status interaction	39	10	21	5.74	0.001	R inf frontal sulcus

Figure 11.2: Main effect of HD gene status on local grey matter volume.

This contrast shows regions of grey matter loss in gene positive relative to gene negative subjects. For illustrative purposes the threshold for display is $p \leq 0.005$ uncorrected. The colour bar represents the T score. Grey matter volume reduction is shown in the left head and body of caudate, putamen and globus pallidus extending into nucleus accumbens and orbito-frontal cortex. On the right, volume loss in the caudate nucleus reaches only borderline significance. There is also grey matter volume loss in the midbrain tectum on the left extending into the medio-dorsal thalamic nucleus.

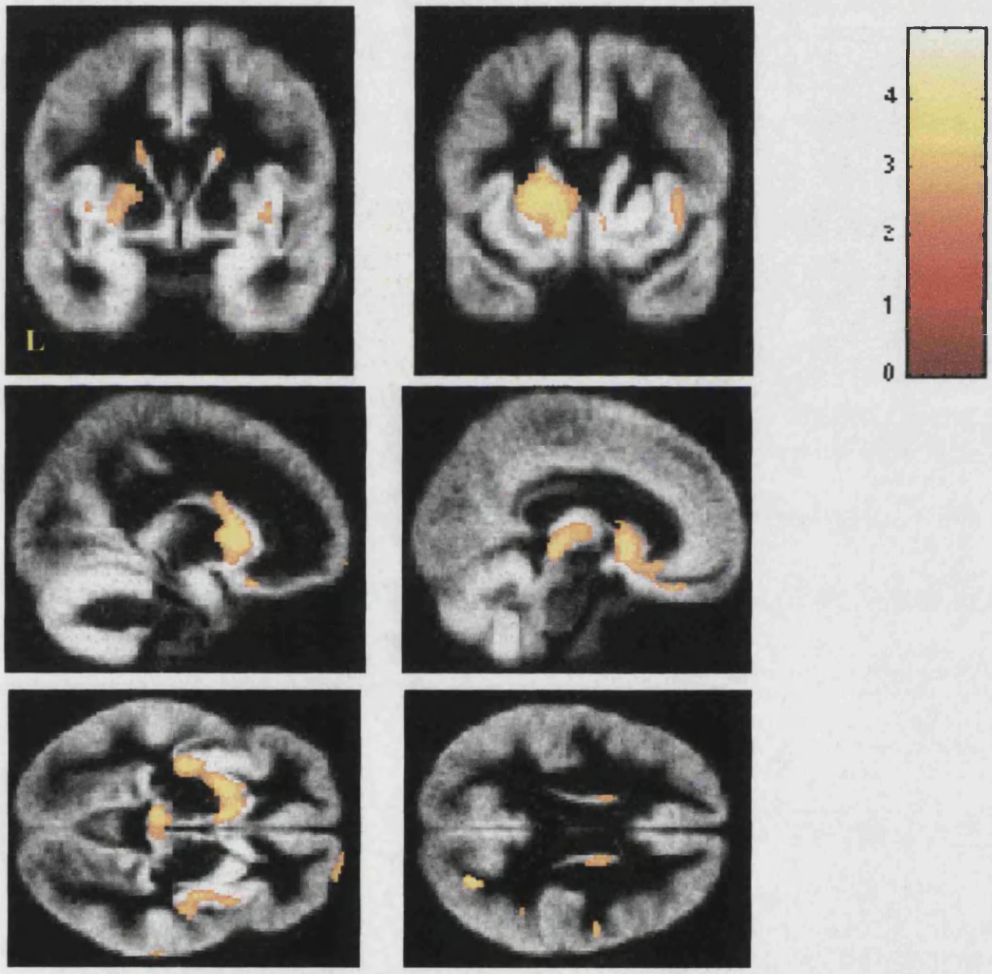

Regarding cortical morphological changes, bilateral grey matter loss was seen in the posterior insula on the left extending ventro-medially into the amygdala. There was also bilateral volume loss in the posterior intra-parietal sulcus, reaching corrected significance on the right. A gene status analysis for white matter revealed a reciprocal significant increase in white matter volume in gene positive subjects beneath the right

intra-parietal sulcus (not shown). There were no other significant changes in the white matter or CSF gene status analyses.

When the grey matter gene status analysis was performed without including global voxel intensity as a confound, the distribution and magnitude of the effects remained unchanged, suggesting that these local effects do not reflect distributed changes in grey matter volume. When the optimal clinical score was included as a confound, grey matter volume loss was similarly distributed remaining significant in the head of the left caudate nucleus (Fig. 11.3).

Figure 11.3: Main effect of HD gene status on local grey matter volume.

Regions marked in red reflect the main effect of gene status (as in Fig. 11.2). Regions marked in yellow remain significant when the optimal clinical score is included as a confound demonstrating that within the gene-positive group there is significant structural neuropathology, which has no clinical correlate apparent on thorough testing.

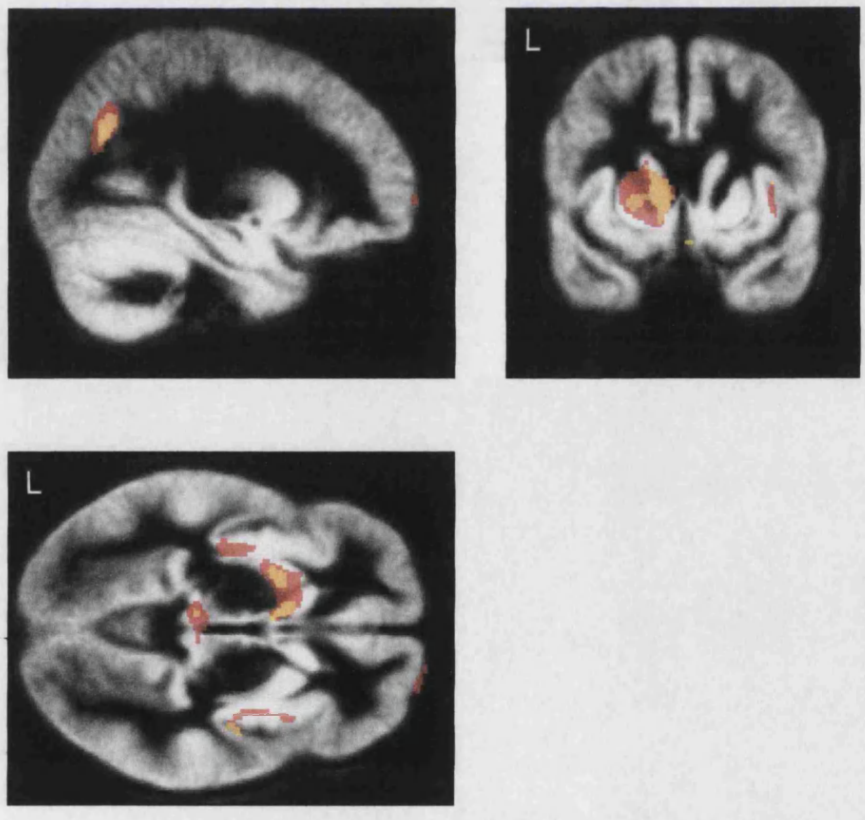

Fig.11.4 shows the distribution and significance of white matter loss with age in gene positive relative to gene negative subjects. Asymmetric left more than right periventricular white matter volume loss was noted, most marked around the left frontal horn. A similar distribution of white matter loss with age was found in a separate analysis of gene positive subjects. In contrast, significant white matter loss with age in gene negative subjects was localised to the posterior limb of internal capsule bilaterally. No significant changes in grey matter or CSF volume were identified in the age by gene status interaction.

Figure 11.4: Interaction of age and gene status on local white matter volume

This contrast shows periventricular white matter loss with increasing age in gene positive relative to gene negative subjects. The threshold for display is $p \leq 0.005$ uncorrected, T score indicated by colour bar.

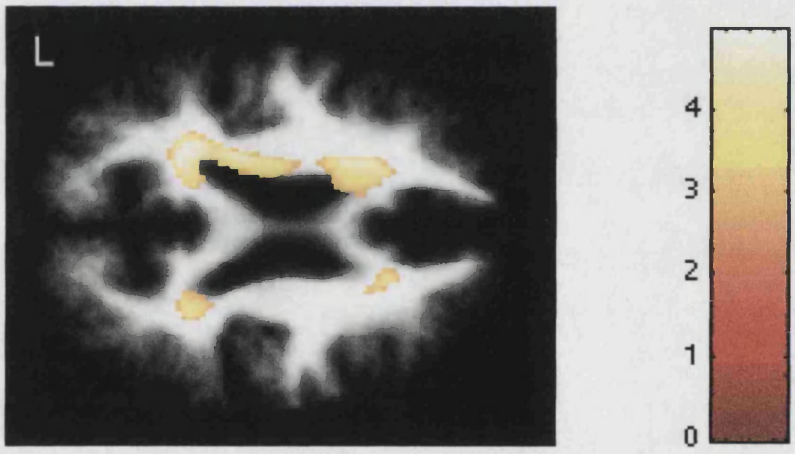

A significant interaction of CAG repeat number with gene status condition was found only in the right inferior frontal sulcus (Fig. 11.5). This reflects a decrease in local grey matter volume and a reciprocal increase in white matter volume with increasing repeats in the gene positive group.

Figure 11.5: Interaction of repeat length and gene status on local grey matter volume.

This contrast identifies regions of greater loss of grey matter volume with increasing repeats in the gene-positive relative to the gene-negative group. This condition-by-covariate interaction effectively tests for a non-linear parametric effect of genetic load on brain structure. The threshold for display is $p \leq 0.005$ uncorrected, T-score indicated by colour bar. Significant voxels are shown in the right inferior frontal sulcus.

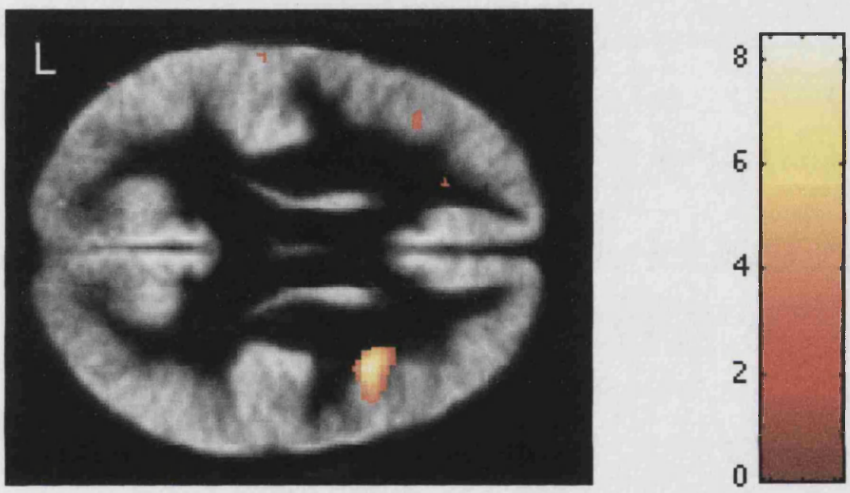

Discussion

The whole brain approach to volumetric analysis adopted in this study allowed the demonstration of widely distributed cortical and subcortical pathological structural changes. Conventional morphometric techniques constrained to a small number of structures and metrics would inevitably have missed many of these areas. The versatile statistical framework of VBM allowed regional prior hypotheses to be tested in a principled way and sensitivity has been improved by using small volume corrections. Importantly, by introducing appropriate confounding covariates into design matrices, I have been able to control for effects of no interest while highlighting several different effects of interest. The conventional approach is more restrictive: precise matching of disease and control groups for all potential confounding variables is necessary if group means are to be compared by a simple t-test, but this inevitably renders the design inflexible for testing multiple hypotheses, or attributing variance among a number of

continuous and discrete explanatory variables.

The principal regional prior hypothesis in this study was that caudate and putamen volume would be reduced in subjects carrying the HD triplicate repeat expansion, relative to controls of normal genotype. While this was confirmed, the asymmetry of volume loss was surprising. A previous MR spectroscopy study of HD showed an asymmetric pattern of elevated lactate levels in the left relative to right striatum. These results were attributed to increased motor activation in the dominant hemisphere, particularly increased glutamatergic synaptic input to striatal cells (Jenkins *et al.* 1998). Even if impairment in mitochondrial function were symmetrical, differential oxidative stress could lead to asymmetrical striatal neuronal loss. In a murine model of HD, manipulation of sensory input and motor activity does indeed alter striatal volume (Van Dellen *et al.* 2000). Another surprising feature of the striatal volume loss was that it appeared to be concentrated rostrally and ventrally in contrast to pathological predictions (Vonsattel *et al.* 1985). A previous histopathological study of a pre-symptomatic case identified degenerative changes confined to the dorsal striatum (Gutekunst *et al.* 1999) supporting the idea that there is a dorsal to ventral gradient of neuronal loss with advancing disease. The reason for this discrepancy with our results is unclear. Involvement of ipsilateral orbitofrontal cortex, globus pallidus and medio-dorsal thalamus, which together with the ventral striatum constitute the orbito-frontal basal ganglia loop, suggest that the VBM findings are real.

The orbito-frontal cortex plays an important role in decision making (Bechara *et al.* 1998; Rogers *et al.* 1999) and reversal learning (Watkins *et al.* 2000). Subjects with early HD generally perform these functions normally but fail tests of planning (Watkins *et al.* 2000) and make perseverative errors in attentional set switching paradigms (Lawrence *et al.* 1996). Such deficits are usually attributed to malfunction of the dorso-lateral prefrontal cortex or interruption of its efferent connections in the dorsal caudate nucleus. In this study, grey matter loss was not seen in dorso-lateral prefrontal cortex, premotor cortex or frontal eye fields that provide input to the motor and oculomotor basal ganglia loops respectively. In order to resolve this apparent conflict between clinical and imaging data more focussed cognitive testing and larger patient groups will be required.

The expectation of regional grey matter loss outside the basal ganglia was confirmed. Bilateral volume loss in the insular cortex is in accordance with loss of recognition of the facial expression of disgust in a similar cohort of pre-symptomatic

gene positive subjects (Gray *et al.* 1997). These subjects were unimpaired in the recognition of fearful expressions, a function previously attributed to the left amygdala (Morris *et al.* 1996), yet in my study the grey matter loss encroached partially into the left amygdala (Fig. 11.2).

The gene positive subjects in my study had early HD. Nevertheless, the distribution of regional volume loss at this stage of disease provides an insight into the pathophysiology underlying clinical deficits which manifest later in the course of HD. For example, focal pathology of the intra-parietal sulcus and midbrain tectum might account for the abnormal eye movement of HD patients. In HD delayed initiation of voluntary saccades is commonly attributed to disruption of descending input to the superior colliculus from the frontal eye fields (Zasker and Zee 1997). The superior colliculus also receives inhibitory input from the oculomotor basal ganglia loop, disruption of which is thought to underlie an inability to suppress reflexive saccades. In this study focal structural change was observed in the midbrain, including the superior colliculus. The burst neurons that generate commands for vertical saccades are located in the rostral interstitial nucleus of the medial longitudinal fasciculus (MLF), allowing a single midbrain lesion to explain both the initiation deficit and saccadic slowing. An alternative possibility is that grey matter loss in the parietal eye fields could impair saccadic eye movement, particularly in the context of the anti-saccade task where deficits are most apparent in HD.

Evidence of neuropathology beyond that which could have been predicted from thorough clinical testing confirms the commonly held belief that pathological changes of HD precede clinical onset. The time course of this process remains unknown, but CAG repeat length plays a role, with greater numbers of repeats resulting in earlier clinical onset (Brinkman *et al.* 1997; Duyao *et al.* 21993). However, increasing CAG repeat length is not necessarily associated with reduced striatal volume (Harris *et al.* 1999; Sieradzan and Mann 1997). In this study, the only area of significant volume change with increasing CAG repeats specific to the gene positive group was the right inferior frontal sulcus (Fig. 11.3) but this could reflect the narrow range of repeat lengths in the gene-positive group who had all reached adulthood without symptoms. There is some evidence that repeat expansion in the HD gene alters regional cerebral development prior to progressive neurodegeneration. In pre-symptomatic gene-positive subjects the caudate histology is suggestive of abnormal morphogenesis (Gómez-Tortosa *et al.* 1996). It seems more likely though, that the striatal grey matter volume

loss in the gene-positive group reflects progressive neuronal loss. Paradoxically, in the age-by-condition interaction, the only structural change with age specific to the gene positive group was white matter loss around the lateral ventricles, not caudate atrophy. This may reflect differing time courses for volume change in different tissues.

Conclusion

This study demonstrates that the VBM approach is ideally suited to answer more subtle questions in HD. Imaging of large numbers of preclinical subjects may in future allow stratification into prognostic groups, enabling prediction of clinical onset in individual cases. Pre-clinical subjects approaching disease onset are likely candidates for preliminary clinical trials of neuroprotective agents. In order to evaluate such agents a reliable measure of pathologic burden in pre-clinical subjects is needed, particularly to measure pathology progression within the time window of a realistic clinical trial. These data suggest that VBM may prove to be a useful surrogate marker of disease progression in pre-clinical HD.

CHAPTER 12

GENOTYPE-PHENOTYPE MAPPING FAMILIAL ATAXIC MIGRAINE

Guide to Reader

In Chapter 7, I showed no evidence of structural change within brainstem regions that demonstrate functional ictal changes in patients with migraine. One of the possibilities I suggested for this negative imaging result was that the phenotype of migraineurs is heterogeneous making the chance of detecting systematic structural change small. In order to test whether putative brainstem structural changes are present in a more refined migraine phenotype, I have chosen a select patient group with a specific genotype and a homogeneous phenotype. In this particular kindred with autosomal dominant familial ataxic migraine, a specific calcium channel gene mutation has been identified and the phenotype comprises migraine and cerebellar symptoms. Moreover, several family members without the mutation have a similar phenotype. This allows me to perform correlations between genotype, clinical phenotype and structural brain phenotype. Importantly, in a very similar autosomal dominant form of migraine with a calcium channel gene mutation and a more heterogeneous genotype and phenotype (familial hemiplegic migraine), standard neuroimaging reveals cerebellar atrophy in a proportion of affected patients. It follows that cerebellar atrophy is likely to be present in affected members of this particular family and this should be easily detectable on MRI. This allows me to test firstly whether VBM can detect cerebellar atrophy in some affected family members, secondly whether VBM can detect brainstem structural changes which, if present, are likely to be more subtle and thirdly whether there is a clear genotype-structural brain phenotype correlation.

Introduction

Familial hemiplegic migraine (FHM) is an autosomal dominant form of migraine (Headache Classification Committee of the International Headache Society

1988). This condition often manifests in childhood with attacks of prolonged hemiparetic aura lasting for hours or days and patients may exhibit nystagmus and mild progressive ataxia between attacks (Terwindt *et al.* 1998). Neuroimaging shows cerebellar atrophy in approximately 20% of FHM patients (Elliot *et al.* 1996) but it is unclear how this relates to the underlying genotype. The FHM genotype is known to be heterogeneous. Approximately half of identified families are linked to mutations of the $\alpha_1$2.1 subunit of the Ca_v2.1 P/Q type brain voltage-gated calcium channel gene, CACNA1A, on chromosome 19p13.1 (Ophoff *et al.* 1997). This neuronal calcium channel is widely expressed in the brain with particularly high levels in cerebellar Purkinje and granule cells and modulates release of neurotransmitters such as monoamines, catecholamines, excitatory amino acids, CGRP and Substance P. About a third of families are linked to chromosome 1q (Ducros *et al.* 1997; Gardner *et al.* 1997) and the remainder are as yet undefined. A genotype-phenotype correlation can be demonstrated - 50% of CACNA1A mutations exhibit progressive ataxia whereas mutations at the other loci are not associated with a cerebellar syndrome (Ducros *et al.* 2001).

The CACNA1A mutations in FHM are usually missense mutations causing amino acid substitutions. Allelic mutations such as splice and frame shift mutations from base pair deletions within CACNA1A (Ophoff *et al.* 1997) are associated with a different phenotype; episodic ataxia type 2 (EA-2). This is an autosomal dominant disorder characterised by intermittent attacks of midline cerebellar ataxia, interictal nystagmus and in about 50% of families migraine attacks with headache and nausea. Some patients exhibit mild progressive cerebellar ataxia with gait unsteadiness, limb ataxia and dysarthria (Kramer *et al.* 1995) and neuroimaging often shows cerebellar atrophy (Vahedi *et al.* 1995; Vighetto *et al.* 1988)(9, 10);

A kindred with a variant of FHM, familial ataxic migraine, linked to a novel CACNA1A mutation has recently been identified (Terwindt, Giffin and colleagues, unpublished data). This mutation is a C-to-G transformation at position 5838 of the coding sequence, predicting a premature stop codon, rather than the missense mutations more typical of FHM. The mutation is located at the beginning of the intracellular C-terminus of the $\alpha_1$2.1 subunit. Affected family members have episodes of unsteadiness, slurred speech and occasional disorientation and 50% have associated attacks of migraine. Several family members are phenocopies: despite having a

strikingly similar clinical phenotype with intermittent attacks with migraine, they do not have the CACNA1A mutation. There is no difference in age at onset, duration of attacks, frequency of attacks and clinical characteristics of attacks between clinically affected family members with and without the mutation however the interictal cerebellar features are present only in the carriers.

In patients with migraine headache functional neuroimaging has identified activations in the brainstem during acute attacks (Bahra *et al.* 2001; Weiller *et al.* 1995), but no corresponding brainstem structural changes have been identified (see Chapter 7). However, in another primary headache disorder, cluster headache, VBM has revealed regional structural change within the hypothalamus (May *et al.* 1999b), exactly matching functional changes on PET imaging (May *et al.* 1998a). The reason for the negative imaging findings in the migraine study (Chapter 7) is unclear, but possible explanations include 1) insufficient power of the VBM study to detect very subtle macroscopic change, 2) heterogeneous phenotype of migraine making the likelihood of detecting a systematic structural difference in migraineurs small and 3) microscopic or no structural change.

In this study I use VBM to further investigate putative brainstem structural changes in a more homogenous phenotype of primary headache disorders, and I hypothesize that if such changes are present they are more likely to occur in the genotype positive group. Since cerebellar atrophy has been shown in FHM, it is likely that members of this particular family will also have cerebellar atrophy and this should be detectable with VBM. This will allow me to characterise the structural brain phenotype (regional grey and white matter) in family members with the FHM phenotype with and without the CACNA1A mutation and show genotype-phenotype correlations.

Methods

Approval for the study was obtained from the Local Research Ethics Committee of the National Hospital for Neurology and Neurosurgery (UCLH, NHS Trust) and the Institute of Neurology (UCL). All subjects gave written informed consent.

Subjects

The kindred are members of a five-generation British family who have

undergone genetic analysis (Fig.12.1). All available members of the family were interviewed by a semi-structured questionnaire and full neurological examination was performed by members of Professor Goadsby's clinical team, in particular Dr Nicola Giffin. Clinical data are summarised in Figure 12.2.

Six family members with the affected genotype (G+P+), 3 family members with the phenotype but without the genotype (G-P+) and 4 with neither the genotype nor phenotype (G-P-) were studied. Of the G-P- group, 2 had infrequent migraine without aura, but neither had any attacks of unsteadiness or hemiparesis.

Age and sex matched normal control structural MRI scans were obtained from my MRI database at the Wellcome Department of Functional Imaging. All control subjects were interviewed and those with a personal history of migraine according to International Headache Society (IHS) criteria (1) or other major neurological disorder were excluded. All controls and subjects were imaged on the same MR scanner with identical parameters to remove any scanner dependent bias.

Figure 12.1: Pedigree with familial ataxic migraine

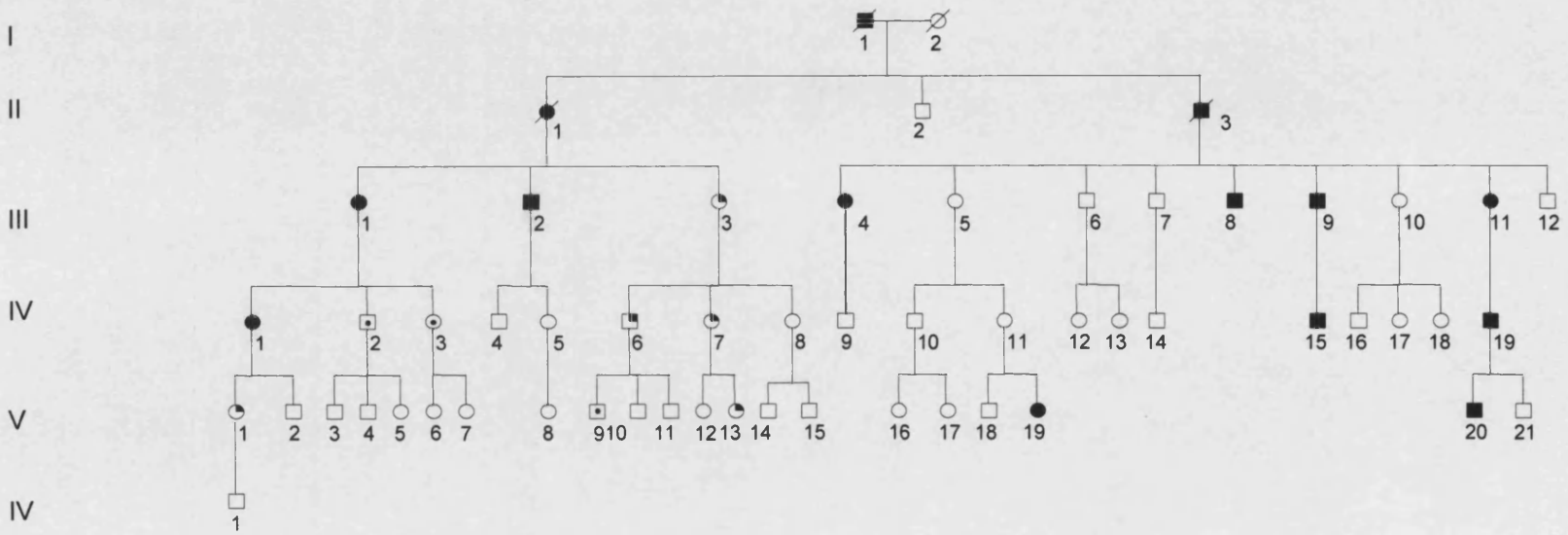

Table 12.1: Clinical details of familial ataxic migraine kindred

	Genotype	Age (yr)	Onset (decade)	Duration	Attacks/yr (min-max)	Attacks with ataxia	Dysarthria	Migraine during ataxia	Separate migraine attacks	Vertigo	Interictal cerebellar symptoms
III-1	+	63	2nd	5-45mins	0-4	+	+	-	+	-	-
III-2	+	65	2nd	minutes	?	+	-	-	+	-	-
III-4	+	63	1st	15-30mins	52-156	+	+	-	-	+	+
III-11	+	49	1st	10mins-few hours	4-156	+	+	-	-	+	+
IV-15	+	21	2nd	1-15 mins	4-6	+	-	-	-	-	-
IV-19	+	26	1st	2-8hrs	12-104	+	+	+	-	+	+
IV-6	-	37	2nd	minutes	rare	+	-	-	+	-	-
V-1	-	25	2nd	5mins	2-24	+	+	+	+	+	?
III-3	-	55	1st	few hours	2-4	+	+	+	+	-	-
III-7	-	59	-	-	-	-	-	-	-	-	-
III-10	-	51	-	-	-	-	-	-	-	-	-
IV-2	-	44	-	-	-	-	-	-	+	-	-
IV-3	-	34	-	-	-	-	-	-	+	-	-

MRI scanning

High resolution volumetric MR imaging was performed on a Siemens 2T Magnetom scanner using an optimised MPRAGE sequence which affords enhanced grey /white matter contrast and segmentation. The acquisition parameters included: TR/TE/TI 11/4/1000, flip angle 12, matrix 256 × 224, FOV 256 × 224mm; 176 sagittal slices, 1mm isotropic voxels (Deichmann).

Voxel-based morphometry

The optimised method of VBM was used for pre-processing (see Chapter 2) of images using the SPM apriori grey and white matter templates for spatial normalisation.

VBM statistical analysis

To analyse the main group effect of gene status I constructed separate design matrices for grey and white matter. I compared genotype/phenotype positive (G+P+), genotype negative/phenotype positive (G-P+) and genotype negative/phenotype negative (G-P-) groups against separate age and sex matched control groups. I also included age, sex and global grey matter voxel intensity as confounding covariates (Fig. 12.2). I also conducted the above analyses without including the global voxel intensity as a confound. In separate design matrices I compared individual G+P+, G-P+ and G-P- family members against age and sex matched control groups. In a further analysis I compared the group of individuals with migraine headache against those without migraine, irrespective of prolonged aura symptoms.

Significance levels were set at $p<0.05$, corrected for multiple comparisons. When a prior hypothesis about regional pathology existed (see introduction), correction was limited to a small volume around this location, of a size appropriate to the volume of the structure. For the cerebellum I used a sphere of radius 5 cm, for the brainstem I used a sphere of radius 2 cm.

Figure 12.2: Design matrix

Rows represent individual subjects. Columns represent conditions: 1= control group I, 2 = G+P+, 3 = control group II, 4 = G-P-, 5 = control group III and 6 = G-P+. Age, sex and global grey matter volume are modelled as confounding covariates.

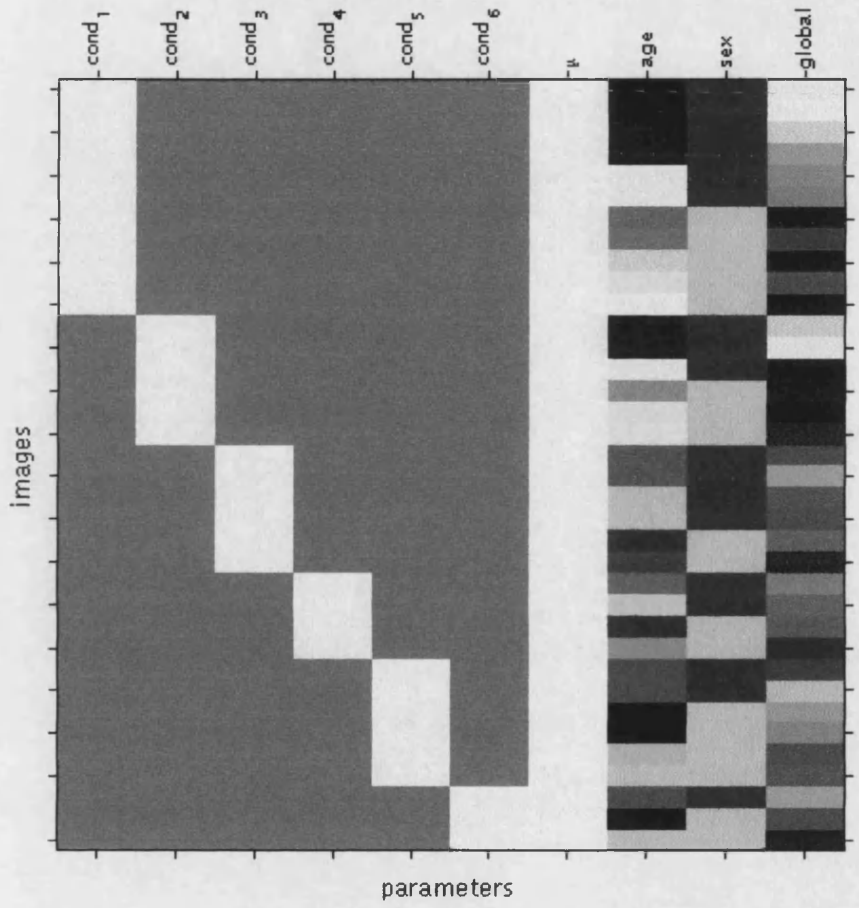

Results

Grey matter

VBM detected cerebellar atrophy within the vermis and cerebellar hemispheres of the G+P+ group, but not the G-P+ or G-P- or control groups (see Fig. 12.4 and 12.6). These within-group cerebellar changes were also seen within each G+P+ patient, but not in any of the G-P+ or G-P- family members. There were no additional differences between the group with headache and the group without headache. No brainstem grey matter structural changes were detected.

Figure 12.3: Main effect of gene status- grey matter.

VBM detected grey matter volume loss in the cerebellar vermis and hemispheres of the G+P+ group projected over the normalised mean grey matter image from the study group. The colour bar represents the T score.

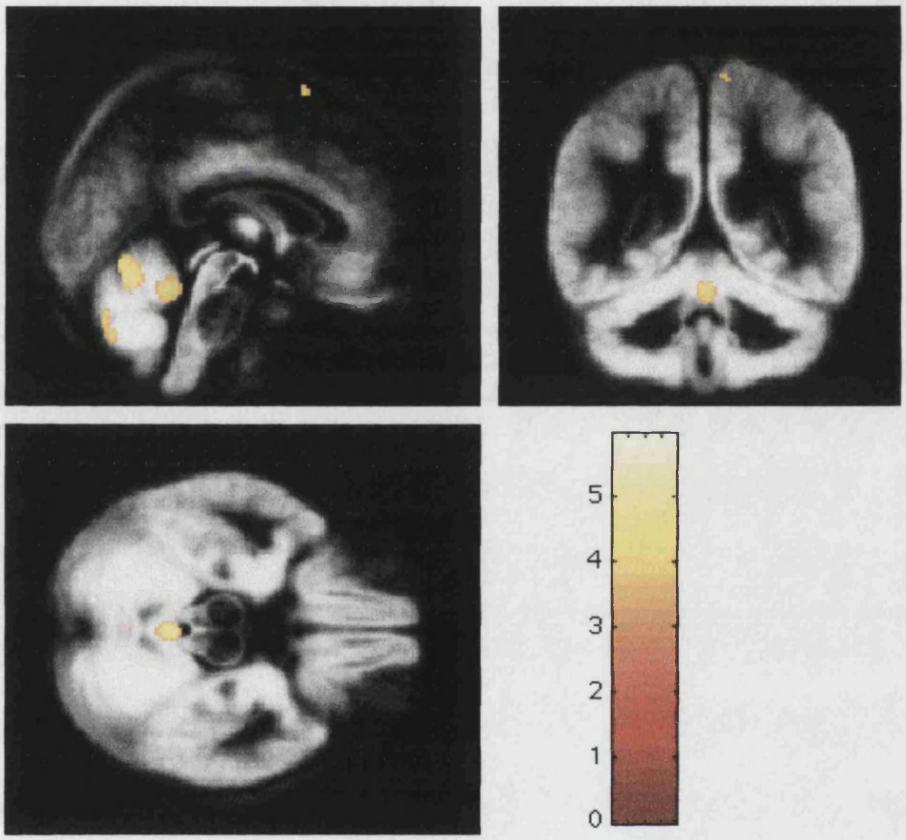

Figure 12.4: Plot of parameter estimates

Parameter estimates of a local maxima in the cerebellar vermis (3, -63, -15, p = 0.026 corrected, T = 5.10) showing regional grey matter atrophy in the G+P+ group only

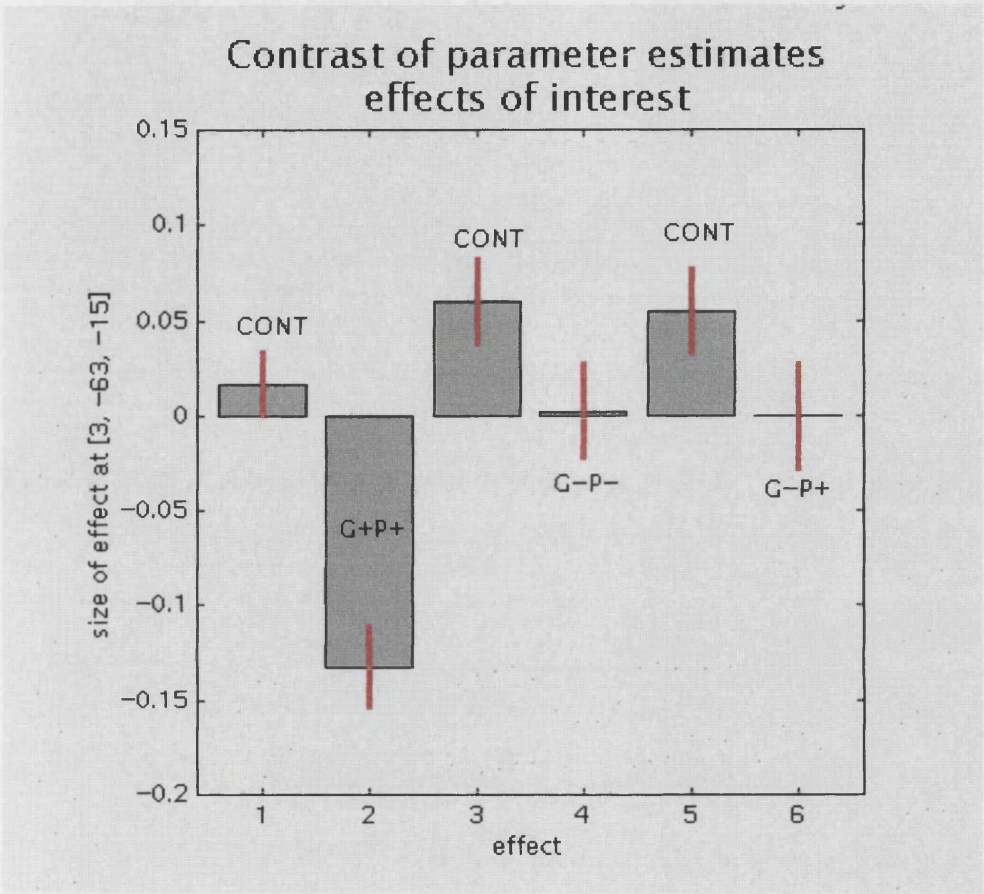

White matter

VBM detected cerebellar white matter atrophy involving the vermis (Fig. 12.5) and cerebellar hemispheres in the G+P+ group, but not in the G-P+ or G-P- or control groups. These within-group cerebellar changes were also seen within each G+P+ patient but not in any of the G-P+ or G-P- family members. There were no additional differences between the group with headache and the group without headache. No brainstem white matter structural changes were detected.

Figure 12.5: Main effect of gene status-white matter

White matter volume loss in the cerebellar vermis in the G+P+ group only projected over the normalised mean white matter image. The colour bar represents the T score

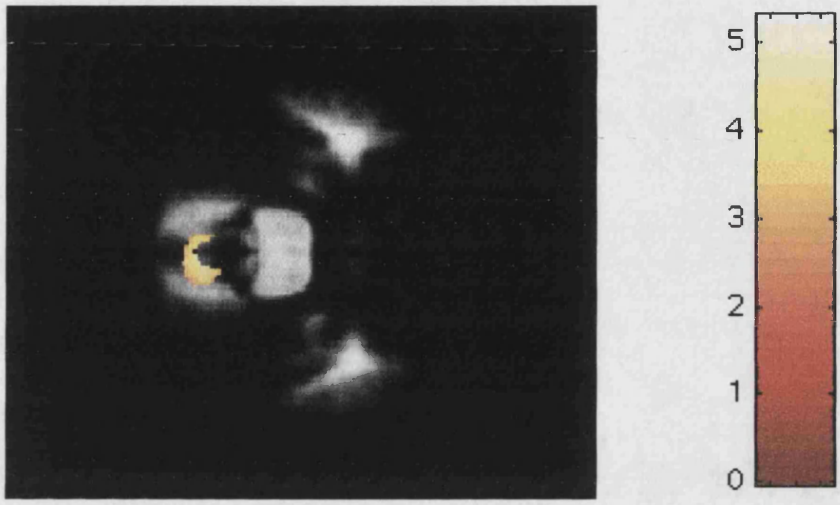

Discussion

I have characterised the structural brain phenotype of a kindred with a novel CACNA1A mutation and a specific clinical phenotype. I have shown a main effect of gene status, namely cerebellar atrophy in the genotype positive phenotype positive (G+P+) group but not in those clinically affected but without the mutation (G-P+). Cerebellar atrophy is seen not only as a G+P+ group effect but also within each carrier. These data demonstrate a precise genotype/phenotype correlation that predicts specific structural change in the brain offering the exciting prospect of selecting patients for study based on the powerful combination of the genetic mapping and MRI structural imaging.

Cerebellar atrophy was diffuse involving grey and white matter of the vermis and cerebellar hemispheres. This concurs with earlier neuroimaging studies that have shown CT and MRI evidence of cerebellar vermis and hemisphere atrophy in FHM (Elliot *et al.* 1996; Fitzsimons and Wolfenden 1985; Joutel *et al.* 1993) and EA-2 (Vahedi *et al.* 1995; Vighetto *et al.* 1988). One of these FHM kindreds has been linked to chromosome 19, but as yet no mutation has been identified (Elliot *et al.* 1996). The kindred in this study may be regarded as part of a spectrum of phenotypes between

FHM and EA-2. Most affected family members had attacks fulfilling the criteria for EA-2. Furthermore this mutation codes for a stop codon which is more typical of EA-2 than FHM. However, the frequency of migraine with, or in addition to ataxic episodes is higher than would be expected in EA-2, and the frequency and severity of nystagmus is more in keeping with FHM than EA-2. Therefore the term familial ataxic migraine has been coined for this particular kindred to emphasise the continuum between the two allelic conditions. The presence of phenocopies (G-P+) has been described before (Terwindt *et al.* 1998) and there may be a number of possible explanations. Firstly 'mimicking' of the phenotype by non-carriers; secondly, a chance association of migraine without aura, and thirdly, an unlinked gene for episodic ataxia within the family.

What is the underlying mechanism of cerebellar atrophy in these subjects? Ictal cerebellar features may be a form of migraine aura. Animal models of cortical spreading depression (Lauritzen 1994) and perfusion weighted imaging in humans (Sanchez del Rio *et al.* 1999) suggest that cortical hypoperfusion in aura occurs secondary to neuronal depolarisation. The cortical perfusion deficit does not reach ischaemic levels (Astrup *et al.* 1981) and therefore it is unlikely that cerebellar atrophy results from recurrent ischaemia due to repeated episodes of prolonged cerebellar hypoperfusion. In the present study, there was no diagnostic neuroimaging evidence of significant ischaemic change in any of the family members. The association of cerebellar atrophy only with genotype and not with phenotype adds weight to the argument that cerebellar atrophy is genetically determined, probably by a direct effect of the $Ca_v2.1$ channel on cerebellar Purkinje and granule cell function (Dove *et al.* 1998). Furthermore, nystagmus and ataxia frequently precede the onset of the migraine attacks (Young *et al.* 1970). More recently it has been noted that some FHM mutations (in particular I1811L and T666M missense mutations) are associated with cerebellar disturbance and others not (Terwindt *et al.* 1998). Interictal features of cerebellar dysfunction are frequently found in FHM, including 50% of those with CACNA1A mutations, but the underlying mechanism is unclear. In some kindreds linked to chromosome 19 nystagmus and associated vermis atrophy can be detected (Elliot *et al.* 1996). Sub-clinical cerebellar dysfunction can be observed in patients with more common forms of non-hemiplegic migraine, both with and without aura (Sandor *et al.* 2001). Whether this latter finding represents involvement of calcium channel genes in the common types of migraine remains to be determined.

Regarding the prior hypothesis of putative structural change in brain stem regions based on previous PET studies of acute migraine (Bahra *et al.* 2001; May and Goadsby 1999; Weiller *et al.* 1995), despite the homogeneous genotype and phenotype I did not demonstrate any structural changes in the brainstem. There are potential explanations for this negative result. This particular family could be more susceptible to aura than headache. CACNA1A may be regarded as an aura, rather than a headache, susceptibility gene. Only half of the G+P+ subjects had migraine headache and furthermore, some G-P- subjects had migraine without aura. Genetic susceptibilities to aura and headache are likely to produce different changes to the function and structure of the brain. However, separate analysis of the groups with and without migraine headache within the family did not show any brainstem changes. The lack of brainstem change could also reflect insufficient power of the study to detect subtle effects, even within a homogeneous phenotype. The midbrain and hypothalamus have relatively poor contrast resolution, owing to their intrinsic anatomy, with embedded nuclei and adjacent white matter connections, providing a challenge for segmentation, but VBM should still be sensitive to a systematic difference in the anatomy, and for this reason, I performed separate grey and white matter analyses. Furthermore the hypothalamus, where VBM showed structural changes matching PET activations in patients with cluster headache (Bahra *et al.* 2001; May *et al.* 1999b; Weiller *et al.* 1995), has similarly poor contrast resolution. It is possible that functional changes within the brainstem in primary headache disorders are not associated with macroscopic change detectable by VBM or even microscopic structural change. Following the first VBM study of a small group of patients with cluster headache (Bahra *et al.* 2001; May *et al.* 1999b; Weiller *et al.* 1995) I performed a study of a larger group of cluster headache divided into episodic and chronic progressive groups using the optimised VBM method (unpublished data) and was unable to replicate the earlier findings and as yet there has been no microscopic confirmation of any brainstem morphological change in this patient group. Similarly, despite a region in the midbrain being reported to show ictal hyperactivity in migraine, further evidence for macro or microscopic structural change is lacking (Bahra *et al.* 2001; Matharu *et al.* 2003; Weiller *et al.* 1995). Postmortem data from a 16-year-old girl with FHM with ataxia linked to a CACNA1A mutation showed no detectable changes in the midbrain or pons but abnormalities of the Purkinje, molecular and granule cell layers of the cerebellar hemispheres and vermis (Bahra *et al.* 2001; Kors *et al.* 2001; Weiller *et al.* 1995). These findings further

support my VBM findings.

Conclusion

I have confirmed reports of cerebellar atrophy in a variant of FHM using VBM. Importantly, there is a clear genotype-phenotype correlation - these changes are only apparent in carriers of a CACNA1A mutation and not in those without the mutation even when displaying a similar phenotype. This emphasises that cerebellar atrophy is a function of the gene, not a consequence of the attacks. Despite the select patient group with a specific genotype and a more refined migraine phenotype, I did not detect any structural change in the brainstem of symptomatic family members.

The results from the last three chapters demonstrate that VBM is a useful tool to characterise the structural brain phenotypes of diseases with a known genetic basis. The versatile statistical framework of VBM allows genotype – phenotype correlations and deletion mapping strategies and demonstrates that the structural brain phenotype often matches the underlying genotype more closely than the clinical or cognitive phenotype. Importantly the structural changes often precede clinical symptoms allowing identification of groups of patients that would be suitable for clinical trials of disease modifying agents, offering an exciting example of the possibilities for translating genetic studies into clinical practice.

CHAPTER 13

CONCLUSIONS

General discussion

Summary of VBM studies

This thesis examines the clinical usefulness of voxel-based morphometry for characterising human brain structure within a standardised anatomical framework.

Chapter 1 addresses the importance of brain structure and suggests that it plays an integral role in neuroscience by providing the anatomical framework for functional brain mapping. The evolution of macroscopic structural characterisation is described from early crude descriptions to current in vivo morphometric characterisation of high-resolution MRI brain scans. Current morphometric methods, namely expertly performed region of interest-based metrics (regarded by many as the gold standard) are contrasted with the requirement for whole brain techniques that are not biased to particular brain regions or dependent upon the skill of the operator. The concept of computational neuroanatomy is introduced as a versatile method of analysis of structural images that is based upon the framework of statistical parametric mapping (SPM). The various types of computational morphometrics, namely the triad of voxel-based morphometry (VBM), deformation-based morphometry (DBM) and tensor-based morphometry (TBM) are defined. Finally the role of this method in clinical neuroradiological assessment is examined with reference to diagnosis, monitoring of disease processes before and after treatment and the characterisation and monitoring of brain structure for clinical research. Flaws in the current methods are revealed and discussed with particular emphasis on the need for techniques that can offer appraisal of brain structure in a holistic reproducible way whilst accommodating intrinsic physiological variability in neuroanatomy.

In order to ascertain the clinical usefulness of VBM the term "usefulness" needs to be better defined. The criteria I have used to characterise clinical usefulness include: 1) Reproducibility - can the analysis be performed on the same data set in

different laboratories to produce identical results? 2) Sensitivity - is the method sensitive to subtle neuroanatomical changes in a manner that is comparable or better than the best available gold standard? 3) Biologically plausible - does the method reveal structural alterations that biologically credible. In other words, with what degree of certainty can it be concluded that VBM detects changes that are not artefactual false positives? 4) Practical - can the analyses be performed within a practical time frame using readily available software? 5) Validity - what is the evidence for construct and face validity of the method?

Firstly VBM has been used in the analysis of a large normal data set to provide information about anatomical characteristics and variability (Chapters 3 and 4). By using large data sets, problems with the standard VBM methodology were revealed which prompted the development of a series of optimisations that are detailed and discussed in Chapter 2. The optimised method incorporates additional information derived from the deformation fields used to normalise brain images into standard anatomical space, incorporating a modulation step that enables voxel-wise detection of changes in grey or white matter **volume** (modulated data) or **concentration** (unmodulated data). The optimised method can be considered to be a hybrid between VBM and TBM analyses in the sense that factors describing voxel-wise volume distortions (Jacobian determinants) are incorporated to improve performance.

Chapter 2 also addresses the reproducibility and practicality of the optimised technique. A scan-rescan study demonstrates that tissue classification is highly reproducible and that the VBM analyses show no significant differences between first and second scans even when liberal thresholds are used. Since VBM is a fully automated technique, results for a given data set are identical between laboratories if the same analysis parameters are used. The technique is practical and the required software is freely available so that analyses can be performed on standard personal computers (preferably a minimum of a Pentium 3 processor and 256 RAM) or on Sun workstations. The time for pre-processing and analyses depends upon studied group sizes, complexity of statistical design matrices and computer speed. For a standard Pentium 3 processor and a group comparison of 10 patients and 10 controls pre-processing (optimised method) takes approximately 24 hours allowing for checking each pre-processing step and each analysis takes approximately 2 hours. In order to put this into context, expert delineation of each and every gyrus in a single brain MRI, if a willing neuroanatomist could be persuaded to do the task, would take many weeks.

Having established reproducibility, validity and practicality, the optimised method is then assessed for clinical usefulness in health and disease. In Chapter 3, VBM is used on a large normal database to characterise global and regional effects of the ageing process. VBM shows a linear pattern of global decline in grey matter, more pronounced in males than females, that corroborates a number of previous studies. In accordance with most previous reports, VBM shows little global change in the white matter compartment with age. Some researchers have suggested that white matter loss is accelerated in the later decades in life and it is possible I may be missing a non-linear trend in elderly subjects in their eighth and ninth decades owing to a paucity of subjects over 75 years of age in my study. Importantly, VBM reveals regionally specific effects of age over and above global change within grey and white matter and CSF compartments. Relatively faster loss of cortical volume occurs with age in the insula, superior parietal gyri, central sulci and cingulate sulci bilaterally. Areas exhibiting little or no age effect (relative preservation) include the amygdala, hippocampi and entorhinal cortex bilaterally. These are new findings and as such cannot be currently confirmed or refuted owing to the paucity of regionally specific ageing data in the literature. They will serve as a guide for further morphometric studies of ageing.

In Chapter 4, I use VBM to characterise asymmetries in human brain anatomy and the effects of sex and handedness on brain morphology. VBM confirms the well known lobar and Sylvian fissure asymmetries, in this way establishing face and construct validity, whilst expanding on regional information, in particular by revealing an interaction of sex and asymmetry in Heschl's gyrus. The well-recognised global difference in grey matter between males and females is confirmed and subtle regional sex differences in temporal lobe structure are revealed. Since the imaging literature on cerebral asymmetry and effects of sex is large and conflicting with a relative paucity of regionally specific details, these new findings cannot be presently definitively confirmed or refuted but correspondence with functional imaging findings adds to their plausibility. Such findings will need further scrutiny in future imaging studies. Despite the large group studied, VBM revealed no main effect of handedness on brain structure, even within the banks of the central sulcus in the vicinity of the hand area. This suggests that either VBM is insensitive to real but subtle macroscopic change (masked by interindividual variability in sulcal topography and difficulty in accurately classifying handedness leading to heterogeneous groups) or that functional

lateralisation is not accompanied by macroscopic structural change. Since the spatial normalisation implicit in VBM is relatively low dimensional and does not aim to accurately match cortical sulci, it seems likely that VBM in its current state of evolution is missing subtle structural change in this region. Further studies with carefully selected homogeneous handedness groups and accurate cortical mapping techniques or tensor-based morphometry will be needed to help resolve this question.

VBM is then been applied to a number of disease groups (Chapters 5-9) to test the usefulness of this technique in diffusely distributed cortical and deep grey matter pathology (e.g. Alzheimer's disease) and regionally specific lobar pathology (e.g. frontotemporal lobar degeneration of the semantic type)(Chapter 5). In these disease groups, VBM has been rigorously compared with the current best gold standard namely region of interest measurements performed by experts and also with post mortem data and PET studies of altered glucose metabolism. VBM confirms the most consistent previous imaging findings whilst expanding upon regionally specific effects in grey and white matter. In many regions, VBM is shown to be more sensitive than classical region of interest metrics (e.g. regional hippocampal volumes in Alzheimer's disease)

VBM is then applied to patients with temporal lobe epilepsy with established mesial temporal sclerosis (Chapter 6). Here VBM confirms the results of independent ROI analyses of ipsilateral hippocampal volume loss and shows additional structural differences outside the affected hippocampus that correlate with clinical outcome after temporal lobe surgery. Patients with an unfavourable postoperative outcome show additional extra hippocampal structural changes in ipsilateral orbitofrontal cortex whereas patients with a favourable postoperative outcome show greater volume loss within the ipsilateral hippocampus within the resection site. The importance of this observation is that VBM detects clinically relevant structural changes that were missed on visual appraisal and classical morphometrics.

Having demonstrated that VBM is a valid technique for characterising global and regional cortical and deep grey matter pathology in dementia, I examined a number of other diseases in which the structural correlates of known clinical and functional imaging features are less clear or previously unknown (migraine, schizophrenia and pure autonomic failure (PAF)). In schizophrenia (Chapter 8) and PAF (Chapter 9) VBM confirms the more consistent imaging findings in the literature whilst revealing new structural changes that match proven functional imaging deficits

in biologically plausible locations. In this setting, VBM offers new insights into the underlying pathological mechanisms of disease. On the other hand, in migraine (Chapter 7), VBM detects no structural changes in areas previously thought to be affected functionally (e.g. brain stem activity changes in functional imaging studies). I conclude that VBM does not always find structural changes in patients with neurological disease. This is not surprising because the method informs about macroscopic and mesoscopic levels of structural change but cannot give information about microscopic changes. Also, functional abnormalities are not necessarily associated with structural change. Finally, VBM may be insensitive to very subtle but real macroscopic/mesoscopic structural changes either due to lack of power (an inadequate group size) or limitations of the technique. Phenotypically migraine is a heterogeneous condition so there may be no reason to expect a consistent anatomical change in a group of patients.

In order to test this possibility, VBM was tested in a specific homogeneous phenotype characterised by a known uniform genotype, namely a pedigree with familial ataxic migraine (Chapter 12). VBM again showed no brainstem structural changes, but clearly revealed cerebellar atrophy in those genotype positive family members with an ataxic phenotype, but not in genotype negative kindred. This result provides compelling evidence that there is no macroscopic structural change within the brainstem of migraine sufferers.

In light of major advances in molecular mapping and new insights provided by the human genome project, genotype-phenotype correlations are now practically possible. Since VBM has been shown to be sensitive to alterations of brain structure that anticipate the onset of clinical symptoms in a number of diseases, it follows that the structural phenotype may match the genotype better. Furthermore the versatile statistical framework on which VBM is based allows application of gene deletion mapping strategy revealing. For example, in Turner syndrome a small locus on the short arm of the X chromosome is responsible for abnormally formed amygdalae in affected females who show abnormal fear conditioning (chapter 10). The implication of significance is that the deleted locus normally contains a putative gene (or genes) that code for amygdala development. Following successful mapping of the X chromosome genotype-phenotype relationship, I have explored genotype-phenotype relationships in genotyped pre-symptomatic subjects at risk for Huntington's disease (HD)(Chapter 11). In this case, use of VBM confirms structural alterations within the

caudate nucleus and other basal ganglia components in genotype positive subjects before the onset of HD symptoms. Furthermore the VBM-based study reveals new insights, including demonstration of asymmetric involvement of the caudate nucleus in genotype positive subjects that recapitulates the asymmetry of presentation of another basal ganglion degenerative disorder, Parkinson's disease. There is also involvement of neocortex which has previously been overlooked in region of interest based studies. This study demonstrates that VBM is suitable for characterisation and monitoring of structural change within genetically at risk pre-symptomatic subjects in clinical trials of potential new therapies.

Strengths of the VBM technique

VBM is a fully automated technique that is therefore by definition reproducible and not subject to inter- or intra- rater variability. It is practical in the sense that the software is freely available, methodological assistance is available on the SPM help line; it can be performed on most standard computers and is relatively time efficient (in comparison with operator dependent techniques). It can therefore be applied to large data sets. One of the greatest strengths of the technique is the ability to characterise brain structure in a holistic way. Each and every voxel in an image is tested so that hypotheses can be examined in a spatially unconstrained manner. Brain function can be accurately localised by mapping brain structure into a standardised anatomical framework, and comparisons can be made with complementary information, from cytoarchitectonics and receptor distributions, to provide a more complete appraisal of the implementation of neural mechanisms.

The image pre-processing steps in VBM allow brains of different size, shape and orientation to be registered into a standard space so that appropriate cross sectional and longitudinal comparisons are feasible. The versatile statistical components of SPM incorporate voxel-wise estimates of variance and allow structure to be correlated with effects of interest (such as disease severity scores) whilst accommodating confounding factors (such as age and sex and global volumes). An additional advantage is that the triad of computational neuroanatomy techniques are complementary. VBM informs about voxel-wise differences in grey (or white matter) volume and concentration. DBM informs about global shape differences. TBM informs about regionally specific shape differences with high precision. The optimised method of VBM (incorporating the modulation step and thus information from the deformation fields) is a hybrid

between VBM and TBM. When high dimensional deformation warps can be practically utilised for large data sets, currently it is too computer intensive, then TBM will be a particularly interesting tool.

Weaknesses of the VBM technique

Many of the strengths of the technique also have down sides. VBM comprises a series of fully automated operations. None of these is perfect.

Spatial normalisation.

The spatial normalisation step uses relatively low dimensional warps to match global brain characteristics such as size and shape but does not aim to accurately match each and every gyrus. Since the human brain is characteristically variable, both between individuals and between brain regions in the same individual, it follows that individual gyri and sulci are not precisely matched. VBM aims to detect regionally specific differences in brain structure that remain after spatial normalisation, using a smoothing kernel to accommodate the imperfect gyral matching. The spatial localisation of VBM is thus limited to the chosen smoothing kernel which for most VBM applications is 10-12mm. Thus any local maximum relates not to the specific voxel coordinates but to the surrounding region defined by the smoothing kernel. In practical terms this means that a maximum in the amygdala may allow inferences about structural change within the amygdala and adjacent portion of entorhinal cortex and/or hippocampus. Smoothing kernels also render the data more normally distributed for the parametric statistical tests. Since group comparisons are, and have been show to be, robust to violations of normality even without smoothing kernels, there is the temptation to do away with smoothing kernels and enhance spatial localisation of inferences. It is important to resist this temptation since the spatial normalisation in VBM produces imperfect gyral matching. Once high deformation warps can be shown to produce accurate and reproducible gyral and sulcal matching, then VBM (with the modulation step) and TBM will be used without smoothing to inform about local differences with high-resolution spatial localisation.

Diseased brains provide a challenge for spatial normalisation. The linear and non-linear registration algorithms aim to map each brain to the template. If the patient brain differs substantially from the template brain there is potential for over fitting of the data. For this reason customised disease, age and sex specific templates are

usefully created and regularisation is adjusted. The VBM study of Alzheimer's disease and semantic dementia shows that spatial normalisation is accurate even for severely atrophic brains (diffuse and regional) when using customised grey and white matter templates. Brain scans with focal complex lesions such as tumours and haemorrhagic infarcts may not be reliably normalised and different additional strategies are needed in these cases (see Indications and cautions below). A number of systematic differences between patients and controls can potentially affect registration, such as systematic differences in grey and white matter intensity or motion artefact. These produce systematic differences in registration accuracy between groups. Such differences in spatial normalisation accuracy have not been formally studied, but it is important to note that these will not produce bias or false positives *per se*. Any differences detected by VBM will reflect systematic differences in anatomy between the groups, but caution about local inferences will need to be observed.

Segmentation

The segmentation step partitions the brain into grey and white matter, CSF and other compartments based upon an *a priori* knowledge of the spatial and signal distribution of voxels. Segmentation is not perfect and therefore some voxels will be misclassified. The optimised VBM methods automatically removes non brain voxels, so misclassification in normal brains is minimal. When the composition and resultant brain tissue signal is altered, as in disease processes or at the extremes of age, then classification of voxels becomes less precise, as can be shown around the hippocampus of patients with Alzheimer's disease and semantic dementia (Chapter 5). Similarly in disease processes with multiple focal lesions in variable locations, such as multiple sclerosis or small vessel ischaemia, a template (even one customised to the disease group) will not be appropriate for a group of patients and thus segmentation will be unreliable.

Indications and cautions

VBM was originally designed to characterise brain structural changes between groups of subjects. For group studies the VBM statistical framework is robust to violations of normality (and thus false positives). Some researchers have been using VBM to detect structural changes within single subjects against a group of controls. Strictly speaking, such study designs are unbalanced and may be vulnerable to false

positives. In these designs large smoothing kernels (12mm) are essential (Salmond *et al.* 2002). This concern should however be balanced with common radiological practice where an individual scan is reported based upon a radiologist's personal perception of what constitutes a normal range. This method is equally unbalanced, which explains why visual inspection of a single scan (for example MR of an elderly subject to exclude atrophy) is often unreliable. VBM will probably prove more reliable than simple visual appraisal for the assessment of atrophy in single subjects compared to a large local age matched control group and customised templates (see Clinical applications below).

VBM is an automated method with a number of pre processing steps. Potential processing errors may enter at each stage and impact on the interpretation of the statistical output. For this reason, images should be evaluated after each processing step for potential errors of normalisation and segmentation. Though an automated technique, VBM is sufficiently complex that it should be preferably used by operators who understand the method and have a good working knowledge of MR and neuroanatomy.

As noted above, spatial normalisation aims to map MRI scans into standard stereotaxic space. For normal scans and those with distributed pathology, the spatial normalisation provides accurate global matching. Where there is marked focal pathology with complex signal changes, for example a large complex tumour or an infarct, there will be problems as spatial normalisation attempts to match the abnormal region to a corresponding normal region on the template. This will generally result in over fitting of the data and marked local distortions may occur. For these reasons, a different strategy is needed such as masking out the lesion zone manually or semi automatically using customised software such as MRIcro (http://www.psychology.Nottingham.ac.uk/staff/cr1/mricro.html). This software allows spatial normalised in situations such as those described without introducing artefacts from complex focal lesions. In general, VBM should thus be avoided or used with caution (with careful attention to each preprocessing step) in subject groups with complex focal lesions.

Clinical implications

This thesis demonstrates that VBM is a reproducible, sensitive and practical

tool for the characterisation of brain morphology. The results are biologically plausible and valid in the sense that they confirm the most consistent findings from histopathological and classical morphometric studies and correspond to functional imaging studies.

VBM is becoming an established tool in the research domain in cross sectional studies of healthy and diseased populations. VBM is increasingly being used to examine the structural brain correlates of diseases with known functional deficits but previously occult or unclear morphological alterations. I have not yet formally evaluated VBM in longitudinal studies, but preliminary data show that this is a robust tool for evaluation of cerebral changes over 1-2 year time scales (within the time window of a MRI scanner). It is likely that VBM and similar whole brain techniques will be used as surrogate markers for disease progression in clinical trials of disease modifying agents

The role for VBM in clinical neuroradiology has yet to be established. Potential areas where the technique could be an asset to a neuroradiology department include assisting in diagnosis and clinical follow up of single cases. In certain instances diagnosis of pathology may be difficult owing to a wide overlap with normality. A typical example is the differentiation of atrophy from normal involution in elderly subjects on a single brain scan. Typical radiological appraisal depends upon the experience of the neuroradiologist and is likely to yield false positive or false negative diagnoses as well as intra-rater variability. A simple VBM analysis comparing the single subject scan to a group of local age and sex matched subjects from a local database will provide objective evidence of whether the scan in question is significantly different from the local norm. A second possibility would be to use core components of the VBM framework to co-register a single subject's scans to a local age and sex-matched template and to assess and interpret a deformation image.

These strategies may also prove useful for pattern recognition in groups of diseases with clinical and imaging overlap. For example, atypical Parkinsonian syndromes such as multiple system atrophy (MSA), progressive supranuclear palsy (PSP) and idiopathic Parkinson's disease may be difficult to differentiate. By creating disease specific templates, it may be possible to sub classify patients more accurately. A VBM study is currently in progress to examine this role.

In order to assist practicality in a busy neuroradiology department, these image analysis algorithms implicit in VBM could potentially be incorporated into the MR

scanner software so that the results are made available at the time of reporting. The most obvious advantage of using such post-processing methods is their suitability for longitudinal evaluation of cases since the scans are in a standard anatomical framework. Furthermore longitudinal evaluation of a single patient will prevent subtle dynamic changes from being masked by interindividual variation. In this particular scenario, VBM is not intended to replace an experienced neuroradiologist, but rather to be a useful tool at his/her disposal and discretion.

Final conclusions

I have shown voxel-based morphometry to be a practical, reproducible and sensitive tool for the characterisation of human brain structure in cross sectional or longitudinal studies. The validity and biological plausibility of VBM detected results have been assessed in the context of the best currently available methods, and in this sense VBM replicates the most consistent and established reported results while offering new regionally specific detail, which in most cases corresponds with functional imaging data. By employing the same anatomical and statistical framework, direct correlations of structure and function are possible. With further improvements in computational power, more accurate mapping of cortical gyri and sulci will facilitate the detection of more subtle structural differences in brain morphology in health and disease. Importantly VBM is a fully automated reproducible whole brain technique that avoids the subjectivity of classical ROI morphometrics and can be practically applied to large study groups. The software is freely available and so the technique can now be applied practically not only within research units, but also within the clinical domain. I therefore conclude that VBM is indeed a useful tool for characterising and mapping brain structure in health and disease.

REFERENCE LIST

Abell F, Krams M, Ashburner J *et al.* The neuroanatomy of autism: a voxel-based whole brain analysis of structural scans. Neuroreport 1999; 10: 1647-51.

Adolphs R, Tranel D, Hamann S *et al.* Recognition of facial emotion in nine individuals with bilateral amygdala damage. Neuropsychologia 1999; 37: 1111-7.

Alexander GE, DeLong MR. Parallel organisation of functionally segregated circuits linking basal ganglia and cortex. Annual Reviews of Neuroscience 1986; 9: 357-381.

Allen LS, Gorski RA. Sexual dimorphism of the anterior commissure and massa intermedia of the human brain. J Comp Neurol 1991; 312: 97-104.

Allen LS, Gorski RA. Sexual orientation and the size of the anterior commissure in the human brain. Proc Natl Acad Sci U S A 1992; 89: 7199-202.

Amaral DG. The primate amygdala and the neurobiology of social behavior: implications for understanding social anxiety. Biol Psychiatry 2002; 51: 11-17.

Amunts K, Jancke L, Mohlberg H, Steinmetz H, Zilles K. Interhemispheric asymmetry of the human motor cortex related to handedness and gender. Neuropsychologia 2000; 38: 304-12.

Amunts K, Schlaug G, Schleicher A *et al.* Asymmetry in the human motor cortex and handedness. Neuroimage 1996; 4: 216-22.

Amunts K, Schmidt-Passos F, Schleicher A, Zilles K. Postnatal development of interhemispheric asymmetry in the cytoarchitecture of human area 4. Anat Embryol (Berl) 1997; 196: 393-402.

Andreasen NC. The role of the thalamus in schizophrenia. Can.J Psychiatry 1997; 42: 27-33.

Andreasen NC, Arndt S, Swayze V *et al.* Thalamic abnormalities in schizophrenia visualized through magnetic resonance image averaging. Science 1994; 266: 294-298.

Andreasen NC, O'Leary DS, Cizadlo T *et al.* Schizophrenia and cognitive dysmetria: a positron-emission tomography study of dysfunctional prefrontal-thalamic-cerebellar circuitry. Proc Natl Acad Sci U S A 1996; 93: 9985-9990.

Andreasen NC, Paradiso S, O'Leary DS. "Cognitive dysmetria" as an integrative theory of schizophrenia: a dysfunction in cortical-subcortical-cerebellar circuitry? Schizophr.Bull. 1998; 24: 203-218.

Andreasen NC, Swayze V, O'Leary DS *et al.* Abnormalities in midline attentional circuitry in schizophrenia: evidence from magnetic resonance and positron emission tomography. Eur.Neuropsychopharmacol. 1995; 5 Suppl: 37-41.

Annett M. A classification of hand preference by association analysis. Br J Psychol 1970; 61: 303-21.

Annett M. Handedness and the cerebral representation of speech. Ann Hum Biol 1976; 3: 317-28.

Ansari KA, Loch J. Decreased myelin basic protein content of the aged human brain. Neurology 1975; 25: 1045-1050.

Arciniegas D, Rojas DC, Teale P, Sheeder J, Sandberg E, Reite M. The thalamus and the schizophrenia phenotype: failure to replicate reduced volume. Biol Psychiatry 1999; 45: 1329-1335.

Aronin N, Chase K, Young C *et al.* CAG expansion affects the expression of mutant huntingtin in the Huntington's Disease brain. Neuron 1995; 15: 1193-1201.

Ashburner J, Andersson JL, Friston KJ. Image registration using a symmetric prior-in three dimensions. Hum Brain Mapp 2000; 9: 212-25.

Ashburner J, Friston K. Multimodal image coregistration and partitioning-a unified framework. Neuroimage 1997; 6: 209-17.

Ashburner J, Friston KJ. Nonlinear spatial normalization using basis functions. Hum Brain Mapp 1999; 7: 254-66.

Ashburner J, Friston KJ. Voxel-based morphometry-the methods. Neuroimage 2000; 11: 805-21.

Ashburner J, Friston KJ. Why voxel-based morphometry should be used. Neuroimage 2001; 14: 1238-1243.

Ashburner J, Hutton C, Frackowiak R, Johnsrude I, Price C, Friston K. Identifying global anatomical differences: deformation-based morphometry. Hum Brain Mapp 1998; 6: 348-57.

Ashburner J, Neelin P, Collins DL, Evans A, Friston K. Incorporating prior knowledge into image registration. Neuroimage 1997; 6: 344-52.

Astrup J, Siesjo BK, Symon L. Thresholds in cerebral ischaemia - the ischaemic penumbra. Stroke 1981; 12: 723-725.

Aylward EH, Andreson NB, Bylsma FW *et al.* Frontal lobe volume in patients with Huntington's disease. Neurology 1998; 50: 252-258.

Aylward EH, Brandt J, Codori AM *et al.* Reduced basal ganglia volume associated with the gene for Huntington's disease in asymptomatic at-risk persons. Neurology 1994; 44: 823-828.

Aylward EH, Li Q, Stine OC *et al.* Longitudinal change in basal ganglia volume in patients with Huntington's disease. Neurology 1997; 48: 394-399.

Aziz Q, Thompson DG, Ng VW *et al.* Cortical processing of human somatic and visceral sensation. J Neurosci 2000; 20: 2657-2663.

Bahra A, Matharu MS, Buchel C, Frackowiak RSJ, Goadsby PJ. Brainstem activation specific to migraine headache. Lancet 2001; 357: 1016-1017.

Barch DM, Carter CS, Braver TS *et al.* Selective deficits in prefrontal cortex function in medication-naive patients with schizophrenia. Arch.Gen.Psychiatry 2001; 58: 280-288.

Baron-Cohen S, Jolliffe T, Mortimore C, Robertson M. Another advanced test of theory of mind: evidence from very high functioning adults with autism or asperger syndrome. J Child Psychol.Psychiatry 1997; 38: 813-822.

Baron JC, Chetelat G, Desgranges B *et al.* In vivo mapping of gray matter loss with voxel-based morphometry in mild Alzheimer's disease. Neuroimage 2001; 14: 298-309.

Bear D, Schiff D, Saver J, Greenberg M, Freeman R. Quantitative analysis of cerebral asymmetries. Fronto-occipital correlation, sexual dimorphism and association with handedness. Arch.Neurol 1986; 43: 598-603.

Bechara A, Damasio A, Tranel D, Andersson JL. Dissociation of working memory from dicision making within the human prefrontal cortex. J Neurosci 1998; 18: 428-437.

Becher MW, Kotzuk JA, Sharp AH *et al.* Intranuclear neuronal inclusions in HUntington's Disease and dentatorubral and pallidoluysian atrophy: correlation between the density of inclusions and IT15 CAG triplet repeat length. Neurobiology of Disease 1998; 4: 387-397.

Berkovic SF, Andermann F, Olivier A *et al.* Hippocampal sclerosis in temporal lobe epilepsy demonstrated by magnetic resonance imaging. Ann Neurol 1991; 29: 175-182.

Berkovic SF, McIntosh AM, Kalnins RM *et al.* Preoperative MRI predicts outcome of temporal lobectomy: an actuarial analysis. Neurology 1995; 45: 1358-1363.

Betancur C, Corbex M, Spielewoy C *et al.* Serotonin transporter gene polymorphisms and hyperserotonemia in autistic disorder. Mol Psychiatry 2002; 7: 67-71.

Bishop KM, Wahlsten D. Sex differences in the human corpus callosum: myth or reality? Neurosci Biobehav.Rev 1997; 21: 581-601.

Blaschke RJ, Rappold GA. SHOX in short stature syndromes. Horm.Res 2001; 55 Suppl 1: 21-23.

Bloch F, Hansen W, Packard M. The nuclear induction experiment. Physics Review 2003; 70: 474-485.

Bohnen NI, Koeppe RA, Meyer MD *et al.* Decreased striatal monoaminergic terminal in Huntington's disease. Neurology 2000; 54: 1753-1759.

Bookstein FL. Landmark methods for forms without landmarks: morphometrics of group differences in outline shape. Med Image Anal. 1997; 1: 225-243.

Boumil RM, Lee JT. Forty years of decoding the silence in X-chromosome inactivation. Hum Mol Genet 2001; 10: 2225-2232.

Braak H, Braak E. Alzheimer's disease: striatal amyloid deposits and neurofibrillary changes. J Neuropathol Exp Neurol 1990; 49: 215-24.

Braak H, Braak E. Neuropathological stageing of Alzheimer-related changes. Acta Neuropathol (Berl) 1991; 82: 239-59.

Braak H, Braak E. Evolution of the neuropathology of Alzheimer's disease. Acta Neurol Scand Suppl 1996; 165: 3-12.

Braak H, Braak E, Bohl J, Bratzke H. Evolution of Alzheimer's disease related cortical lesions. J Neural Transm Suppl 1998; 54: 97-106.

Brinkman RR, Mezei MM, Theilmann J, Almqvist E, Hayden MR. The likelihood of being affected with Huntington's disease by a particular age. Am J Hum Genet 1997; 60: 1201-1210.

Brodmann, K. Vergleichende lokalisationslehre der grosshirnrinde in ihren prinzipien dargestellt auf grund des zellenbaues. Smith Gordon. 1909. London.
Ref Type: Serial (Book,Monograph)

Brody H. The aging brain. Acta Neurol Scand.Suppl 1992; 137: 40-44.

Brothers L. Friday's Footprint. Oxford: Diane Publisjing Co., 1997.

Buchel C, Wise RJ, Mummery CJ, Poline JB, Friston KJ. Nonlinear regression in parametric activation studies. Neuroimage 1996; 4: 60-6.

Buchsbaum MS, Someya T, Teng CY *et al.* PET and MRI of the thalamus in never-medicated patients with schizophrenia. Am J Psychiatry 1996; 153: 191-199.

Bugiani O, Salvarani S, Perdelli F, Mancardi GL, Leonardi A. Nerve cell loss with aging in the putamen. Eur.Neurol 1978; 17: 286-291.

Butcher KS, Cechetto DF. Autonomic responses of the insular cortex in hypertensive and normotensive rats. Am J Physiol 1995; 268: R214-R222.

Byne W, Bleier R, Houston L. Variations in human corpus callosum do not predict gender: a study using magnetic resonance imaging. Behav Neurosci 1988; 102: 222-7.

Byne W, Buchsbaum MS, Kemether E *et al.* Magnetic resonance imaging of the thalamic mediodorsal nucleus and pulvinar in schizophrenia and schizotypal personality disorder. Arch.Gen.Psychiatry 2001; 58: 133-140.

Byne W, Buchsbaum MS, Mattiace LA *et al.* Postmortem assessment of thalamic nuclear volumes in subjects with schizophrenia. Am J Psychiatry 2002; 159: 59-65.

Calabresi P, Centonze D, Bernardi G. Cellular factors controlling neuronal vulnerability in the brain. Neurology 20032; 55: 1249-1255.

Calder AJ, Keane J, Manes F, Antoun N, Young AW. Impaired recognition and experience of disgust following brain injury. Nat Neurosci 2000; 3: 1077-1078.

Callicott JH, Bertolino A, Mattay VS *et al.* Physiological dysfunction of the dorsolateral prefrontal cortex in schizophrenia revisited. Cereb Cortex 2000; 10: 1078-1092.

Campbell R, Elgar K, Kuntsi J *et al.* The classification of 'fear' from faces is associated with face recognition skill in women. Neuropsychologia 2002; 40: 575-584.

Canli T, Desmond JE, Zhao Z, Gabrieli JD. Sex differences in the neural basis of emotional memories. Proc Natl Acad Sci U S A 2002; 99: 10789-10794.

Carrel L, Cottle AA, Goglin KC, Willard HF. A first-generation X-inactivation profile of the human X chromosome. Proc Natl Acad Sci U S A 1999; 96: 14440-14444.

Carrel L, Willard HF. Heterogeneous gene expression from the inactive X chromosome: an X-linked gene that escapes X inactivation in some human cell lines but is inactivated in others. Proc Natl Acad Sci U S A 1999; 96: 7364-7369.

Caspi A, McClay J, Moffitt TE *et al.* Role of genotype in the cycle of violence in maltreated children. Science 2002; 297: 851-854.

Caviness VS, Kennedy DN, Richelme C, Rademacher J, Filipek PA. The human brain age 7-11 years: a volumetric analysis based on magnetic resonance images. Cereb Cortex 1996; 6: 726-36.

Chan D, Fox NC, Scahill RI *et al.* Patterns of temporal lobe atrophy in semantic dementia and Alzheimer's disease. Ann Neurol 2001; 49: 433-432.

Chen ZY, Powell JF, Hsu YP, Breakefield XO, Craig IW. Organization of the human monoamine oxidase genes and long-range physical mapping around them. Genomics 1992; 14: 75-82.

Chetelat G, Desgranges B, De La Sayette V, Viader F, Eustache F, Baron JC. Mapping gray matter loss with voxel-based morphometry in mild cognitive impairment. Neuroreport. 2002 Oct 28;13(15):1939-43.

Chiu HC, Damasio AR. Human cerebral asymmetries evaluated by computed tomography. J Neurol Neurosurg Psychiatry 1980; 43: 873-878.

Christensen GE, Joshi SC, Miller MI. Volumetric transformation of brain anatomy. IEEE Trans Med Imaging 1997; 16: 864-877.

Clark CV, Ewing DJ. Ocular autonomic function in progressive autonomic failure. Doc.Ophthalmol. 1988; 70: 309-321.

Clarke S, Miklossy J. Occipital cortex in man: organization of callosal connections, related myelo- and cytoarchitecture, and putative boundaries of functional visual areas. J Comp Neurol 1990; 298: 188-214.

Coffey CE, Lucke JF, Saxton JA *et al.* Sex differences in brain aging: a quantitative magnetic resonance imaging study. Arch Neurol 1998; 55: 169-79.

Connolly JD, Goodale MA, Desouza JF, Menon RS, Vilis.T. A comparison of frontoparietal fMRI activation during anti-saccades and anti-pointing. J Neurophysiol 2000; 84: 1645-1655.

Constant D, Ruther H. Sexual dimorphism in the human corpus callosum? A comparison of methodologies. Brain Res 1996; 727: 99-106.

Cook MJ. Mesial temporal sclerosis and volumetric investigations. Acta Neurol Scand Suppl 1994; 152: 109-14.

Corfield DR, Fink GR, Ramsay SC *et al.* Evidence for limbic system activation during CO2-stimulated breathing in man. J Physiol 1995; 488 (Pt 1): 77-84.

Cowell PE, Turetsky BI, Gur RC, Grossman RI, Shtasel DL, Gur RE. Sex differences in aging of the human frontal and temporal lobes. J Neurosci 1994; 14: 4748-55.

Craig AD, Chen K, Bandy D, Reiman EM. Thermosensory activation of insular cortex. Nat Neurosci 2000; 3: 184-190.

Creswell CS, Skuse DH. Autism in association with Turner syndrome: genetic implications for male vulnerability to pervasive developmental disorders. Neurocase 1999; 5: 101-108.

Critchley HD, Corfield DR, Chandler MP, Mathias CJ, Dolan RJ. Cerebral correlates of autonomic cardiovascular arousal: a functional neuroimaging investigation in humans. J Physiol 2000a; 523 Pt 1: 259-270.

Critchley HD, Elliott R, Mathias CJ, Dolan RJ. Neural activity relating to generation and representation of galvanic skin conductance responses: a functional magnetic resonance imaging study. J Neurosci 2000b; 20: 3033-3040.

Critchley HD, Mathias CJ, Dolan RJ. Neural activity in the human brain relating to uncertainty and arousal during anticipation. Neuron 2001a; 29: 537-545.

Critchley HD, Mathias CJ, Dolan RJ. Neuroanatomical basis for first- and second-order representations of bodily states. Nat Neurosci 2001b; 4: 207-212.

Critchley HD, Mathias CJ, Dolan RJ. Fear conditioning in humans: the influence of awareness and autonomic arousal on functional neuroanatomy. Neuron 2002; 33: 653-663.

Critchley HD, Melmed RN, Featherstone E, Mathias CJ, Dolan RJ. Brain activity during biofeedback relaxation: a functional neuroimaging investigation. Brain 2001c; 124: 1003-1012.

Cunningham D. Contribution to the surface anatomy of the cerebral hemispheres. Royal Irish Academy.Dublin. 1892.

Damasio AR. The feeling of what happens: Body and emotion in the making of consciousness. New York: Harcourt Brace, 1999.

Dasari M, Friedman L, Jesberger J *et al.* A magnetic resonance imaging study of thalamic area in adolescent patients with either schizophrenia or bipolar disorder as compared to healthy controls. Psychiatry Res 1999; 91: 155-162.

Davatzikos C. Spatial normalization of 3D brain images using deformable models. J Comput Assist Tomogr 1996; 20: 656-665.

Davatzikos C. Spatial transformation and registration of brain images using elastically deformable models. Comput Vis.Image Underst. 1997a; 66: 207-222.

Davatzikos C. Spatial transformation and registration of brain images using elastically deformable models. Comput Vis.Image Underst. 1997b; 66: 207-222.

Davatzikos C, Genc A, Xu D, Resnick SM. Voxel-based morphometry using the RAVENS maps: methods and validation using simulated longitudinal atrophy. Neuroimage 2001a; 14: 1361-1369.

Davatzikos C, Resnick SM. Sex differences in anatomic measures of interhemispheric connectivity: correlations with cognition in women but not men. Cereb Cortex 1998; 8: 635-40.

Davatzikos C, Shen D, Mohamed A, Kyriacou SK. A framework for predictive modeling of anatomical deformations. IEEE Trans Med Imaging 2001b; 20: 836-843.

Davies S, Bishop D, Manstead AS, Tantam D. Face perception in children with autism and Asperger's syndrome. J Child Psychol.Psychiatry 1994; 35: 1033-1057.

Davies SW, Turmaine M, Cozens BA *et al.* Formation of neuronal intranuclear inclusions underlies the neurological dysfunction in mice transgenic for the HD mutation. Cell 1997; 90: 537-548.

Davis MH, Khotanzad A, Flamig DP, Harms SE. A physics-based coordinate transformation for 3-D image matching. IEEE Trans Med Imaging 1997; 16: 317-328.

De la Monte SM, Vonsattel JP, Richardson EP. Morphometric demonstration of atrophic changes in the cerebral cortex, white matter and neostriatum in Huntington's disease. J Neuropathol Exp Neurol 1988; 47: 516-525.

de Leon MJ, Convit A, DeSanti S *et al.* The hippocampus in aging and Alzheimer's disease. Neuroimaging Clin N Am 1995; 5: 1-17.

de Leon MJ, Golomb J, Convit A, DeSanti S, McRae TD, George AE. Measurement of medial temporal lobe atrophy in diagnosis of Alzheimer's disease. Lancet 1993; 341: 125-6.

DeCarli C, Hatta J, Fazilat S, Fazilat S, Gaillard WD, Theodore WH. Extratemporal atrophy in patients with complex partial seizures of left temporal origin. Ann Neurol 1998; 43: 41-45.

Deichmann R, Good CD, Josephs O, Ashburner J, Turner R. Optimization of 3-D MP-RAGE sequences for structural brain imaging. Neuroimage 2000a; 12: 112-27.

Deichmann R, Good CD, Turner R. RF inhomogeneity compensation in structural brain imaging. Magn Reson.Med 2002b; 47: 398-402.

Dekaban AS. Changes in brain weights during the span of human life: relation of brain weights to body heights and body weights. Ann Neurol 1978; 4: 345-356.

Delacourte A, David JP, Sergeant N *et al.* The biochemical pathway of neurofibrillary degeneration in aging and Alzheimer's disease. Neurology 1999; 52: 1158-65.

DeLeo JM, Schwartz M, Creasey H, Rapoport SI. Computer-assisted categorization of brain computerized tomography pixels into cerebrospinal fluid, white matter, and gray matter. Comput Biomed Res 1985; 18: 79-88.

Den Heijer JC, Bollen WLEM, Reulen JPH *et al* . Autonomic nervous function in Huntington's disease. Arch Neurol 1988; 45: 312.

Desgranges B, Baron JC, de la Sayette V *et al.* The neural substrates of memory systems impairment in Alzheimer's disease. A PET study of resting brain glucose utilization. Brain 1998; 121: 611-31.

DiFiglia M, Sapp E, Chase KO *et al.* Aggregation of huntingtin in neuronal intranuclear inclusions and dystrophic neurites in brain. Science 1997; 277: 1990-1993.

Diforio D, Walker EF, Kestler LP. Executive functions in adolescents with schizotypal personality disorder. Schizophr.Res 2000; 42: 125-134.

Disteche CM. Escapees on the X chromosome. Proc Natl Acad Sci U S A 1999; 96: 14180-14182.

Dolan RJ, Bench CJ, Liddle PF *et al.* Dorsolateral prefrontal cortex dysfunction in the major psychoses; symptom or disease specificity? J Neurol Neurosurg Psychiatry 1993; 56: 1290-1294.

Domaradzka-Pytel B, Ludkiewicz B, Morys J, Wisniewski HM. Expression and distribution of various antigens of developing microglial cells in the rat telencephalon. J Hirnforsch 1999; 39: 283-91.

Dove LS, Abbott LC, Griffit WH. Whole-cell and single channel analysis of P-type calcium currents in cerebellar purkinje cells of leaner mutant mice. J Neurosci 1998; 18: 7687-7699.

Dreifuss S, Vingerhoets FJ, Lazeyras F *et al* . Volumetric measurements of subcortical nuclei in patients with temporal lobe epilepsy. Neurology 2001; 57: 1636-1641.

Ducros A, Denier C, Joutel A, et al. The clinical spectrum of familial hemiplegic migraine associated with mutations in a neuronal calcium channel. N Engl J Med 2001; 345: 17-24.

Ducros A, Joutel A, Vahedi K *et al.* Mapping of a second locus for familial hemiplegic migraine to 1q21-q23 and evidence of further heterogeneity. Ann Neurol 1997; 42: 885-890.

Duvernoy HM. The Human Brain: Surface, blood supply and three-dimensional sectional anatomy. Second edition. Wien New York: Springer-Verlag, 1999.

Duyao M, Ambrose C, Myers R *et al.* Trinucleotide repeat length instability and age of onset in Huntington's disease. Nat Genet 21993; 4: 387-392.

Ekman, P. Pictures of Facial Affect. Consulting Psycholgists Press . 1976. Palo Alto. Ref Type: Newspaper

Elgar K, Campbell R, Skuse D. Are you looking at me? Accuracy in processing line-of-sight in Turner syndrome. Proc R.Soc.Lond B Biol Sci 2002; 269: 2415-2422.

Elias LJ, Bryden MP, Bulman-Fleming MB. Footedness is a better predictor than is handedness of emotional lateralization. Neuropsychologia 1998; 36: 37-43.

Elliot MA, Peroutka SJ, Welch S, May EF. Familial hemiplegic migraine, nystagmus and cerebellar atrophy. Ann Neurol 1996; 39: 100-106.

Engel JJ, Van Ness P, Rasmussen T, Ojemann L. Outcome with respect to seizures. In: Engel JJ, editor. Surgical treatment of the epilepsies. New York: Raven, 1993: 609-21.

Evans A, Collins D, Mills S, Brown E, Kelly P, Peters T. 3D statistical neuroanatomical models from 305 MRI volumes. IEEE-Nuclear science symposium and medical imaging conference 1993; 1813-1817.

Falzi G, Perrone P, Vignolo LA. Right-left asymmetry in anterior speech region. Arch Neurol 1982; 39: 239-40.

Fannon D, Chitnis X, Doku V *et al.* Features of structural brain abnormality detected in first-episode psychosis. Am J Psychiatry 2000; 157: 1829-1834.

Fein G, Van Dyke C, Davenport L *et al.* Preservation of normal cognitive functioning in elderly subjects with extensive white-matter lesions of long duration. Arch.Gen.Psychiatry 1990; 47: 220-223.

Ferrari MD. Migraine. Lancet 1998; 351: 1043-1051.

Filipek PA, Richelme C, Kennedy DN, Caviness VS, Jr. The young adult human brain: an MRI-based morphometric analysis. Cereb Cortex 1994; 4: 344-60.

Fish DR, Gloor P, Quesney FL, Olivier A. Clinical responses to electrical brain stimulation of the temporal and frontal lobes in patients with epilepsy. Pathophysiological implications. Brain 1993; 116 (Pt 2): 397-414.

Fitzsimons RB, Wolfenden WH. Migraine coma-meningitic migraine with cerebral edema associated with a new form of autosomal dominant cerebellar-ataxia. Brain 1985; 108: 555-557.

Flood D and Coleman P. Neuron numbers and size in aging brain: comparison of human, monkey and rodent data. Neurobiol Aging 1988; 9: 453-463.

Florian CL, Williams SR, Bhakoo KK, Noble MD. Regional and developmental variations in metabolite concentration in the rat brain and eye: a study using 1H NMR spectroscopy and high performance liquid chromatography. Neurochem Res 1996; 21: 1065-74.

Folstein MF, Folstein SE, McHugh PR. "Mini-mental state". A practical method for grading the cognitive state of patients for the clinician. J Psychiatr Res 1975; 12: 189-98.

Folstein SE, Rosen-Sheidley B. Genetics of autism: complex aetiology for a heterogeneous disorder. Nat Rev Genet 2001; 2: 943-955.

Foong J, Symms MR, Barker GJ *et al.* Neuropathological abnormalities in schizophrenia: evidence from magnetization transfer imaging. Brain 2001; 124: 882-892.

Forstl H, Zerfass R, Geiger-Kabisch C, Sattel H, Besthorn C, Hentschel F. Brain atrophy in normal ageing and Alzheimer's disease. Volumetric discrimination and clinical correlations. Br J Psychiatry 1995; 167: 739-46.

Foster NL, Chase TN, Fedio P, Petronas NJ, Brooks RA, Di Chiro G. Alzheimer's disease: focal cortical changes shsowed by positron emission tomography. Neurology 1983; 33: 961-965.

Foundas AL, Eure KF, Luevano LF, Weinberger DR. MRI asymmetries of Broca's area: the pars triangularis and pars opercularis. Brain Lang 1998a; 64: 282-96.

Foundas AL, Eure KF, Luevano LF, Weinberger DR. MRI asymmetries of Broca's area: the pars triangularis and pars opercularis. Brain Lang 1998b; 64: 282-296.

Foundas AL, Faulhaber JR, Kulynych JJ, Browning CA, Weinberger DR. Hemispheric and sex-linked differences in Sylvian fissure morphology: a quantitative approach using volumetric magnetic resonance imaging. Neuropsychiatry Neuropsychol Behav Neurol 1999; 12: 1-10.

Foundas AL, Leonard CM, Gilmore RL, Fennell EB, Heilman KM. Pars triangularis asymmetry and language dominance. Proc Natl Acad Sci U S A 1996; 93: 719-22.

Foundas AL, Leonard CM, Heilman KM. Morphologic cerebral asymmetries and handedness. The pars triangularis and planum temporale [see comments]. Arch Neurol 1995; 52: 501-8.

Fox NC, Cousens S, Scahill R, Harvey RJ, Rossor MN. Using serial registered brain magnetic resonance imaging to measure disease progression in Alzheimer disease: power calculations and estimates of sample size to detect treatment effects. Arch Neurol 2000; 57: 339-44.

Fox NC, Freeborough PA. Brain atrophy progression measured from registered serial MRI: validation and application to Alzheimer's disease. J Magn Reson Imaging 1997; 7: 1069-75.

Fox NC, Freeborough PA, Rossor MN. Visualisation and quantification of rates of atrophy in Alzheimer's disease. Lancet 1996a; 348: 94-7.

Fox NC, Warrington EK, Freeborough PA *et al.* Presymptomatic hippocampal atrophy in Alzheimer's disease. A longitudinal MRI study. Brain 1996b; 119: 2001-7.

Fox NC, Warrington EK, Rossor MN. Serial magnetic resonance imaging of cerebral atrophy in preclinical Alzheimer's disease. Lancet 1999; 353: 2125.

Fox NC, Warrington EK, Stevens JM, Rossor MN. Atrophy of the hippocampal formation in early familial Alzheimer's disease. A longitudinal MRI study of at-risk members of a family with an amyloid precursor protein 717Val-Gly mutation. Ann N Y Acad Sci 1996c; 777: 226-32.

Frackowiak RS, Pozzilli C, Legg NJ *et al.* Regional cerebral oxygen supply and utilization in dementia. A clinical and physiological study with oxygen-15 and positron tomography. Brain 1981; 104: 753-78.

Frederikse M, Lu A, Aylward E, Barta P, Sharma T, Pearlson G. Sex differences in inferior parietal lobule volume in schizophrenia. Am J Psychiatry 2000; 157: 422-7.

Frederikse ME, Lu A, Aylward E, Barta P, Pearlson G. Sex differences in the inferior parietal lobule. Cereb Cortex 1999; 9: 896-901.

Free SL, Sisodiya SM, Cook MJ, Fish DR, Shorvon SD. Three-dimensional fractal analysis of the white matter surface from magnetic resonance images of the human brain. Cereb Cortex 1996; 6: 830-836.

Freeborough PA, Fox NC. Modeling brain deformations in Alzheimer disease by fluid registration of serial 3D MR images. J Comput Assist Tomogr 1998; 22: 838-43.

Freeborough PA, Fox NC, Kitney RI. Interactive algorithms for the segmentation and quantitation of 3-D MRI brain scans. Comput Methods Programs Biomed 1997; 53: 15-25.

Freeborough PA, Woods RP, Fox NC. Accurate registration of serial 3D MR brain images and its application to visualizing change in neurodegenerative disorders. J Comput Assist Tomogr 1996; 20: 1012-22.

Frisoni GB, Laakso MP, Beltramello A *et al.* Hippocampal and entorhinal cortex atrophy in frontotemporal dementia and Alzheimer's disease. Neurology 1999; 52: 91-100.

Friston KJ. Testing for anatomically specified regional effects. Hum Brain Mapp 1997; 5: 133-6.

Friston KJ, Holmes A, Poline JB, Price CJ, Frith CD. Detecting activations in PET and fMRI: levels of inference and power. Neuroimage 1996; 4: 223-35.

Friston KJ, Holmes A, Worsley KJ, Poline JB, Frith CD, Frackowiak RSJ. Statistic parametric maps in functional imaging: A general linear approach. Hum Brain Mapp 1995; 2: 189-210.

Frith CD, Friston KJ, Herold S *et al.* Regional brain activity in chronic schizophrenic patients during the performance of a verbal fluency task. Br.J Psychiatry 1995; 167: 343-349.

Galaburda AM, Sanides F, Geschwind N. Human brain. Cytoarchitectonic left-right asymmetries in the temporal speech region. Arch Neurol 1978; 35: 812-7.

Galton CJ, Gomez-Anson B, Antoun N *et al.* Temporal lobe rating scale: application to Alzheimer's disease and frontotemporal dementia. J Neurol Neurosurg Psychiatry 2001; 70: 165-173.

Gardner K, Barmada MM, Ptacek LJ, Hoffman EP. A new locus for hemiplegic migraine maps to chromosome 1q31. Neurology 1997; 49: 1231-1238.

Ge Y, Fitzpatrick JM, Votaw JR *et al.* Retrospective registration of PET and MR brain images: an algorithm and its stereotactic validation. J Comput Assist Tomogr 1994; 18: 800-810.

Geschwind N, Galaburda AM. Cerebral lateralization. Biological mechanisms, associations, and pathology: I. A hypothesis and a program for research. Arch Neurol 1985a; 42: 428-59.

Geschwind N, Galaburda AM. Cerebral lateralization. Biological mechanisms, associations, and pathology: II. A hypothesis and a program for research. Arch Neurol 1985b; 42: 521-52.

Geschwind N, Galaburda AM. Cerebral lateralization. Biological mechanisms, associations, and pathology: III. A hypothesis and a program for research. Arch Neurol 1985c; 42: 634-54.

Geschwind N, Levitsky W. Human brain: left-right asymmetries in temporal speech region. Science 1968; 161: 186-187.

Giedd JN, Snell JW, Lange N *et al.* Quantitative magnetic resonance imaging of human brain development: ages 4-18. Cereb Cortex 1996; 6: 551-60.

Gilbert AR, Rosenberg DR, Harenski K, Spencer S, Sweeney JA, Keshavan MS. Thalamic volumes in patients with first-episode schizophrenia. Am J Psychiatry 2001; 158: 618-624.

Gilissen EP, Ghosh P, Jacobs RE, Allman JM. Topographical localization of iron in brains of the aged fat-tailed dwarf lemur (Cheirogaleus medius) and gray lesser mouse lemur (Microcebus murinus). Am J Primatol 1998; 45: 291-9.

Goadsby PJ. Migraine, aura, and cortical spreading depression: why are we still talking about it? Ann Neurol 2001; 49: 4-6.

Goldstein JM, Seidman LJ, Horton NJ *et al.* Normal sexual dimorphism of the adult human brain assessed by in vivo magnetic resonance imaging. Cereb Cortex 2001; 11: 490-497.

Goldszal AF, Davatzikos C, Pham DL, Yan MX, Bryan RN, Resnick SM. An image-processing system for qualitative and quantitative volumetric analysis of brain images. J Comput Assist Tomogr 1998; 22: 827-837.

Gomez-Isla T, Price JT, McKeel DW, Jr., Morris JC, Growdon JH, Hyman BT. Profound loss of layer II entorhinal cortex neurons occurs in very mild Alzheimer's disease. J Neurosci 1996; 16: 4491-4500.

Good CD, Ashburner J, Frackowiak RS. Computational neuroanatomy: new perspectives for neuroradiology. Rev Neurol.(Paris) 2001a; 157: 797-806.

Good CD, Johnsrude I, Ashburner J, Henson RN, Friston KJ, Frackowiak RS. Cerebral asymmetry and the effects of sex and handedness on brain structure: a voxel-based morphometric analysis of 465 normal adult human brains. Neuroimage 2001b; 14: 685-700.

Good CD, Johnsrude IS, Ashburner J, R.N.A H, Friston KJ, Frackowiak RSJ. A voxel-based morphometric study of ageing in 465 normal adult human brains. Neuroimage 2001c; 14: 21-36.

Good CD, Scahill RI, Fox NC *et al.* Automatic differentiation of anatomical patterns in the human brain: validation with studies of degenerative dementias. Neuroimage 2002; 17: 29-46.

Gómez-Tortosa, del Barrio A, Barroso T, Garcia Ruiz PJ. Visual processing disorders in patients with Huntington's disease and asymptomatic carriers. J Neurol 1996; 243: 286-292.

Gray JM, Young AW, Barker WA, Curtis A, Gibson D. Impaired recognition of disgust in Huntington's disease gene carriers. Brain 1997; 120: 2029-2038.

Grelotti DJ, Gauthier I, Schultz RT. Social interest and the development of cortical face specialization: what autism teaches us about face processing. Dev.Psychobiol. 2002; 40: 213-225.

Grimsby J, Toth M, Chen K *et al.* Increased stress response and beta-phenylethylamine in MAOB-deficient mice. Nat Genet 1997; 17: 206-210.

Guimond A, Meunier J, Thirion JP. Average brain models: a convergence study. Comp.Vision and Image Understanding 2000; 77: 192-210.

Gundara N, Zivanovic S. Asymmetry in East African skulls. Am J Phys.Anthropol. 1968; 28: 331-337.

Gunning-Dixon FM, Head D, McQuain J, Acker JD, Raz N. Differential aging of the human striatum: a prospective MR imaging study. AJNR Am J Neuroradiol 1998; 19: 1501-7.

Gur RC, Gunning-Dixon FM, Turetsky BI, Bilker WB, Gur RE. Brain region and sex differences in age association with brain volume: a quantitative MRI study of healthy young adults. Am J Geriatr Psychiatry 2002; 10: 72-80.

Gur RC, Mozley PD, Resnick SM *et al.* Gender differences in age effect on brain atrophy measured by magnetic resonance imaging. Proc Natl Acad Sci U S A 1991; 88: 2845-9.

Gur RC, Turetsky BI, Matsui M *et al.* Sex differences in brain gray and white matter in healthy young adults: correlations with cognitive performance. J Neurosci 1999; 19: 4065-72.

Gur RE, Maany V, Mozley PD, Swanson C, Bilker W, Gur RC. Subcortical MRI volumes in neuroleptic-naive and treated patients with schizophrenia. Am J Psychiatry 1998; 155: 1711-1717.

Gutekunst C, Li S, Yi H *et al.* Nuclear and neuropil aggregates in Huntington's disease: relationship to neuropathology. J Neurosci 1999; 19: 2522-2534.

Guttmann CR, Jolesz FA, Kikinis R *et al.* White matter changes with normal aging. Neurology 1998a; 50: 972-8.

Guttmann CR, Jolesz FA, Kikinis R *et al.* White matter changes with normal aging. Neurology 1998b; 50: 972-8.

Habib M, Gayraud D, Oliva A, Regis J, Salamon G, Khalil R. Effects of handedness and sex on the morphology of the corpus callosum: a study with brain magnetic resonance imaging. Brain Cogn 1991; 16: 41-61.

Halliday GM, McRichie DAMV, Double KL, Trent RJ, McCusker E. Regional specificity of brain atrophy in Huntington's disease. Exp.Neurol 1998; 154: 663-672.

Hamilton JM, Murphy C, Paulsen JS. Odor detection, learning and memory in Huntington's disease. J Int.Neuropsychol.Soc. 1999; 5: 609-615.

Hampel H, Teipel SJ, Alexander GE *et al.* Corpus callosum atrophy is a possible indicator of region- and cell type-specific neuronal degeneration in Alzheimer disease: a magnetic resonance imaging analysis. Arch Neurol 1998; 55: 193-8.

Harris GJ, Codori AM, Lewis RF, Schmidt E, Bedi A, Brandt J. Reduced basal ganglia blood flow and volume in pre-symptomatic, gene tested persons at risk for Huntington's disease. Brain 1999; 122: 1667-1678.

Harro M, Eensoo D, Kiive E *et al.* Platelet monoamine oxidase in healthy 9- and 15-years old children: the effect of gender, smoking and puberty. Prog Neuropsychopharmacol.Biol Psychiatry 2001; 25: 1497-1511.

Harvey I, Ron MA, Du BG, Wicks D, Lewis SW, Murray RM. Reduction of cortical volume in schizophrenia on magnetic resonance imaging. Psychol.Med 1993; 23: 591-604.

Haug H. Effect of secular acceleration on the human brain weight and its changes during aging. Gegenbaurs.Morphol.Jahrb. 1984; 130: 481-500.

Hazlett EA, Buchsbaum MS, Byne W *et al.* Three-dimensional analysis with MRI and PET of the size, shape, and function of the thalamus in the schizophrenia spectrum. Am J Psychiatry 1999; 156: 1190-1199.

Hazlett EA, Buchsbaum MS, Mohs RC *et al.* Age-related shift in brain region activity during successful memory performance. Neurobiol Aging 1998; 19: 437-45.

Headache Classification Committee of the International Headache Society. Classification and diagnostic criteria for headache disorders, cranial neuralgias and facial pain. Cephalgia 1988; 8 (Suppl 7): 1-96.

Heckers S, Curran T, Goff D *et al.* Abnormalities in the thalamus and prefrontal cortex during episodic object recognition in schizophrenia. Biol Psychiatry 2000; 48: 651-657.

Hendriks RW, Chen ZY, Hinds H, Schuurman RK, Craig IW. An X chromosome inactivation assay based on differential methylation of a CpG island coupled to a VNTR polymorphism at the 5' end of the monoamine oxidase A gene. Hum Mol Genet 1992; 1: 187-194.

Hochberg FH, Le May M. Arteriographic correlates of handedness. Neurology 1975; 25: 218-222.

Hodges JR, Garrard P, Patterson K. Semantic dementia. In: Kertesz A, Munoz DG, editors. Pick's disease and Pick complex. new York: Wiley-Liss, 1998: 83-104.

Hodges JR, Patterson K, Oxbury S, Funnell E. Semantic dementia. Progressive fluent aphasia with temporal lobe atrophy. Brain 1992; 115: 1783-806.

Holland GN, Hawkes RC, Moore WS. Nuclear magnetic resonance (NMR) tomography of the brain: coronal and sagittal sections. J Comput Assist Tomogr 1980a; 4: 429-433.

Holland GN, Moore WS, Hawkes RC. Nuclear magnetic resonance tomography of the brain. J Comput Assist Tomogr 1980b; 4: 1-3.

Holsinger AE, Riederer SJ. The importance of phase-encoding order in ultra-short TR snapshot MR imaging. Magn Reson.Med 1990; 16: 481-488.

Hornak J, Rolls ET, Wade D. Face and voice expression identification in patients with emotional and behavioral changes following ventral frontal lobe damage. Neuropsychologia 1996; 34: 247-261.

Howard MA, Cowell PE, Boucher J *et al.* Convergent neuroanatomical and behavioral evidence of an amygdala hypothesis of autism. Neuroreport 2000; 11: 2931-5.

Hubbard BM, Anderson JM. A quantitative study of cerebral atrophy in old age and senile dementia. J Neurol Sci 1981; 50: 135-145.

Huntington's Disease Collaborative Research Group. A novel gene containing a trinucleotide repeat that is expanded and unstable on Huntington's disease chromosomes. Cell 1993; 72: 971-983.

Huntington Study Group. Unified Huntington's disease rating scale: reliability and consistency. Movement Disorders 1996; 11: 136-142.

Igarashi H, Sakai F, Kan S, Okada J, Tazaki Y. Magnetic resonance imaging of the brain in patients with migraine. Cephalalgia 1991; 11: 69-74.

Insausti R, Juottonen K, Soininen H *et al.* MR volumetric analysis of the human entorhinal, perirhinal, and temporopolar cortices. AJNR Am J Neuroradiol 1998; 19: 659-71.

International Huntington's Association (IHA) and the World Federation of Neurology (WFN) Research group on Huntington's Chorea. Guidelines for the molecular genetics predictive test in Huntington's disease. Neurology 1994; 44: 1533-1536.

Ishiwata A, Kitamura S, Nagazumi A, Terashi A. Cerebral blood flow of patients with age-associated memory impairment and the early stage of Alzheimer's disease. A study by SPECT using the ARG method. Nippon Ika Daigaku Zasshi 1998; 65: 140-7.

Jack CR, Jr. Brain and cerebrospinal fluid volume: measurement with MR imaging. Radiology 1991; 178: 22-4.

Jack CR, Jr., Gehring DG, Sharbrough FW *et al.* Temporal lobe volume measurement from MR images: accuracy and left-right asymmetry in normal persons. J Comput Assist Tomogr 1988; 12: 21-9.

Jack CR, Jr., Petersen RC, Xu YC *et al.* Hippocampal atrophy and apolipoprotein E genotype are independently associated with Alzheimer's disease. Ann Neurol 1998; 43: 303-10.

Jack CR, Jr., Petersen RC, Xu YC *et al.* Medial temporal atrophy on MRI in normal aging and very mild Alzheimer's disease. Neurology 1997; 49: 786-94.

Jack CR, Jr., Twomey CK, Zinsmeister AR, Sharbrough FW, Petersen RC, Cascino GD. Anterior temporal lobes and hippocampal formations: normative volumetric measurements from MR images in young adults. Radiology 1989; 172: 549-54.

Jackson GD, Berkovic SF, Tress BM, Kalnins RM, Fabinyi GC, Bladin PF. Hippocampal sclerosis can be reliably detected by magnetic resonance imaging. Neurology 1990; 40: 1869-1875.

Jacobs PA, Dalton P, James RS, Mosse K, Power M, Robinson D. Turner syndrome: a cytogenetic and molecular study. Ann Hum Genet 1997; 61: 471-483.

James RS, Coppin B, Dalton P *et al.* A study of females with deletions of the short arm of the X chromosome. Hum Genet 1998; 102: 507-516.

Jenkins BG, Rosas HD, Chen YCI *et al.* ^{1}H NMR spectroscopy studies of Huntington's disease. Correlations with CAG repeat numbers. Neurology 1998; 50: 1357-1365.

Jenkins R, Fox NC, Rossor AM, Harvey RJ, Rossor MN. Intracranial volume and Alzheimer disease: evidence against the cerebral reserve hypothesis. Arch Neurol 2000; 57: 220-4.

Jernigan TL, Archibald SL, Berhow MT, Sowell ER, Foster DS, Hesselink JR. Cerebral structure on MRI, Part I: Localization of age-related changes. Biol Psychiatry 1991a; 29: 55-67.

Jernigan TL, Archibald SL, Fennema-Notestine C *et al.* Effects of age on tissues and regions of the cerebrum and cerebellum. Neurobiol Aging 2001; 22: 581-594.

Jernigan TL, Press GA, Hesselink JR. Methods for measuring brain morphologic features on magnetic resonance images. Validation and normal aging. Arch.Neurol 1990; 47: 27-32.

Jernigan TL, Salmon DP, Butters N, Hesselink JR. Cerebral structure on MRI, Part II: Specific changes in Alzheimer's and Huntington's diseases. Biol Psychiatry 1991b; 29: 68-81.

Jernigan TL, Trauner DA, Hesselink JR, Tallal PA. Maturation of human cerebrum observed in vivo during adolescence. Brain 1991c; 114 (Pt 5): 2037-2049.

Johnson HJ, Christensen GE. Consistent landmark and intensity-based image registration. IEEE Trans Med Imaging 2002; 21: 450-461.

Johnstone EC, Frith CD, Lang FH, Owens DG. Determinants of the extremes of outcome in schizophrenia. Br.J Psychiatry 1995; 167: 604-609.

Joutel A, Bousser MG, Biousse V, et al. A gene for familial hemiplegic migraine maps to chromosome 19. Nat Genet 1993; 5: 40-45.

Juottonen K, Laakso MP, Insausti R *et al.* Volumes of the entorhinal and perirhinal cortices in Alzheimer's disease. Neurobiol Aging 1998; 19: 15-22.

Juottonen K, Laakso MP, Partanen K, Soininen H. Comparative MR analysis of the entorhinal cortex and hippocampus in diagnosing Alzheimer disease. AJNR Am J Neuroradiol 1999; 20: 139-44.

Kaada BR. Somato-motor, autonomic and electrocorticographic responses to electrical stimulation of rhinencephalic and other structures in primates, cat and dog. Acta Physiol.Scand 1951; 24 (Suppl. 83): 1-285.

Kansaku K, Yamaura A, Kitazawa S. Sex differences in lateralization revealed in the posterior language areas [In Process Citation]. Cereb Cortex 2000; 10: 866-72.

Katz S, Ford A, Moskowitz R, Jaffe M. Studies of illness in the aged; the index of ADL; a standardized measure of biological and psychosocial function. J.Am.Med.Assoc. 1965; 185: 914-919.

Keller SS, Mackay CE, Barrick TR, Wieshmann UC, Howard MA, Roberts N. Voxel-based morphometric comparison of hippocampal and extrahippocampal abnormalities in patients with left and right hippocampal atrophy. Neuroimage 2002; 16: 23-31.

Kemper TL. The relationship of cerebral cortical changes to nuclei in the brainstem. Neurobiol Aging 1993; 14: 659-660.

Kennedy DN, Lange N, Makris N, Bates J, Meyer J, Caviness VS, Jr. Gyri of the human neocortex: an MRI-based analysis of volume and variance. Cereb Cortex 1998; 8: 372-384.

Kennedy DN, O'Craven KM, Ticho BS, Goldstein AM, Makris N, Henson JW. Structural and functional brain asymmetries in human situs inversus totalis. Neurology 1999; 53: 1260-1265.

Kennedy L, Shelbourne PF. Dramatic mutation instability in HD mouse striatum: does polyglutamine load contribute to cell specific vulnerability in HD? Hum Mol Genet 2000; 9: 2539-2544.

Kertesz A, Polk M, Black SE, Howell J. Sex, handedness, and the morphometry of cerebral asymmetries on magnetic resonance imaging. Brain Res 1990; 530: 40-8.

Killiany RJ, Moss MB, Albert MS, Sandor T, Tieman J, Jolesz F. Temporal lobe regions on magnetic resonance imaging identify patients with early Alzheimer's disease. Arch Neurol 1993; 50: 949-54.

Kimber JR, Watson L, Mathias CJ. Distinction of idiopathic Parkinson's disease from multiple-system atrophy by stimulation of growth-hormone release with clonidine. Lancet 1997; 349: 1877-1881.

Kimura D. The asymmetry of the human brain. Sci Am 1973; 228: 70-8.

Kirkwood SC, Siemers E, Hodes ME, Conneally PM, Christian JC, Foroud T. Subtle changes among presymptomatic carriers of the Huntington's disease gene. J Neurol Neurosurg Psychiatry 2000; 69: 779.

Koeppen AH. The nucleus pontis centralis caudis in H. J Neurol Sci 1989; 91: 129-141.

Konick LC, Friedman L. Meta-analysis of thalamic size in schizophrenia. Biol Psychiatry 2001; 49: 28-38.

Kors EE, Terwindt GM, Vermeulen FLMG, et al. Delayed cerebral edema and fatal coma after minor head trauma: role of CACNA1A calcium channel subunit gene and relationship with familial hemiplegic migraine. Ann Neurol 2001; 49: 753-760.

Kramer PL, Yue Q, Gancher ST, Nutt JG, Baloh R, Smith E. A locus for the nystagmus-associated form of episodic ataxia maps to an Ii-Cm region on chromosome 19p. Am J Hum Genet 1995; 57: 182-185.

Krams M, Quinton R, Ashburner J *et al.* Kallmann's syndrome: mirror movements associated with bilateral corticospinal tract hypertrophy. Neurology 1999; 52: 816-22.

Kremer B, Almqvist E, Theilmann J *et al.* Sex-dependent mechanisms for expansions and contractions of the CAG repeat on affected Huntington disease chromosomes. Am J Hum Genet 1005; 57: 343-350.

Kulynych JJ, Vladar K, Jones DW, Weinberger DR. Gender differences in the normal lateralization of the supratemporal cortex: MRI surface-rendering morphometry of Heschl's gyrus and the planum temporale. Cereb Cortex 1994; 4: 107-18.

Laakso MP, Frisoni GB, Kononen M *et al.* Hippocampus and entorhinal cortex in frontotemporal dementia and Alzheimer's disease: a morphometric MRI study. Biol Psychiatry 2000; 47: 1056-63.

Laakso MP, Soininen H, Partanen K *et al.* MRI of the hippocampus in Alzheimer's disease: sensitivity, specificity, and analysis of the incorrectly classified subjects. Neurobiol Aging 1998; 19: 23-31.

Lamm C, Windischberger C, Leodolter U, Moser E, Bauer H. Co-registration of EEG and MRI data using matching of spline interpolated and MRI-segmented reconstructions of the scalp surface. Brain Topogr. 2001; 14: 93-100.

Landfield PW. Hippocampal neurobiological mechanisms of age-related memory dysfunction. Neurobiol Aging 1988; 9: 571-579.

Lange H, Thörner G, Hopf A, Schröder KF. Morphometric studies of the neuropathological changes in choreatic diseases. J Neurol Sci 1976; 28: 401-425.

Lange N, Giedd JN, Castellanos FX, Vaituzis AC, Rapoport JL. Variability of human brain structure size: ages 4-20 years. Psychiatry Res 1997; 74: 1-12.

Last RJ, Tompsett DH. Casts of cerebral ventricles. Br.J.Surg 1953; 40: 525-543.

Lauritzen M. Pathophysiology of the migraine aura. The spreading depression theory. Brain 1994; 117: 199-210.

Lawrence AD, Sahakian BJ, Hodges JR, Rosser AE, Lange KW, Robbins.T.W. Executive and mnemonic functions in early Huntington's disease. Brain 1996; 119: 1633-1645.

Lawrence AD, Watkins LHA, Sahakian BJ, Robbins.T.W., Hodges JR. Visual object and visuospatial cognition in Huntington's disease: implications for information processing in corticostriatal circuits. Brain 2000; 123: 1349-1364.

Lawrence K, Kuntsi J, Coleman M, Campbell R, Skuse DH. Face and emotion recognition deficits in Turner syndrome: A possible role for X-linked genes in amygdala development. Neuropsychology 2003.

Lawrie SM, Whalley H, Kestelman JN *et al.* Magnetic resonance imaging of brain in people at high risk of developing schizophrenia. Lancet 1999; 353: 30-33.

Lee JW, Andermann F, Dubeau F *et al.* Morphometric analysis of the temporal lobe in temporal lobe epilepsy. Epilepsia 1998; 39: 727-736.

Leigh RJ, Newman SA, Folstein SE, Lasker AG, Jensen BA. Abnormal ocular motor control in Huntington's disease. Neurology 1983; 33: 1268-1275.

Leigh RJ, Parhad IM, Clark AW, Buettner-Ennever JA, Folstein SE. Brainstem findings in Huntington's disease. Possible mechanisms for slow vertical saccades. J Neurol Sci 1985; 71: 247-256.

LeMay M. Left-right temporal region asymmetry in infants and children [letter]. AJNR Am J Neuroradiol 1986; 7: 974.

Liddle PF, Morris DL. Schizophrenic syndromes and frontal lobe performance. Br.J Psychiatry 1991; 158: 340-345.

Lieb JP, Dasheiff RM, Engel J, Jr. Role of the frontal lobes in the propagation of mesial temporal lobe seizures. Epilepsia 1991; 32: 822-837.

Lim KO, Tew W, Kushner M, Chow K, Matsumoto B, DeLisi LE. Cortical gray matter volume deficit in patients with first-episode schizophrenia. Am J Psychiatry 1996; 153: 1548-1553.

Lim KO, Zipursky RB, Watts MC, Pfefferbaum A. Decreased gray matter in normal aging: an in vivo magnetic resonance study. J Gerontol 1992; 47: 26-30.

Lipton RB, Scher AI, Steiner TJ *et al.* Patterns of health care utilization for migraine in England and in the United States. Neurology 2003; 60: 441-448.

Loftus WC, Tramo MJ, Thomas CE, Green RL, Nordgren RA, Gazzaniga MS. Three-dimensional quantitative analysis of hemispheric asymmetry in the human superior temporal region. Cereb Cortex 1993; 3: 348-55.

Luft AR, Skalej M, Schulz JB *et al.* Patterns of age-related shrinkage in cerebellum and brainstem observed in vivo using three-dimensional MRI volumetry. Cereb Cortex 1999; 9: 712-21.

Lyon MF. Gene action in the X-chromosome of the mouse (Mus musculus L). Nature 1961; 190: 372-373.

Magnifico F, Misra VP, Murray NM, Mathias CJ. The sympathetic skin response in peripheral autonomic failure-evaluation in pure failure, pure cholinergic dysautonomia and dopamine-beta-hydroxylase deficiency. Clin Auton.Res 1998; 8: 133-138.

Maguire EA, Gadian DG, Johnsrude IS *et al.* Navigation-related structural change in the hippocampi of taxi drivers. Proc Natl Acad Sci U S A 2000; 97: 4398-4403.

Mansour A, Fox CA, Akil H, Watson SJ. Opioid-receptor mRNA expression in the rat CNS: anatomical and functional implications. Trends Neurosci 1995; 18: 22-29.

Matharu MS, Good CD, May A, Bahra A, Goadsby PJ. No change in the structure of the brain in migraine: a voxel-based morphometric study. Eur.J Neurol 2003; 10: 53-57.

Mathias CJ. Disorders of the Autonomic Nervous System. In: Bradley WG, Daroff RB, Fenichel GM, et al, editors. Neurology in Clinical Practice. Woburn MA: Butterworth-Heinemann, 2000: 2131-65.

Mathias CJ, Bannister R. Investigation of autonomic disorders. In: Mathias CJ, Bannister R, editors. Autonomic Failure: A Textbook of Clinical Disorders of the Autonomic Nervous System. Oxford: Oxford University Press, 1999: 169-95.

Mathias CJ, Mallipeddi R, Bleasdale-Barr K. Symptoms associated with orthostatic hypotension in pure autonomic failure and multiple system atrophy. J Neurol 1999; 246: 893-898.

Matthews M. Autonomic ganglia and preganglionic neurons in autonomic failure. In: Mathias CJ, Bannister R, editors. Autonomic failure: A Textbook of Clinical Disorders of the Autonomic nervous System. Oxford: Oxford University Press, 1999: 169-95.

May A, Ashburner J, Buchel C *et al.* Correlation between structural and functional changes in brain in an idiopathic headache syndrome. Nat Med 1999b; 5: 836-838.

May A, Bahra A, Buchel C, Frackowiak RS, Goadsby PJ. Hypothalamic activation in cluster headache attacks. Lancet 1998a; 352: 275-278.

May A, Bahra A, Buchel C, Frackowiak RS, Goadsby PJ. PET and MRA findings in cluster headache and MRA in experimental pain. Neurology 2000; 55: 1328-1335.

May A, Bahra A, Buchel C, Turner R, Goadsby PJ. Functional MRI in spontaneous attacks of SUNCT: short-lasting neuralgiform headache with conjunctival injection and tearing. Ann Neurol 1999c; 46: 791-793.

May A, Goadsby PJ. The trigeminovascular system in humans: pathophysiologic implications for primary headache syndromes of the neural influences on the cerebral circulation. J Cereb Blood Flow Metab 1999; 19: 115-127.

May A, Goadsby PJ. Hypothalamic involvement and activation in cluster headache. Curr.Pain Headache Rep. 2001; 5: 60-66.

May A, Kaube H, Buchel C *et al.* Experimental cranial pain elicited by capsaicin: a PET study. Pain 1998b; 74: 61-66.

Mazziotta J, Toga A, Evans A *et al.* A probabilistic atlas and reference system for the human brain: International Consortium for Brain Mapping (ICBM). Philos.Trans R.Soc.Lond B Biol Sci 2001; 356: 1293-1322.

McCauley E, Kay T, Ito J, Treder R. The Turner syndrome: cognitive deficits, affective discrimination, and behavior problems. Child Dev 1987; 58: 464-73.

McDonald V, Halliday GM, Trent RJ, McCusker EA. Significant loss of pyramidal neurons in the angular gyrus of patients with Huntington's disease. Neuropathol Appl Neurobiol 1997; 23: 495.

McKhann G, Drachman D, Folstein M, Katzman R, Price D, Stadlan EM. Clinical diagnosis of Alzheimer's disease: report of the NINCDS-ADRDA Work Group under the auspices of Department of Health and Human Services Task Force on Alzheimer's Disease. Neurology 1984; 34: 939-44.

Mehler MF, Gokhan S. Mechanisms underlying neuronal cell death in neurodegenerative diseases: alterations of a developmentally -mediated cellular rheostat. Trends Neurosci 2000; 23: 599-605.

Meier-Ruge W, Ulrich J, Bruhlmann M, Meier E. Age-related white matter atrophy in the human brain. Ann N.Y.Acad Sci 1992; 673: 260-269.

Melsbach G, Wohlschlager A, Spiess M, Gunturkun O. Morphological asymmetries of motoneurons innervating upper extremities: clues to the anatomical foundations of handedness? Int J Neurosci 1996; 86: 217-24.

Menken M, Munsat TL, Toole JF. The global burden of disease study: implications for neurology. Arch.Neurol 2000; 57: 418-420.

Menon V, Adleman NE, White CD, Glover GH, Reiss AL. Error-related brain activation during a Go/NoGo response inhibition task. Hum Brain Mapp. 2001; 12: 131-143.

Messert B, Wannamaker BB, Dudley AW, Jr. Reevaluation of the size of the lateral ventricles of the brain. Postmortem study of an adult population. Neurology 1972; 22: 941-51.

Meyer JS, Rauch GM, Crawford K *et al.* Risk factors accelerating cerebral degenerative changes, cognitive decline and dementia. Int J Geriatr Psychiatry 1999; 14: 1050-61.

Miller AK, Corsellis JA. Evidence for a secular increase in human weight during the past century. Ann Hum Biol 1977; 4: 253-257.

Minoshima S, Giordani B, Berent S, Frey KA, Foster NL, Kuhl DE. Metabolic reduction in the posterior cingulate cortex in very early Alzheimer's disease. Ann Neurol 1997; 42: 85-94.

Moberg PJ, Doty RL. Olfactory function in Huntington's disease patients and at-risk offspring. J Neurosci 1997; 89: 133-139.

Moffat SD, Hampson E, Lee DH. Morphology of the planum temporale and corpus callosum in left handers with evidence of left and right hemisphere speech representation. Brain 1998; 121: 2369-79.

Moran NF, Lemieux L, Kitchen ND, Fish DR, Shorvon SD. Extrahippocampal temporal lobe atrophy in temporal lobe epilepsy and mesial temporal sclerosis. Brain 2001; 124: 167-175.

Moran NF, Lemieux L, Maudgil D, Kitchen ND, Fish DR, Shorvon SD. Analysis of temporal lobe resections in MR images. Epilepsia 1999; 40: 1077-1084.

Morris JS, Frith CD, Perrett DI *et al.* A differential neural response in the human amygdala to fearful and happy facial expressions. Nature 1996; 383: 812-815.

Mugler JP, III, Brookeman JR. Three-dimensional magnetization-prepared rapid gradient-echo imaging (3D MP RAGE). Magn Reson.Med 1990; 15: 152-157.

Mummery CJ, Patterson K, Price CJ, Ashburner J, Frackowiak RS, Hodges JR. A voxel-based morphometry study of semantic dementia: relationship between temporal lobe atrophy and semantic memory. Ann Neurol 2000; 47: 36-45.

Murphy DG, DeCarli C, McIntosh AR *et al.* Sex differences in human brain morphometry and metabolism: an in vivo quantitative magnetic resonance imaging and positron emission tomography study on the effect of aging. Arch Gen Psychiatry 1996; 53: 585-94.

Neary D, Snowden JS, Gustafson L *et al.* Frontotemporal lobar degeneration: a consensus on clinical diagnostic criteria. Neurology 1998; 51: 1546-54.

Neelin P, Crossman J, Hawkes DJ, Ma Y, Evans AC. Validation of an MRI/PET landmark registration method using 3D simulated PET images and point simulations. Comput Med Imaging Graph. 1993; 17: 351-356.

Neumann CS, Walker EF. Motor dysfunction in schizotypal personality disorder. Schizophr.Res 1999; 38: 159-168.

Nordin S, Paulsen JS, Murphy C. Sensory- and memory-mediated olfactory dysfunction in Huntington's disease. J Int.Neuropsychol.Soc. 1995; 1: 281-290.

Oguro H, Okada K, Yamaguchi S, Kobayashi S. Sex differences in morphology of the brain stem and cerebellum with normal ageing. Neuroradiology 1998; 40: 788-92.

Oldfield RC. The assessment and analysis of handedness: the Edinburgh inventory. Neuropsychologia 1971; 9: 97-113.

Olesen J, Tfelt-Hansen P, Welch KMA. The Headaches. Philadelphia: Lippincott, Williams & Wilkins, 2000.

Ophoff RA, Terwindt GM, Vergouwe MN, Frants RR, Ferrari MD. Familial hemiplegic migraine: involvement of a calcium neuronal channel. Neurologia 1997; 12 Suppl 5: 31-37.

Oppenheimer SM, Gelb A, Girvin JP, Hachinski VC. Cardiovascular effects of human insular cortex stimulation. Neurology 1992; 42: 1727-1732.

Osterlund MK, Hurd YL. Estrogen receptors in the human forebrain and the relation to neuropsychiatric disorders. Prog Neurobiol 2001; 64: 251-267.

Pakkenberg B. Pronounced reduction of total neuron number in mediodorsal thalamic nucleus and nucleus accumbens in schizophrenics. Arch.Gen.Psychiatry 1990; 47: 1023-1028.

Patwardhan AJ, Brown WE, Bender BG, Linden MG, Eliez S, Reiss AL. Reduced size of the amygdala in individuals with 47,XXY and 47,XXX karyotypes. Am J Med Genet 2002; 114: 93-98.

Penhune VB, Zatorre RJ, MacDonald JD, Evans AC. Interhemispheric anatomical differences in human primary auditory cortex: probabilistic mapping and volume measurement from magnetic resonance scans. Cereb Cortex 1996; 6: 661-72.

Peters A, Morrison JH, Rosene DL, Hyman BT. Feature article: are neurons lost from the primate cerebral cortex during normal aging? Cereb Cortex 1998; 8: 295-300.

Peters A, Rosene DL, Moss MB *et al.* Neurobiological bases of age-related cognitive decline in the rhesus monkey. J Neuropathol.Exp.Neurol 1996; 55: 861-874.

Petersen A, Mani K, Brundin P. Recent advances on the pathogenesis of Huntington's disease. Exp.Neurol 1999; 157: 1-18.

Pfefferbaum A, Mathalon DH, Sullivan EV, Rawles JM, Zipursky RB, Lim KO. A quantitative magnetic resonance imaging study of changes in brain morphology from infancy to late adulthood. Arch Neurol 1994; 51: 874-87.

Pfefferbaum A, Sullivan EV, Jernigan TL *et al.* A quantitative analysis of CT and cognitive measures in normal aging and Alzheimer's disease. Psychiatry Res 1990; 35: 115-136.

Pfefferbaum A, Zatz LM, Jernigan TL. Computer-interactive method for quantifying cerebrospinal fluid and tissue in brain CT scans: effects of aging. J Comput Assist.Tomogr. 1986; 10: 571-578.

Phillips ML, Young AW, Senior C *et al.* A specific neural substrate for perceiving facial expressions of disgust. Nature 1997; 389: 495-498.

Pool JL, Ransohoff J. Autonomic effects on stimulating the rostral portion of the cingulate gyri in man. J.Neurophysiol. 1949; 12: 385-392.

Popken GJ, Bunney WE, Jr., Potkin SG, Jones EG. Subnucleus-specific loss of neurons in medial thalamus of schizophrenics. Proc Natl Acad Sci U S A 2000; 97: 9276-9280.

Porrino LJ, Goldman-Rakic PS. Brainstem innervation of prefrontal and anterior cingulate cortex in the rhesus monkey revealed by retrograde transport of HRP. J Comp Neurol 1982; 205: 63-76.

Portas CM, Goldstein JM, Shenton ME *et al.* Volumetric evaluation of the thalamus in schizophrenic male patients using magnetic resonance imaging. Biol Psychiatry 1998; 43: 649-659.

Pruessner JC, Collins DL, Pruessner M, Evans AC. Age and gender predict volume decline in the anterior and posterior hippocampus in early adulthood. J Neurosci 2001; 21: 194-200.

Purcell E, Torrey H, Pound R. Resonance absorption by nuclear magnetic moment. Physics Review 1945; 69: 37-38.

Rabinowicz T, de Courten-Myers GM, Petetot JM, Xi G, de los Reyes E. Human cortex development: estimates of neuronal numbers indicate major loss late during gestation. J Neuropathol Exp Neurol 1996; 55: 320-8.

Rabinowicz T, Dean DE, Petetot JM, de Courten-Myers GM. Gender differences in the human cerebral cortex: more neurons in males; more processes in females. J Child Neurol 1999; 14: 98-107.

Rademacher J, Burgel U, Geyer S *et al.* Variability and asymmetry in the human precentral motor system. A cytoarchitectonic and myeloarchitectonic brain mapping study. Brain 2001; 124: 2232-2258.

Rademacher J, Caviness VS, Jr., Steinmetz H, Galaburda AM. Topographical variation of the human primary cortices: implications for neuroimaging, brain mapping, and neurobiology. Cereb Cortex 1993; 3: 313-329.

Rajkowska G, Goldman-Rakic PS. Cytoarchitectonic definition of prefrontal areas in the normal human cortex: I. Remapping of areas 9 and 46 using quantitative criteria. Cereb Cortex 1995a; 5: 307-322.

Rajkowska G, Goldman-Rakic PS. Cytoarchitectonic definition of prefrontal areas in the normal human cortex: II. Variability in locations of areas 9 and 46 and relationship to the Talairach Coordinate System. Cereb Cortex 1995b; 5: 323-337.

Ranen N, Stine OC, Abbott MH *et al.* Anticipation and instability of IT-15(CAG) repeats in parent-offspring pairs with Huntington's disease. Am J Hum Genet 1995; 57: 593-602.

Ratcliff G, Dila C, Taylor L, Milner B. The morphological asymmetry of the hemispheres and cerebral dominance for speech: a possible relationship. Brain Lang 1980; 11: 87-98.

Raz N, Gunning-Dixon FM, Head D, Dupuis JH, Acker JD. Neuroanatomical correlates of cognitive aging: evidence from structural magnetic resonance imaging. Neuropsychology 1998; 12: 95-114.

Raz N, Gunning FM, Head D *et al.* Selective aging of the human cerebral cortex observed in vivo: differential vulnerability of the prefrontal gray matter. Cereb Cortex 1997; 7: 268-82.

Raz N, Torres IJ, Spencer WD, White K, Acker JD. Age-related regional differences in cerebellar vermis observed in vivo. Arch Neurol 1992; 49: 412-6.

Reichardt M. Uber die bestemmung der schadelkapazikat an der leiche. Allgemeine zeitschrift fur psychiatrie. 1905; 62: 787-801.

Resnick SM, Goldszal AF, Davatzikos C *et al.* One-year age changes in MRI brain volumes in older adults. Cereb Cortex 2000; 10: 464-472.

Richardson MP, Friston KJ, Sisodiya SM *et al* . Cortical grey matter and benzodiazepine receptors in malformations of cortical development. A voxel-based comparison of structural and functional imaging data. Brain 1997; 120: 1961-73.

Rogers RD, Owen AM, Middleton HC *et al.* Choosing between small, likely rewards and large, unlikely rewards activates inferior and orbitofrontal cortex. J Neurosci 1999; 20: 9029-9038.

Roland PE, Zilles K. Structural divisions and functional fields in the human cerebral cortex. Brain Res Brain Res Rev 1998; 26: 87-105.

Rolls ET. In: Angleton JP, editor. The amygdala. Oxford: Oxford University Press, 2003: 447-78.

Rombouts SA, Barkhof F, Witter MP, Scheltens P. Unbiased whole-brain analysis of gray matter loss in Alzheimer's disease. Neuroscience Letters 2000; 285: 231-233.

Ross JL, Roeltgen D, Kushner H, Wei F, Zinn AR. The Turner syndrome-associated neurocognitive phenotype maps to distal Xp. Am J Hum Genet 2000; 67: 672-81.

Ross JL, Stefanatos GA, Kushner H, Zinn A, Bondy C, Roeltgen D. Persistent cognitive deficits in adult women with Turner syndrome. Neurology 2002; 58: 218-225.

Rubia K, Russell T, Bullmore ET *et al.* An fMRI study of reduced left prefrontal activation in schizophrenia during normal inhibitory function. Schizophr.Res 2001; 52: 47-55.

Russell TA, Rubia K, Bullmore ET *et al.* Exploring the social brain in schizophrenia: left prefrontal underactivation during mental state attribution. Am J Psychiatry 2000; 157: 2040-2042.

Salat D, Ward A, Kaye JA, Janowsky JS. Sex differences in the corpus callosum with aging. Neurobiol Aging 1997; 18: 191-7.

Salmond CH, Ashburner J, Vargha-Khadem F, Connelly A, Gadian DG, Friston KJ. Distributional assumptions in voxel-based morphometry. Neuroimage 2002; 17: 1027-1030.

Salmond CH, Ashburner J, Vargha-Khadem F, Gadian DG, Friston KJ. Detecting bilateral abnormalities with voxel-based morphometry. Hum Brain Mapp 2000; 11: 223-32.

Salonen O, Autti T, Raininko R, Ylikoski A, Erkinjuntti T. MRI of the brain in neurologically healthy middle-aged and elderly individuals. Neuroradiology 1997; 39: 537-45.

Sanchez del Rio M, Bakker D, Wu O, et al. Perfusion weighted imaging during migraine: spontaneous visual aura and headache. Cephalalgia 1999; 19: 701-707.

Sandor PS, Mascia A, Seidel L, de Pasqua V, Schoenen J. Subclinical cerebellar impairment in the common types of migraine: a three dimensional analysis of reaching movements. Ann Neurol 2001; 49: 668-672.

Scahill RI, Schott JM, Stevens JM, Rossor MN, Fox NC. Mapping the evolution of regional atrophy in Alzheimer's disease: Unbiased analysis of fluid-registered serial MRI. Proc Natl Acad Sci U S A 2002; 99: 4703-4707.

Scalaidhe SP, Wilson FA, Goldman-Rakic PS. Face-selective neurons during passive viewing and working memory performance of rhesus monkeys: evidence for intrinsic specialization of neuronal coding. Cereb Cortex 1999; 9: 459-475.

Schlaepfer TE, Harris GJ, Tien AY, Peng L, Lee S, Pearlson GD. Structural differences in the cerebral cortex of healthy female and male subjects: a magnetic resonance imaging study. Psychiatry Res 1995; 61: 129-35.

Schuff N, Amend DL, Knowlton R, Norman D, Fein G, Weiner MW. Age-related metabolite changes and volume loss in the hippocampus by magnetic resonance spectroscopy and imaging. Neurobiol Aging 1999; 20: 279-85.

Schultz SK, Andreasen NC. Schizophrenia. Lancet 1999; 353: 1425-1430.

Schulz JB, Skalej M, Wedekind D *et al.* Magnetic resonance imaging-based volumetry differentiates idiopathic parkinson's syndrome from multiple system atrophy and progressive supranuclear palsy. Ann Neurol 2002; 45: 65-74.

Schwartz M, Creasey H, Grady CL *et al.* Computed tomographic analysis of brain morphometrics in 30 healthy men aged 21 to 81 years. Ann Neurol 1985; 17: 146-157.

Shah PJ, Ebmeier KP, Glabus MF, Goodwin GM. Cortical grey matter reductions associated with treatment-resistant chronic unipolar depression. Controlled magnetic resonance imaging study. Br.J Psychiatry 1998; 172: 527-532.

Shen D, Davatzikos C. Very high-resolution morphometry using mass-preserving deformations and HAMMER elastic registration. Neuroimage 2003; 18: 28-41.

Shergill SS, Brammer MJ, Williams SC, Murray RM, McGuire PK. Mapping auditory hallucinations in schizophrenia using functional magnetic resonance imaging. Arch.Gen.Psychiatry 2000; 57: 1033-1038.

Shih JC, Thompson RF. Monoamine oxidase in neuropsychiatry and behavior. Am J Hum Genet 1999; 65: 593-598.

Sieradzan K, Mann DMA. Clinical presentation and patterns of regional cerebral atrophy related to the length of trinucleotide repeat expansion in patients with adult-onset Huntington's disease. Neurosci Lett 1997; 225: 45-48.

Sieradzan KA, Mann DMA. Selective vulnerability of nerve cells in Huntington's disease. Neuropathol Appl Neurobiol 2001; 27: 1-21.

Silbersweig DA, Stern E, Frith C *et al.* A functional neuroanatomy of hallucinations in schizophrenia. Nature 1995; 378: 176-179.

Sisodiya SM, Moran N, Free SL *et al.* Correlation of widespread preoperative magnetic resonance imaging changes with unsuccessful surgery for hippocampal sclerosis. Ann Neurol 1997; 41: 490-496.

Sisodiya SM, Stevens JM, Fish DR, Free SL, Shorvon SD. The demonstration of gyral abnormalities in patients with cryptogenic partial epilepsy using three-dimensional MRI. Arch.Neurol 1996; 53: 28-34.

Skuse DH, James RS, Bishop DV *et al.* Evidence from Turner's syndrome of an imprinted X-linked locus affecting cognitive function. Nature 1997; 387: 705-8.

Small GW, Ercoli LM, Silverman DH *et al.* Cerebral metabolic and cognitive decline in persons at genetic risk for Alzheimer's disease. Proc Natl Acad Sci U S A 2000; 97: 6037-42.

Snowden JS, Goulding PJ. Semantic dementia: a form of circumscribed cerebral atrophy. Behavioural Neurology 1989; 2: 167-182.

Soges LJ, Cacayorin ED, Petro GR, Ramachandran TS. Migraine: evaluation by MR. AJNR Am J Neuroradiol. 1988; 9: 425-429.

Sowell ER, Toga AW, Asarnow R. Brain abnormalities observed in childhood-onset schizophrenia: a review of the structural magnetic resonance imaging literature. Ment.Retard.Dev.Disabil.Res Rev 2000; 6: 180-185.

Sprengelmeyer R, Young AW, Calder AJ *et al.* Loss of disgust. perception of faces and emotions in Huntington's disease. Brain 1996; 119: 1647-1665.

Spyer KM. Central nervous system control of the cardiovascular system. In: Mathias CJ, Bannister R, editors. Autonomic failure: A Textbook of Clinical Disorders of the Autonomic Nervous System. Oxford: Oxford University Press, 1999: 45-55.

Staal WG, Hulshoff Pol HE, Schnack H, van der Schot AC, Kahn RS. Partial volume decrease of the thalamus in relatives of patients with schizophrenia. Am J Psychiatry 1998; 155: 1784-1786.

Steinmetz H. Structure, functional and cerebral asymmetry: in vivo morphometry of the planum temporale. Neurosci Biobehav Rev 1996; 20: 587-91.

Steinmetz H, Jancke L, Kleinschmidt A, Schlaug G, Volkmann J, Huang Y. Sex but no hand difference in the isthmus of the corpus callosum [see comments]. Neurology 1992; 42: 749-52.

Steinmetz H, Rademacher J, Huang YX *et al.* Cerebral asymmetry: MR planimetry of the human planum temporale. J Comput Assist Tomogr 1989; 13: 996-1005.

Stewart WF, Lipton RB, Celentano DD, Reed ML. Prevalence of migraine headache in the United States. Relation to age, income, race, and other sociodemographic factors. JAMA 1992; 267: 64-69.

Stout JC, Bondi MW, Jernigan TL, Archibald SL, Delis DC, Salmon DP. Regional cerebral volume loss associated with verbal learning and memory in dementia of the Alzheimer type. Neuropsychology. 1999; 13: 188-197.

Subsol G, Roberts N, Doran M, Thirion JP, Whitehouse GH. Automatic analysis of cerebral atrophy. Magn Reson.Imaging 1997; 15: 917-927.

Sudbrack R. X chromosome-specific cDNA arrays: identification of genes that escape from X-inactivation and other applications. Hum Mol Genet 2001; 10: 77-83.

Talairach J, Tournoux P. Coplanar stereotaxic atlas of the human brain. New York: Thieme, 1988.

Teipel SJ, Hampel H, Pietrini P *et al.* Region-specific corpus callosum atrophy correlates with the regional pattern of cortical glucose metabolism in Alzheimer disease. Arch Neurol 1999; 56: 467-73.

Temple CM, Carney R. Reading skills in children with Turner's syndrome: an analysis of hyperplexia. Cortex 1996; 32: 335-45.

Temple CM, Carney RA. Intellectual functioning of children with Turner syndrome: a comparison of behavioural phenotypes. Dev Med Child Neurol 1993; 35: 691-8.

Terwindt GM, Ophoff RA, Haan J *et al.* Variable clinical expression of mutations in the P/Q-type calcium channel gene in familial hemiplegic migraine. Dutch Migraine Genetics Research Group. Neurology 1998; 50: 1105-1110.

Thompson AJ, Schwartz C, Lin RT, Khan AA, Toga AW. Three-dimensional statistical analysis of sulcal variability in the human brain. J Neurosci 1996a; 16: 4261-4274.

Thompson AJ, Schwartz C, Toga AW. High-resolution random mesh algorithms for creating a 3D probabilistic surface atlas of the human brain. Neuroimage 1996b; 3: 19-34.

Thompson PM, Mega MS, Woods RP *et al.* Cortical change in Alzheimer's disease detected with a disease -specific population-based brain atlas. Cerebral Cortex 2001a; 11: 1-16.

Thompson PM, Moussai J, Zohoori S *et al.* Cortical variability and asymmetry in normal aging and Alzheimer's disease. Cereb Cortex 1998; 8: 492-509.

Thompson PM, Schwartz C, Toga AW. High-resolution random mesh algorithms for creating a probabilistic 3D surface atlas of the human brain. Neuroimage 1996c; 3: 19-34.

Thompson PM, Toga AW. Detection, visualization and animation of abnormal anatomic structure with a deformable probabilistic brain atlas based on random vector field transformations. Med Image Anal 1997; 1: 271-94.

Thompson PM, Vidal C, Giedd JN *et al.* Mapping adolescent brain change reveals dynamic wave of accelerated gray matter loss in very early-onset schizophrenia. Proc Natl Acad Sci U S A 2001b; 98: 11650-11655.

Thompson PM, Woods RP, Mega MS, Toga AW. Mathematical/computational challenges in creating deformable and probabilistic atlases of the human brain. Hum Brain Mapp 2000; 9: 81-92.

Tokgozoglu SL, Batur MK, Top uoglu MA, Saribas O, Kes S, Oto A. Effects of stroke localization on cardiac autonomic balance and sudden death. Stroke 1999; 30: 1307-1311.

Tononi G, Edelman GM. Schizophrenia and the mechanisms of conscious integration. Brain Res Brain Res Rev 2000; 31: 391-400.

Tranel D. Electrodermal activity in cognitive neuroscience: neuroanatomical and neurophysiological correlates. In: Lane RD, Nadel L, editors. Cognitive Neuroscience of Emotion. New York: Oxford University Press, 2000: 192-2224.

Tranel D, Damasio H. Neuroanatomical correlates of electrodermal skin conductance responses. Psychophysiology 1994; 31: 427-438.

Tzourio C, Kittner SJ, Bousser MG, Alperovitch A. Migraine and stroke in young women. Cephalalgia 2000; 20: 190-199.

Vahedi K, Joutel A, van Bogaert P, et al. A gene for hereditary paroxysmal cerebellar ataxia maps to chromosome 19p. Ann Neurol 1995; 37: 289-293.

Valenzuela MJ, Sachdev PS, Wen W, Shnier R, Brodaty H, Gillies D. Dual voxel proton magnetic resonance spectroscopy in the healthy elderly: subcortical-frontal axonal N-acetylaspartate levels are correlated with fluid cognitive abilities independent of structural brain changes. Neuroimage 2000; 12: 747-56.

Van Dellen A, Blakemore C, Deacon R, York D, Hannan AJ. Delaying the onset of Huntington's in mice. Nature 2000; 404: 721-722.

Vargha-Khadem F, Watkins KE, Price CJ *et al.* Neural basis of an inherited speech and language disorder. Proc Natl Acad Sci U S A 1998; 95: 12695-700.

Vighetto A, Froment JC, Trillet M, Aimard G. Magnetic resonance imaging in familial paroxysmal ataxia. Arch Neurol 1988; 45: 547-549.

Vijayashankar N, Brody H. A quantitative study of the pigmented neurons in the nuclei locus coeruleus and subcoeruleus in man as related to aging. J Neuropathol.Exp.Neurol 1979; 38: 490-497.

Vonsattel JP, DiFiglia M. Huntington's Disease. J Neuropathol Exp Neurol 1998; 57: 369-384.

Vonsattel JP, Myers RH, Stevens TJ, Ferrante RJ, Bird ED, Richardson EP. Neuropathological classification of Huntington's disease. J Neuropathol Exp Neurol 1985; 44: 559-577.

Wada JA, Clarke R, Hamm A. Cerebral hemispheric asymmetry in humans. Cortical speech zones in 100 adults and 100 infant brains. Arch Neurol 1975; 32: 239-46.

Wahlund LO, Agartz I, Almqvist O *et al.* The brain in healthy aged individuals: MR imaging. Radiology 1990; 174: 675-9.

Wahlund LO, Almkvist O, Basun H, Julin P. MRI in successful aging, a 5-year follow-up study from the eighth to ninth decade of life. Magn Reson Imaging 1996; 14: 601-8.

Walker E, Lewis N, Loewy R, Palyo S. Motor dysfunction and risk for schizophrenia. Dev.Psychopathol. 1999; 11: 509-523.

Warrington EK. The selective impairment of semantic memory. Q J Exp Psychol 1975; 27: 635-57.

Watkins KE, Paus T, Lerch JP *et al.* Structural asymmetries in the human brain: a voxel-based statistical analysis of 142 MRI scans. Cereb Cortex 2001; 11: 868-877.

Watkins LHA, Rogers RD, Lawrence AD, Sahakian BJ, Rosser AE, Robbins.T.W. Impaired planning but intact decision making in Huntington's disease: implications for specific fronto-striatal pathology. Neuropsychologia 2000; 38: 1112-1125.

Weiller C, May A, Limmroth V *et al.* Brain stem activation in spontaneous human migraine attacks. Nat Med 1995; 1: 658-660.

Weinberger DR. Computed tomography (CT) findings in schizophrenia: speculation on the meaning of it all. J Psychiatr.Res 1984; 18: 477-490.

Weinberger DR. Schizophrenia and the frontal lobe. Trends Neurosci 1988; 11: 367-370.

Weinberger DR, Luchins DJ, Morihisa J, Wyatt RJ. Asymmetrical volumes of the right and left frontal and occipital regions of the human brain. Ann Neurol 1982; 11: 97-100.

Weinberger DR, Torrey EF, Neophytides AN, Wyatt RJ. Lateral cerebral ventricular enlargement in chronic schizophrenia. Arch.Gen.Psychiatry 1979a; 36: 735-739.

Weinberger DR, Torrey EF, Neophytides AN, Wyatt RJ. Structural abnormalities in the cerebral cortex of chronic schizophrenic patients. Arch.Gen.Psychiatry 1979b; 36: 935-939.

Westbury CF, Zatorre RJ, Evans AC. Quantifying variability in the planum temporale: a probability map. Cereb Cortex 1999; 9: 392-405.

White LE, Andrews TJ, Hulette C *et al.* Structure of the human sensorimotor system. II: Lateral symmetry. Cereb Cortex 1997; 7: 31-47.

White LE, Lucas G, Richards A, Purves D. Cerebral asymmetry and handedness [letter]. Nature 1994; 368: 197-8.

Winston JS, Strange BA, O'Doherty J, Dolan RJ. Automatic and intentional brain responses during evaluation of trustworthiness of faces. Nat Neurosci 2002; 5: 277-83.

Witelson SF. The brain connection: the corpus callosum is larger in left-handers. Science 1985; 229: 665-8.

Witelson SF, Glezer II, Kigar DL. Women have greater density of neurons in posterior temporal cortex. J Neurosci 1995; 15: 3418-3428.

Witelson SF, Kigar DL. Sylvian fissure morphology and asymmetry in men and women: bilateral differences in relation to handedness in men. J Comp Neurol 1992; 323: 326-40.

Woermann FG, Free SL, Koepp MJ, Ashburner J, Duncan JS. Voxel-by-voxel comparison of automatically segmented cerebral gray matter-A rater-independent comparison of structural MRI in patients with epilepsy. Neuroimage 1999b; 10: 373-84.

Woermann FG, Free SL, Koepp MJ, Sisodiya SM, Duncan JS. Abnormal cerebral structure in juvenile myoclonic epilepsy demonstrated with voxel-based analysis of MRI. Brain 1999c; 122: 2101-2108.

Worsley K, Marrett S, Vandal AC, Friston KJ, Evans AC. A unified statistical approach for determining significant voxels in images of cerebral activation. Hum Brain Mapp. 1996; 4: 58-73.

Wright IC, Ellison ZR, Sharma T, Friston KJ, Murray RM, McGuire PK. Mapping of grey matter changes in schizophrenia. Schizophr.Res 1999; 35: 1-14.

Wright IC, McGuire PK, Poline JB *et al.* A voxel-based method for the statistical analysis of gray and white matter density applied to schizophrenia. Neuroimage 1995b; 2: 244-252.

Wright IC, McGuire PK, Poline JB *et al.* A voxel-based method for the statistical analysis of gray and white matter density applied to schizophrenia. Neuroimage 1995a; 2: 244-52.

Wright IC, Rabe-Hesketh S, Woodruff PW, David AS, Murray RM, Bullmore ET. Meta-analysis of regional brain volumes in schizophrenia. Am J Psychiatry 2000a; 157: 16-25.

Xu J, Burgoyne PS, Arnold AP. Sex differences in sex chromosome gene expression in mouse brain. Hum Mol Genet 2002; 11: 1409-1419.

Xu J, Kobayashi S, Yamaguchi S, Iijima K, Okada K, Yamashita K. Gender effects on age-related changes in brain structure. Am J Neuroradiol 2000a; 21: 112-8.

Xu Y, Jack CR, Jr., O'Brien PC *et al.* Usefulness of MRI measures of entorhinal cortex versus hippocampus in AD. Neurology 2000b; 54: 1760-7.

Yamada M, Tsuji S, Takahashi H. Pathology of CAG repeat diseases. Neuropathology 2000; 20: 319-325.

Yamamoto A, Lucas JL, Hen R. Reversal of neuropathology and motor dysfunction in a conditional model of Huntington's disease. Cell 2000; 101: 57-66.

Yamano S, Sawai N, Minami S *et al.* The relationship between brain atrophy and asymptomatic cerebral lesions. Nippon Ronen Igakkai Zasshi 1997; 34: 913-919.

Yamauchi H, Fukuyama H, Harada K *et al.* Callosal atrophy parallels decreased cortical oxygen metabolism and neuropsychological impairment in Alzheimer's disease. Arch Neurol 1993; 50: 1070-4.

Yamauchi H, Fukuyama H, Nagahama Y *et al.* Comparison of the pattern of atrophy of the corpus callosum in frontotemporal dementia, progressive supranuclear palsy, and Alzheimer's disease. J Neurol Neurosurg Psychiatry 2000; 69: 623-9.

Young AW, Aggleton JP, Hellawell DJ, Johnson M, Broks P, Hanley JR. Face processing impairments after amygdalotomy. Brain 1995; 118: 15-24.

Young AW, Hellawell DJ, Van De Wal C, Johnson M. Facial expression processing after amygdalotomy. Neuropsychologia 1996; 34: 31-39.

Young GF, Leon-Barth CA, Green J. familial hemiplegic migraine, retinal degeneration, deafness and nystagmus. Arch Neurol 1970; 23: 201-209.

Zasker AG, Zee DS. Ocular motor abnormalities in Huntington's disease. Vision Research 1997; 37: 3639-3645.

Zechner U, Wilda M, Kehrer-Sawatzki H, Vogel W, Fundele R, Hameister H. A high density of X-linked genes for general cognitive ability: a run-away process shaping human evolution? Trends Genet 2001; 17: 697-701.

Zilles K, Dabringhaus A, Geyer S *et al.* Structural asymmetries in the human forebrain and the forebrain of non-human primates and rats. Neurosci Biobehav Rev 1996; 20: 593-605.

Zweig RM, Ross CA, Hedreen JC *et al.* Locus coeruleus involvement in Huntington's disease. Arch Neurol 1992; 49: 156.